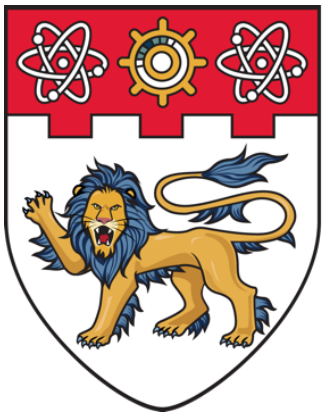

NANYANG TECHNOLOGICAL UNIVERSITY
SINGAPORE

MODELLING AND IN-PROCESS MONITORING OF ABRASIVE BELT GRINDING PROCESS

VIGNEASHWARA PANDIYAN SOLAIRAJA PANDIYAN

G1400568K

SCHOOL OF MECHANICAL AND AEROSPACE ENGINEERING

THESIS REPORT SUBMITTED IN PARTIAL FULFILLMENT FOR DEGREE OF DOCTOR OF PHILOSOPHY

2019

MODELLING AND IN-PROCESS MONITORING OF ABRASIVE BELT GRINDING PROCESS

by

VIGNEASHWARA PANDIYAN SOLAIRAJA PANDIYAN

Thesis Supervisor: Prof. Tegoeh Tjahjowidodo

A thesis submitted to the School of Mechanical and Aerospace Engineering in partial fullfilment of the requirements for the degree of DOCTOR OF PHILOSOPHY

SCHOOL OF MECHANICAL AND AEROSPACE ENGINEERING

Nanyang Technological University

2019

Statement of originality

I hereby certify that the work embodied in this thesis is the result of original research, is free of plagiarised materials, and has not been submitted for a higher degree to any other University or Institution.

Date : 7-March-2019 [Vigneashwara Pandiyan]

Supervisor declaration statement

I have reviewed the content and presentation style of this thesis and declare it is free of plagiarism and of sufficient grammatical clarity to be examined. To the best of my knowledge, the research and writing are those of the candidate except as acknowledged in the Author Attribution Statement. I confirm that the investigations were conducted in accord with the ethics policies and integrity standards of Nanyang Technological University and that the research data are presented honestly and without prejudice.

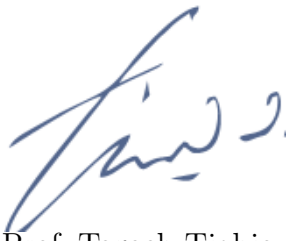

Date : 7-March-2019 [Assoc. Prof. Tegoeh Tjahjowidodo]

Author attribution statement

This thesis contains material from four papers published in the following peer-reviewed journal(s) / from papers accepted at conferences in which I am listed as an author.

Chapter 3 is published as Vigneashwara Pandiyan, Wahyu Caesarendra, Tegoeh Tjahjowidodo, and Gunasekaran Praveen. "Predictive modelling and analysis of process parameters on material removal characteristics in abrasive belt grinding process." Applied Sciences 7, no. 4 (2017): 363. doi.org/10.3390/app7040363

The contributions of the co-authors are as follows:

- Assoc/Prof Tegoeh provided the project direction and edited the manuscript drafts.
- All experimentation, including sample preparation, was conducted by me in the Rolls-Royce @ NTU Corp Lab.
- Gunasekaran Praveen assisted me during experimentation and in the measuring the depth of cut data.
- I prepared the manuscript drafts. The manuscript was revised by Dr Wahyu Caesarendra.

Chapter 6 is published as Vigneashwara Pandiyan, Wahyu Caesarendra, Tegoeh Tjahjowidodo, and Hock Hao Tan. "In-process tool condition monitoring in compliant abrasive belt grinding process using support vector machine and genetic algorithm." Journal of Manufacturing Processes 31(2018): 199-213. doi.org/10.1016/j.jmapro.2017.11.014

The contributions of the co-authors are as follows:

- Assoc/Prof Tegoeh provided the project direction and edited the manuscript drafts.
- All experimentation, including sample preparation, was conducted by me in the Rolls-Royce @ NTU Corp Lab.
- Hock Hao Tan assisted me during experimentation and in the preparation of belt tools with different cycle time.
- I prepared the manuscript drafts. The manuscript was revised by Dr Wahyu Caesarendra.

Chapter 7 is published as Vigneashwara Pandiyan and Tegoeh Tjahjowidodo. "In-process endpoint detection of weld seam removal in robotic abrasive belt grinding process." The International Journal of Advanced Manufacturing Technology 93, no. 5-8 (2017): 1699-1714. doi.org/10.1007/s00170-017-0646-x

The contributions of the co-authors are as follows:

- Assoc/Prof Tegoeh provided the project direction and edited the manuscript drafts.
- All experimentation, including sample preparation, was conducted by me in the Rolls-Royce @ NTU Corp Lab.

Chapter 7 is published as Vigneashwara Pandiyan, Pushparaja Murugan, Tegoeh Tjahjowidodo, Wahyu Caesarendra, Omey Mohan Manyar, and David Jin Hong Then. "In-process virtual verification of weld seam removal in robotic abrasive belt grinding process using deep learning." Robotics and Computer-Integrated Manufacturing 57 (2019): 477-487. doi.org/10.1016/j.rcim.2019.01.006

The contributions of the co-authors are as follows:

- Assoc/Prof Tegoeh provided the project direction and edited the manuscript drafts.
- All experimentation, including sample preparation, was conducted by me in the Rolls-Royce @ NTU Corp Lab.
- Pushparaja Murugan assisted me during experimentation and in measuring the weld seam depth.
- I prepared the manuscript drafts. The manuscript was revised by Dr Wahyu Caesarendra, Omey Mohan Manyar, and David Jin Hong Then.

Date : 7-March-2019 [Vigneashwara Pandiyan]

Abstract

Automation and self-monitoring implementation of manufacturing processes will support the development of interoperable ecosystem relevant to the Industry 4.0 concept. Among many industrial cases, abrasive belt grinding is a tertiary machining process used to achieve desired surface quality and to machine off features such as burrs and weld seams. Manufacturers are in the need of an ability to closely monitor and optimise the performance of abrasive belt grinding processes to meet tight tolerances.

The abrasive belt grinding process is highly nonlinear due to the complexity of the underlying physical mechanisms, some of which remain unknown. Existing research in the literature on in-situ tool wear prediction were primarily focused on hard tools, but limited effort can be found on that of compliant belt tools. Although many advanced machining cells are equipped with belt grinder and robotic manipulators for surface finishing, industries still rely on skilled operators to manually remove weld seams using belt sanders. Self monitoring of such a dynamic process in industrial robot cell environment is essential in having a fully automated system. This research aims to model the robotic abrasive belt grinding process in dry conditions appropriate for monitoring purposes.

The first part of this thesis discusses the influence of the process parameters on material removal and surface quality in abrasive belt grinding process. Interpretation of Taguchi's Design of Experiments (DoE) experimental results revealed that abrasive grain distribution on backing material has significant influence on material removal and surface quality. Subsequently, a systematic approach to mathematically model the belt grinding process using regression techniques based on soft computing is presented.

The second part of the thesis deals with real-time monitoring of the belt grinding tool life. Predicting belt tool life helps to determine whether it is under-utilised, overused or it is due for replacement. Unlike other rigid abrasive machining tools, in abrasive belts the grains are not regenerated. The influence of grain wear on material removal mechanisms namely cutting, ploughing and rubbing were investigated with single grit scratch tests and Acoustic Emission (AE) sensor reading analysis. Having understood the effect of abrasive grain wear on belt grinding performance, a methodology to virtually monitor the coated abrasive belt tool life in real time with the help of physical sensors and machine learning classifiers is developed.

In the last part of this thesis, an automated weld seam removal method is proposed. The method offers a real time endpoint verification system for weld seam removal using accelerometer, force and vision-based sensors along with machine learning and deep learning algorithms. Expectedly, this will reduce unnecessary costs and also increase the safety level of operators. In general, the proposed modelling and virtual metrology techniques will add values to the entire manufacturing process, in particular to those involving abrasive belt grinding, and will comply to Industry 4.0 objectives.

Acknowledgements

I would like to convey my sincere gratitude and appreciation to my professor Dr. Tegoeh Tjahjowidodo, for his invaluable suggestions, support, encouragement and unending support throughout this research work. I am proud and grateful to have the good fortune of his mentorship. The experience of working under his guidance helped me to develop as a person and an engineer. I am truly thankful to my project Managers Mr. Arthur Wee and Mr. David Jin Hong Then for their unflagging support throughout this research. I feel deeply honoured in expressing my sincere thanks to Rolls-Royce, Singapore for providing the resources available at the right time. I also convey my gratitude to Mr. Sudhan Raj, Mr. Mohammed Izzat and Mr. Omey Manyar for providing valuable insights. Special appreciation is extended to the Rolls-Royce @ NTU corp lab staff for their assistance and encouragement over the years both past and present, which made all of the endeavors here memorable and irreplaceable. I wish to thank Dr. Wahyu Caesarendra for allowing me to have time off in putting the finishing touches to my thesis and offering continued help. Thanks to all the other academic staff I may have missed out on their kind interactions that have also allowed me to get this far and triggered great levels of inspiration. I would like to thank Shanmuga Sundaram Durairaj, Adhithya Plato Sidharth, Vijay Santhanam and Shanmuga Sundaram Selvadurai for constant tea breaks, stimulating discussions, sleepless nights, indoor crickets and for all the fun we have had in the last four years.

I wish to thank all my friends at the Nanyang Technological University both past and present, their support and inspiration are second to none which makes it a pleasure to work with them. I wish to say thanks to all the Lab technicians who are so valued within the School of Mechanical and Aerospace at the Nanyang Technological University. I wish to thank my friends Dinesh Sathiyamoorthy, Javid Latif, Kalai Selvan, Venkatesan Annadurai, Kamal Raj, Wiselam Ashokan, Glinton dhas, Mahesh kumar Murali, Stephen Jayapaul, Sirajudeen, Thines kumar, Srikanth, Vignesh Gandhiram, Ramala Manohar Babu, Kamal Selvam, Riaz Ahamed, Siva Srinivasan, Pushparaja, Esther Jemi Sandiag and Manoj Manoharan for their kind words in difficult times and for their continued support. Special thanks to Sowmika Akka, Sujatha Akka, Senthalir Akka and Nivethitha Venkatesh, without them, I would not have made this far as what I am today.

Love to my parents for their support and encouragement which made my dream of higher studies a reality. I wish to thank my Amma, Selvamathy, my Appa, Solai raja Pandiyan, my Akka, Dr. Moogaambiga and my brother-in-law, Dr. Jayaraman for their kind words, love, and inspiration. Most importantly, none of this could have happened without my Aunt Mangayarkarasi and late Uncle Dr. Doraipandy for inspiring me even when I was a kid. I would like to express my very profound gratitude to my father-in-law Dr. Jawahar for having believed in me. Lastly, this list would be incomplete without my wife Mala who was always there through the process of writing this thesis providing me with unfailing support and continuous encouragement. Keeping the best for last, thank you is never sufficient to express my feelings to my grand father A.G.A. Ganapathy for his blessings. Honestly, I would say that these last four years were one of my best parts in my life.

List of publications

The following publications have been generated from this research work:

International Journals

- Vigneashwara Pandiyan, Pushparaja Murugan , Tegoeh Tjahjowidodo, Wahyu Caesarendra, Omey Mohan Manyar, David Jin Hong Then. In-Process Virtual Verification of Weld Seam Removal in Robotic Abrasive Belt Grinding Process Using Deep Learning, Robotics and Computer-Integrated Manufacturing 57 (2019): 477-487.

- Vigneashwara Pandiyan, Wahyu Caesarendra, Tegoeh Tjahjowidodo, Hock Hao Tan (2018). In-process tool condition monitoring in compliant abrasive belt grinding process using support vector machine and genetic algorithm, Journal of Manufacturing Processes 31 (2018): 199-213.

- Vigneashwara Pandiyan, Tegoeh Tjahjowidodo. In-process endpoint detection of weld seam removal in robotic abrasive belt grinding process. The International Journal of Advanced Manufacturing Technology, 93(5-8) (2017): 1699-1714.

- Vigneashwara Pandiyan, Wahyu Caesarendra, Tegoeh Tjahjowidodo, and Praveen Gunasekaran. Predictive Modelling and Analysis of Process Parameters on Material Removal Characteristics in Abrasive Belt Grinding Process. 7, no. 4 (2017): 363.

- Vigneashwara Pandiyan, Tegoeh Tjahjowidodo, Wahyu Caesarendra. Use of Acoustic Emissions to Detect Change in Material Removal Mechanism in Abrasive Belt Grinding Processes Caused by Tool Wear. Wear, 2019. [To be submitted]

- Vigneashwara Pandiyana, Tegoeh Tjahjowidodo, Wahyu Caesarendra, Omey Mohan Manyar, David Jin Hong Then. Regression Analysis in Modeling Material Removal for Abrasive Belt Grinding. The International Journal of Intelligent Manufacturing, 2019. [To be submitted]

International Paper Conferences

- Vigneashwara Pandiyan, Tegoeh Tjahjowidodo. In-Process Surface Roughness Estimation Model for Compliant Abrasive Belt Machining Process, Procedia CIRP, Volume 46, 2016, Pages 254-257, ISSN 2212-8271.

- Vigneashwara Pandiyan, Tegoeh Tjahjowidodo, Wahyu Caesarendra, Gunasekaran Praveen, Tomi Wijaya and Bobby Pappachan. Analysis of Contact Conditions based on Process Parameters in Abrasive Belt Grinding Using Dynamic Pressure Sensor. International Conference on Soft Computing and Intelligent Systems,2018.

List of Abbreviations and Acronyms

ANOVA	Analysis of Variance
DoE	Design of Experiments
RPM	Revolutions per Minute
FEM	Finite Element Method
MRR	Material Removal Rate
AE	Acoustic Emission
TCMS	Tool Wear Monitoring System
ANN	Artificial Neural Network
SVM	Support Vector Machine
HMM's	Hidden Markov Model
DT	Decision Trees
SVR	Support Vector Regression
STFT	Short-Time Fourier Transform
FFT	Fast Fourier Transform
S/N	Signal-to-Noise ratio
ANFIS	Adaptive Neuro-Fuzzy Inference System
RF	Random Forest
RMSE	Root Mean Squared Error
MSE	Mean Squared Error
PCA	Principal Component Analysis
VGG	Visual Graphics Group
2D	Two Dimensional
3D	Three Dimensional
CNN	Convolution Neural Networks
NN	Neural Networks
CCD	Charge-Coupled Device
SEM	Scanning Electron Microscope
RMS	Root Mean Square
PSD	Power Spectral Density
WT	Wavelet Transform
CWT	Continous Wavelet Transform

DWT	Discrete Wavelet Transform
kHz	Kilohertz
MHz	Megahertz
SSA	Singular Spectrum Analysis
ARMA	Auto-Regressive Moving Average
DFI	Dominant Feature Identification
MIG	Metal Inert Gas
PSI	Pound per Square Inch
BP	Back-Propagation
MISO	Multiple Input Single Output
OOB	Out-of-Bag data
DAQ	Data Acquisition
k-NN	K-Nearest Neighbours
Db4	Daubechies-4
RSSQ	Root Sum of Squares
FIS	Fuzzy Inference System
RBF	Radial Basis Function
IoU	Intersection over Union
DSLR	Digital Single Lens Reflex
EDCNN	Encoder-Decoder Convolutional Neural Networks

Nomenclature

F	Force
l	Length
C_A	Belt grinding constant
K_A	Resistance factor of the work coupon and grinding ability factor of the belt
k_t	Belt wear factor
V_b	Grinding rate
V_w	Feed-in rate
L_w	Machining width
F_A	Normal force
R_v	Relative velocity
F_n	Normal load
S	Sliding distance
K	Dimensionless constant
V_z	Wear volume
σ	Variance
ϵ_i	Residuals
β_0	Intercept
β_n	Slopes or coefficients
w_{ji}	Weights
η	Learning parameter
b	Bias
$\phi(x)$	Nonlinear mapping function
ξ_i	Slack variable
(C)	Box Constraint
P	Polishing pressure
σ	Standard deviation
R_a	Surface Roughness
J	Boundary of the elastic body
J_F	Area where the external forces are imposed
J_D	Fixed area that cannot be moved and deformed
J_c	Contact area

Contents

List of Tables

List of Figures

Chapter 1

Introduction

Robots are becoming widely implemented in the industry to reduce dependency on operators, while they also offer great performance for repetitive work at relatively lower costs. In machining and manufacturing industry, in particular, robotic assistance plays a vital and significant role. High level of accuracy and repeatability are among several advantages that industrial robots offer compared to manual labour. Repeatability of an industrial robot is defined as its ability to achieve consistent performance in performing repetitive tasks, while accuracy refers to the deviation between the targeted and obtained result [1]. In manual processes, accuracy and repeatability are typically restricted by human capability related to varying factors, e.g. fatigue, loss of concentration and personal skills. Given this, along with the requirements of high volumes of production of components requiring high levels of precision and accuracy in aerospace and automotive industries, industrial robots are the most efficient 'labourers' suitable for the job.

Nowadays, moving forwards, most industries strive towards optimizing the manufacturing processes through automation. Higher output and increased productivity have been two of the biggest reasons for justifying the use of automation. Automation systems can be leveraged by introducing a capability for self-monitoring of the production processes in real time. The capability to monitor the process inputs and outputs, in turns, will allow the system to compensate for any possible process faults to guarantee the output quality. The Figure 1.1 schematically illustrates how the process consistency will be maintained over time.

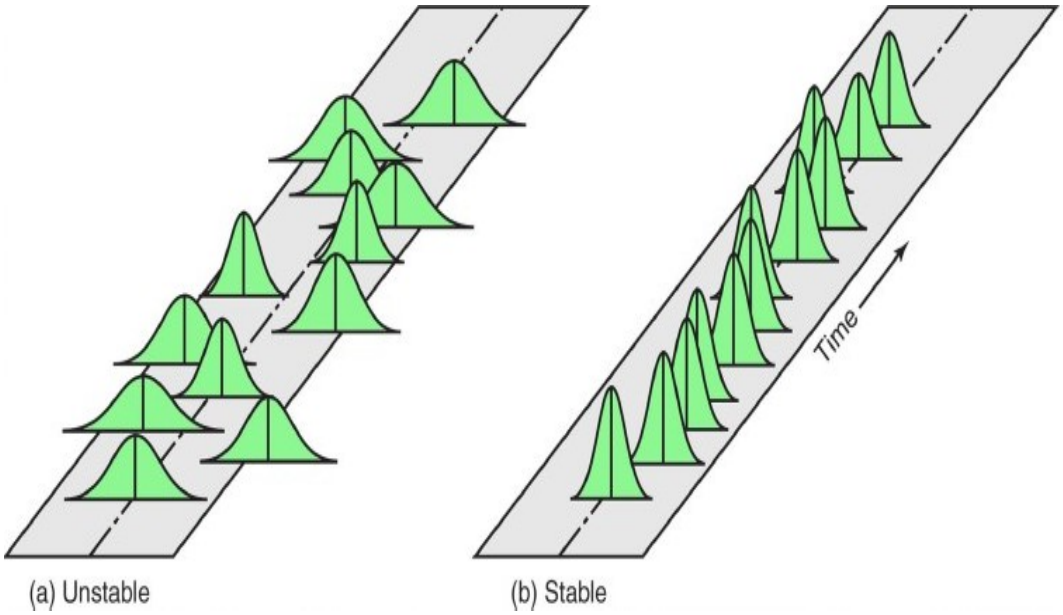

Figure 1.1: Comparison between stable and unstable process quality [2].

A simple monitoring using physical sensors will enable us to observe some phenomena in real time from the process. However, for highly complex processes involving non-linear patterns in the sensor data, the monitoring of the process states requires decision making methods, e.g. artificial intelligence techniques. This monitoring approach also opens its feasibility for prediction, detection, classification, regression, and forecasting purposes.

Integration of manufacturing processes with robots and enabling them with self monitoring and decision-making capabilities will help industries to redefine the manufacturing processes. Adoption of such automation strategies will enable them to move towards realization of Industry 4.0.

1.1 Abrasive surface finishing

All manufacturing processes involve the transformation of material from the initial geometry and property to the final outputs. The manufacturing processes are majorly classified into primary and secondary processes. The primary group comprises extrusion, casting, forming and forging, where the resulting components require a secondary operation to achieve their final shape [3]. Primary manufacturing processes are intended to give a basic property, shape, and size so that it can be further finished in the secondary manufacturing processes. In the latter processes, the re-

sulting components from the primary processes are machined to the required size, shape and tolerance targeting for the precision and accuracy as per design specifications.

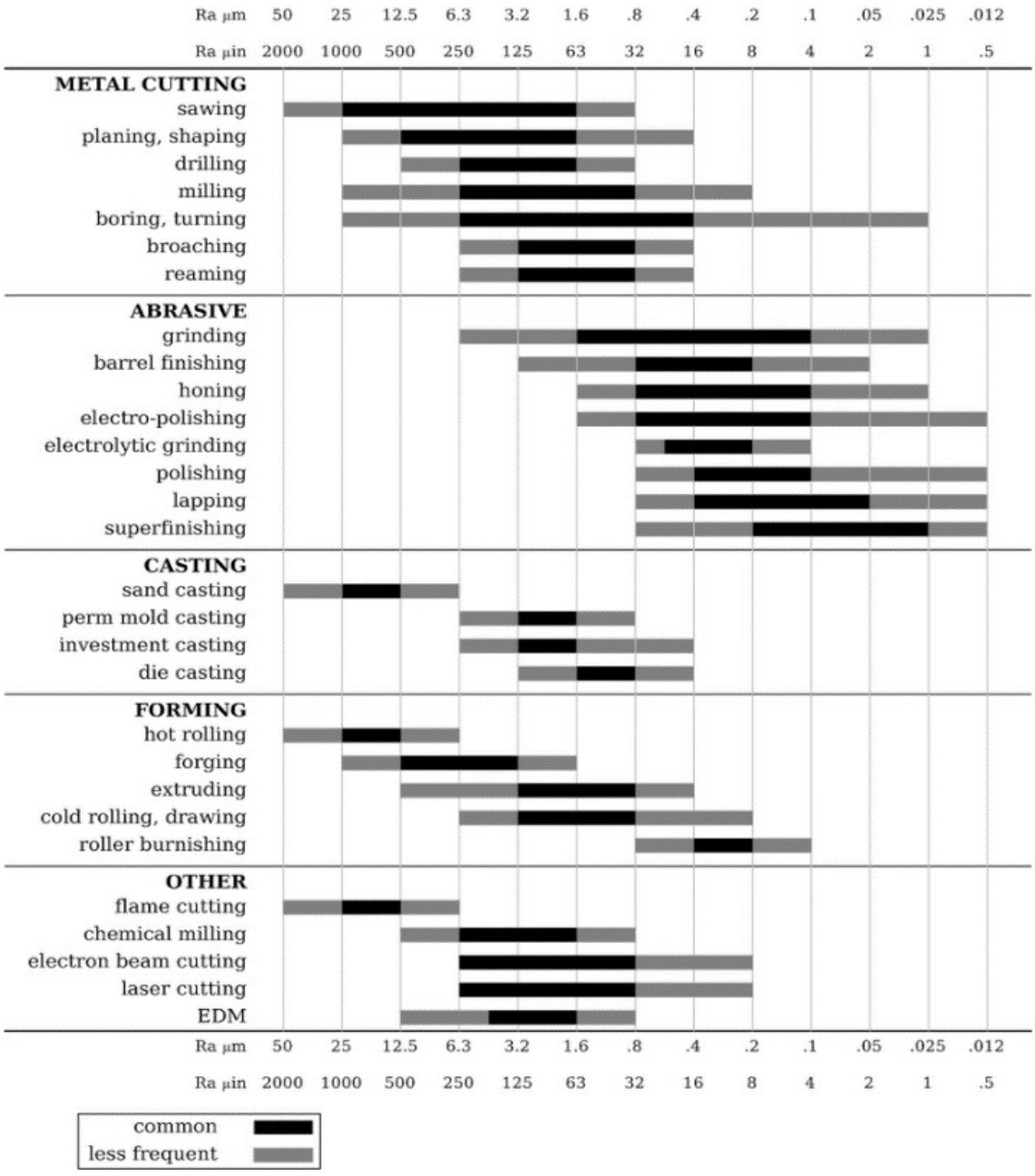

Figure 1.2: Surface quality that can be reached using different manufacturing methods [4].

Traditional secondary manufacturing processes include milling, turning, broaching, etc. Unconventional secondary manufacturing techniques, such as abrasive machining, are now on the rise as the traditional secondary manufacturing processes suffer from lower repeatability and lower accuracy.

Though abrasive machining processes are costly, it performs with higher tolerances and finer surface quality than other conventional machining processes. The Figure 1.2 illustrates the comparison of the range of accuracy achievable by abrasive machining to that of traditional secondary manufacturing techniques. The process of abrasive machining works similar to other traditional machining as the abrasive grain is a form of cutting tool. The difference is that the grains are of small geometry and are randomly distributed with different orientation.

Unconventional machining technique has multiple benefits [5] over the traditional ones. As the tool radius of a traditional tool is typically larger than that of an unconventional tool in order of microns, traditional machining process will generate higher internal stress and heat affected zone. Furthermore, the likelihood for the traditional machining tools to encounter a void or micro level defect is very high as metals are non-homogenous at micro level. This creates microcracks that propagate to the next void giving rise to a discontinuity in chip formation and uneven surface.

In abrasive micromachining, material removal occurs due to the interaction of randomly oriented multipoint grain edges and the workpiece material. An abrasive particle is typically made from a mineral, where the finishing process is achieved through scratching mechanism, which results in a fraction of removed workpiece. As the abrasive grain has a negative rake angle of different values and orientation, the tooltips are referred to as undefined cutting edges. Due to undefined tooltips and negative rake angle the specific energy is very high at the machining point. The abrasive machining process is a track-bound undefined tool engagement, where the forefront of the grain penetrates the workpiece along a pathway and, after a phase of elastic deformation, plastic flow of the workpiece material occurs.

All abrasive machining processes are intended to generate surfaces for defined tolerance as per design quality [6, 7]. Based on the interaction of the cutting edges and workpiece surface, abrasive interaction is classified into two body interaction and three body interaction [8]. The two-body abrasive cutting tool is made up of matrix material on which the abrasive particles are embedded. The matrix materials can be resin, paper, cloth, rubber. Three body interaction is also known as free or loose abrasive interactions. As the name suggests, the abrasives are free and not bound within a matrix. The process could be with or without the lubrication.

The abrasives could be dry or in the form of a slurry. These abrasive grains move freely over the machining surface. Figure 1.3 shows the bonded and free abrasives interacting with workpieces.

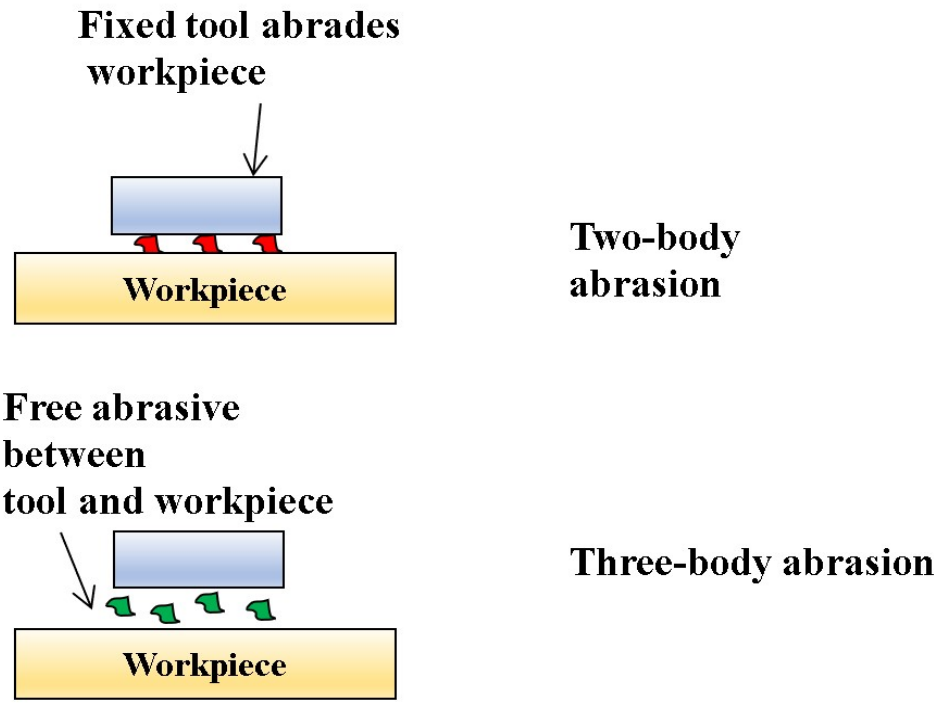

Figure 1.3: Illustration of two-body and three-body abrasive interaction.

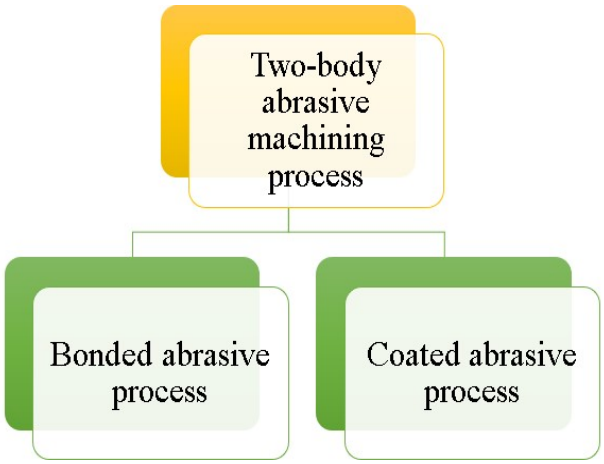

Figure 1.4: Classification of two-body abrasive interaction.

From an energy point of view, three body interaction is a less efficient process since each collision leads to energy dissipation whereas in two body interaction energy is completely transferred. However, as the new cutting edges are present during the process, the surface quality increases at a high rate. Two body interaction

can cut much more in-depth than three body abrasion because the grains are held rigidly.

Two-body abrasive machining process can be further classified into two categories such as bonded abrasive and coated abrasive process as shown in Figure 1.4. Bonded abrasives are mixtures of grains, fillers, and adhesive bonds. In bonded abrasives, the grain particles are bind together within a matrix, and their combined shape determines the geometry of the finished workpiece. Common processes involving bonded abrasive are grinding, honing, buffing, super finishing and abrasive sawing [9]. Coated abrasive is characterized by three main properties, namely grain particles, adhesives, and backing. The particle grains are bind by adhesive films onto the backing material such as cloths, paper, and fiber. Coated compliant abrasive tools in the form of a disk, flap wheel and belt are widely used in industries for tertiary finishing operations as shown in Figure 1.5. Typical processes in coated abrasive processes are bench grinders, die grinders and belt sanders [9].

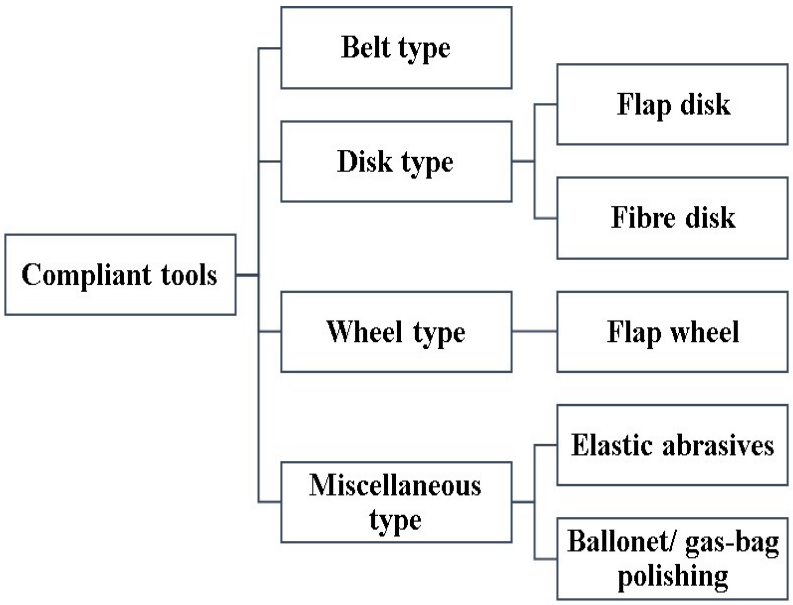

Figure 1.5: Types of compliant tools [10].

An advantage of coated abrasives over other types of abrasive cutting tools is attributed to its compliance as it conforms to the shape of the workpiece surface regardless of complexities, giving rise to higher quality surface finishes as illustrated in Figure 1.6. Being compliant means that the machining tool will always adhere and take the shape of the desired manufactured product. In this thesis, we adopt 'belt type' compliant tool as the subject of our study.

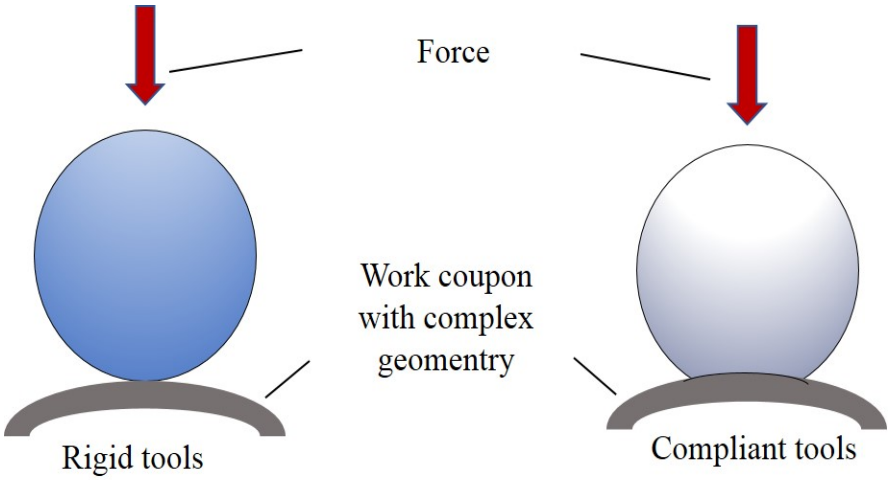

Figure 1.6: Comparison of contact characteristics of rigid and compliant tools.

1.2 Abrasive belt grinding process

Abrasive belt grinding is a two-body abrasive compliant machining process used to improve the surface quality of components. Abrasive belt grinding is a modification of the traditional grinding processes such that the outer layer of the contact wheel is made of soft materials. Unlike rigid abrasive wheels, the abrasives belts are not bonded to the matrix structure rather is coated over a flexible system as shown in Figure 1.7. The flexible system ranges from paper, cloth, synthetic resin.

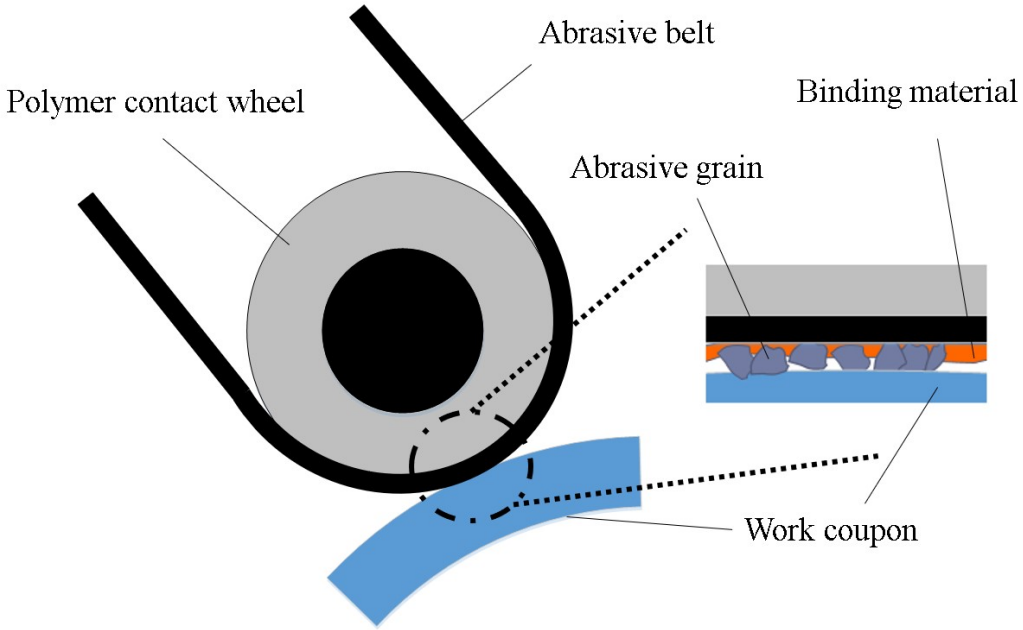

Figure 1.7: Principle of belt grinding process [11, 12].

The abrasive belt grinder is made up of coated abrasives and is fastened around at least two rotating rubber contact wheels [13]. The abrasive belt grinding process is a form-adaptive machining technique; this is due to the inherent hyperelastic property of polymer rubber contact wheels. Flexibility arises from the shape adaptive characteristics of the backing material [14]. The form adaptive characteristics make the abrasive belt to act as a compliant tool. Compliant belt grinding resembles the elastic grinding and has potentials of milling, grinding and polishing [15]. Coated abrasive belts use the same working speed range as bonded wheels and have no performance lagging to that of wheel grinding. The belt grinding has an elastic contact roller wheel made up of thermosetting polyurethane elastomer which can be deformed to assist the coated abrasive belt that functions as cutting edge as shown in Figure 1.8.

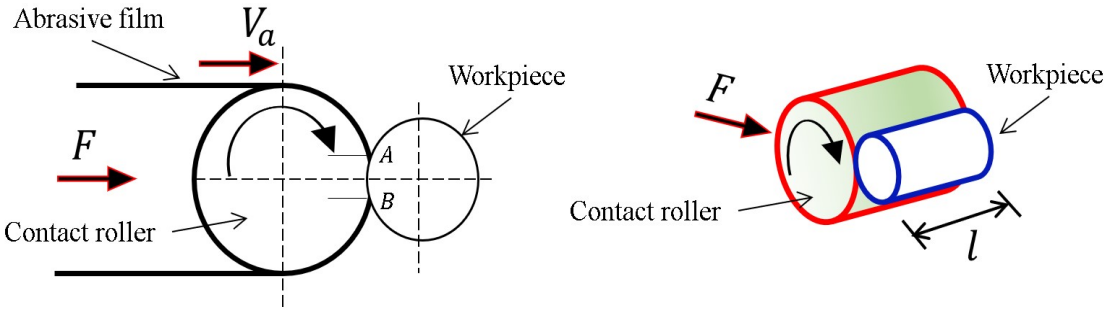

Figure 1.8: Elastic deformation of the contact area [16].

As indicated in the figure, l is the length of the contact area sandwiched between the work piece and the belt surface. The width of this area l varies on the force F applied on the work coupon and on the Young's modulus of the contacting elastic wheel is interrelated to the shore A stiffness of the material. The soft contact rubber wheel enables this machining process, which is very appropriate to manufacture free-form surfaces due to its capability to adapt to the work piece surface [11]. The materials are machined off under non-permanent compliant touches between the work piece and the abrasive belt. Belt grinding has been widely used in manufacturing industries, especially where machining of complex geometries is involved, for example, turbine blades in the aerospace industry as shown in Figure 1.9.

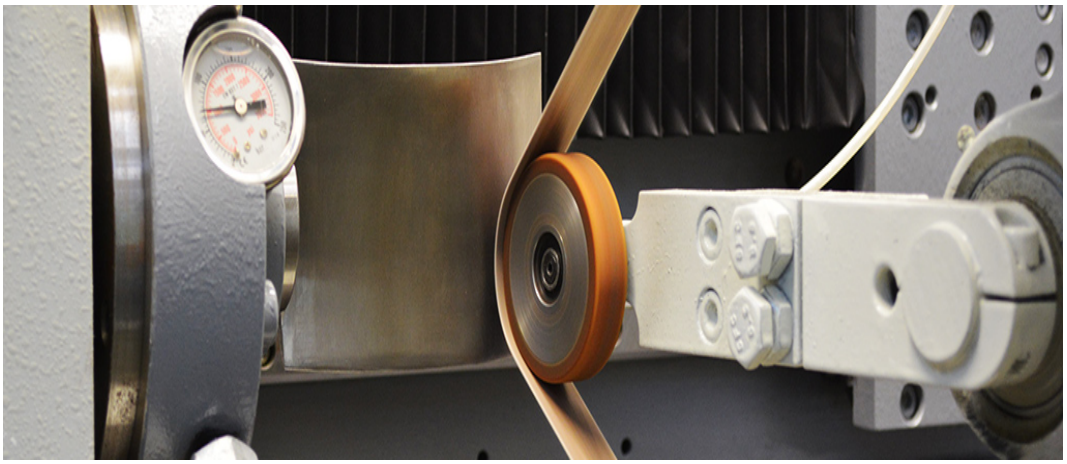

Figure 1.9: Example of belt grinding of a turbine blade [17].

One of the common applications in industries, where complaint tooling are used, is tertiary finishing and localised error correction. Abrasive belts are mainly used for light stock removal and polishing operations, and recently are being increasingly employed for heavier stock removal [18]. Coated abrasive belt grinding is different from traditional machining. The difference is in the way of chip production, the order of specific cutting pressure faced and surface integrity of machined components. Like any other abrasive machining, there are many grinding parameters influencing the final ground surface quality, along with the grinding belt topography features. The grinding parameters include belt speed, infeed rate, workpiece geometry and belt preloaded tension, while belt topography features include the information such as grit size, grain distance, and wear rate [16]. Many aspects of interactions between cutting tool, workpiece, and material removal during compliant belt grinding are not fully understood due to high nonlinearity of the process. The manufacturing industries that involve abrasive belt grinding process still heavily rely on operators knowledge and experience [19].

1.2.1 Advantages of abrasive belt grinding process

Apart from the ability of the belt grinding to produce high material removal rates, and conforming to workpiece geometries there exist other advantages that are listed below.

- Versatility is the major advantage, since machines can be quickly converted from heavy stock removal to finishing operations, or for grinding various mate-

rials or parts, by simply changing the belts, and contact wheels. Furthermore, the process can be carried out in dry and wet conditions without bringing any major changes to the setup.

- Truing and balancing are costly setup operations which are eliminated in robotic abrasive belt grinding process [20].
- Owing to its large working area, the heat generated in abrasive belt grinding process is very less compared to that in abrasive wheels. There is no requirement of a coolant system as the grinding belts with typical length of 2 to 5 m are able to cool down during the return strokes on the process [21].
- Abrasive belt grinding system is safe to operate as they produce low noise and the heat accumulation during the grinding is small [22].

1.2.2 Robot-assisted belt grinding process

The robot-assisted belt grinding process is gaining popularity in industries, that move towards automation of manufacturing process. Integration of the belt grinder setup on the robot helps in easing the axis of motion and also ensures that the force applied and repeatability are maintained [16, 23]. It further secures the safety of the workforce.

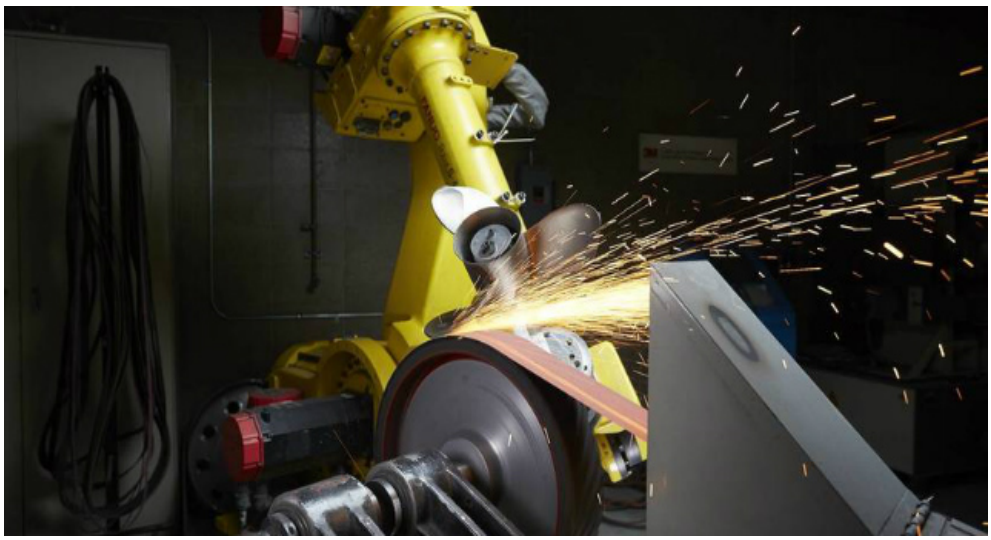

Figure 1.10: Robotic arm holds the components and presses against the static grinding wheel setup [24].

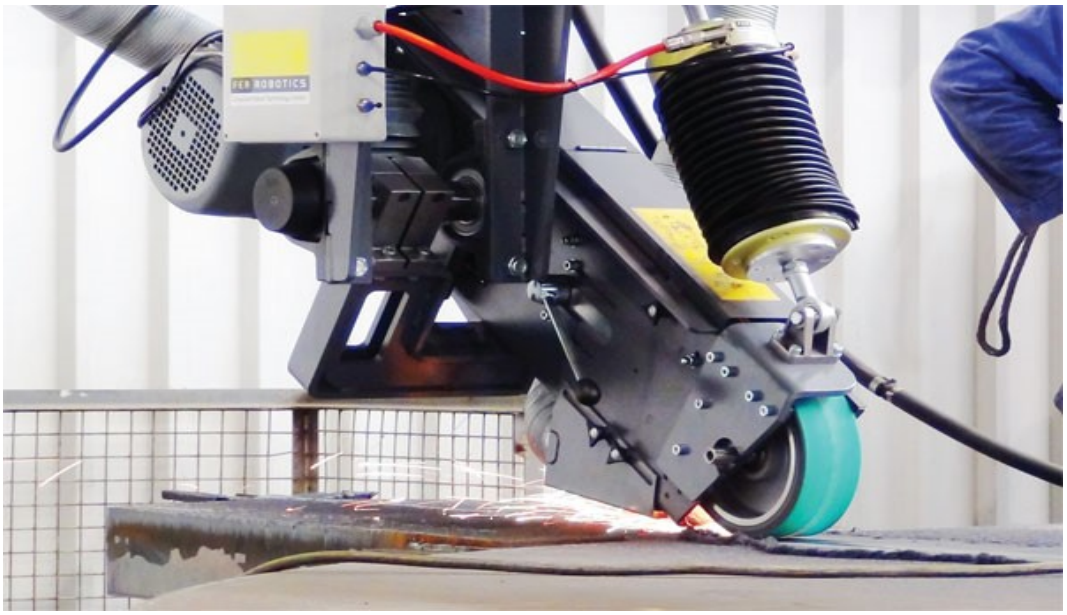

Figure 1.11: Robotic arm holds the abrasive belt machine and presses against the stationary target (components) [25].

There are two variants of robotic-assisted belt grinding process based on the application prevalent in industries. The first variant has the robotic arm holding the component, and arm movement adapt a specific path wherein the part is machined as shown in Figure 1.10. Less complex shapes where the part is small to medium, in size are machined using this method with its belt grinding setup is kept stationary. In the second variant, the robotic arm holds the grinding tool and tool is made to press against the component in a predefined path as illustrated in Figure 1.11. Heavy complex components and free-form surfaces are machined using this method. In both cases, the path to be followed needs to be taught and must be programmed accordingly.

1.3 Motivation and background

The surface finishing and stock removal of complicated geometries is the principal objective for grinding with compliant abrasive tools. To understand and achieve optimum material removal in a tertiary finishing process, such as abrasive belt grinding, it is essential to look in more detail at the process parameters/variables that affect the stock removal rate. Though belt grinding is remarkably straightforward and inexpensive, nitty-gritties of the process are not well-grasped and reported in

the literature. Manufacturing industries that involve abrasive belt grinding process still choose the parameters based on empirical rules.

Developing analytical models for such a nonlinear process with various parameters and assumptions may introduce a lot of randomnesses and will not be a viable option to model the process. A systematic approach to quantify the material removal and to achieve the desired stock removal using modelling techniques has to be established.

Tool life is a significant criterion in coated abrasive machining since deterioration of abrasive grains increases the surface irregularity and adversely affects the finishing quality. The life cycle of a coated abrasive belt tool vitiates due to continuing grain wear resulting to tool failure. As the abrasive belt tool approaches the end of its life, the degradation in the surface quality of the machined workpiece is apparent. Unlike other abrasive machining processes the grains are not regenerated. The pre-planned tool replacement methodologies are no longer suitable in belt grinding process as the machining conditions vary extensively. As tool grain wear has a direct influence on the uniform material removal, monitoring such coated abrasive tool condition in real time helps in quality control of surface in finished components.

Though surface finishing is done using belt grinders with robot manipulators in highly sophisticated machining cell, the industry still depends primarily on skilled operators in removing weld seam using belt sanders manually. Current industrial practice in removing weld seam involve a manual belt grinder, either pneumatic or electric, where flat spots are created in and around neighbouring surfaces of the weld and finally removed by the operator. Such a process is laborious and also unsafe as the operator has to appropriately define the grinding paths for free-form workpieces during the weld seam removal process. Moreover, manual belt grinding process is also time consumptive as the part has to be taken from robot cell to the manual machining station and vice versa.

1.4 Objective, approach and scope

Overall objective of thesis is to model and monitor abrasive belt grinding process. A reliable process model and in-situ monitoring system will transform manufacturing

environment from manually operated production machines to unsupervised robotic machining centre's. This is significant in a manufacturing domain to realise Industry 4.0 implementation.

The belt grinding process is highly nonlinear, and in industries still based on empirical rules and operator experience. A systematic approach to quantification on such dynamic process is not reported previously. Firstly, this thesis studies the magnitude of relationship between various process parameters on material removal and surface quality using Taguchi's Design of Experiment (DoE).

Secondly, the thesis attempts to mathematically model the process using soft computing regression techniques to determine material removal. The material removal data are acquired from Taguchi's Design of Experiment (DoE).

In abrasive machining, it is known that there are three material removal modes, namely cutting, ploughing and rubbing. This thesis aims to investigate how material removal modes change with respect to tool wear by analysing frequency components of the data acquired from Acoustic Emission (AE) sensor using single grit scratch tribometer experiments. The adequate knowledge developed from scratch experiments, is used to develop an in-process tool wear prediction system based on machine learning classifier and sensor data. This is the third objective of this thesis.

The final objective of the thesis is to close the gap in automating belt grinding process to precisely estimate the endpoints during weld seam removal. A real time endpoint prediction system for weld seam removal during abrasive belt grinding is developed with the help of accelerometer, force, and vision sensors using machine learning classifiers and deep learning algorithms.

1.4.1 Scope

The scope of the research work to model and monitor robotic abrasive belt grinding process is listed below.

- All the experimental trials are performed in dry condition on aluminium and mild steel work pieces.
- All the experiments are done using a variable speed electrical belt grinder mounted to the end effector of the robot using a suitable fixture. The belt

grinder is always pressed against the stationary work piece by the robot.

- The tool paths are always performed normally to the surface of the work piece and force control resolution achieved is based on the operating range of the ATI Omega force sensor.

1.5 Report organization

This thesis is organized into eight chapters. Chapter 1 is the present chapter, which provides background information of this study, an overview on the abrasive belt grinding process, the motivation of the research, objectives of the research and the organization of this report.

Chapter 2 presents a comprehensive review on the compliant tools, belt grinding parameters and previous research work on modelling of the abrasive machining process. The chapter then discusses the various modes of material removal mechanism involved during abrasive processes. The chapter also explains the previous works in sensing techniques, provides a review of sensor selection, dominant frequency components and signal processing methods. The chapter outlines the past research works on monitoring techniques for machining in real time and decision mechanisms such as machining classifier. The last section of this chapter gives an overview the recent trends in machine vision and deep learning. The goal of the review is to understand the previous research effort in this domain and to bridge this gap in real-time monitoring of compliant tools.

Chapter 3 and 4 deals with the modelling of the abrasive belt grinding process. Chapter 3 figures out the dominant belt grinding parameter influencing material removal and surface quality. It starts with discussing the customised belt grinding tool setup, tool path planning, Taguchi based DoE and finally the method to measure the depth of cut and surface roughness using profilometer. The chapter presents the prominence of factors and their interaction using ANOVA on material removal and surface quality. The chapter also shows the influence of the process parameters in real time on contact conditions using dynamic pressure sensor setup. Chapter 4 discusses the development of predictive regression modelling techniques to model material removal in detail. The chapter also discusses on validation of

model accuracy and draws a comparison on the different regression techniques used.

Chapter 5 is the opening chapter in understanding the effect of the tool wear on material removal mechanism. The chapter discusses in detail on how the material removal modes changes with respect to abrasive grain wear using single grit tribometer scratching experiments. The last part of this chapter 5 presents the existence of these dominant frequencies in actual belt grinding and how they can be used to predict tool state.

Chapter 6 and 7 deals with the monitoring of the abrasive belt grinding process. Having the knowledge of tool wear on material removal mechanism the effect of tool wear on material removal and surface quality is established initially in chapter 6. Chapter 6 proposes a methodology based on classification for in-process tool wear prediction. This chapter also introduces the methods applied to extract features from time and frequency domain from the data acquired from physical sensors, optimization of the feature space and finally the performance of the different machine learning classifiers.

Chapter 7 initially proposes a methodology based on wavelet transform for in-process weld seam detection using physical sensors. In the last section of chapter 7 a novel methodology to determine the end point of weld seam removal using visual inspection system and deep learning segmentation algorithm is presented. The chapter also compares both methods developed.

Finally, chapter 8 draws some appropriate general conclusions, contributions and proposes recommendations for the future work.

Chapter 2

Literature review

2.1 Parameter analysis and modelling

Compliant belt grinding corresponds to elastic grinding and has the capabilities of grinding, milling, and polishing [15]. In fact, about 33% of the rigid abrasive grinding processes have changed to belt grinding [26]. The belt grinding process has characteristics of good workpiece-shape adaptability with uniform material removal, low grinding temperature, maintenance of residual compressive stresses, and resistance to workpiece burning. The soft contact rubber wheel enables this machining process to manufacture free-form surfaces due to its capability to adapt to the workpiece surface. Figure 2.1 illustrates the grinding process relationship between the contact wheel and the workpiece.

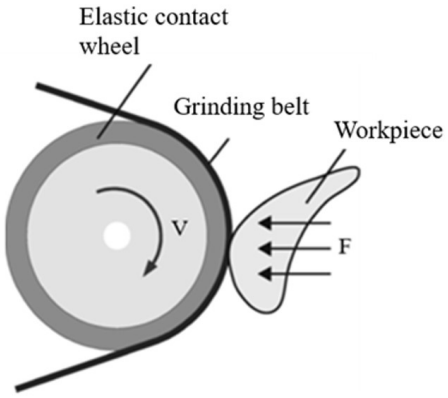

Figure 2.1: Sketch of a typical belt surface grinding system [5].

The elastic contact wheel enables the grinding process to machine many form features due to its capability to absorb shock and adapt to the workpiece surface [27–

29]. The application and scope for coated abrasive machining is not only for precision machining and finishing but also widely used in roughing. The belt grinding process can quickly generate surfaces with high levels of precision and smoothness.

Table 2.1: Parameters affecting abrasive belt grinding performance.

Parameters	Types
Belt	tension, backing material, abrasive type, grit size, grain removal rate
Test Coupon	initial surface roughness, the surface topography of the material
Wheel	width of the contact wheel, the topography of the wheel, the hardness of the wheel
Other Parameters	speed (RPM), force applied

Since the polymer contact wheel rotates exactly like the grinding wheel and they do not wear out, it is possible for abrasive belt grinding to achieve a constant cutting speed, which is a prerequisite for automated grinding. Analogous to other abrasive machining processes, many process parameters in the belt grinding impact the material removal performance, which include cutting speed, loading belt tension, the force imparted, infeed rate, workpiece topographies, polymer wheel hardness, wheel geometry and belt topography features, e.g. backing material, grain composition, and grit size [16].

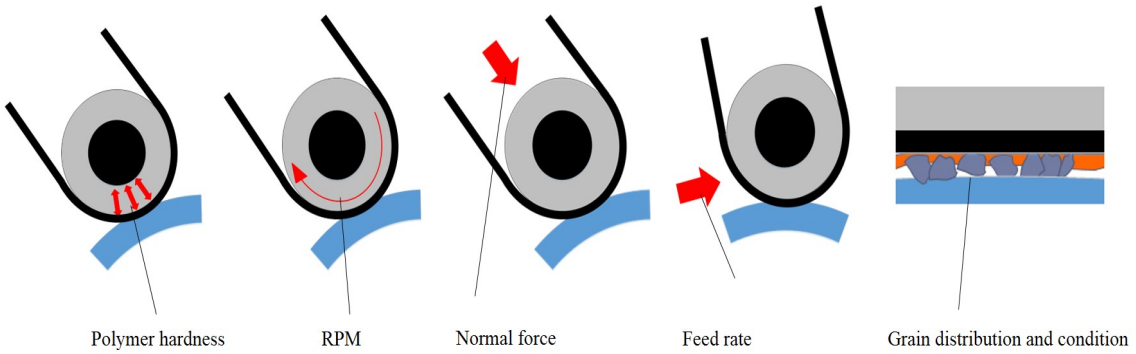

Figure 2.2: Parameters affecting the belt grinding performance.

Abrasive machining parameter study mostly is determined by the process objectives such as surface finish, stock removal (heavy or light stock removal), time-saving, and the efficiency of the cutting tools [30]. There are many parameters to look into

for operating the belt grinding to its full usefulness. However, the most critical parameters are shown in Table 2.1 and illustrated in Figure 2.2.

Though the removal of material in the belt grinding process from the workpiece surface can be written as a function of several parameters, their influence and interaction have not been reported in literature and that will be covered and bridged in this thesis. Changing any of these parameters will cause a resultant shift in the belt grinding performance. However, the degree of the effect will vary from parameter to parameter [31]. The material removal intensifies when the number of the interactions of the abrasive grains per unit time increases [32]. Therefore, it is evident that material removal is directly proportional to the cutting speed (grinding rate) of the polymer contact wheel on the belt grinder. However, the higher the speed, the lower the stability due to vibration. Thus this vibration effect will influence the surface quality [33].

The depth of penetration depends on the topography and the geometry of the belt/wheel surfaces which serves as an undefined cutting-edge. Coarser grain sizes exhibit a greater ability to achieve higher cutting depth, which results in higher material removal than finer sizes. Furthermore, coarse-grained abrasive belts increase the material removal rate by its ability to cut thicker than finer-grained abrasive belts. Finer-grained abrasive belts are mostly used for polishing and finishing to achieve a smooth surface. Grit refers merely to the size of the abrasive grains present in a belt. Varying grit sizes give abrasive belts varying degrees of durability and machining capacity [34].

In general, higher material removal is possible by having higher speed and contact pressure. Material removal increases with a higher dwell time of interaction between the cutting grain edges and workpiece surface, i.e., material removal, is inversely proportional to the feed-in rate [32]. The slower feed rate leads to more significant material removal because of longer dwell time but increases the surface roughness. Meanwhile, higher feed rate leads to diminishing surface roughness thus increasing the smoothness of the workpiece [33].

Adequate force is required for the cutting edge to penetrate deeply into the workpiece to achieve grain cutting depth resulting in material removal. The penetration depth of the grains into the work coupon surface predominantly depends on

the force imparted for grinding [32]. Belt finishing with contact wheels of different hardnesses results in dynamic changes in contact pressure, leading to a change in the mechanism of material removal. Force needs to be uniformly distributed to remove material uniformly.

The material removal rate, the surface quality, and the tool life rely mainly on the design of the contact wheel [21]. The serrated belt grinder wheel is very beneficial compared to the plain wheel in belt grinding. The serrated wheel provides faster cut and thus gives longer belt life. The serration allows the belt to cool in between the gaps [35]. Changing the serration of the rubber backing can make significant changes in the wide belt grinding results [18]. The selection of the contact wheel and abrasive to match the grinding parameters required for a specific operation is very critical.

Selection of working parameters depend on the final requirement such as fine or rough finish as both are adopted widely in industries. Stock removal commonly requires a harder polymer contact wheel, coarse abrasive grains, greater force, reduced feed, and better cutting speed. Finishing requires the use of a softer contact wheel and fine grade abrasive grains.

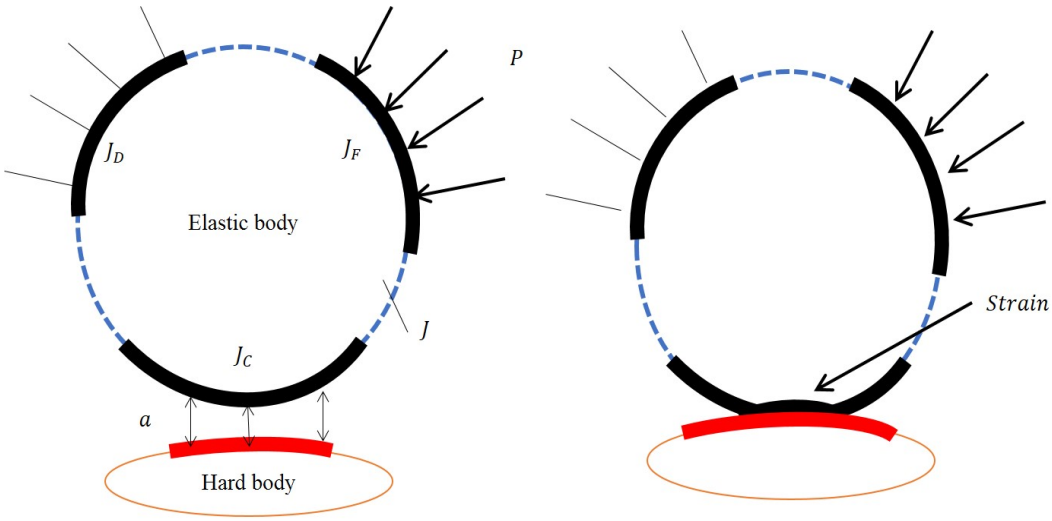

Figure 2.3: Signorini contact problem [11].

Table 2.2: Research efforts in modelling of belt grinding process.

Investigators	Contribution
Y. Wang *et al.* [36]	Developed a controllable material removal strategy to control the acting force and grinding dwell time by modelling global and local material removal process of belt grinding. A finite element method (FEM) was adopted to calculate the local force and global grinding model based on the Hertz contact theory.
X. Zhang *et al.* [11,37]	Formed a local grinding model based on support vector regression (SVR) and neural network to get the force distribution faster than conventional FEM in the contact area between the workpiece and the elastic contact wheel.
X. Ren *et al.* [38]	Created a local process model based on localisation algorithm simulation to calculate the material removal before machining enabling to optimise the tool path planning.
X. Ren *et al.* [39]	Established a simulation system using $Surfel$ to visualise the material removal process interactively and to optimise the tool path planning.
X. Ren *et al.* [16]	Presented a local process model to estimate the material removal rate in robotic belt grinding by calculating the force acting from the information on the local geometry of the workpiece.
S. Wu *et al.* [40]	Presented a comprehensive platform to simulate belt grinding system incorporating a kinematic model of the robot for tool path planning, dynamic model of the robot joint, along with the material removal model of the grinding process.
Jourani *et al.* [41].	Developed a three-dimensional numerical model, which could determine pressure distribution and distribution of real contact of the abrasive grain. The study proved that real contact areas strongly depends on the attack angle distribution of the abrasive.
Mezgahani *et al.* [42]	Performed a comparative study of contact pressure and abrasive grit size to material removal keeping parameters such as speed of workpiece, tool hardness, cycle time, coolant, abrasive feed, and tool wear constant. The study showed that decrease in grain size results in more ploughing action rather than cutting action.
J. Shibata *et al.* [43]	Offered a material removal model incorporating the belt wear factor to explain the belt grinding characteristics quantitatively.
Khellouki *et al.* [12]	Theoretically modelled contact conditions between abrasive film and the surface and investigated the effect of average contact pressure, contact duration and the number of active grains in the contact.
V.T. Thien *et al.* [44] and Y. Sun *et al.* [45]	Demonstrated that pressure distribution obtained from pressure films can be correlated with Hertzian model under different loads and hardness of the polymer wheel.
H. Lv *et al.* [46]	Presented a material removal modelling technique for free-form surface using eco sate network.
W. Wang *et al.* [47]	Proposed a grinding depth predicting frame working using local stress model and a local material removal model taking into account the contact wheel deformation.
Y. Sun *et al.* [48]	Proposed a novel methodology using a dynamic pressure sensor to predict material removal considering belt grinding parameters such as force, workpiece geometry and different types of contact wheel geometry.
Y.J. Wang *et al.* [49]	Demonstrated that nonlinear material model performs better than the linear material removal model.

Belt grinding depends on the operator's skill and knowledge, resulting in poor consistency and reproducibility. There are numerous process variables in belt grinding process and their combined effect is still not well understood. The amount of material removed from the workpiece surface results from the distinct local contact conditions, which are completely influenced by the process parameters/variables. Material removal in the belt grinding process is determined by the force distribution in the contact area between the workpiece and the elastic contact [11]. The contact between an elastic polymer wheel and a rigid work coupon has been regarded as a Signorini contact problem as shown in the Figure 2.3 and solved with the help of the FEM [11].

Table 2.2 lists the previous research effort performed so far on abrasive belt grinding to predict material removal and model the contact conditions. Hamann [50] had proposed a simple linear mathematical material removal model which involves C_A (constant of the grinding process), K_A (combination constant of resistance factor of the work coupon and grinding ability factor of the belt), k_t (belt wear factor), V_b (grinding rate), V_w (feed-in rate), L_w (machining width), and F_A (normal force). The model states that the overall material removal rate (MRR) r is either proportional or inversely proportional to belt grinding parameters such as shown in equation (2.1). However, this model has its limitation as it does not take into account the interaction between belt grinding parameters.

$$r = C_A.K_A.k_t.\frac{V_b}{V_w L_w}.F_A \tag{2.1}$$

Preston's fundamental polishing equation as shown in equation (2.2) states that material removal rate, $\frac{dR}{dt}$ of belt grinding process has a direct relationship with relative velocity R_v and polishing pressure P [51, 52]. A constant C established to denote other influential parameters is determined experimentally for each polishing system.

$$\frac{dR}{dt} = CPR_v \tag{2.2}$$

Archard's wear based on equation (2.3) predicts wear volume V_z to be a function of normal load F_n, sliding distance S and hardness of the softest contacting surface

H. K is a dimensionless constant [48].

$$V_z = \frac{KFnS}{H} \tag{2.3}$$

Although the equations from Preston, Archard, and Hammann give a holistic view on the relationship between material removal rate and the few process parameters, the dimensionless constant in each equation (C_A, K and C) needs to be determined after many exhaustive physical or simulation experimentations. Developing analytical models for such a nonlinear process with large parameter and assumptions may introduce many uncertainties and will not be a viable option to model the process. An overall process model of material removal incorporating belt grinding parameters without any assumptions with regression techniques in such a dynamic process has not yet been studied. A systematic approach to mathematically model material removal using regression techniques will be reported in this thesis.

2.2 Material removal modes in abrasive machining

In abrasive micro-machining, material removal occurs due to the interaction of randomly oriented multipoint cutting edges and the surface of workpiece material. Each abrasive particle removes a tiny bit of material when the abrasive machining forces its grains onto the surface of the workpiece.

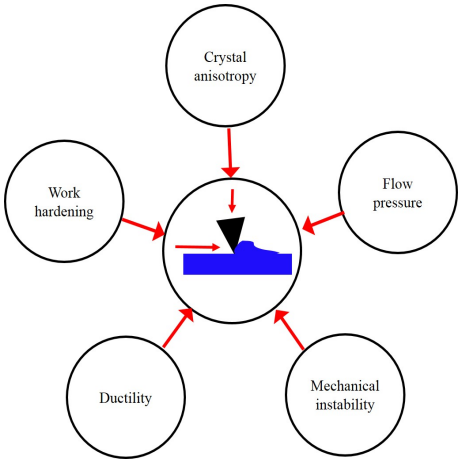

Figure 2.4: Properties of materials that influence abrasive grain interaction.

The material removal performance of the abrasive grains is influenced greatly by the material property as shown in Figure 2.4. The contact area of the grain on the surface is determined by the hardness property of the material [53]. K. H. Zum Gahr [54] studied the interaction between the abrasive particle and workpiece material. The study revealed that abrasive machining exhibits different types of material removal mechanism as shown in the Figure 2.5.

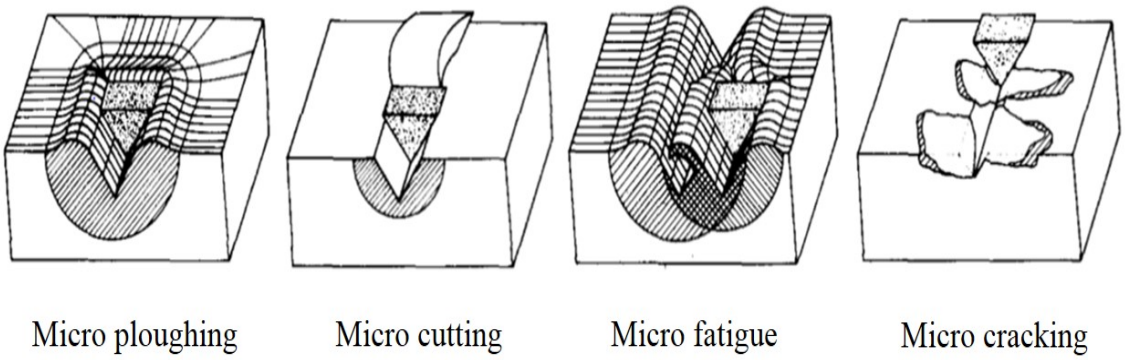

Figure 2.5: Surface wears generated from abrasive machining processes [54].

Based on the surface wear the material removal mechanism can be categorized into microploughing, microcutting, microcracking and microfatigue. Microploughing results in displacement of the material unlike microcutting where the material is detached from the surface. Microfatigue is the removal of material from the surface due to cyclic displacement as result of microploughing. Microcracking is a phenomenon of material removal where the material is detached by propagation of cracks and stress concentration. Microcutting is the dominant processes on ductile materials while microcracking is predominant in brittle materials.

Many events occur in the interaction zone of the grain and workcoupon. Out of the various events occurring in the interaction zone only three events namely rubbing, ploughing and cutting, that are significantly responsible for the modification of the surface, i.e., material removal or surface wear in abrasive machining process [55–57]. Rubbing is typically characterised by the interaction between both the abrasive grain and the material without any plastic deformation on the surface. Ploughing is often considered to have negligible wear on the surface as it creates continuous groove with ridges on both sides resulting in dislocation rather than removal due to plastic deformation. Cutting is the actual material removal process as the cutting tool tip with sufficient force enters deeply into the workpiece causing

chip formation. The cutting and ploughing phenomena from single-point scratch tests is represented in the Figure 2.6 .

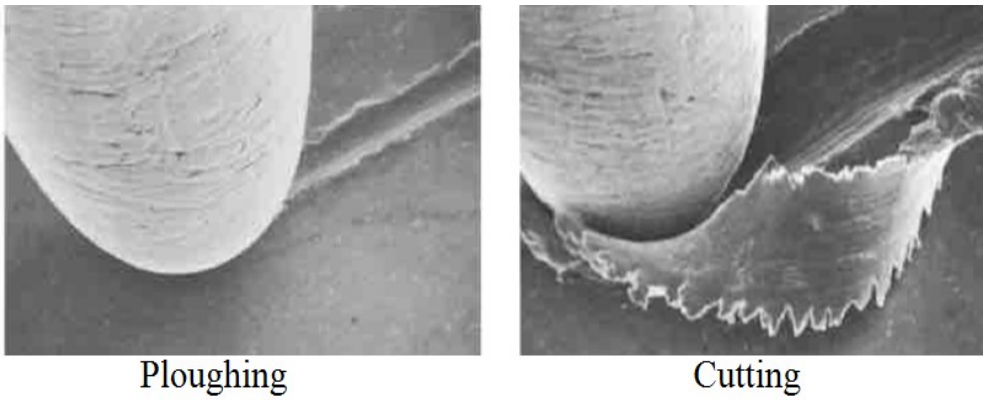

Figure 2.6: Scanning electron microscope (SEM) image depiction of ploughing and cutting on workpiece surface [58].

For belt grinding process, the belt tool is made up of three components i.e. backing, adhesive bond, and the abrasive grains. As seen as in Figure 2.7, the first layer is the backing which is usually made out of either one of three primary materials such as papers, cloth, and fiber. The second layer is adhesives such as base coat and size coat as bonding agents to the abrasive grain which is the third layer. The additional coat shown in Figure 2.7 is just a coat layer which is optional. Unlike rigid abrasive tools, the grains are not regenerative that makes the belt to wear with cycle time.

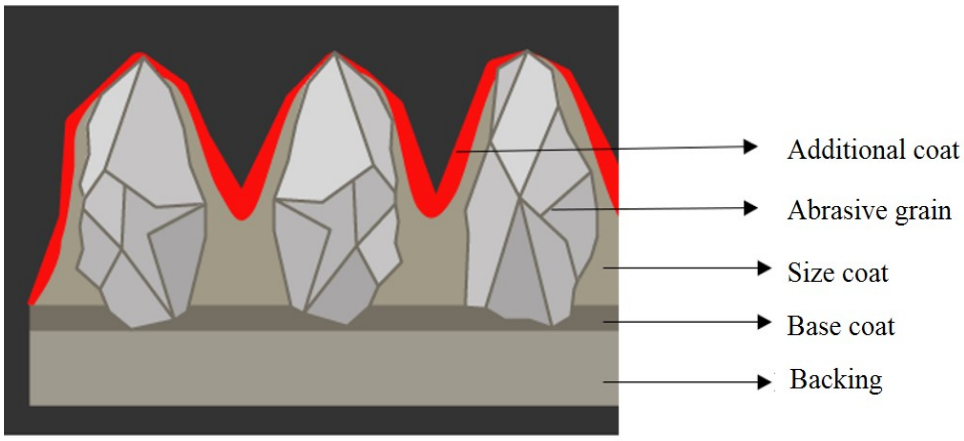

Figure 2.7: Structure of coated abrasive belt.

Generally the penetration depth of the abrasive tool depends on the topography of tool surfaces and the geometry of the undefined cutting-edge [31]. The granularity

of a coated abrasive belt tool vitiates with cycle time resulting in change of the material removal mechanism. Many aspects of the interactions between cutting grain granularity on the material surface and resulting three material removal modes (rubbing, ploughing and cutting) are not fully understood for coated abrasive tool and will be covered in this thesis.

2.3 Toolwear monitoring

The concept of tool life monitoring has earned significant importance in manufacturing industries. Automated manufacturing processes have resulted in the revolution of manufacturing industries, requiring little or no human intervention. In this environment, tool changing decisions cannot be made by operators. Thus, there is a great demand for tool condition monitoring systems that ensure optimum performance of the automated machining centres. The pre-planned tool replacement approaches are no longer appropriate when the machining conditions vary extensively. Useful tool life is the period when a tool cuts effectively and is generally expressed as the time between consecutive tool change. The life of a cutting tool can be brought to an end either due to gradual wear leading to tool failure or premature edge failure due to chipping [59].

Characterization of the surface topography of a machined workpiece can act as a fingerprint of the machining process and, more specifically, the condition of the cutting tool [60,61]. This is attributed to the change in the textural characteristics of the machined workpiece that is becoming apparent as the cutting tool approaches the end of its life. In production, it is a high disadvantage to use a tool until breakage occurs, as it affects severely the quality of the work. Twenty percent of the downtime for modern machine tools is attributed to tool failure, resulting in reduced productivity and economic losses [62]. In general, predicting tool life helps to optimise the utilization of the tool's life cycle. A reliable real time monitoring system could allow ideal exploitation of the tool and avert these problems. It aids to make the process more effective and the energy more efficient by reducing the production time and the dependency on the operator.

2.3.1 Tool wear monitoring systems (TCMS)

In general, tool wear is the gradual degradation of the cutting tool that causes failure in the process during regular operation. Tool monitoring includes both instantaneous tool breakage detection and progressive wear detection [59]. Unnoticed breakage can cause harm to the machinery, along with substantial stoppage delays in manufacturing facilities. Tool wear increases cutting forces and temperatures that further results in tool breakdown.

Metal cutting is associated with high temperatures in the tool-chip interface zone which significantly affect the accuracy of the machining process [62]. As wear level of the tool increases on the work coupon interface, there is a temperature hike which affects workpiece surface integrity. The most significant source of machining error originates from excessive cutting temperatures that have a high impact on tool wear, tool life, workpiece surface integrity, chip formation mechanisms and also contribute to thermal deformation of the cutting tool [59, 63].

In case of unsupervised machining centres, it has been established that the addition of sensor competences can sense the signal either directly from the tool or indirectly from the workpiece and predict the tool wear state in real time [58]. Experiments have been performed to study effects of tool wear on cutting force signals when drilling copper alloy to achieve on-line drill wear monitoring [64]. The correlation between flank wear and tangential cutting force coefficient were used with cutting parameters such as cutting speed, depth of cut and feed per tooth to evaluate tool wear for milling [65]. A time series modelling technique was developed to monitor coated carbide tool condition based on AE signal [66]. These works on tool wear monitoring were focused on time series and frequency domain analysis. Wherein, an upper limit is set among the normal and abnormal states of the tool. Conversely, the threshold value changes with time and cutting environment which makes these techniques in-accurate. For increasing the performance, more novel logic, such as pattern recognition and statistical techniques have been developed in the region of tool wear assessment. A neural network-based sensor fusion model for estimation of the average flank wear of the primary cutting edge based on features isolated from the fused data of some machining zone signals such as cutting forces, spindle vibration, spindle current, and sound pressure level has also been investigated [67].

Table 2.3: Research efforts in predicting tool wear states of rigid tools.

Process	Year	Investigators	Sensors used	Decision-making techniques
Milling	1994	S. Kakade *et al.* [68]	AE	Statistical analysis
	1995	S.C. Lin and R. J. Yang [69]	Force	Statistical analysis
	2000	S.L. Chen and Y.W. Jen [70]	Force, vibration	Neural network
	2007	Ghosh *et al.* [71]	Force, vibration, Current, and Sound pressure	Backpropagation neural network
	2009	M. Malekian *et al.* [72]	Force, vibration, and AE	Neuro-fuzzy method
	2010	J.H. Zhou *et al.* [73]	AE and force	Auto-Regressive Moving Average (ARMA)/ Dominant Feature Identification (DFI)
	2017	B. Cuka and D.W. Kim [74]	Force, vibration, current, and microphone	fuzzy logic
	2017	D. Wu *et al.* [75]	Force, vibration, and AE	Random Forest
Turning	2000	D.E. Dimla and P.M. Lister [76]	Force, accelerometer	Time series and frequency analysis
	2008	Alonso and Salgado [77]	Accelerometer	Singular Spectrum Analysis (SSA) and cluster analysis
	1999	Ghasempoor [78]	Force	Neural network
	2002	L.Wang *et al.* [79]	Accelerometer	Hidden Markov models (HMMs)
	2010	A.Gajate [80]	Force, vibration, and AE	Neuro-fuzzy
Drilling	1995	S.C. Lin and C.J. Ting [81]	Force and power	Statistical analysis
	2000	X. Li *et al.* [82]	Accelerometer	Neural network model with fuzzy logic (FNN)
	2001	H. M. Ertunc *et al.* [83]	Force and power	HMM
	2005	C. Sanjay *et al.* [84]	Force	Backpropagation neural networks
Broaching	2007	D. Shi and N. N. Gindy [85]	Force, strain sensor and accelerometer	SVM and Principal Component Analysis (PCA)
Grinding	1992	E. Brinksmeier and F. Werner [86]	Optical sensor	Statistical analysis
	2001	P. Lezanski [87]	Force, vibration, and AE	Neural network and fuzzy logic
	2007	T. Warren Liao *et al.* [88]	AE	Adaptive genetic clustering algorithm

A new modelling outline for tool wear monitoring using Hidden Markov Models (HMM's) based on feature vectors extracted from the vibration signals in turning operation of AISI 8620 steel has also been proposed [89]. The tool wear monitoring system (TCMS) can be accomplished using a varied range of different indirect sensing techniques that include acoustic emission, tool temperature, cutting forces and vibrations [90–92]. All these signals from indirect sensors considerably rise with wear [59, 60, 93]. Other tool wear and failure sensing systems have also been developed in the past using optical techniques such as CCD camera and TV camera [94]. A successful tool condition monitoring system requires an appropriate

decision-making algorithm to predict the tool condition from the signal data acquired from the indirect sensors [95]. Works on tool wear monitoring using indirect sensing techniques combined with a decision-making algorithm for different machining processes are listed in Table 2.3.

2.3.2 Previous work on abrasive tool wear monitoring

The grain/bond breakdown modes that are commonly found in abrasive grinding wheels is illustrated in Figure 2.8. Many research works have been accomplished in conventional abrasive grinding wheel wear monitoring in the past [96–99]. A. Hassui *et al.* [100] tried to determine the exact moment at which abrasive grinding wheel wears to accomplish the dressing using vibration and acoustic emission sensor.

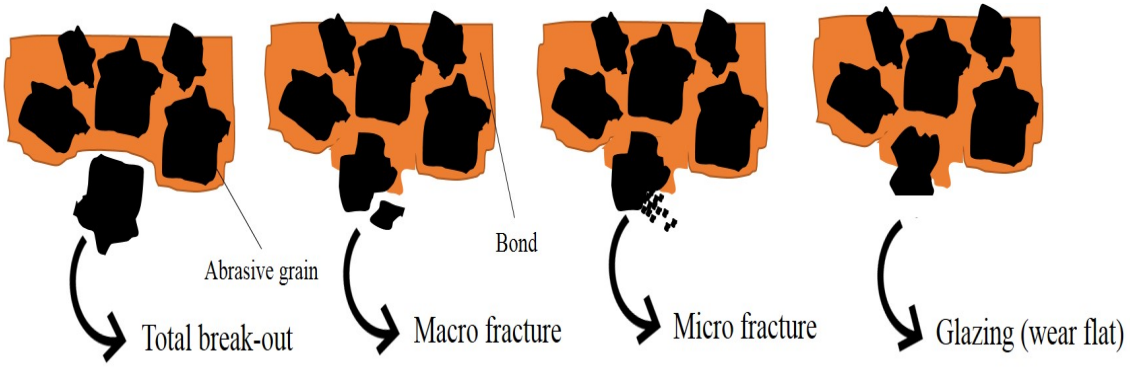

Figure 2.8: Grain/bond break down modes common in abrasive grinding [101].

AE_{RMS} signals and the vibration signal showed relationships with wheel wear and was used to establish the end of wheel life indirectly. P.Lezansk [87] developed an intelligent system for grinding wheel condition monitoring by application of a neural network and fuzzy logic combining the outputs of several sensors measuring vibration, acoustic emission and grinding forces. AE and force signals have been used for classifying the tool conditions into four distinct classes namely sharp tool, used tool, chip noise, and tool breakage using pattern recognition [102]. Force signal could be better processed using wavelet de-noising than FFT filtering in surface plunge grinding to monitor tool sate [103]. Frequency spectrum signals of grinding along with neural network technique have been used to develop wheel surface condition monitoring system [104]. A methodology of evaluation of the level of changes in geometric features of the tool during the grinding process was developed using laser

scanning microscopy to monitor the condition of abrasive tool [105].

Industrial interest in tool condition monitoring for coated abrasives has significantly augmented in recent years as unlike other rigid abrasive machining tools the grains are not regenerated. Figure 2.9 shows the SEM (Scanning Electron Microscope) image of the new and old abrasive belt tool. In the old coated abrasive tool, we can see deformations that will severely affect the surface's quality. As the coated abrasive tool is being worn down, edge geometry of abrasive grains are modified continuously.

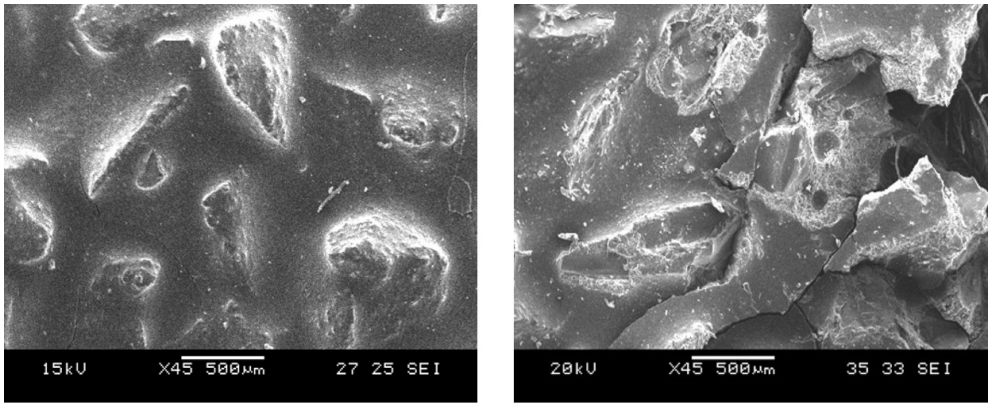

Figure 2.9: Scanning electron microscope (SEM) image of coated abrasive new and old belt tool.

Though not much work has been explored in tool wear of coated abrasive tools, other works on coated abrasive tools provide some insight into the importance of tool monitoring coated abrasive tools. The influence of abrasive grain's wear and contact conditions on surface texture in belt finishing process and concluded that material removal rate changes based on the wear level of active grains and becomes stable after the effective contact duration [12].

A study by W.Wang *et al.* had shown that adhesion wear might dramatically decline the cutting effectiveness [106]. The reason is that adhesion wear flats those belt surface, which brings additional rubbing friction between grain and workpiece. The changes of grinding force and metal removal rate with time in coated abrasive belt grinding are caused principally by the formation and increase of the worn flat area on grain tips [43]. Khellouki *et al.* [107] studied the influence of the interactions of the belt finishing parameters such as abrasive film parameters, cutting parameters on the surface texture. The study proved that among the parameters of

belt finishing, the granularity of abrasive films is the most influential parameter on surface roughness and quality.

These studies on belt finishing process emphasise the tool condition monitoring for the effectiveness of the process. There is a lot to be considered before the implementation since abrasive machining at different speeds involve different rates of wear (as cutting speeds increase, the cutting process becomes more adiabatic, and heat generated in the shear deformation zone cannot be conducted away during the brief duration of contact) [108]. A better understanding of the types of tool wear will lead to better implementation of real-time tool wear monitoring systems.

2.4 In-direct sensing and monitoring

The technology for measuring surface quality has undergone tremendous evolution. New techniques are developed from the existing and requirement for such techniques are still in rise. Variety of techniques have been developed for measuring vertical and lateral surface quality features. The measurement approaches are classified into three basic types, linear profiling, area profiling (or areal topography), and area averaging [109] as shown in Figure 2.10. Profiling and areal topography methods are in particular the widely used measurement approaches.

Two categories are available based on which measurement approaches can be achieved, namely contact/mechanical measurement and non-contact/optical measurement [110].

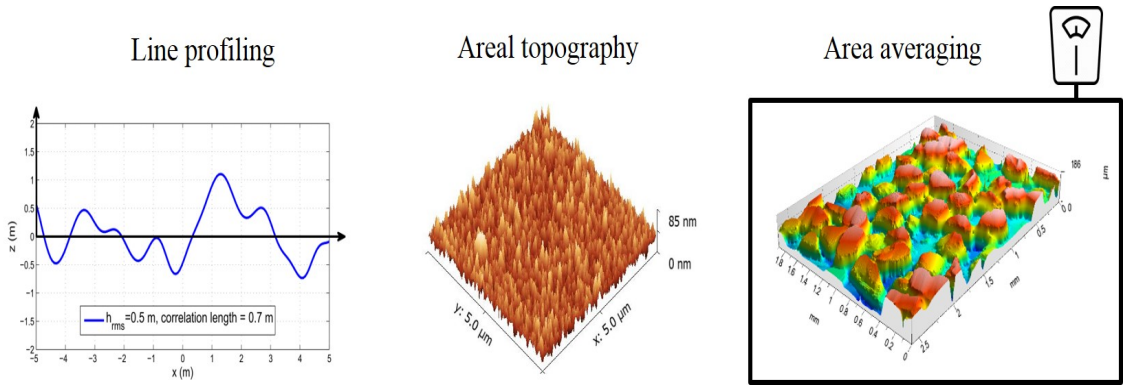

Figure 2.10: Classification of surface finish measurement methods [109].

Contact measurement means a physical contact is made between the measuring device and the test surface. Non-contact measurement does not have any material

contact. Metrology application for most engineering and manufacturing can be satisfied using both contact or non-contact methods [111]. Contact and non-contact measuring technique can be further classified based on the applied technology as shown in Figure 2.11.

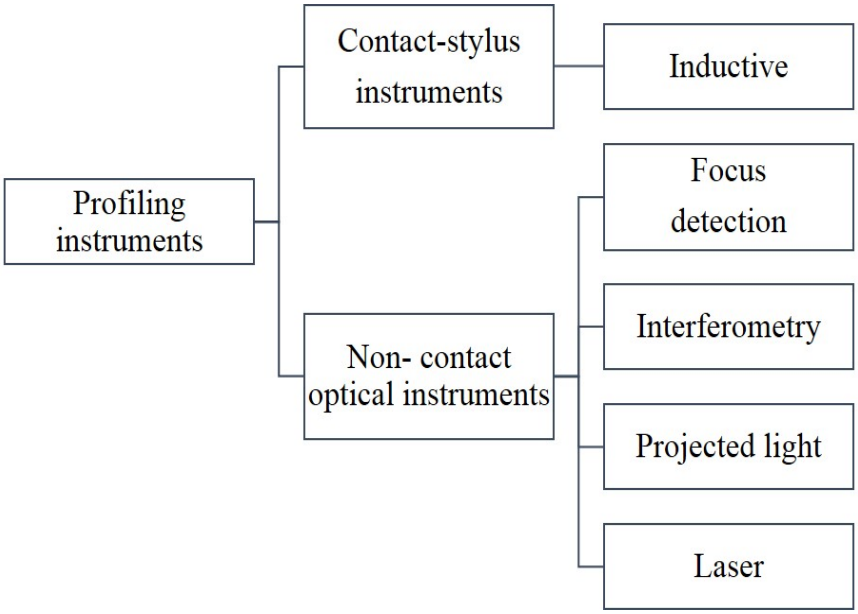

Figure 2.11: Classification of profiling instruments-contact and non-contact [110].

A stylus profiler is a device typically used for contact measurement as illustrated in Figure 2.12. Stylus profilers are the most common instruments of measurement, and are profoundly used in industry and research laboratories because of their consistency, ease of interpretation and relatively low cost. The stylus tip is continuously in contact with the surface, and a transducer transforms vertical motion of the stylus to an electrical signal, which represents the surface profile $z(x)$ in case of line scanning or topography image $z(x, y)$ in case of area profiling. The perpendicular resolution of a contact measuring tip can be as small as around 0.05 nm and lateral resolution can be as small as about 100 nm [112]. Stylus instruments have also been criticized for being too slow [113] which makes it to be ignored when productivity is to be improved.

Optical measurement systems such as phase shifting interferometry, vertical scanning (white light) interferometry, and confocal microscopy etc. are used in measuring surface quality as non-contact methods. Non-contact methods have great benefits because they are non-destructive. Non-contact optical methods have higher speed than contacting methods, which is an advantage over contacting stylus probe.

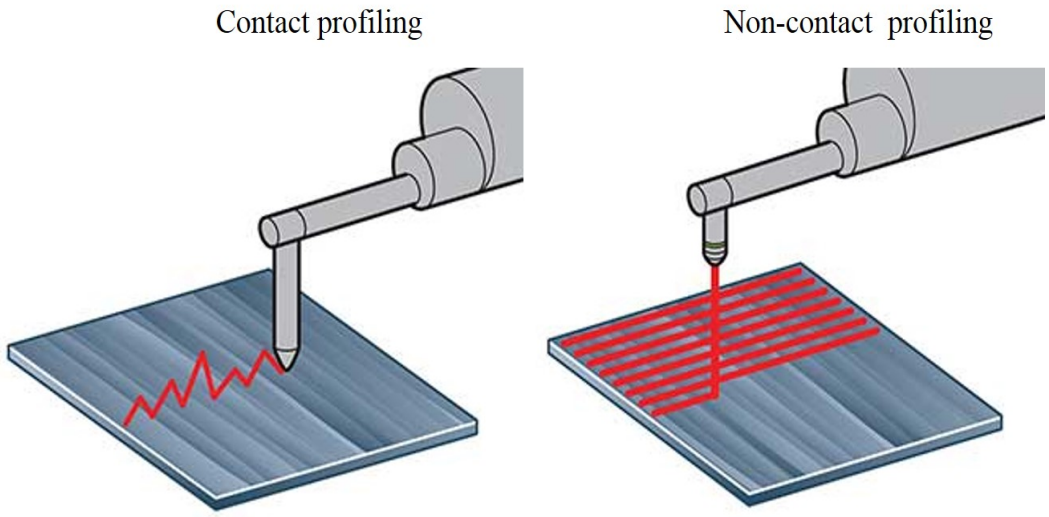

Figure 2.12: Contact and non-contact methods of measuring surface quality.

Optical methods are susceptible to surface properties that include surface optical properties, surface slopes, and fine surface features causing diffraction and stray light. Correctness of an optical profiling method can be affected due to dissemination generated from stray light from other surfaces within the optical system [113].

Loading, unloading and reloading of the machined part for measurement using any of the techniques discussed above consumes much time. Loading, unloading and reloading can further lead to damage or distortion, which will ultimately lead to deviation of the machined part from original dimension. Moreover, the part may require a separate fixture for proper orientation during measuring which adds to the additional cost.

These measuring methods discussed above, however, cannot be applied in real-time in a machining operation. While a workpiece is machined, it is unlikely to measure its surface quality by contact and non-contact techniques. An indirect measuring technique should be employed instead. The measuring techniques employed should be competent enough of sensing and co-relating evidence or parameters related to the machined surface or the machining condition.

2.4.1 Sensing technologies for machining

In manufacturing, typically machining processes involve various cutting operations. To enhance the productivity of a manufacturing process, sensors are needed for real-time monitoring which can serve as a feedback for controllers. The focus of

in-process monitoring in any machining environment can be grouped into four categories i.e. on the machine (diagnostics and performance monitoring), tooling (state of wear etc.), the workpiece (geometry and dimensions, surface features and roughness, metallurgical damage), and the process itself (chip formation, temperatures, energy consumption) as shown in Figure 2.13. Sensors that are used to retrieve quality information from the process should be in such a way that it does not intrude in the actual process or require extensive alteration on the machine.

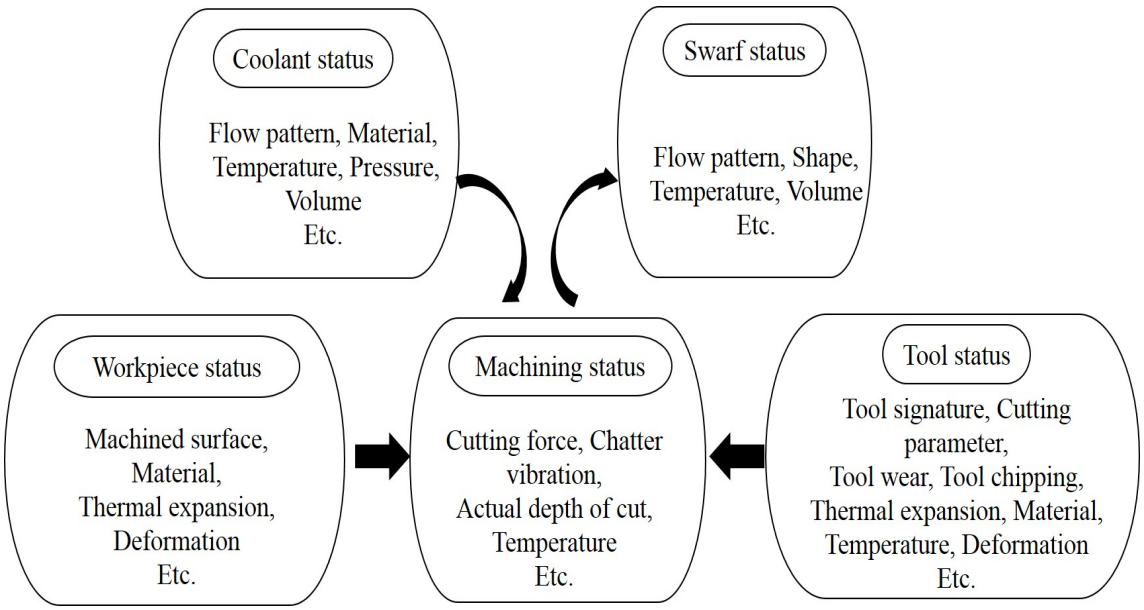

Figure 2.13: Sensing objective during machining conditions [114].

A multiple-modal sensor system is essential for process scrutinising to identify the states of the individual components of a machining system as illustrated in Figure 2.14. For monitoring in precision manufacturing regime where the tolerances on the surface finish are very tight, this approach is of particular importance [115]. The way by which various sensors are incorporated into the operation of the system is usually a significant factor in the overall design of an intelligent system [116, 117]. Due to the evolution of automated manufacturing, there is a mandate for a real-time sensor for surface quality prediction by an accurate assessment of surfaces produced during the tertiary machining. Integration of an in-process sensor for optimising manufacturing environment demands a good confidence in the sensor as it should be capable of detecting the desired process characteristic consistently. One significant advantage of using in-process sensor is that it is possible to bring together data over a much greater zone of the work coupon compared to the conventional metrological

technique that has been traditionally practised.

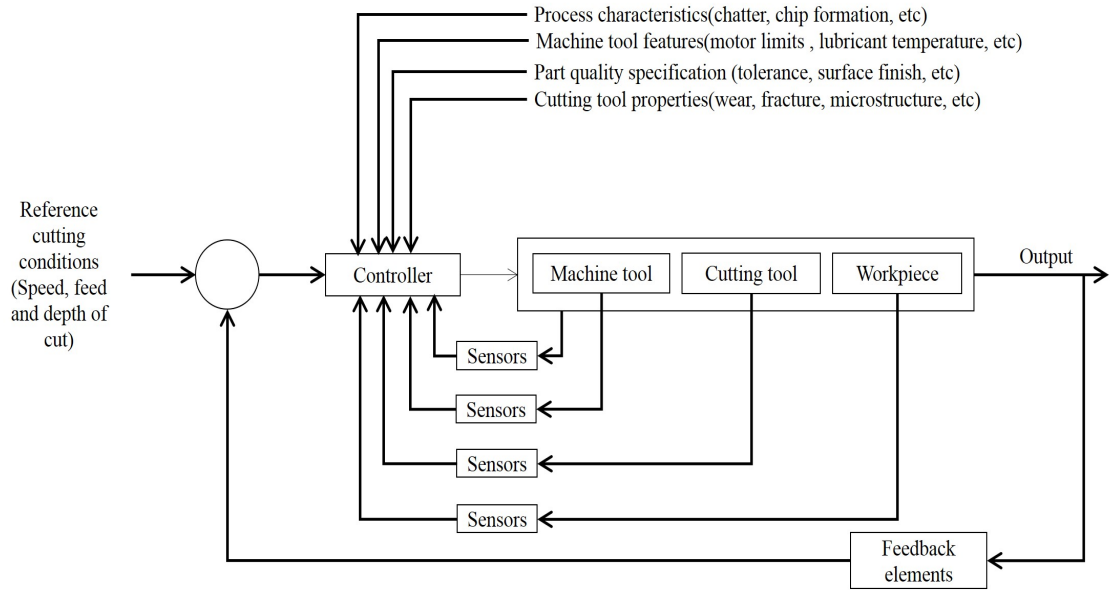

Figure 2.14: Multiple-sensor systems essential for process monitoring [118].

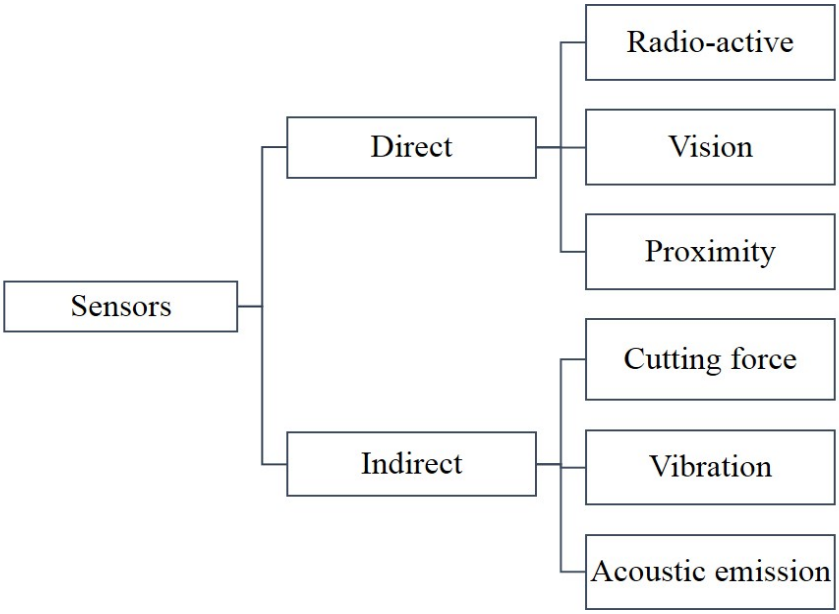

Figure 2.15: Classification of sensing techniques [62].

Sensors play a critical role in the acquirement of data relating to the machine, process and part to enhance the machine tool functioning. In a case of unsupervised machining centers, it has been established that the addition of sensor competences can intensely slash the downtime and enrich product quality.

Over years, a wide number of sensing techniques have been fostered. Most of these systems have been restricted to a clean room environment, and only a handful

have emerged as a suitable tool for in-process measurement. Generally, these sensing techniques are classified into two categories of direct sensors and indirect sensors as shown in Figure 2.15. The former methods are reliable, but they cannot provide continuous in-process measurements because cutting edges are generally inaccessible during cutting [95]. Direct methods are very costly, and incorporation of them in the machining process environment is also difficult [119]. The indirect methods can take measurements while cutting tools are actively engaged in cutting, which makes it possible to monitor the machining condition in real time.

2.4.2 Sensors for machine monitoring

The indirect methods are more economical for monitoring machining processes and are capable of measuring a variety of physical quantities that characterise them. Force sensors, AE sensors, accelerometers, current/power sensors, thermistors, etc., transform a physical quantity into the corresponding electrical signals from which process state could be acquired. Force sensors, accelerometers and AE sensors are the three sensors that have been widely applied to monitor machining systems [95]. Figure 2.16 shows the relative frequency of usage of these three sensors in monitoring the machining conditions. The sub-sections that follow reviews the use of these sensors with special attention paid to monitoring surface quality and tool wear condition.

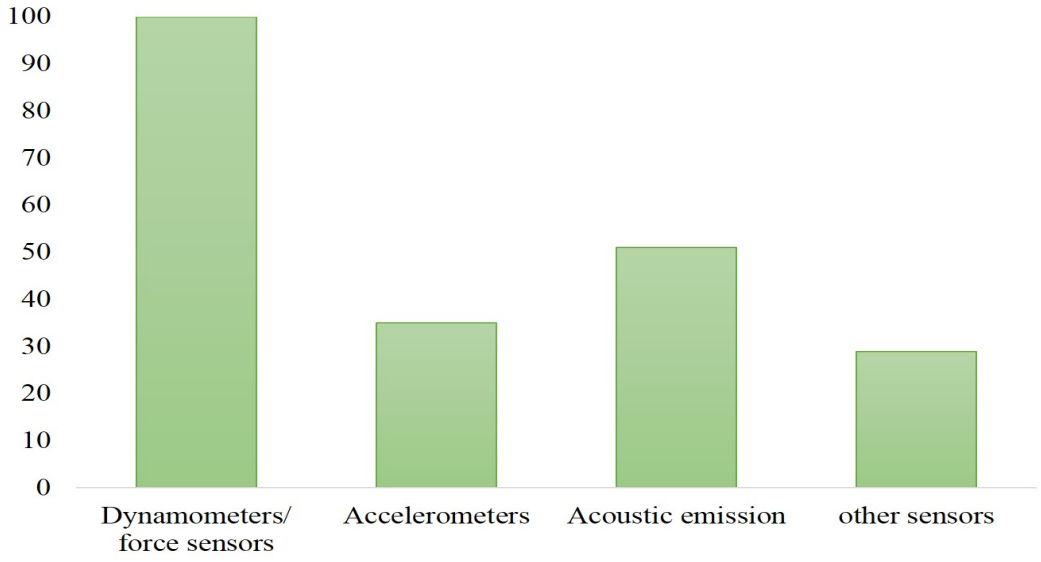

Figure 2.16: Relative frequency of usage of sensors in monitoring the machining conditions [95, 119].

Force sensors

Cutting force is one crucial characteristic parameter to monitor during machining processes [120]. Numerous force measurement devices like dynamometers have been built which are capable of measuring tool forces with higher accuracy and its application can be regarded as state of the art. Research results show that surface quality is intensely related to cutting force [121,122]. Cutting force is considered to be the parameter that best represents the cutting condition [123]. Research results show that tool breakage, tool wear and workpiece surface quality are strongly related to cutting force [121,122]. Force sensors can be incorporated into the tool where the tool applies force to work coupon, and sensor reading is got because of the reaction force. Force sensors can also be incorporated into the work coupon provided that the word coupon is stationary and it does not hinder the cutting region.

Accelerometers/ vibration sensors

The monitoring systems using accelerometers are very simple to use and are cost-effective [124]. The cutting vibration at a specific frequency determines the roughness profile of a machined surface [125]. This correlation between cutting vibration and roughness can be used to verify the surface finish during machining without disruption as shown in Figure 2.17. It is essential to examine the outcomes of vibrations on the characteristics of the surface roughness profile. Studies indicate that relative vibration between work and tool affects surface finish [126,127]. A small amount of resistance is only offered by the line contact between the work coupon and the new tool. As a result, the tool vibration tends to be higher. However, with cycle time the tool tends to wear off, and there is no more line contact on the work coupon. As a result there is a decrease in the magnitude of vibration which helps as an indicator to monitor the tool condition as well as surface quality.

Lin *et al.* [127] established a surface topography simulation model to study the effects of single-direction vibrations on the surface finish profile on machining S45C carbon steel. Surface roughness estimated from simulation model is very close with the difference of less than 15% with the experimental results. They concluded that surface roughness is not only dependent on vibration amplitude but also vibration

frequency and both have a stronger effect on the surface finish profile.

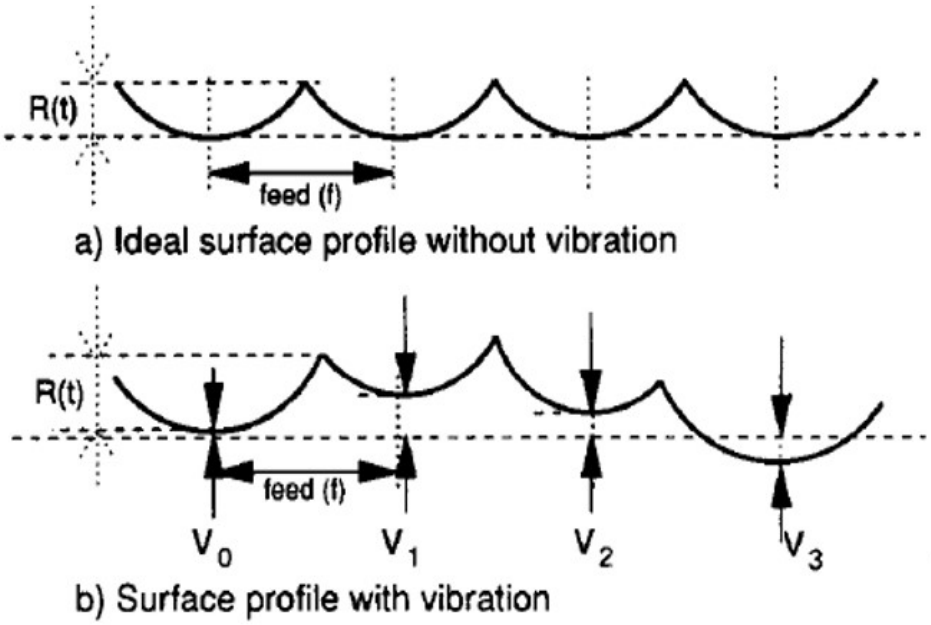

Figure 2.17: Surface profile due to vibration between tool and workpiece [125] .

Placement of the accelerometer sensor is crucial as the strength of the vibrational signal decreases with an increase in the distance from the cutting zone.

Acoustic Emission sensors

During machining, the workpiece undertakes considerable plastic deformation as the tool thrusts through it. Within the deformation zones, strain energy is released. This released energy is commonly stated as an acoustic emission. An acoustic emission (AE) sensor is small and easy to position on the workpiece or tool holders. The use of AE sensing for tool condition monitoring is becoming an attractive sensing method due to its non-intrusiveness, simplicity of operation and fast dynamic response. Sensitivity loss of force and vibration sensors are higher at an high frequency where most of the micro-cutting components are dominant as shown in Figure 2.18. Acoustic emission does not capture low-frequency disturbance signals but is very sensitive at high-frequency range which makes it a suitable contender to monitor any abrasive machining process.

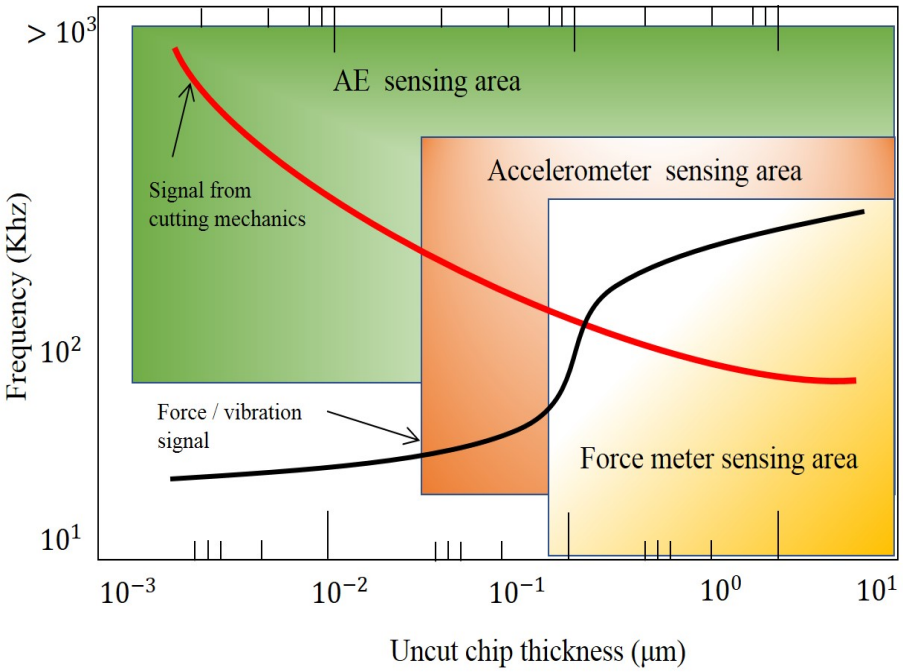

Figure 2.18: Sensor classification based on operating frequency range and chip thickness [128] .

Most of the micro-cutting such as abrasive machining can be sensed by Acoustic emission (AE) as it sensible at higher frequency range [129]. The frequency spectrum of AE typically spans the kilohertz to megahertz range (usually 10 kHz−10 MHz) [130]. Acoustic emission (AE) has exhibited high reliability in characterising material removal at the microscale, hence lending credence to its suitability for the precision manufacturing process. Raw AE signal (AE_{RAW}) is composed of several high frequencies on different energy levels and is difficult to interpret [131]. Time and frequency domain information from (AE_{RAW}) signals can be exercised to represent the surface profile of the workpiece [132–135]. A.E. Diniz *et al.* [136] results confirmed that acoustic emission could monitor the evolution of surface roughness in finish turning in real-time based on acoustic emission count rate, zero crossing rate, root mean square of the AE signal, standard deviation, skewness and kurtosis. Karpuschewski [137] presented that deformation or stress on a work coupon is based on the contacts that are caused by the grits and is a source for AE in abrasive grinding process. The belt grinding process considered in this research is characterized by simultaneous contact of a significant number of abrasive cutting edges on the surface of the workpiece analogous to the grinding process thus the source of AE signal can be more or less the same. However, the accuracy of this acoustic-based

sensor depends predominantly upon the detection angle and the distance between the sensor and the workpiece to be measured.

Table 2.4: Indirect sensors for predicting machining states.

Sensor	Process	Application	Reference
Dynamometer/ Force	Milling	Tool wear	[123], [69], [72], [74], [75]
		Surface quality	[138], [139], [140]
	Turning	Tool wear	[76], [78], [80]
		Surface quality	[141]
	Drilling	Tool wear	[81], [83], [84]
	Broaching	Tool wear	[85]
	Grinding	Tool wear	[87]
Accelerometer	Milling	Tool wear	[77], [76], [79], [80]
		Surface quality	[142]
	Turning	Tool wear	[77], [76], [79], [80]
		Surface quality	[143] , [144]
	Drilling	Tool wear	[82]
	Broaching	Tool wear	[85]
	Grinding	Tool wear	[87]
		Surface quality	[145]
Acoustic emission	Milling	Tool wear	[68], [72], [75], [146], [147]
		Surface quality	[147], [148]
	Turning	Tool wear	[80], [91], [149]
		Surface quality	[149], [150], [151]
	Grinding	Tool wear	[87], [152], [153]
		Surface quality	[150], [153]

Table 2.4 summarises the list of force, accelerometer and vibration sensors applied in different machining developed for monitoring tool state as well as surface quality.

Tool wear and surface quality are more or less correlated with each other as degradation of the tool will also have effects on the machined surface. Sensors for monitoring the cutting conditions should possess high response and sensitivity even under the influence of various disturbances arising during machining. A most important aspect of the sensor selection for monitoring is its reliability, the cost and its intrusive nature. Furthermore, it should have a compact sensor structure to mount the sensor device near the machining point without much alteration to the system [114]. The use of multiple sensors is principally necessary for applications where the prerequisite is that the system interacts with and operates in a dynamic environment [154].

2.4.3 Sensing technologies in abrasive machining

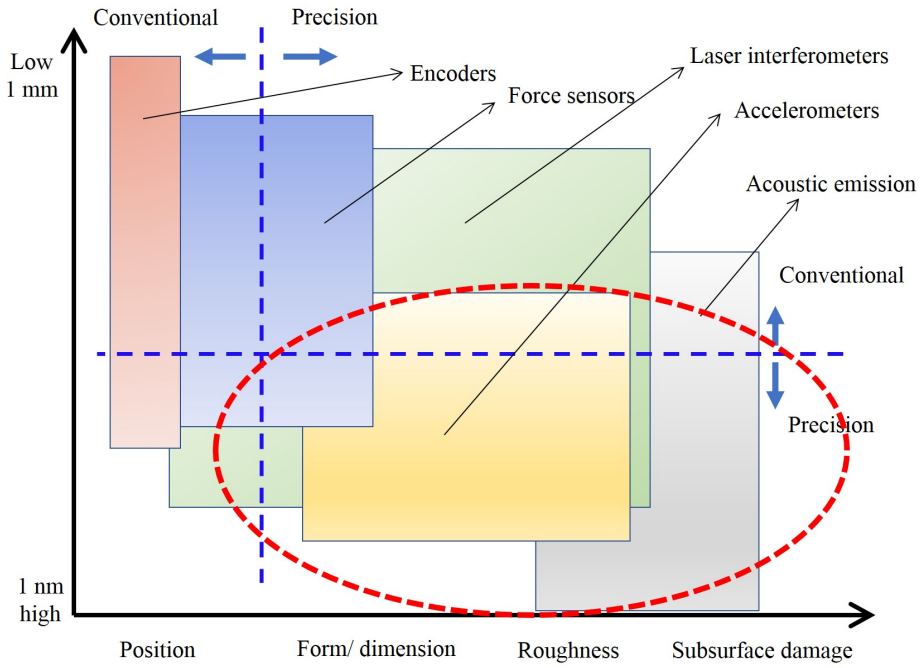

Figure 2.19: Sensor application in various level of precision [115].

Abrasive machining process is capable of achieving very low surface roughness or surfaces finish of very high quality as compared to other machining techniques, i.e. they fall in the precision machining regime. The material removal is in range of submicrometre level in any abrasive machining process. Therefore, sensor incorporated for real-time data retrieval for any abrasive machining process should be capable of detecting any change in the process with high consistency. Incorporation of sensor technology for precision manufacturing process such as abrasive machining process has been investigated by D. A. Dornfeld *et al.* [155]. The study reveals that force, accelerometer, laser and AE are most critical sensors required in-precision machining regime for assessing surface finish at the sub-micrometre level as shown in Figure 2.19.

2.5 Digital signal analysis and features extraction

A signal may be expressed as a physical quantity which can vary with respect to time. The extraction of information from sensor data to correlate with other physical phenomena (i.e. material anomalies/defects) requires signal processing techniques.

The signal processing flow for developing real time monitoring systems for machining is shown in Figure 2.20.

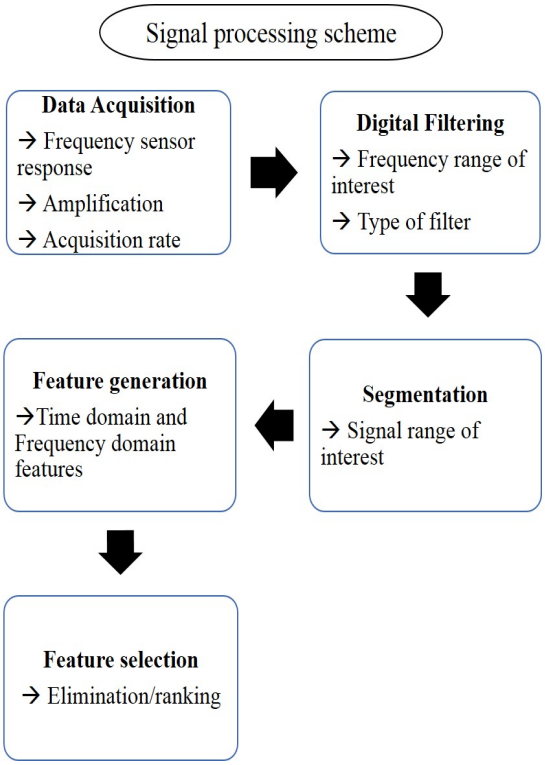

Figure 2.20: A schematic representation of the signal processing system practised in machine monitoring [95].

The processing of sensor signal starts with data acquisition which is governed by the hardware efficiency and sensor characteristics. Selection of proper sensor and its operating range is determined by the significance of the event to be captured that correlates to the process state [156]. As a rule of thumb, data acquisition rate is based on the Nyquist Shannon theorem which states that sampling rate should be at two times that of the maximum frequency range that we are interested in [156]. Failure to fulfil this requirement will result in aliasing of the reconstructed signal.

Moving on from data acquisition process, filtering should be carried out to eliminate unwanted attributes and undesired components that may be present within the signal. Filtering can be an offline process or an online process depending on the hardware capability. The transformed signal has to be segmented in the time domain so only the data of significant interest with respect to time will be processed.

There are various attributes in the signal, including intensity changes, the frequency of those intensity changes, the mixture superimposing of several signals

forming one signal that gives an insight of the process state as well as its correlation. Sensor data in raw form may be challenging to quantify, and conversion to other physical quantities is required for more straightforward analysis. Analysis of the segmented signal is done through mathematical functions where the conversion from continuous to discrete data is achieved. Such conversions allow useful features of the data to be more noticeable. Conversion of the signal from time domain into the frequency domain will facilitate us to focus on frequently occurring dominant frequency bands which will give further insight into the process. Signal analysis methods can be roughly divided into the time domain, frequency domain and time-frequency domain. Last part of the signal processing scheme practised in monitoring is all about identifying the best feature set that is the close representative of the ground condition.

2.5.1 Time domain methods

When a sensor signal is processed in time domain without being transformed into another domain, the signal processing technique is classified as a time domain analysis. Time-domain analysis [157] is based on the time waveform to extract characteristic features such as mean, peak, peak-to-peak interval, standard deviation, crest factor or high-order statistics (root mean square, skewness, kurtosis, etc.) from waveform signals. These features are called time-domain features. The magnitude of the time-domain features could give understandings of the anomalies in the process [70,71,123,124,158–160]. The formulas for these time-domain features are listed in the equations below.

Mean is described as in equation (2.4)

$$Mean = \frac{1}{n}\sum_{i=1}^{n} x_i \tag{2.4}$$

The standard deviation of a set of N is given by equation (2.5) where $\bar{x}$ is the mean of the sample

$$standard\,deviation(\sigma) = \sqrt{\frac{\sum_{i=1}^{n}(x_i - \overline{x})^2}{N-1}} \tag{2.5}$$

Skewness is the asymmetry value of the distribution of a random variable about

its mean. Skewness gives the shape of the signal. Negative skewness and positive skewness is depicted in the Figure 2.21.

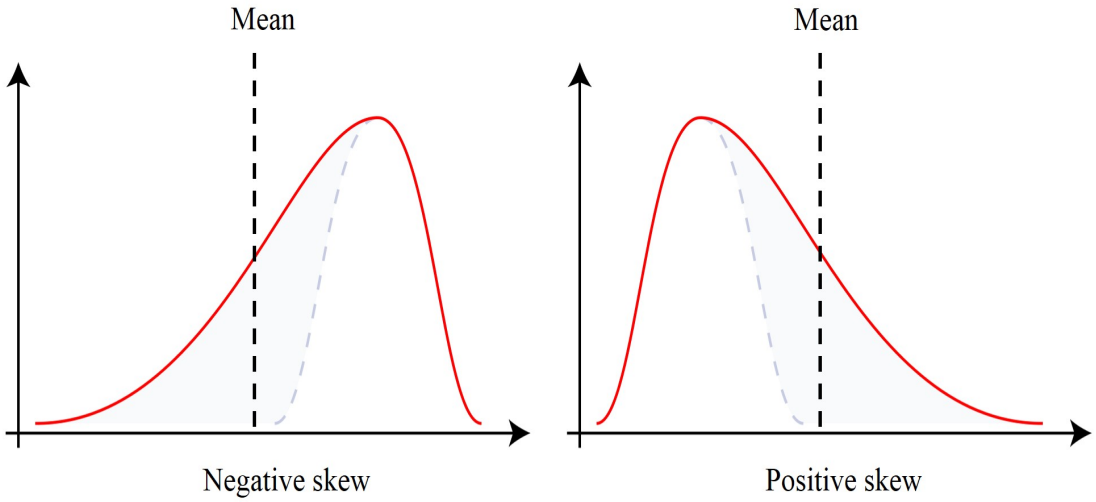

Figure 2.21: Types of skewness profiles.

Skewness is described as in equation (2.6)

$$Skewness = \sum_{i=1}^{n} \frac{(x_i - \overline{x})^3}{(N-1)\sigma^3} \tag{2.6}$$

$\bar{x}$= Mean of data points, x_i= Data point at i,

σ= Standard deviation,N = Number of data points.

Kurtosis is one of the most popular condition indicators used in fault analysis [161] and the mathematical form is written in equation (2.7)

$$Kurtosis = \frac{\sum_{i=1}^{n} \frac{(x_i - \overline{x})^4}{(N)}}{\sigma^4} \tag{2.7}$$

Root mean square (RMS) is the statistical measure of effective value or the magnitude of the set of data points. It can be calculated as given in equation (2.8)

$$RMS = \sqrt{\frac{1}{N}\sum_{i=1}^{n}(x(i) - \overline{x})^2} \tag{2.8}$$

Peak to valley is the difference between the maximum and minimum values of the

sensor signal [162, 163] and the mathematical form is written in equation (2.9).

$$Peak - to - valley = max(x(n)) - min(x(n)) \tag{2.9}$$

Crest factor can be calculated as shown in the equation (2.10) below

$$Creastfactor = \frac{Peak - to - valley}{RMS} \tag{2.10}$$

Table 2.5 lists the time domain features applied in monitoring machining from the various sensor system.

Table 2.5: Time domain features applied in monitoring machining from the various sensor system.

Feature	Sensor signal	Application	Reference
RMS	Cutting forces	Milling	[71], [124]
	Vibrations	Turning	[164]
	Acoustic emission	Turning	[165]
		Grinding	[166], [167]
Peak	Cutting forces	Milling	[168]
	Vibrations	Milling	[168]
	Acoustic emission	Milling	[168]
Mean	Cutting forces	Milling	[123], [70], [158], [159], [160]
		Turning	[169]
	Vibrations	Milling	[159]
		Turning	[169], [170], [142]
	Acoustic emission	Milling	[159]
		Turning	[169], [171], [165]
Standard deviation	Cutting forces	Milling	[123], [70], [159]
	Vibrations	Milling	[159]
	Acoustic emission	Milling	[159]
		Turning	[165]
Skewness	Cutting forces	Milling	[123], [159]
	Vibrations	Milling	[159]
	Acoustic emission	Turning	[172]
		Milling	[159]
		Grinding	[161]
Kurtosis	Cutting forces	Milling	[123], [159]
	Vibrations	Milling	[159]
	Acoustic emission	Turning	[172]
		Milling	[159]
		Grinding	[161]

2.5.2 Frequency domain methods

The shapes of a signals can be described easily in the frequency domain. The frequency domain refers to the analysis of signals in terms of frequency as illustrated in Figure 2.22.

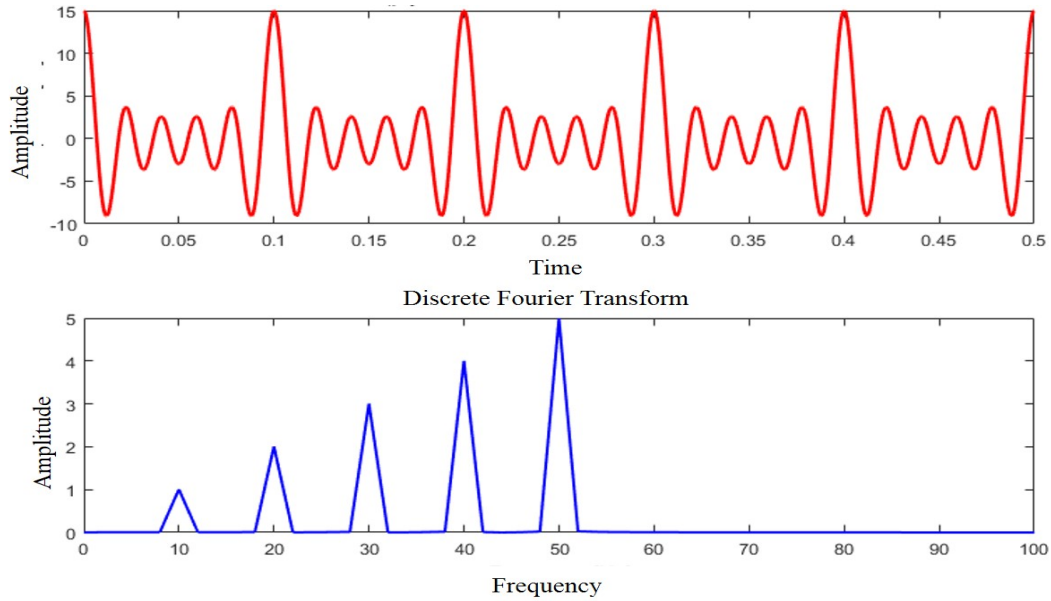

Figure 2.22: Transformation of a signal from time domain to frequency domain.

Table 2.6: Frequency domain features applied in monitoring machining from the various sensor system.

Feature	Sensor signal	Application	Reference
Single H /Frequency	Cutting forces	Milling	[123], [159]
		Turning	[172], [169]
	Vibrations	Milling	[159], [173]
		Turning	[169], [174], [170]
	Acoustic emission	Milling	[159]
		Turning	[169]
		Grinding	[175], [167]
PSD	Cutting forces	Milling	[123], [124], [159]
	Vibrations	Milling	[159], [174]
	Acoustic emission	Milling	[159]
		Turning	[165]

Fast Fourier Transform (FFT) converts a sensor signal from the time domain into a representative frequency domain form by sampling the signal over a period. The FFT algorithm has been used for tool wear monitoring in CNC turning based

on comparing the frequency component between new tool and the degraded tool [176, 177]. The power spectral density (PSD) of a sensor signal explains the power present in the signal as a function of frequency. PSD can also be seen as computing the sum of FFT of a signal. The PSD techniques have been used to monitor motor conditions [178]. Table 2.6 lists the frequency domain features applied in monitoring machining from the various sensor systems.

2.5.3 Time-frequency domain methods

Time-frequency domain is a class of techniques to represent time and frequency domain elements together such as Short-time Fourier Transform (STFT), Wavelet Transform (WT), Wigner–Ville etc.

Short-time Fourier Transform (STFT)

STFT originated from Fourier Transform to represent non-stationary signals in both frequency and time domains. In STFT the time series data is segmented and frequency components of each segment is analysed using Fourier transforms as illustrated in Figure 2.23. Essentially STFT is local frequency representation of a signal over time [179]. The performance of STFT greatly depends upon the shape and size of the window employed. Longer windows give good frequency resolution while shorter windows give good time resolution. A choice of suitable window function (such as Hamming or Kaiser window) in STFT to represent the non-stationary stochastic signal can provide quick and accurate results.

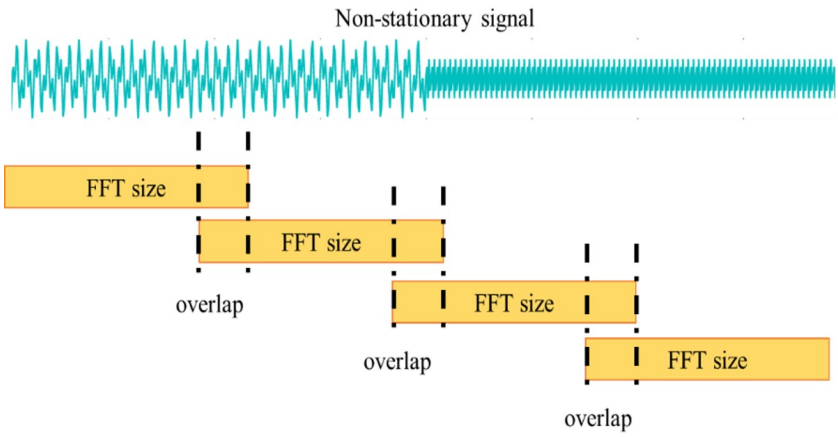

Figure 2.23: Window and overlap used in STFT analysis.

STFT is used to represent the degradation condition of the slew bearing from non-stationary vibration signals [180]. STFT has been also used to identify features for condition monitoring of grinding wheel wear from force signals [181]. STFT provides an excellent solution for correlating both elastic and plastic material removal mechanisms from single grit scratching experiments which can be used for controlling grinding dressing ratios as well as against deviation errors [182].

Discrete Wavelet Transform (DWT)

Wavelet transform is specially adapted for the detection of transient signals, i.e. signal components that last a short period and span a wide frequency range [183]. The main advantage of the wavelet transform is that it allows outstanding localisation in both the frequency and time domains via dilations and translations of the mother wavelet.

The Discrete wavelet transform is a type of the Wavelet transform operation using a distinct set of the wavelet scales (frequency) and translations. It confirms some distinct guidelines that decompose the signal into a mutually orthogonal set of wavelets. The translation and dilation operations applied to the mother wavelet are implemented to determine the wavelet coefficients, which corresponds to the relationship between the wavelet and a localized section of the signal. The discrete wavelet transform is derived from the discretisation of $CWT(i, j)$ as given by equation (2.11)

$$CWT(i,j) = \frac{1}{\sqrt{|i|}} \int_{-\infty}^{\infty} f(t)\Psi^*(\frac{t-j}{i})dt \tag{2.11}$$

$$DWT(i,j) = \frac{1}{\sqrt{2^x}} \int_{-\infty}^{\infty} f(t)\Psi^*(\frac{t-2^x y}{2^x})dt \tag{2.12}$$

where i and j are replaced by 2^x and $2^x y$ (x is the scale parameter, y is the non-negative integer).

The Discrete wavelet transform analysis breaks the signal into several components covering the complete frequency spectrum with various bandwidths. Discrete wavelet transform decomposes the data obtained into approximation coefficients (low-frequency) and detail coefficients (high-frequency) components. Discrete

wavelet transform coefficients can be obtained by filter-bank structure using Mallat (pyramidal) algorithm [184]. The approximation coefficients at subsequent lower levels are passed through a high-pass and a low-pass filter. The frequency bands of the filters are based on the sampling frequency (fs) and the upmost band, which relates to a level-one decomposition, covering between fs/2 to fs/4. This is followed by a downsampling by two to calculate both the detail coefficients (of the high-pass filter) and the approximation coefficients (of the low-pass filter) at a next decomposition level. Wavelet transforms have been used to monitor tool breakage and wear conditions in real time based on the sensed data from currents measured from the spindle and feed motor [185]. The multiresolution, sparsity and localization properties of wavelet transform can be used to monitor the tool state in realtime when combined with a appropriate decision making straetagy [186].

2.6 Intelligent modelling and decision-making mechanism

Theoretical models are very complicated to develop because of inadequate understanding of machining processes [187]. Decision-making strategies are one of the major issues in the development of performance prediction and monitoring of machining processes. Moreover, most prevailing theoretical models are restricted to very few measurable quantities and sensors. The use of soft computing modelling methods is reasonable as they counteract the incompetence, to understand and sufficiently illustrate the process mechanisms.

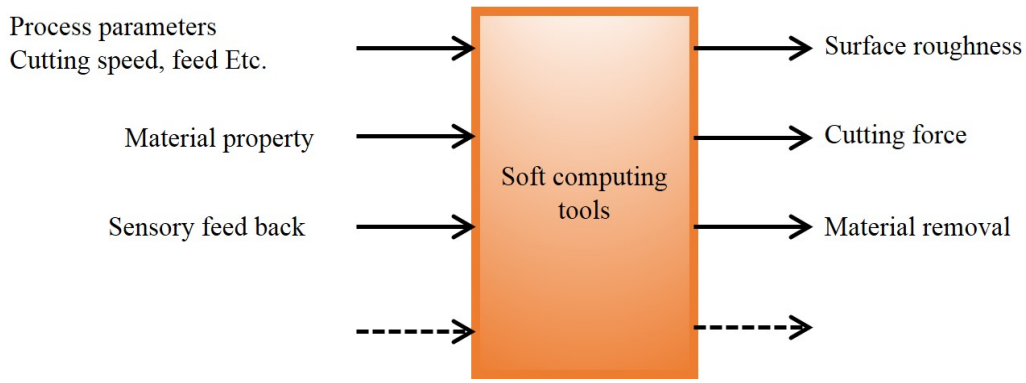

Figure 2.24: Applications of soft computing in machining performance prediction.

Performance prediction can be accomplished even though a large grey area is present between process conditions and human understanding using soft computing techniques as they can recognise patterns. Performance prediction of any machining process such as surface roughness, material removal, depth of cut etc. could be modelled [188] using regression techniques by correlation model to cutting parameters as shown in Figure 2.24.

Monitoring of machining process ranges from simple threshold limit value [189] being exceeded or statistical comparisons as listed in Table 2.7, to systems requiring supervised training and learning to determine the process characteristics of each machining condition. Figure 2.25 shows all the elements which are required for monitoring and control of machine tools, out of which the most critical element is methodologies for decision making [190].

Table 2.7: Previous work on machining state monitoring using thresholds, statistical comparison and visualisation.

Algorithm	Process	Process state	Reference
Thresholds	Turning	Tool wear	[189]
	Milling	Tool wear	[189], [68], [69], [92]
	Drilling	Tool wear	[189], [81]
	Grinding	Grinding wheel wear	[86]

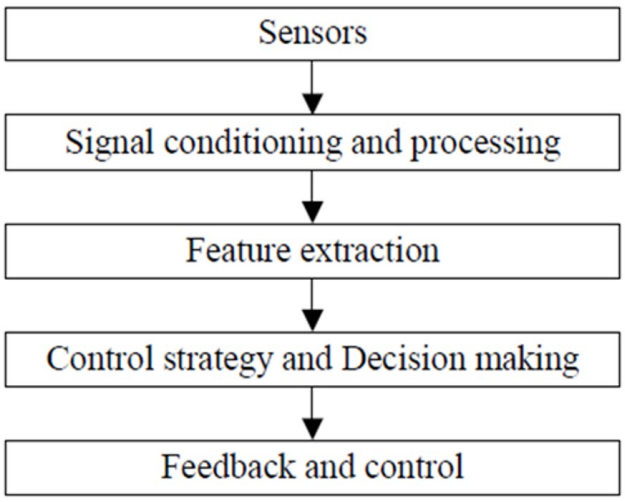

Figure 2.25: Components of a monitoring system [190].

A decision-making process in monitoring is based on the relationship between the process/tool conditions and the feature-bearing signals (monitoring indices). In

monitoring of modern automated machining systems, the soft computing methods play a primary role in the implementation of intelligent sensors and sensorial systems. Tool wear and surface quality have been significant indicators of machining performance and are also interrelated. The features extracted from indirect measurements such as cutting forces, vibrations or AE measurements can be more effective in modelling tool wear and surface quality than raw data when combined with decision-making strategies or soft computing techniques. Soft computing techniques process the signal features from indirect sensor data and accomplish a pattern association assignment, thereby establishing a correlation between the signal feature and appropriate monitoring process state.

Decision mechanisms based on soft computing techniques have already been applied successfully in developing monitoring systems. Several soft computing techniques such as artificial neural networks (ANN), expert systems called fuzzy logic systems and techniques based on hybridisation of these two techniques called neuro-fuzzy inference systems have been widely used in the past for modelling and monitoring machining systems. Among the enormous number of soft computing approaches that have been created in the past on monitoring the conditions of machining state, ANN has frequently been used followed by fuzzy sets as shown in Figure 2.26.

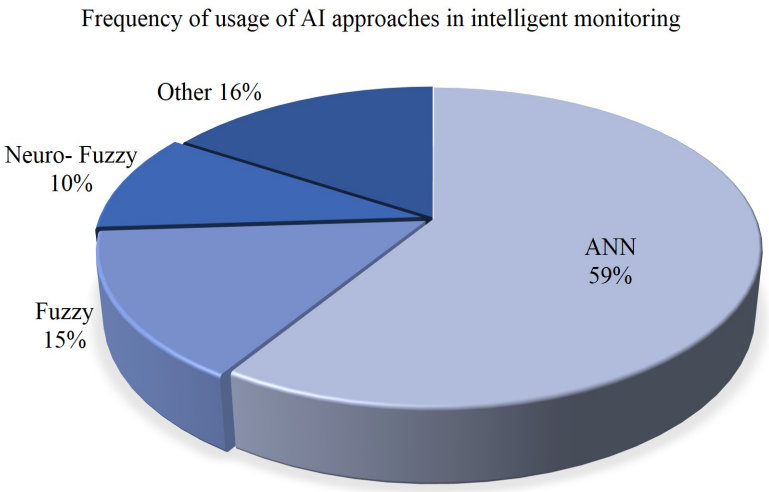

Figure 2.26: Frequency of usage of soft computing in intelligent monitoring [95].

The choice of soft computing techniques depends primarily on previous knowledge of the process, sensor signals data features, monitoring purpose and the experi-

mental data set. Among a large number of decision-making methods that have been developed, Neural Networks (NN) have been applied mostly to monitoring tasks in turning, milling, drilling, and other metal cutting processes compared to other decision-making methods. Previous works on surface quality prediction and tool wear monitoring using ANN on a range of cutting processes are listed in Table 2.8.

During training, neural networks map points in the input space to output space by modifying the weight component in the connections between neurons. The effectiveness of NN modelling based on approaches such as back propagation neural network and feedforward neural network for predicting surface roughness has been proved in hard cutting [138,191–194]. ANN is generally used when the knowledge of the process is not known. ANN is known for their predictive accuracy and also for their excellent generalisation capability. However, they possess an inherent disadvantage as the knowledge acquired and the patterns recognised cannot be extracted and it more or less behaves as a black box model.

Table 2.8: Machining operation monitoring using ANN.

Algorithm	Process	Process state	Reference
Neural	Turning	Tool wear	[195], [196], [197], [198], [199], [200]
		Surface roughness	[196], [201], [202], [194], [187], [203], [204]
		Dimensional accuracy	[181], [181]
	Broaching	Tool wear	[205]
	Milling	Surface roughness	[206], [207], [208], [209], [196], [142]
		Tool wear	[71], [196], [210], [211], [212]
	Abrasive waterjet	Surface roughness	[213]
	Drilling	Surface roughness	[214], [215]
		Tool wear	[216], [217], [218],
	Grinding	Surface quality	[161]
		Tool wear	[219], [87], [220]

Compared to NN, there are a lesser number of applications of fuzzy sets for the prediction of machining performance from literature. Fuzzy inference systems are applied when there is enough knowledge and understanding of the process. In general, fuzzy inference systems are applied for surface roughness and tool wear prediction as listed in Table 2.9. The advantage of the fuzzy systems over neural

networks is that the acquired knowledge could be extracted. Though the human knowledge could be transferred to the model, the methods of transferring to the model are insufficient. To take the advantages of both neural network and fuzzy set a hybrid technique called neuro-fuzzy systems were introduced. A typical neuro-fuzzy system eradicates the fundamental problem in fuzzy if-then rules by exploiting the learning competence of an ANN for automated optimisation of fuzzy if-then rules during training. A significant advantage of such a hybrid approach is that the knowledge of the model could be obtained from ANN which was not possible when it was used standalone [221]. Previous works on surface quality prediction and tool wear monitoring using the neuro-fuzzy system on cutting processes are also listed in Table 2.9.

Table 2.9: Machining operation monitoring using fuzzy and neuro-fuzzy.

Algorithm	Process	Process state	Reference
Fuzzy	Turning	Tool wear	[222] , [223]
		Surface roughness	[224], [225]
		Dimensional accuracy	[226]
	Milling	Tool wear	[227], [228], [72], [229]
		Surface roughness	[230], [231], [232] , [233], [234], [235]
	Grinding	Surface quality	[236], [237], [238]
	Drilling	Tool wear	[239]
Neuro-fuzzy	Milling	Tool Condition	[240], [241], [242]
		Surface roughness	[243], [244]
	Turning	Surface roughness	[245]
		Tool wear	[80], [246]
	Grinding	Wheel condition	[87], [247]
	Deburring	Surface quality	[248]
	Abrasive waterjet	Surface roughness	[249]

Apart from these decision mechanisms some of the efforts were made as listed Table 2.10 to predict machine and machining status using Support Vector Machines (SVM), Hidden Markov Models (HMM's) [250, 251] and Decision Trees (DT) based soft computing paradigm. SVM is a collection of supervised machine learning algorithm that has a robust methodological approach for cracking nonlinear problems [252]. The nonlinear problems can be solved by applying a kernel function trick. The data is mapped onto a high-dimensional feature space where the linear

formulation can be derived from the non-linear from by indirectly mapping feature space and finally train them. SVM posses properties such as generalisation ability, free adjusting parameters, and no requirement for experimentation to find the learning machine architecture, which enables it to exploit highly nonlinear problems with ease [253].

Table 2.10: Machining operation monitoring using SVM, HMM's and DT.

Algorithm	Process	Process state	Reference
Support vectors	Milling	Tool wear	[254], [255], [256]
		Surface roughness	[257], [258], [259]
	Milling	Tool wear	[260]
		Surface roughness	[261]
	Broaching	Surface quality	[85]
	Grinding	Wheel redress-life	[181]
		Tool wear	[253]
HMM's	Milling	Tool wear	[262], [263]
	Drilling	Tool wear	[83]
	Turning	Tool wear	[79]
	Grinding	Wheel condition	[264]
Random Forest	Milling	Tool wear	[75]
Decision Trees	Turning	Tool wear	[265], [266]

Random Forests (RF) operate by constructing a multitude of decision trees. One of the most significant advantages of RF over DT is that the algorithm works on bootstrapping [267]. Decision trees tend to be prone to over-fitting. RF creates a lot of individual DT's by re-sampling the data many times with replacement and makes the final prediction at a new point by averaging the predictions from all the individual binary regression trees on this point. Averaging over all the decision trees results in a reduction of variance thereby enhancing the accuracy of the prediction. The process dependent behaviour of the surface quality, material removal and tool wear mechanism besides the numerous uncontrollable variables make it impossible to find an up-front solution without an empirical prediction model in monitoring its states in real time. The empirical model discussed in this section will suffice to build an intelligent system intended in this thesis. Apart from accuracy, it is to

be noted that the computational time plays a significant role in the choice of the decision-making algorithms or soft computing techniques.

2.6.1 Computer vision and deep learning

Recent advancements in image classification based on computer vision show promising possibilities in developing a cost-effective intelligent system to classify the various stages of weld seam removal. R. Shanmugamani *et al.* [268], studied varies defects such as normal wear, corrosive pitting, rust and erosion in gun barrel based on image processing and machine learning algorithm. In this study, various image segmentation techniques and various machine learning algorithms were extensively studied, and reported that SVM provides the best possibilities for developing visual inspection system. X. Zhang *et al.* [269], carried out a study to develop a multiclass classification inspection system for surface grinding and polishing. In this investigation, image features are extracted through various methods including statistical parameters Gabor filter bank, Laws-filter bank and fed into SVM classifier for image classification. G.S. Kumar *et al.* [270] studied the defect in metal inert gas (MIG) welding joints, where they implemented average grey value as the feature vector and back propagation neural network as the classifier. They classified four different zones of welding joints. Lashkia proposed a methodology based on fuzzy algorithm to detect the small objects by using Xray images [271]. Chongjian *et al.* [272] studied penetration control in aluminium alloy welding where they utilised combined wavelet transform and canny operator to detect the edges. They used piecewise curve fitting for recovering the weld pool edge and developed a controller to control penetration in welding. Ravikumar *et al.* [273] developed a surface crack inspection system to identify various cracks such as minor scratches and deep scratches on mild steel sheet metals. In this study, histogram-based features are extracted from the images and Nave Bayes and DT algorithms were used as the classifier. They reported that histogram based features and DT algorithm showed the potential for being a good candidate for visual inspection system [273]. J. Hongbin *et al.* [274] implemented SVM to identify the defects in a hot rolling process based on features extracted by implementing rough filtering algorithm. H. Zheng *et al.* [275] developed an artificial intelligence system to identify the defects on a metallic surface based on morphology

and genetic algorithms (GA). They also reported that manual selection of feature vectors does not reflect the structural defects due to the complexity of the structural defects.

Though numerous studies are developed, weld seam removal inspection study is hardly found in literature. Moreover, developed inspection systems are based on image processing and machine learning classification algorithm such as SVM, ANN, GA. Recent advancement in deep learning (Convolution Neural Network - CNN) has outperformed all of the classical machine learning algorithms due to its ability of processing raw input images rather than feature vectors [276]. Convolution neural networks known as CovnNets are bio-inspired ANN developed on mathematical representation to analyse visual imagery, pattern recognition and speech recognition. The fundamental design principle of CNN is tailoring the architecture and a learning algorithm such way that it reduces the number of free parameter without compromising the computational power of learning algorithm [277]. As the name refers, it consists of linear mathematical operation of convolution followed by non-linear activators, pooling layers and deep neural network classifier. Unlike machine learning, convolution neural networks can be fed with raw image pixel values rather than feature vectors as input as shown in Figure 2.27 [276].

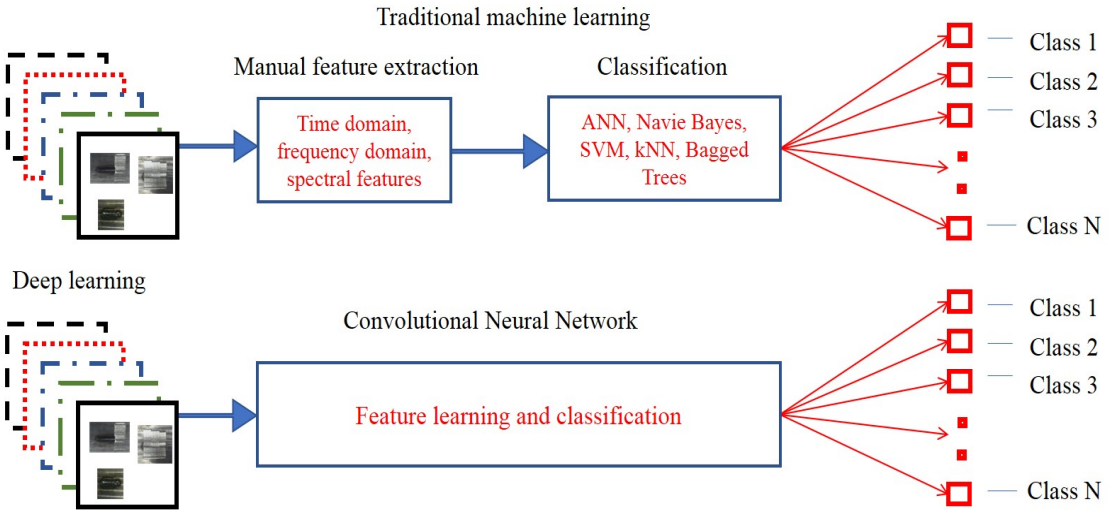

Figure 2.27: Comparison between traditional machine learning and convolutional neural network.

The convolution processes act as appropriate feature detectors that demonstrate the ability to deal with a large amount of low-level information. A complete convolu-

tion layer has different feature detectors so that multiple features can be extracted from the same image. A single feature detector is smaller in size as compared with the input image and is slid over the image for the convolution operation. All the units in that feature detector share the same weight and bias which gives the properties of invariance to transformation and shift of images [278]. Local connections between the pixels are used many times in a the architecture. Using local respective field, neurons can extract the elementary features such as the orientation of edges, corners and end points. So that higher degree of complex features are detected in hidden layers when it is combined. These functions of sparse connectivity between subsequent layers, parameter sharing of weights between the adjacent pixels and equivalent representation enable CNN to use efficiently in image recognition and image classification problems [279]. The typical architecture of ConvNets consists of several layers. There are convolutional layers, pooling layers and fully connected dense layers [279] and model accuracy depends dramatically on the influence of the selection of a set of hyperparameters [280, 281]. The advancement in computer vision and the CNN's are widely used in many application such as trend prediction [282,283], image recognition [284], cancer cell classification, medical image processing application, star cluster classification, and self-driving cars [285, 286].

2.7 Identified gaps and proposed research directions

The literature review discussed in this chapter identifies areas in modelling and real time monitoring of the belt grinding process that are to be bridged. There is only limited understanding of the influence of process variables in belt grinding process and the development of a material removal model.

- The amount of material removed relies heavily on the distinct local contact conditions, which is completely influenced by the state of the grinding parameters. Though the removal of material and surface quality in the belt grinding process can be written as a function of several parameters, their influence, interaction and the magnitude of contribution to material removal and surface quality have not been adequately reported in the literature.

- Most of the efforts on developing local material removal models have concentrated on simulating the contact condition of the tool and surface. These local models have ignored the granularity parameter of the belt tool and have made assumptions during the development of material removal model. Efforts involving in developing material removal model with granularity parameter without any assumptions have not been reported yet. Incorporating parameters with minimum assumptions help in developing a conclusive material removal model. A systematic approach to mathematically model material removal considering all the parameter by means of predictive modelling using soft computing regression techniques has not been reported yet which will be bridged in this thesis.

Developing a real time monitoring system will enable in achieving Industry 4.0 values. Two areas have been identified in real time monitoring of the belt grinding process and are listed below. Virtual metrology with the help of smart sensors adds value for the whole manufacturing process and can provide feedback to the process in real-time.

- Most of the previous research work on tool wear monitoring was on hard tools with defined cutting edges and rigid grinding tools using sensors and decision-making algorithm. As coated abrasives do not regenerate the grains and their performance solely depends on the granularity of the abrasive grains monitoring their degradation with cycle time is important. Principally, the fundamental aim is to determine whether a belt tool is underutilised or overused and is due for a replacement which has practised in the industry based only on the operator experience. Developing a methodology for condition monitoring and predicting tool wear in a compliant belt grinding process in real time will help in empowering the manufacturing line and also in optimising the process. A suitable waveform data analysis using time-domain features and frequency domain features are to be extracted that can correlate with belt tool condition. Furthermore, a suitable supervised machine learning algorithm to predict the tool wear state using these signal feature should also be explored.

- Though belt grinding is optimised by incorporating it to robot arms in highly sophisticated machining cell, the weld seam is still removed by the manual

operators and still requires the operators expertise. Involving manual operators severely affects the process quality, consistency, and decreases the level of safety. Additionally, manual belt grinding process to remove weld seam is also time consumptive as the components have to be moved from automated production lines to the manual machining station and vice versa. For ensuring a thoroughly industrialised time-intensive weld seam removal work, it is vital to construct a prognostic system that can oversee the weld seam removal in real time. The recent development in artificial intelligence can be involved in developing well sophisticated and highly efficient method to automate weld seam removal in a robotic environment. A reliable real-time weld seam removal detection system using smart sensors and artificial intelligence has to be developed and will be presented in this thesis.

This thesis aims to fill these gaps presented in section 2.7 and the work is reported in five chapters of this thesis.

Chapter 3

Process parameters analysis

3.1 Introduction

The surface finishing and stock removal in complicated geometries is the principal objective for grinding with compliant abrasive tools. Abrasive grinding is a widely employed finishing process, with abrasive grains as the cutting edge to accomplish close tolerances and excellent dimensional correctness and surface integrity. The polymer wheel in the tool enables the grinding process to machine free-form surfaces [11].

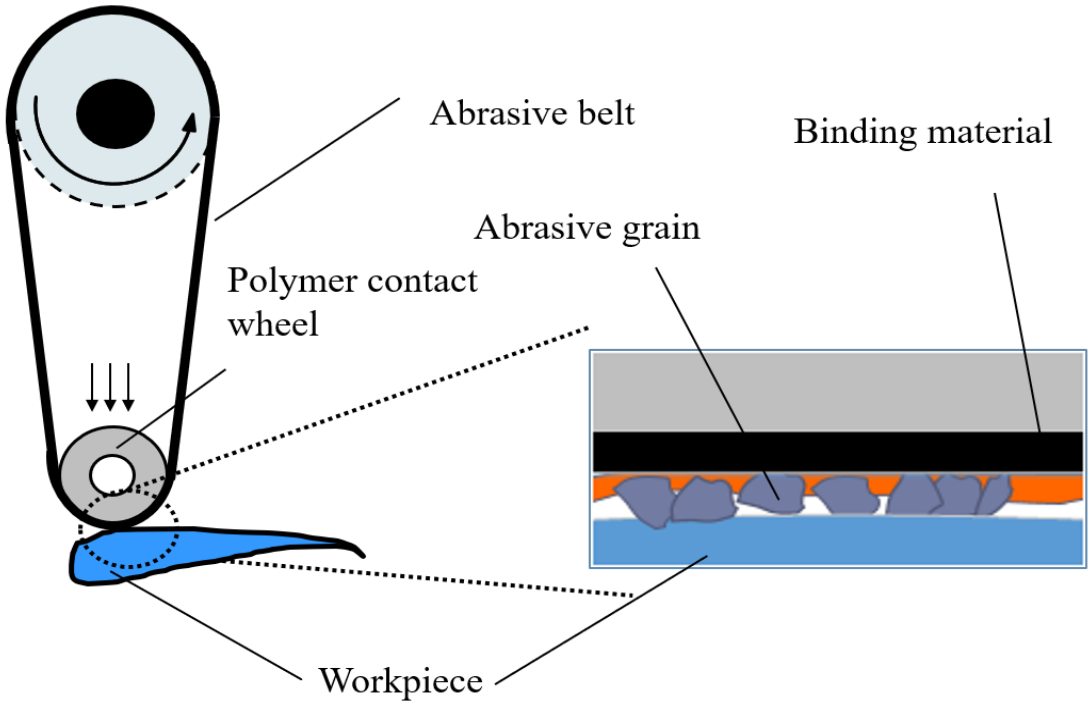

Figure 3.1: Principle of belt grinding process.

Understanding belt grinding process is a problem in industries as it is complex and nonlinear. Behavior of the belt grinding tool is dependent on contacts between the workpiece and the belt tool as shown in Figure 3.1. Most industries operate the belt grinding process based on empirical rules and experience of the operator. This makes it fundamental, to look in more detail at the process parameters/ variables that affect the material removal and surface quality. Changing these process variables will affect the performance of the process, so it is essential to look for the variables that affect the performance the most.

The presence of multiple parameters working in different regimes creates a dynamic condition which is not entirely well understood. Though the stock removal and surface quality in the belt grinding process can be written as a function of several parameters, influence and interaction of these paramaters have not been reported in the literature, this will be covered in this chapter.

Only limited studies have focused in understanding the parametric effects on contact conditions i.e., pressure distribution in the belt grinding process. A dynamic pressure sensor is used to study the parametric effects affecting the pressure distribution in this research. Pressure distribution study will help to understand the effect of individual levels of each process variable affecting the contact conditions.

A systematic approach to analyse process parameters using orthogonal arrays of Taguchi and Analysis of Variance (ANOVA) on the depth of cut, i.e., metal removal rate and surface roughness (R_a), i.e., surface quality in a customised belt grinding setup is discussed in this chapter. Taguchi methods have been widely utilised in engineering analysis to obtain information about the behaviour of a given process [287]. The Taguchi's Design of Experiment (DoE) is used for significant reduction of experimental runs and to identify the prominence of belt grinding parameters along with their inter-relation. Furthermore, the material removal and surface quality DoE trial result are then analysed using ANOVA, which is a statistical based analysis employed to indicate the individual impact of process parameters on the process output that comprises the depth of cut and surface roughness in our case and helps in predicting the significance of all factors and their interactions [288].

This chapter presents the relationship between the abrasive belt grinding parameters on the depth of cut for developing a comprehensive material removal model.

3.2 Experimental setup

A hand held abrasive belt sander, as shown in Figure 3.2, is customised with a fixture designed to be used as a belt grinding tool. A belt sander is an electrically powered abrasive belt tool that can be run at variable speeds. The contact wheel is made up of Ester polyurethane polymer of different Shore A hardnesses as shown in Figure 3.2.

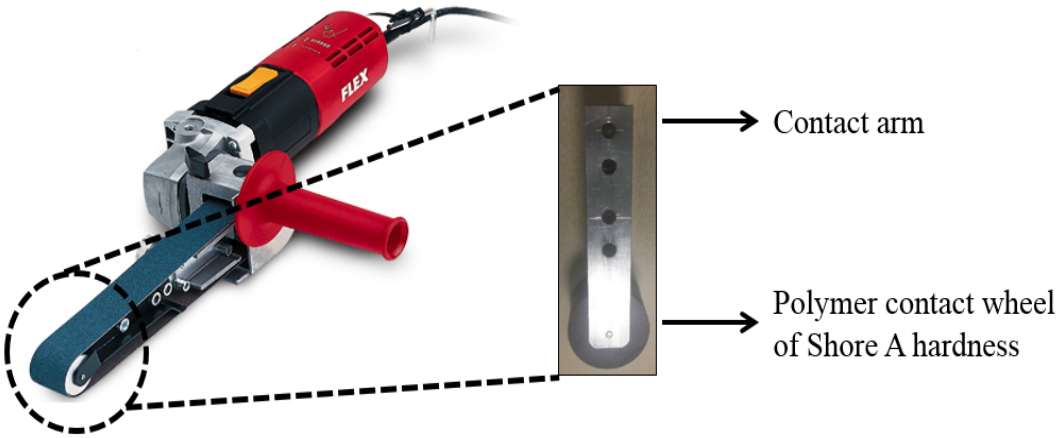

Figure 3.2: Belt sander customised to perform grinding experimental trials.

The use of robots or multiple-axes machining centres improves the finishing efficiency. The experimental trials were conducted on coupling the belt sander and an ABB 6660-205-193 multi-axes robot using a suitable fixture, as shown in Figure 3.3. The robot has a serial arm structure, powerful gears, and motors for handling fluctuating process forces prevalent within applications such as milling, deburring, and grinding. An ATI force sensor (Omega 160) connects the belt sander and the robot arm end effector. This is accomplished by mounting the force sensor to the robot end-effector and then attaching the customised belt grinding tool to the force sensor, as shown in Figure 3.3. The robot controller continuously receives the force/torque signal, compares it with the users input, and compensates the force to ensure that the force exerted is maintained. The robot arm is primarily used for toolpath control and force control.

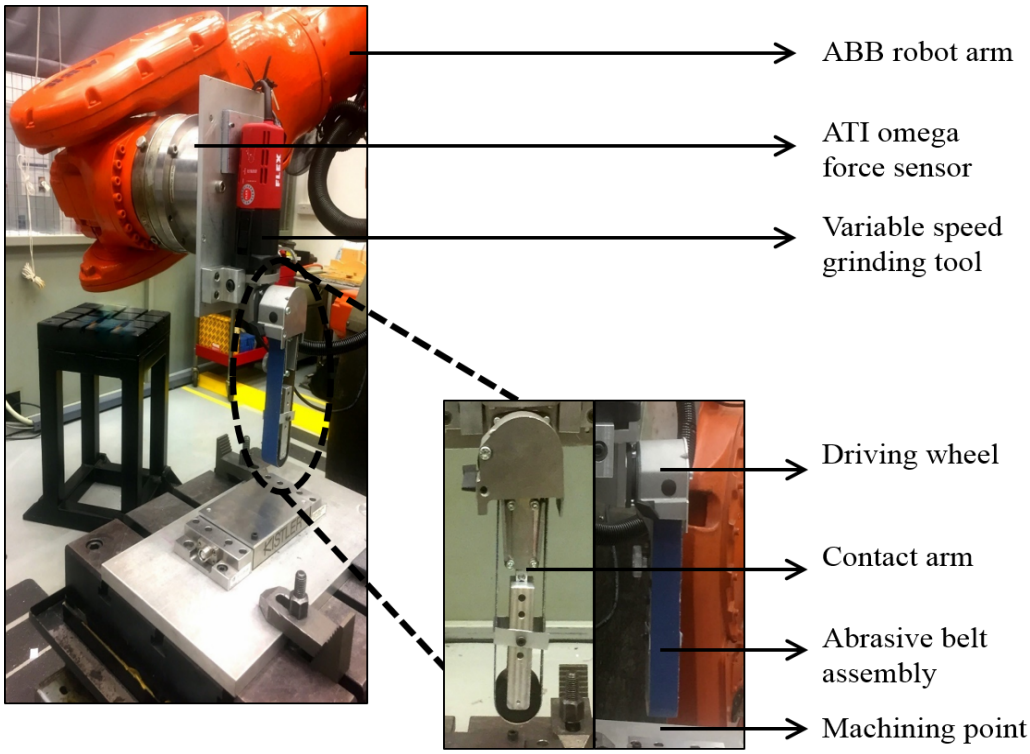

Figure 3.3: Experimental setup for compliant abrasive belt grinding.

3.2.1 Toolpath planning

Force control is essential for avoiding over and under-cutting of the material. Force control is particularly used for uniform material removal along the whole toolpath. Such an adaptive tool for path generation in the system was realised with (ATI Omega 160) force control in the experimental trials. A constant contact force in the normal direction (Z-axis) throughout the process is achieved by using a force sensor (ATI Omega 160). The force sensor maintains an adequate in-feed in the normal direction. Tool path planning has five different zones, as shown in Figure 3.4.

Zone A and Zone B are when the abrasive belt tool enters the machining region, zone C is where the actual machining happens in force control mode, and zones D and E are where the abrasive belt tool exits the machining region. ABB robot studio executes tool path planning. Most belt grinding processes are performed for complicated geometries, where maintaining uniform material removal can be realised only when tool centre point (machining end) interacts with the surface normally. This approach is the current industrial practice employing highly automatic robotic arm manipulators.

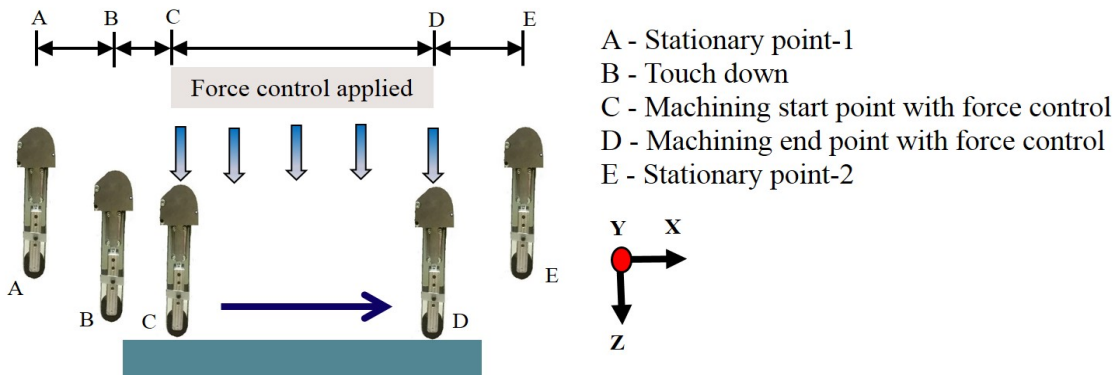

Figure 3.4: Toolpath planning in force control mode by ABB robot studio.

3.3 Pressure film test

Based on the author's knowledge, only limited studies have focused on understanding the parametric effects affecting the contact conditions of the belt grinding process concerning pressure distribution or material removal. The parameters such as RPM, feed rate, force and rubber hardness that influence the contact conditions were investigated by studying pressure distribution patterns during actual machining using a dynamic pressure sensor. Three levels of input for each parameter was considered as listed in Table 3.1.

Table 3.1: Belt grinding parameters and their levels.

Parameter	Unit	Levels		
		L1	L2	L3
RPM	(m/min)	250	500	700
Feed	(mm/s)	10	20	30
Force	(N)	10	20	30
Rubber hardness	(Shore A)	30	60	90

The experimental setup consisted of the ABB robot, customised electric grinder, and pressure sensing system as shown in Figure 3.5. ABB robot arm is used mainly for toolpath control which constrains the tool centre point (machining end) normally with the interacting surface. The experimental trials were accomplished by fastening the belt grinder to the robots end-effector imparting a constant force and uniform contact throughout the pressure sensing trials in the normal direction (Z-axis) using

the force sensor (ATI Omega 160). Static pressure films have the inherent disadvantage of not capturing the pressure distribution in real time. Therefore, dynamic pressure sensor is used in this study as they are capable of capturing the pressure distribution in real-time.

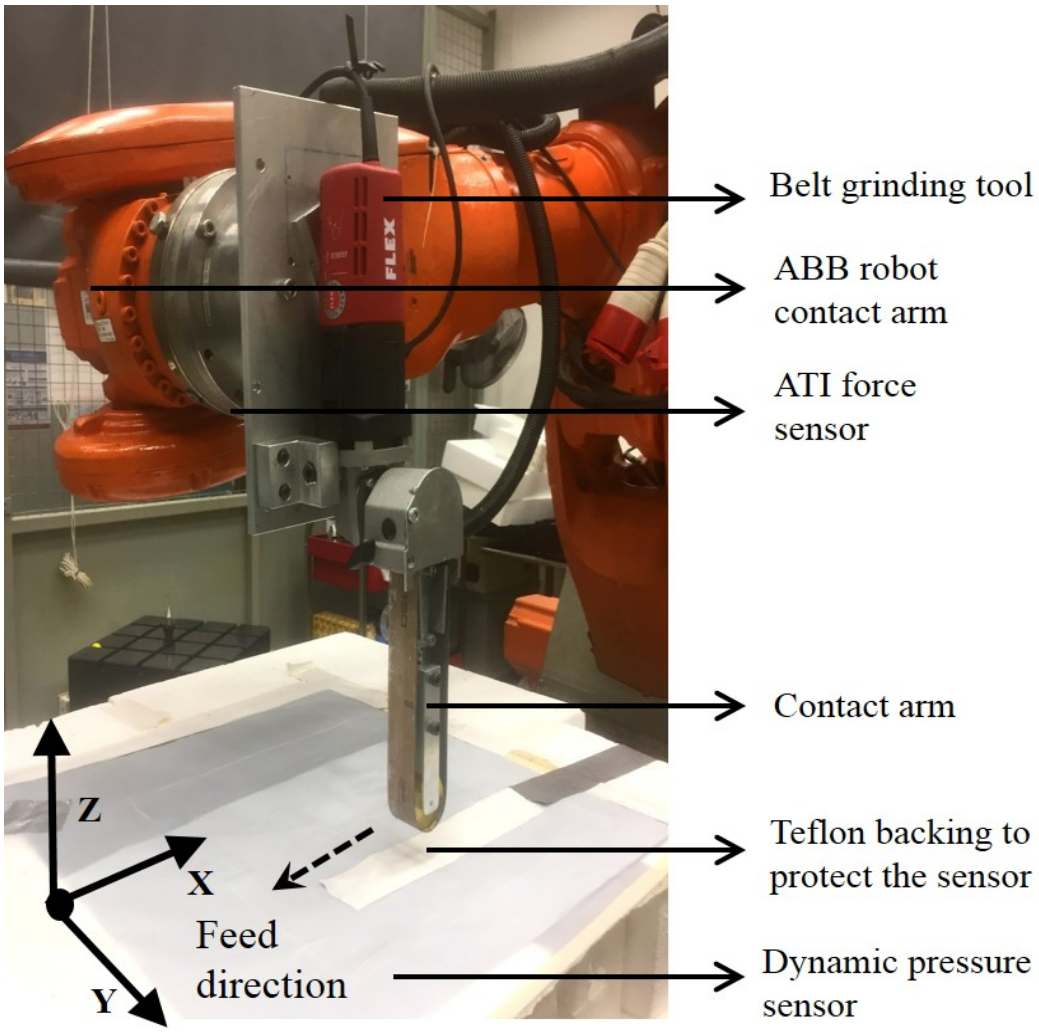

Figure 3.5: Dynamic pressure sensing setup.

The working temperature range of the pressure sensor was between $10°C - 40°C$ which is well below the temperature generated during the actual belt grinding process. As a result, grit parameter was not considered for the dynamic pressure sensing test. Moreover, using belt with abrasive grains can damage the pressure sensor during operation. Therefore, experiments were performed only with nylon backing material of the commercially available belt.

3.3.1 Dynamic pressure sensor

The X3 IX500:128.128.10 dynamic pressure sensor is used to measure the pressure distributions over a contact area during the experimental trials in real time. Pressure sensing measurement is made with a tough urethane cover with 16,384 sensing points and 2.54mm pitch (resolution) [289]. The pressure sensor consists of a capacitive transducer comprising two parallel plates that are separated by air or dielectric medium. The change in distance results in a resultant change in capacitance. The change in capacitance is directly related to the pressure applied to the capacitor as shown in Figure 3.6.

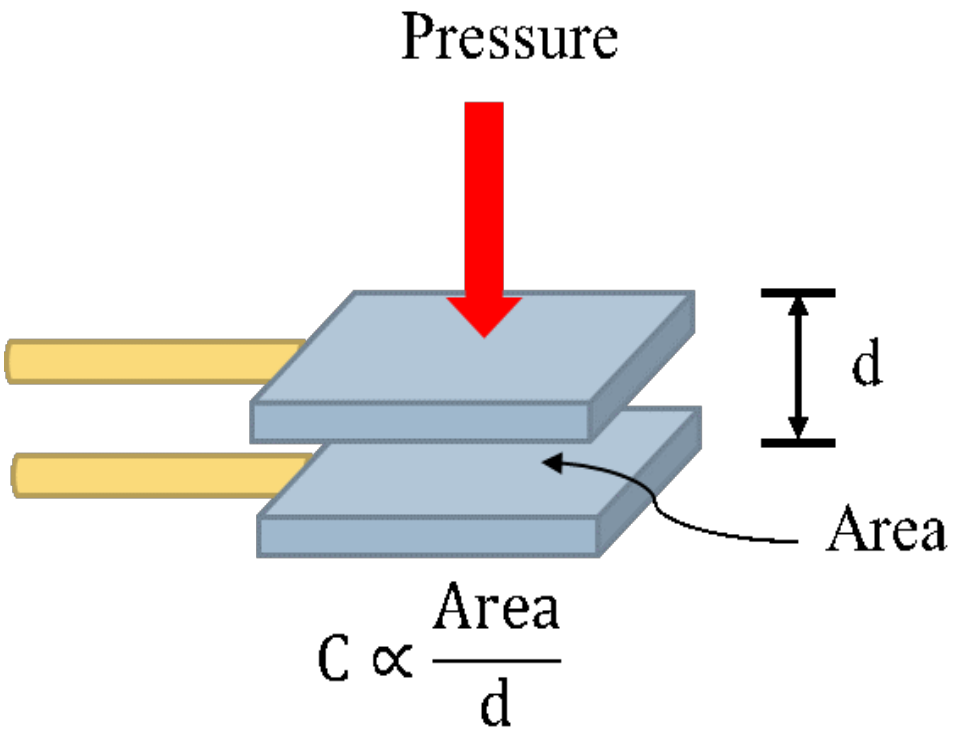

Figure 3.6: Working principle of dynamic pressure sensor [290].

Multiple arrays of pressure sensing variable capacitors from input pulses are then signal conditioned into image data. The pressure sensor has a spatial resolution of 2.54 mm and sensing area of 32.5 cm x 32.5 cm. The pressure sensor has eight frames/s output with withstanding pressure threshold of 30 Bar. The pressure pad is placed on the flat aluminium work coupon and secured to the surface to avoid displacement during the contact of the grinding wheel as shown in Figure 3.7.

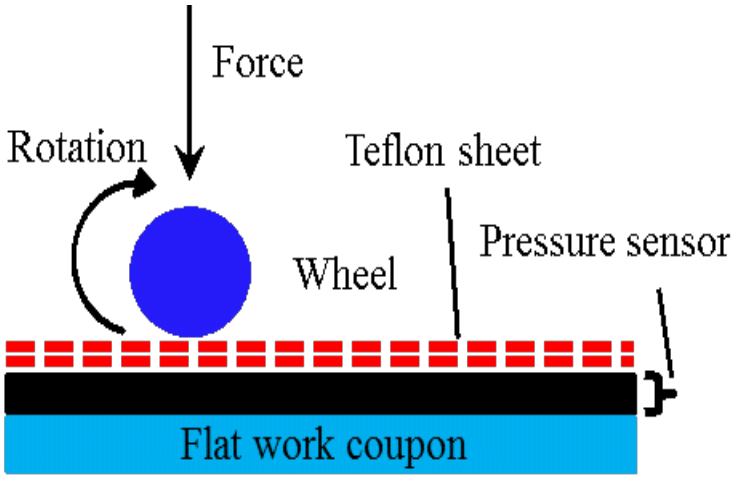

Figure 3.7: Schematic diagram of the pressure sensor.

Table 3.2: Dynamic pressure test input conditions.

Trial	RPM (m/min)	Feed(mm/s)	Force (N)	Hardness (Shore A)
Trial 1	250	20	20	60
Trial 2	500	20	20	60
Trial 3	700	20	20	60
Trial 4	250	10	20	60
Trial 5	500	20	20	60
Trial 6	700	30	20	60
Trial 7	250	20	10	60
Trial 8	500	20	20	60
Trial 9	700	20	30	60
Trial 10	250	20	20	60
Trial 11	500	20	20	30
Trial 12	700	20	20	90

Extra care is taken by isolating the pressure pad contact with the worktable to avoid electronic interferences in the parallel plate capacitor due to metallic objects. The pressure pad sensor surface is protected using a Teflon sheet as the abrasive belt rotates at higher speed. Effect of the Teflon sheet on the sensor is not significant as the sheet weight was negligible. The pressure data were recorded during the grinding experimental trials in real time and later retrieved for post analysis. The experimental layout for finding the correlation between the three levels considered for each parameter is identified based on the contact conditions is provided in Table 3.2.

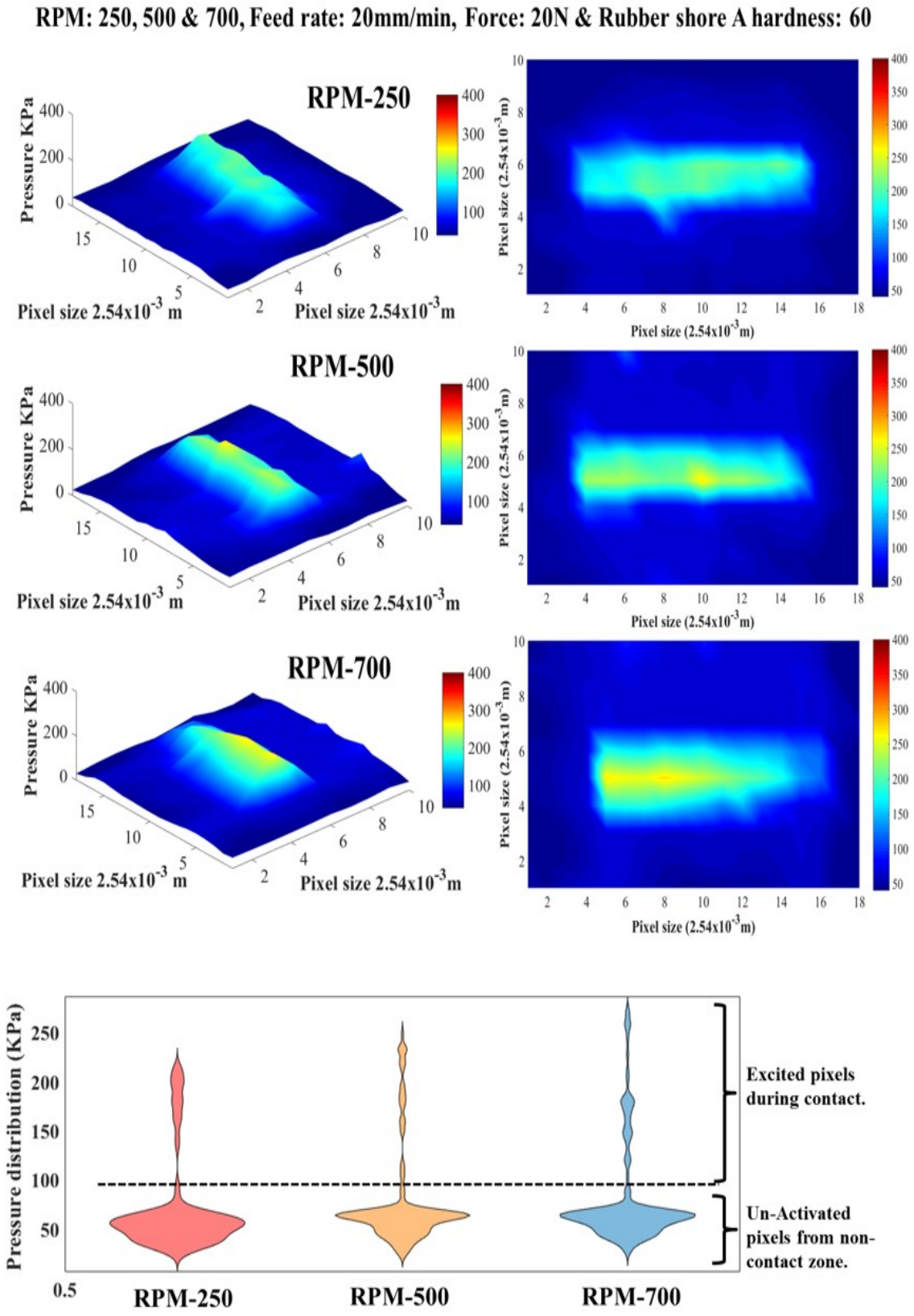

Figure 3.8: 2D, 3D and violin plot comparison of pressure distribution PSI with change in RPM and constant rubber shore A hardness, feed rate, force.

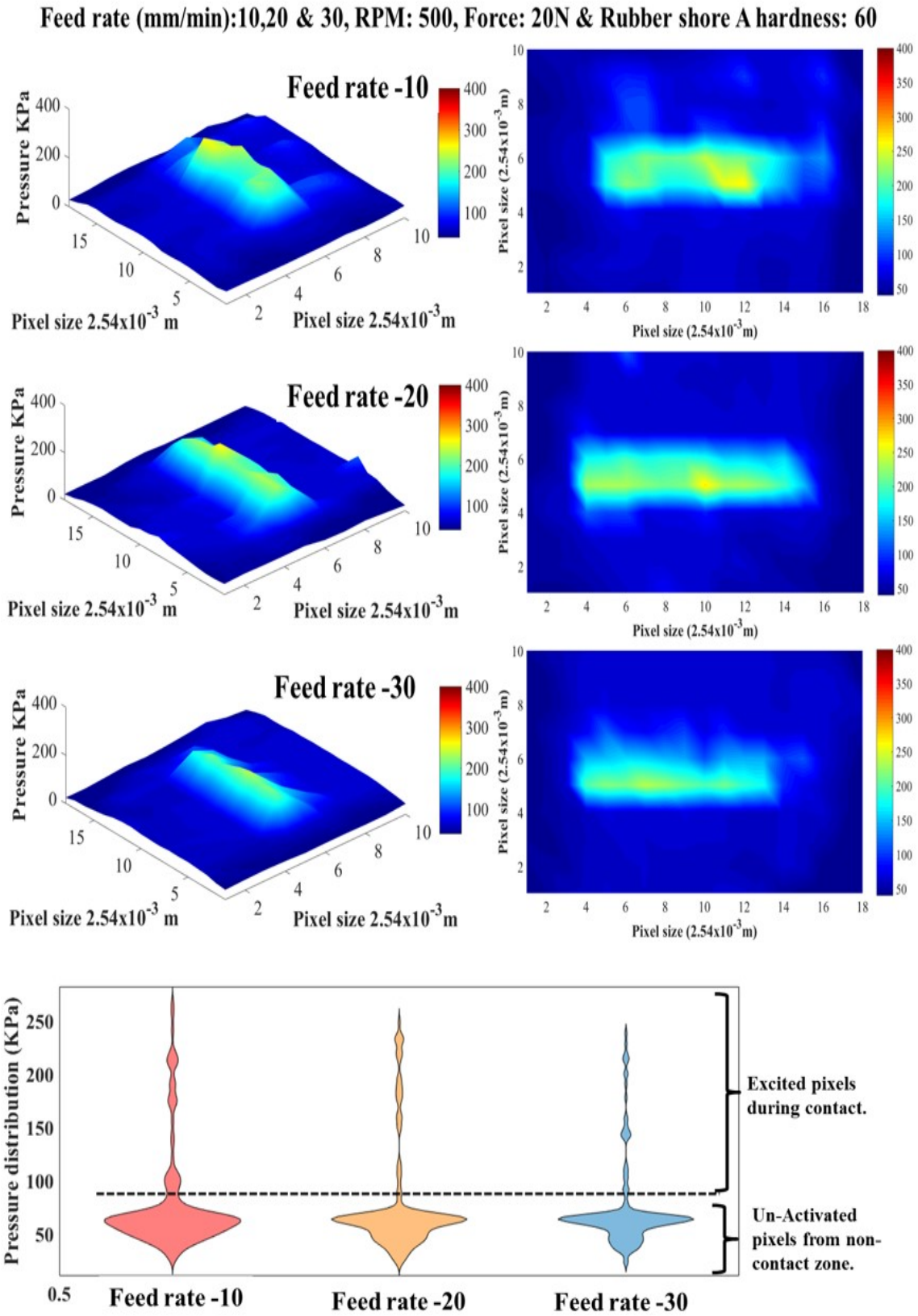

Figure 3.9: 2D, 3D and violin plot comparison of pressure distribution PSI with a change in applied feed rate and constant RPM, force, hardness.

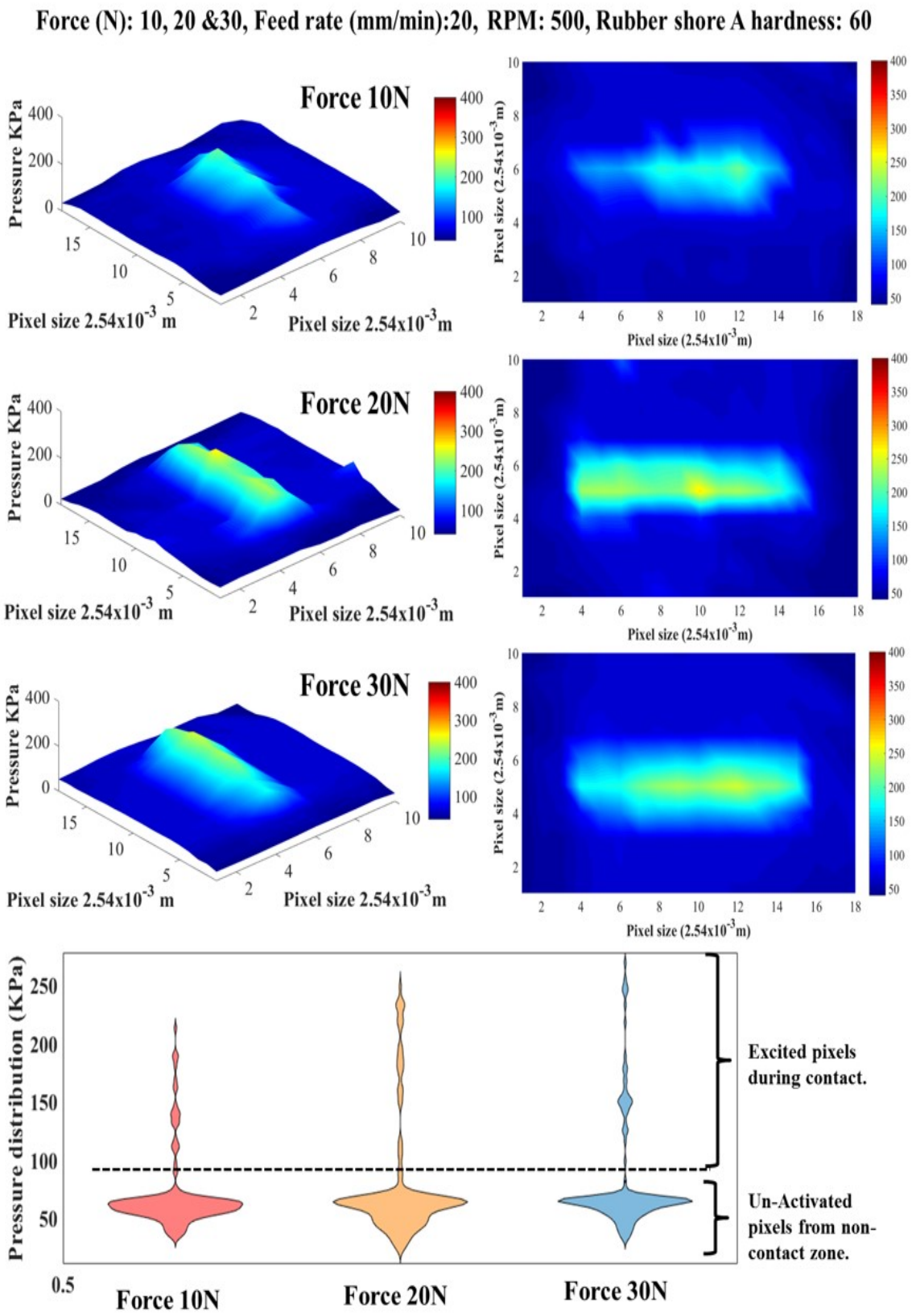

Figure 3.10: 2D, 3D and violin plot comparison of pressure distribution PSI with change in applied force and constant RPM, feed rate, rubber shore A hardness.

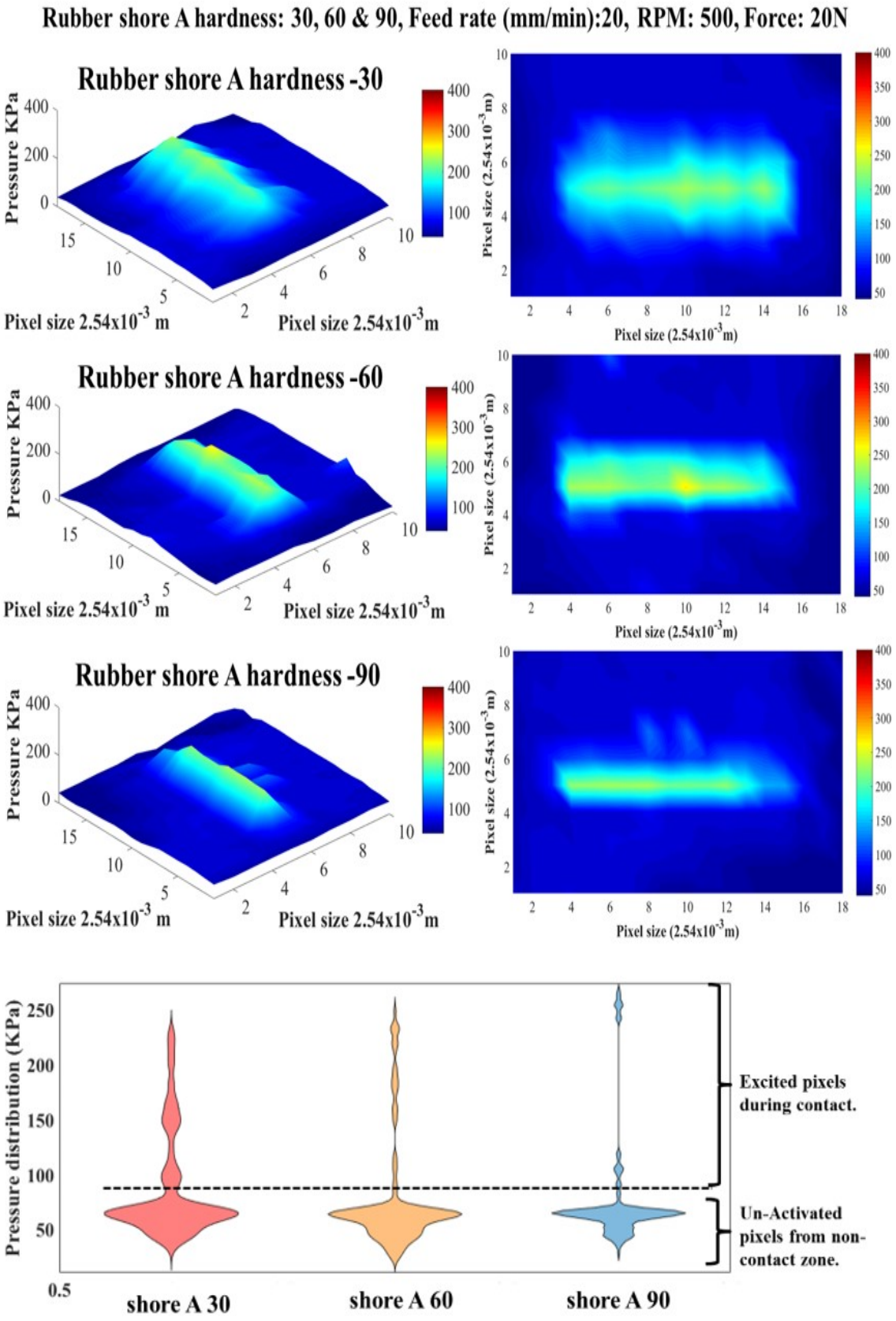

Figure 3.11: 2D, 3D and violin plot comparison of pressure distribution PSI with a change in rubber Shore A hardness 60, 30, 90 and constant RPM, feed rate, force.

Trials were made by varying the parameter under study while keeping the other three parameters fixed at a constant value. Constant values for the remaining three parameters were taken from level 2 from the respective parameter. First three trials have the RPM changed with a constant feed, force, and hardness. The same approach is applied for feed, force, and hardness in subsequent trials. The contribution of each parameter to the material removal based on the contact conditions and pressure distribution are analysed and explained in Section 3.3.2.

3.3.2 Results and analysis

The abrasive belt grinder used in the experimental trials had its contact wheel making a contact length of 24mm. Violin plot is also used to represent the change in density estimates of the pressure distribution for varying the levels of each parameter. As the Violin plots can show the probability density of the data at different values, they were used to show significant details as how pressure data values are distributed along the contact region.

Trials 1, 2 and 3 were used to correlate the relationship between the levels of RPM. Based on the RPM levels 250, 500 and 700 it was found that pressure distribution increased with increase in RPM as shown in Figure 3.8. The contact pressure intensifies when the number of the interactions between the polymer wheel and surface due to the rotation of the polymer wheel per unit time gets maximized. Analysis of pressure distribution for three different RPM's of 250, 500 and 750 suggests that material removal is directly proportional to the cutting speed (grinding rate) of the polymer contact wheel. The width of the violin plot for a lower RPM suggests that pressure distribution are equal among all excited pixels in pressure sensor along the contact region. However, this trend gets peaked with increase in RPM suggesting pressure distribution are unequal among along the contact region.

Pressure distribution results from trials 4, 5 and 6 were used to correlate the relationship between the levels of feed rate. Based on the feed rate levels 10 mm/s, 20 mm/s and 30 mm/s it was found that pressure distribution decreases with the increase in feed rate as shown in Figure 3.9. Contact pressure increases with a higher dwell time of interaction between the polymer wheel, and workpiece surface, i.e., contact pressure pattern is inversely proportional to the feed rate. The width of the

violin plot from Figure 3.7 for different feed rate suggest that pressure distribution are unequal among all excited pixels in pressure sensor along the contact region.

Figure 3.10 shows the pressure distribution variation in force with constant feed, force, and hardness as represented by Trials 7, 8 and 9. 10 N has no significant impact on machining as we could see the pressure exerted on the surface is very low compared to 20 N and 30 N. Adequate force penetrates deeply into the workpiece to achieve grain cutting depth resulting in high-pressure distribution proportional to applied force. From the visual analysis of Figure 3.10, it was evident that pressure distribution increased with increase in force imparted.

Analysing the 2D and 3D plots extracted in Figure 3.11 from experimental trials 10, 11 and 12 by varying the levels of hardness suggests that the pressure concentration increased with increase in hardness of the polymer wheel. However, the distribution pattern area was observed to be inversely proportional. The width of the violin plot for softer wheel suggests that pressure distribution is equal along the contact region but unequal when the hardness increases. The pressure distribution pattern involving polymer wheel of shore A hardness 30 with good compliance effect showed that pressure concentration per unit area was lesser but was distributed to a large area. Due to the decrease in compliance of the contact wheel of shore A 90 hardness, it was found that contact area was like a line contact and the pressure concentration per unit area was observed to be higher.

Pressure distribution pattern obtained based on the trial from Table 3.2 were not symmetric as a result of the low spatial resolution of the pressure sensor. The spatial resolution of the pressure sensor used in the experimental trials was around 2.54 mm, so it is evident that pressure distribution pattern obtained is a simple representative of the contact conditions and does not replicate the actual pressure distribution pattern. Analysis of parameters based on material removal in real belt grinding trials may imitate the actual scenario which has been discussed in the next section

3.4 Analysis of parameters in actual belt grinding trials

In order to understand and achieve optimal material removal and surface quality in abrasive belt grinding, it is essential to look in more detail at the process parameters/variables that affect them during actual machining. In this study, the process parameters such as grit size, rubber shore A hardness, force, feed, and wheel speed are considered to analyse material removal and surface quality. The experimental studies that are done on a belt grinding setup were defined by the Taguchi experimental design, as the knowledge of the likely interactions of the belt grinding parameters was not known. To evaluate the effect of belt grinding parameters on material removal and surface quality Taguchi's L_{27} orthogonal array (five-factor, three-level) model is selected, and experiments were performed using experimental setup discussed in Section 3.2. Table 3.3 shows a summary of process parameters (factors) and their levels used for performing actual grinding trials.

Table 3.3: Belt grinding parameters and their levels.

Parameter	Unit	Levels		
		L1	L2	L3
RPM	(m/min)	250	500	700
Feed	(mm/s)	10	20	30
Force	(N)	10	20	30
Rubber hardness	(Shore A)	30	60	90
Grit Size	-	60	120	220

Material removal was quantified using the depth of cut and surface quality was quantified in terms of surface roughness associated with the grit size of the belt used. Also, the following conditions were continuously maintained throughout to achieve a controlled experimental trial.

- The contact head of the belt grinder is kept at a normal angle to maintain uniformity in contact conditions throughout machining.
- Tool wear effect was ignored as the tests were conducted in the useful lifetime of the belt tool.

- The surface condition of the machined aluminium 6061 coupons was uniform with a surface roughness of 0.8 microns (μm).
- Experiments are carried out in dry conditions.
- Experiments were carried out with three passes for each trial. On each pass, the depth of cut and surface roughness were measured at three different locations resulting in nine measurements. According to the parameter combinations from the Taguchi method, which obtained 27 trials as presented in Table 3.4, 243 depth of cut and surface roughness readings were obtained.

The mean Signal to Noise (S/N) ratio for each level of the other machining parameters is assessed based on the material removal and surface quality, i.e., depth of cut, and surface roughness. A greater S/N ratio corresponds to better material removal and surface quality characteristics.

3.5 Parameters affecting material removal/depth of cut

A Mitutoyo stylus profilometer with a stylus tip radius of 5 μm was used to measure the depth of cut across the grinded path. Mitutoyo profilometer primarily consists of a traverse unit and a processor control module. The grinded workpieces are adjusted such that the area of interest of measurement is across the grinded path. The length is profiled across locations A, B, and C along the tool path, as shown in Figure 3.12.

3D and 2D profiles were extracted from the workpiece surface across the machined length, using the profilometer to measure the depth of cut, as illustrated in Figure 3.13. The depth of cut is measured as the distance between the deepest point in the grinded path and the surface of the word coupon.

The experimental layout for the five cutting parameters using the L_{27} orthogonal array is provided in Table 3.4. The table shows the experimental results for the mean depth of cut and corresponding S/N ratios. Each experimental trial was repeated three times to ensure consistency, and the depth of cut was measured across three locations for each trial, resulting in a total of nine readings per test.

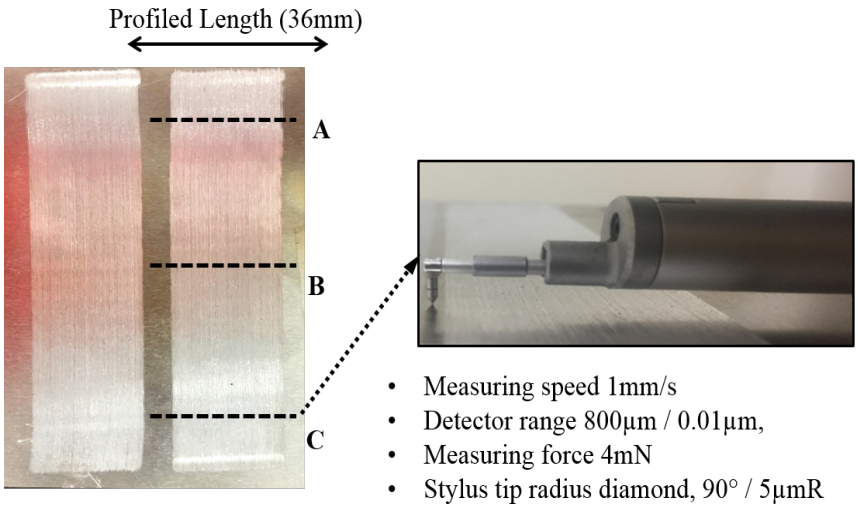

Figure 3.12: Profilometer with the tactile stylus used to measure the depth of cut across the grinded path at three different locations A, B and C.

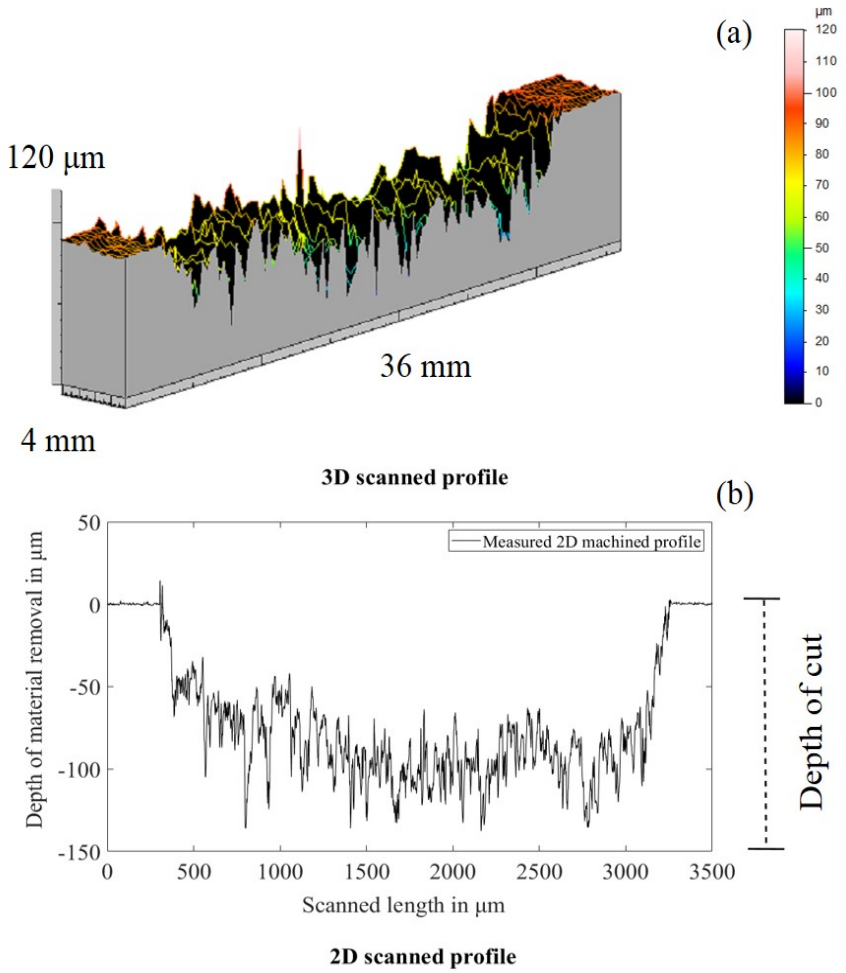

Figure 3.13: (a) 3D profile extracted from the workpiece surface across the machined surface using Taly-scan; (b) 2D profile obtained from the workpiece surface across the grinded path to measure the depth of cut.

Table 3.4: Taguchi experimental design using the L_{27} orthogonal array and corresponding depth of cut and signal-to-noise (S/N) ratio.

Trial no.	Factors					MRR	
	RPM (m/min)	Feed (mm/s)	Force (N)	Hardness (Shore A)	Grit (Grit No.)	Depth of cut (μm)	S/N ratio
1	250	10	10	30	60	65.60	36.33
2	250	10	10	30	120	25.87	28.25
3	250	10	10	30	220	13.34	22.50
4	250	20	20	60	60	86.10	38.70
5	250	20	20	60	120	44.20	32.90
6	250	20	20	60	220	23.53	27.43
7	250	30	30	90	60	93.87	39.45
8	250	30	30	90	120	54.33	34.70
9	250	30	30	90	220	23.55	27.44
10	500	10	20	90	60	142.93	43.10
11	500	10	20	90	120	86.37	38.72
12	500	10	20	90	220	59.38	35.47
13	500	20	30	30	60	120.66	41.63
14	500	20	30	30	120	57.50	35.19
15	500	20	30	30	220	45.55	33.17
16	500	30	10	60	60	77.47	37.78
17	500	30	10	60	120	26.08	28.32
18	500	30	10	60	220	13.54	22.63
19	700	10	30	60	60	134.89	42.59
20	700	10	30	60	120	76.88	37.71
21	700	10	30	60	220	58.97	35.41
22	700	20	10	90	60	103.82	40.32
23	700	20	10	90	120	56.96	35.11
24	700	20	10	90	220	35.31	30.95
25	700	30	20	30	60	114.00	41.13
26	700	30	20	30	120	56.65	35.06
27	700	30	20	30	220	44.31	32.93

Figure 3.14 shows the standard deviation of the depth of cut measure taken from Taguchi's L27 orthogonal array based experimental trials for all 27 test conditions.

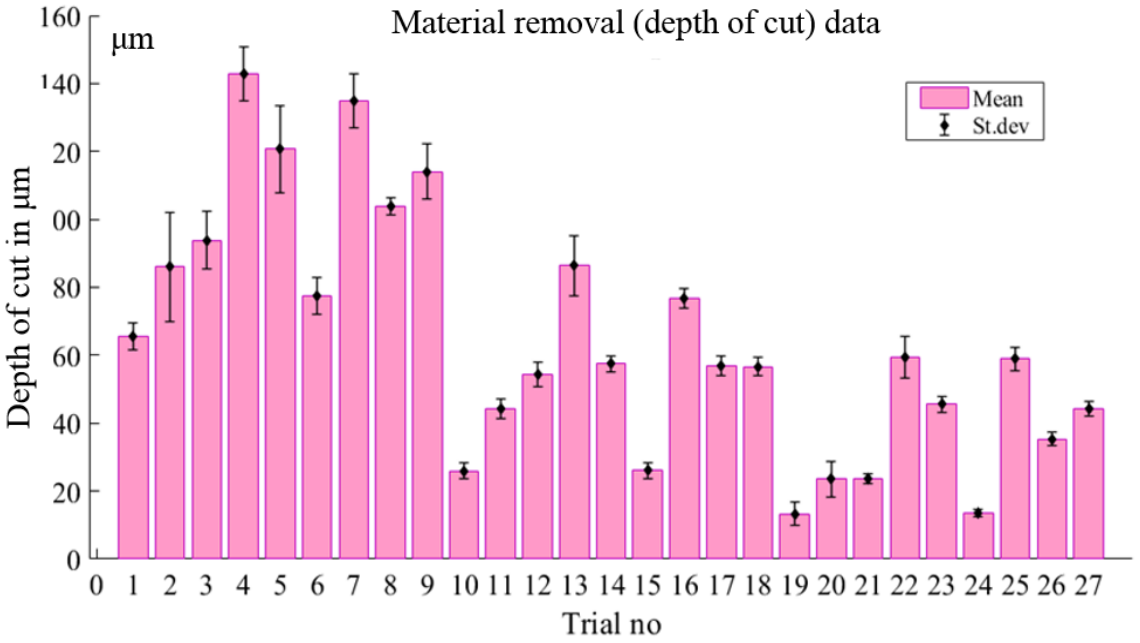

Figure 3.14: Standard deviation of the depth of cut taken from Taguchi based L_{27} orthogonal experimental trials.

The depth of cut, i.e., material removal, was identified as the process output as well as the quality characteristic with the concept 'the larger-the-better'. The S/N ratio for the larger-the-better is: $S/N = -10 \times log$ (mean square deviation):

$$\frac{S}{N} = -10\, log_{10}\, (\frac{1}{n} \sum \frac{1}{y_2}) \tag{3.1}$$

where n is the number of measurements in a trial/row, in this case, $n = 1$, and y is the measured value in a run/row. A higher S/N value agrees with a higher depth of cut. Consequently, the ideal level of the grinding parameters is the level with the most significant S/N value.

Figure 3.15 presents the results of the S/N ratio for the five parameters at three levels. According to Figure 3.15, the optimal parameters for a higher material removal rate were obtained at 700 RPM (level 3), 10 mm/s feed rate (level 1), 30 N force (level 3), 90 shore A hardness (level 3), and 60 grit (level 1). The depth of cut increases with increasing rotation speed (RPM), force, and hardness. On the contrary, depth of cut increases with decreasing feed and grit size. The increase of RPM in the contact wheel causes greater tangential force, thereby causing higher

depth of cut. The decrease in feed rate increases the contact time between the grains and work coupon, resulting in a higher material removal rate. With coarser grain, i.e., larger grit size, the depth of cut increases.

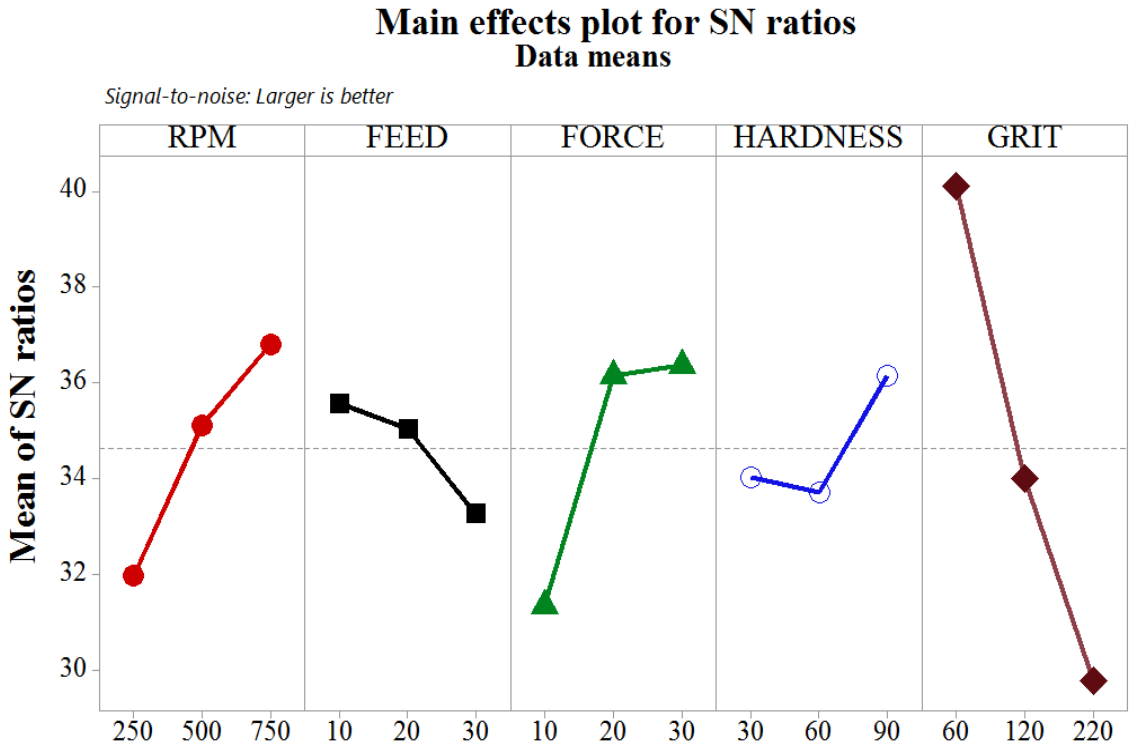

Figure 3.15: Mean signal-to-noise (S/N) ratio graph for depth of cut.

An increase in force imparted on the work coupon and hardness of contact wheel results in an increase of material removal. It is also observed that the depth of cut correlation between the three levels considered for four parameters (belt/wheel rotation speed, feed, rubber hardness, and force) using main effects plots followed the same results as predicted by the pressure sensor.

3.5.1 Statistical analysis of process parameters on material removal

To provide a detailed visualisation of the impact of various factors influencing the depth of cut in the belt grinding of aluminium 6061 specimen, Analysis of Variance (ANOVA) was used. Based on the ANOVA, the comparative significance of the grinding parameters on the depth of cut was examined to define the optimum combination of the grinding parameters for higher material removal accurately. The

analysis is carried out with 5% level of significance. The results are shown in Table 3.5. The last column of the table shows the percentage impact of each parameter on the total variation, signifying the degree of their effect on the results.

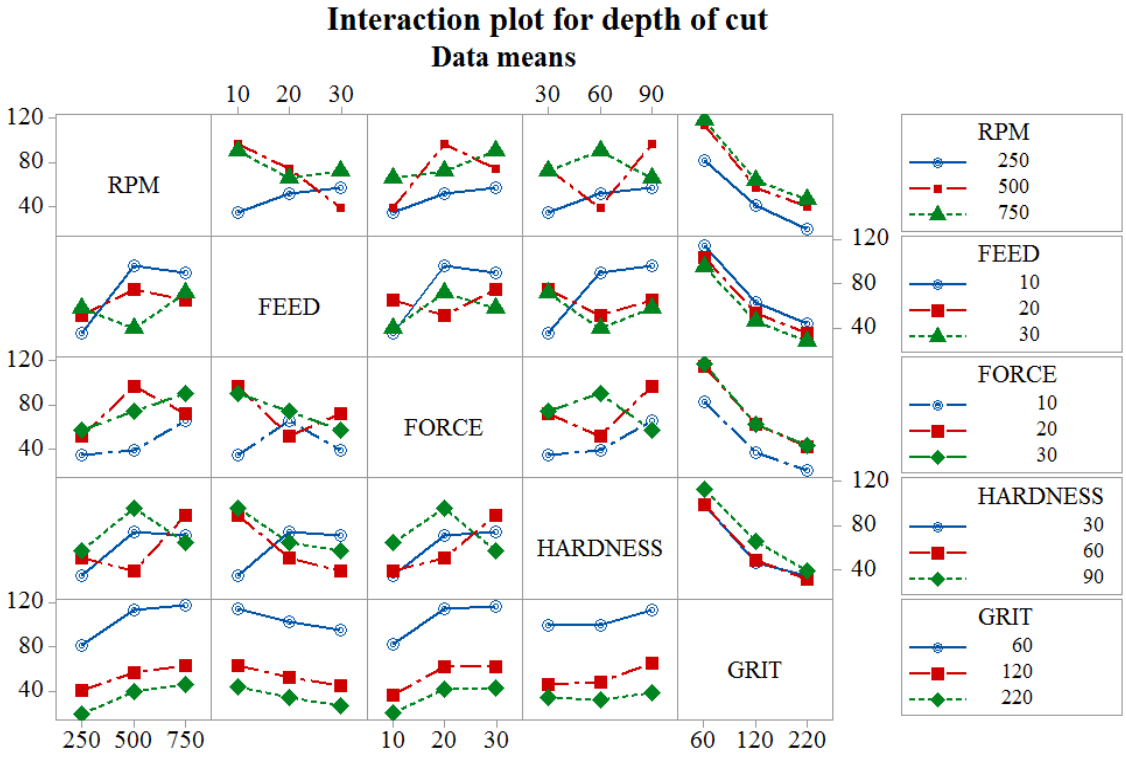

Figure 3.16: Two way interaction effect plots between RPM, feed, force, hardness, and grit on depth of cut at different initial levels of parameters.

Table 3.5: Results of ANOVA for depth of cut.

Machining parameter	Degrees of freedom	Sum of squares	Mean square	F ratio	Contribution (%)
RPM	2	5055.5	2527.7	26.42	13.54
Feed	2	1249.1	624.5	6.53	3.34
Force	2	4782.8	2391.4	25.00	12.79
Hardness	2	867.1	433.6	4.53	2.31
Grit	2	23,903.7	11,951.9	124.93	63.93
Error	16	1530.7	95.7	-	4.09
Total	26	37,388.8	-	-	-

The larger the percentage contribution, the greater the influence of a parameter on the material removal. It can be observed from Table 3 that the grit size (F = 124.93) has the greatest static influence of 63.93%, followed by RPM (F = 26.42), which has an influence of 13.54%, and force (F = 25.00), which has an in-

fluence of 12.79% on material removal rate. The feed and wheel hardnesses have an insignificant effect on the material removal of 3.34% and 2.31%.

Interaction plots are most often used to visualise interactions during ANOVA. The effect of one factor depends on the level of the other factor, and such possible interactions can be envisioned using an interaction plot. The two way interaction effects are shown as line plots in Figure 3.16. The figure indicates the interaction plot among the five belt grinding parameters that have been considered in our study on the depth of cut. In this interaction plot, the lines are not parallel for the process parameter indicating the fact that the relationship between them will affect the depth of cut.

Further statistical data study using Pareto chart as shown in Figure 3.17 on identifying significant individual and interaction factors based on standardized effect value reveals that grit size parameter is dominant.

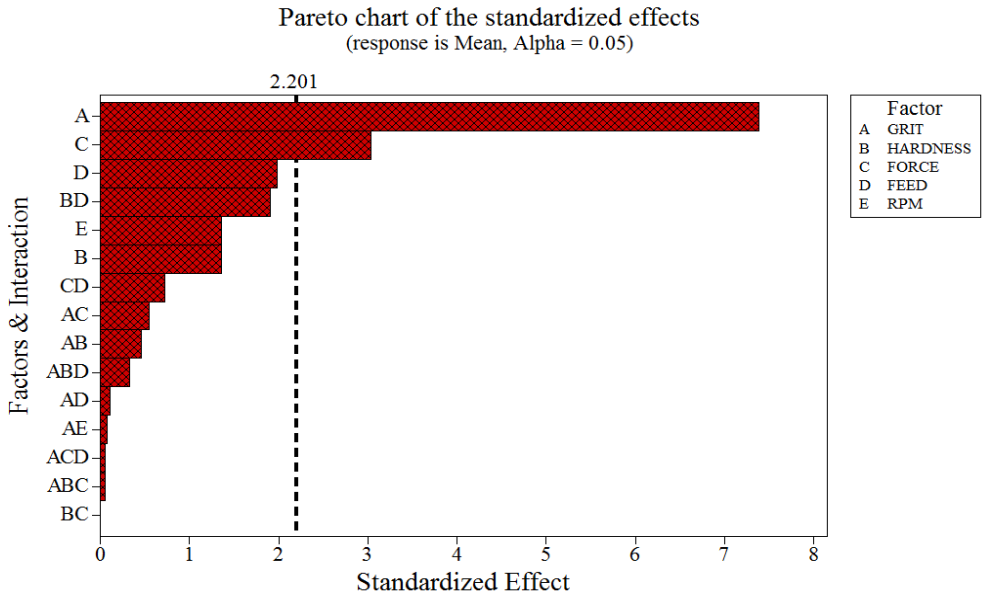

Figure 3.17: Pareto chart on interaction effects of belt grinding parameters on the depth of cut.

3.6 Parameters affecting surface quality/ roughness

The application and scope for belt grinding is not only for precision material removal and fine finishing. It is also widely used for roughing processes. The study on

process parameters that influence the final requirement such as fine or rough finish is discussed in this section. The experimental layout with five cutting parameters using the L_{27} orthogonal array is provided in Table 3.6 and experimental setup discussed in Section 3.2 is used to perform belt grinding trials.

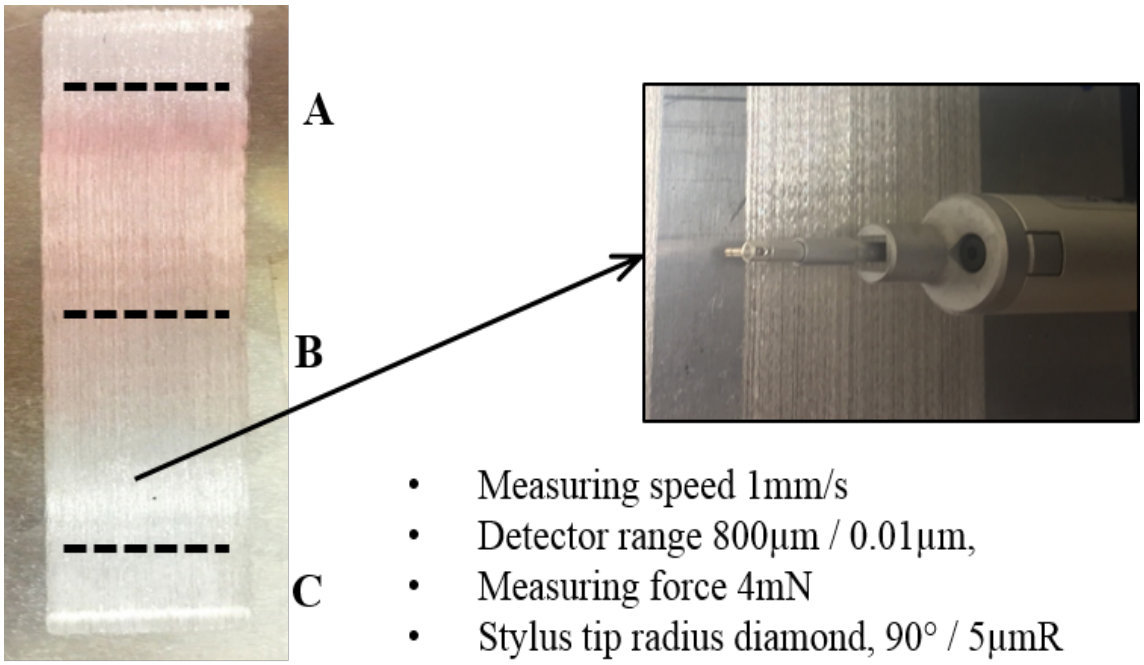

Figure 3.18: Profilometer with the tactile stylus used to measure surface roughness across the grinded path at three different locations A, B and C.

Each experimental trial was repeated three times to have consistency, and depth of cut was measured across three locations for each trial, resulting in a total of nine readings per test condition. A Mitutoyo stylus profilometer with a stylus tip radius of $5\mu m$ was used to measure the surface roughness across the grinded path. The grinded workpieces are adjusted so that the area of interest of surface roughness (R_a) measurement is across the grinded path. The length is profiled across locations A, B, and C along the tool path, as shown in Figure 3.18.

Surface roughness R_a provides a suitable general portrayal of the height discrepancy in the surface profile as it is the average absolute deviation of the roughness asymmetries from the mean line over the sampling length. A sampling length of 15mm at a scanning speed of 1mm/sec was used to calculate surface roughness. Table 3.6 shows the experimental results for the mean surface roughness (R_a) and corresponding S/N ratios.

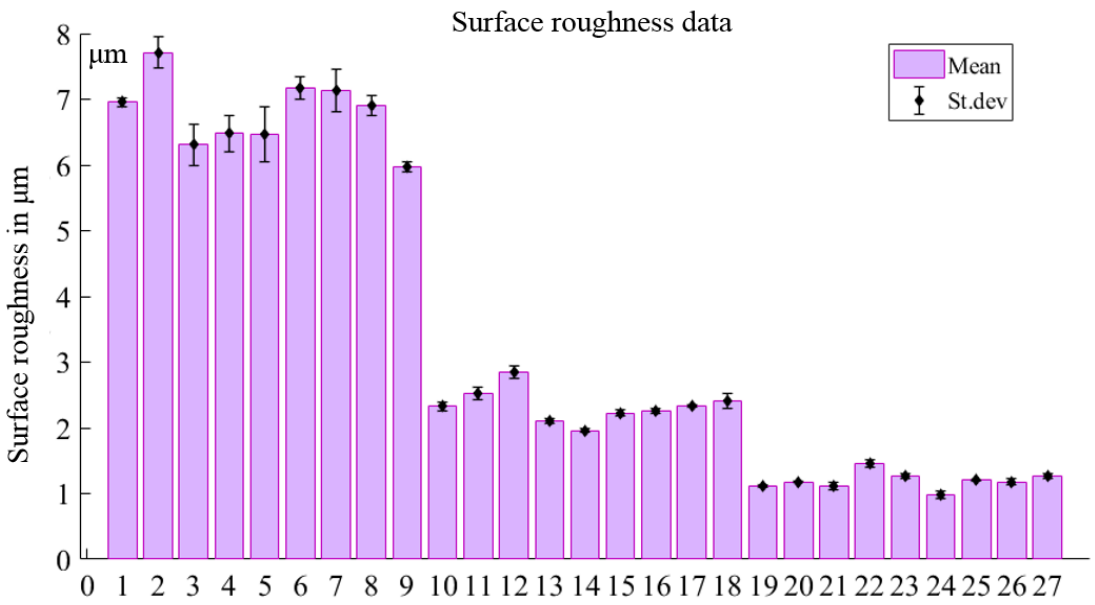

Figure 3.19: Standard deviation of the surface roughness taken from Taguchi based L_{27} orthogonal experimental trials.

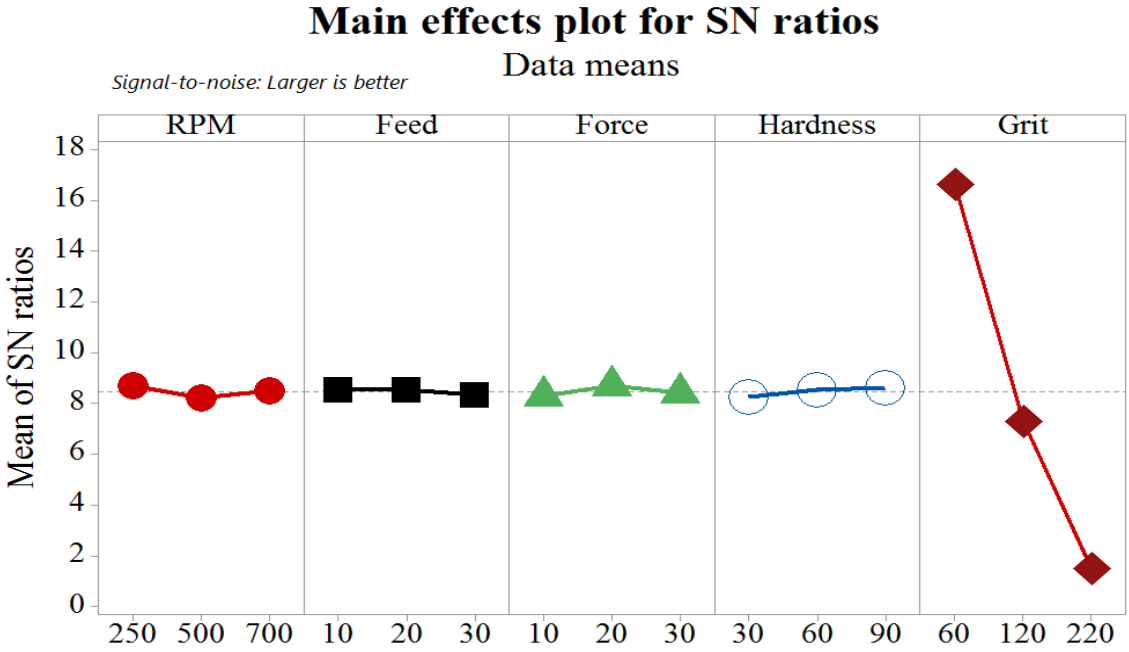

Figure 3.20: Mean signal-to-noise (S/N) ratio graph for surface roughness.

Figure 8 shows the standard deviation of the surface roughness measure taken from Taguchi's L_{27} orthogonal array based experimental trials for all 27 test conditions. Figure 3.20 presents the results of the S/N ratio for the five parameters at three levels. Interpreting the values from Figure 3.20, it is evident that the optimal parameter that determines the surface quality in terms of surface roughness is unanimously the grit size parameter.

Table 3.6: Taguchi experimental design using the L_{27} orthogonal array and corresponding surface roughness(R_a) and signal-to-noise (S/N) ratio.

Trial no.	Factors					Surface roughness	
	RPM (m/min)	Feed (mm/s)	Force (N)	Hardness (Shore A)	Grit (Grit No.)	R_a (μm)	S/N ratio
1	250	10	10	30	60	6.95	16.84
2	250	10	10	30	120	2.33	7.34
3	250	10	10	30	220	1.11	0.93
4	250	20	20	60	60	7.70	17.73
5	250	20	20	60	120	2.52	8.05
6	250	20	20	60	220	1.18	1.43
7	250	30	30	90	60	6.30	15.99
8	250	30	30	90	120	2.84	9.07
9	250	30	30	90	220	1.11	0.93
10	500	10	20	90	60	6.47	16.22
11	500	10	20	90	120	2.1	6.44
12	500	10	20	90	220	1.45	3.26
13	500	20	30	30	60	6.47	16.21
14	500	20	30	30	120	1.95	5.83
15	500	20	30	30	220	1.27	2.07
16	500	30	10	60	60	7.18	17.12
17	500	30	10	60	120	2.22	6.94
18	500	30	10	60	220	0.98	-0.17
19	700	10	30	60	60	7.13	17.06
20	700	10	30	60	120	2.25	7.05
21	700	10	30	60	220	1.20	1.60
22	700	20	10	90	60	6.90	16.78
23	700	20	10	90	120	2.34	7.38
24	700	20	10	90	220	1.18	1.43
25	700	30	20	30	60	5.9	15.51
26	700	30	20	30	120	2.41	7.64
27	700	30	20	30	220	1.26	2.05

3.6.1 Statistical analysis of process parameters on surface roughness

Based on the ANOVA, the relative significance of the grinding parameters on the surface roughness (R_a) was examined to define the optimum combination to achieve the required surface quality. The analysis was carried out at 5% significance level and the results are shown in Table 3.7.

Table 3.7: Results of ANOVA for surface roughness.

Machining parameter	Degrees of freedom	Sum of squares	Mean square	F ratio	Contribution (%)
RPM	2	0.227	0.1136	0.83	0.14
Feed	2	0.087	0.0433	0.32	0.08
Force	2	0.027	0.0134	0.10	0.009
Hardness	2	0.399	0.1997	1.47	0.25
Grit	2	157.331	78.6655	577.77	99.51
Error	16	2.178	0.1362	-	4.09
Total	26	160.249	-	-	-

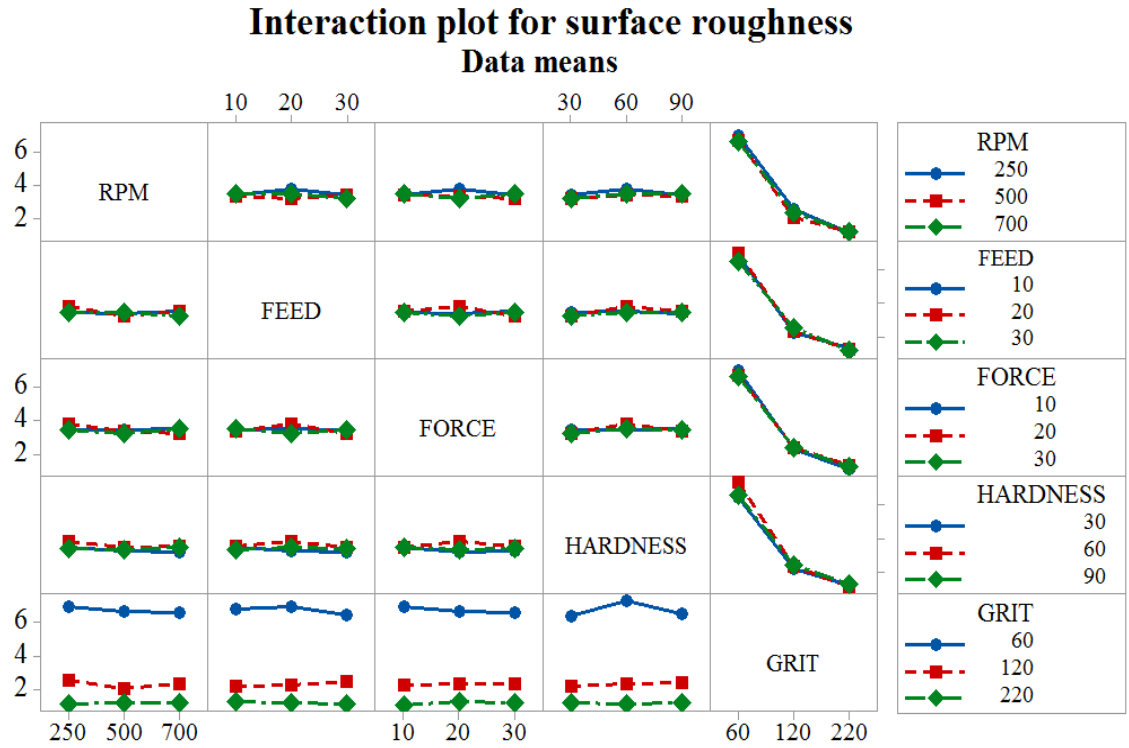

Figure 3.21: Two way interaction effect plots between RPM, feed, force, hardness, and grit on surface roughness at different initial levels of parameters..

It can be observed from Table 3.7 that the grit size (F = 577.77) has the greater

static influence of 99.51% collectively. The feed, wheel hardness, RPM, force parameters had no significant effect on the surface roughness. Envisioning the two-way interaction plot among the parameters on the surface roughness in Figure 3.21 suggests the presence of more parallel lines resulting in no interaction effects that alter the surface quality other than the grit size parameter. Statistical data study using Pareto chart as shown in Figure 3.22 on individual and interaction effect of process parameters on surface roughness also reveals that impact of grit size is more dominant than others. This statistical study shows that the final grinded surface quality relies only on the belt condition and also the characteristic of the abrasive arrangement like any other abrasive machining process.

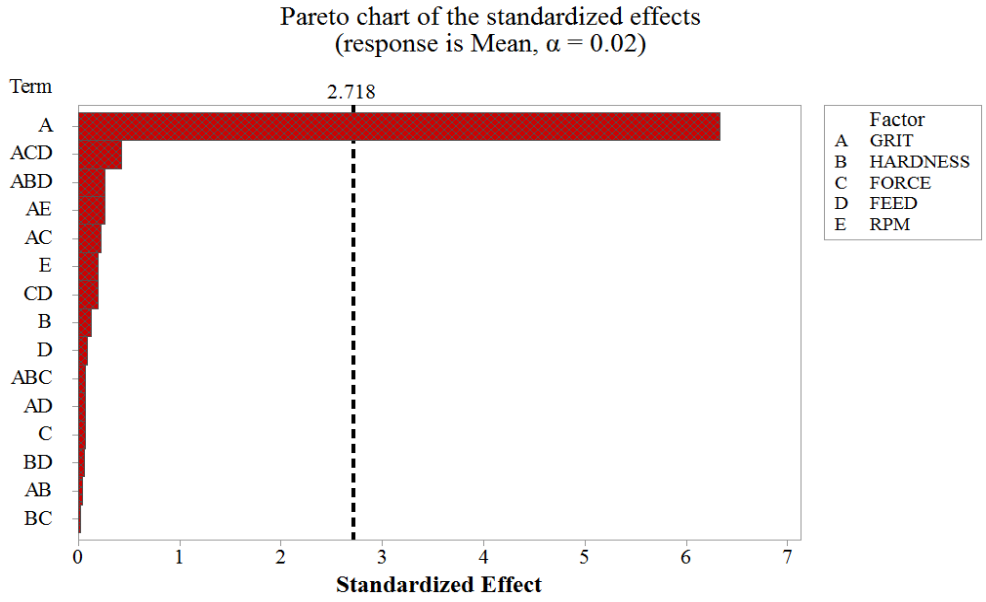

Figure 3.22: Pareto chart on interaction effects of belt grinding parameters on the surface roughness.

3.7 Conclusion

Investigation results in the influence of belt grinding parameters on material removal depth and surface quality from dynamic pressure sensor, Taguchi's parameter design method and parameter analysis using ANOVA have been presented in this section.

The pressure sensor trials with three levels of cutting wheel speed, feed rate, force and rubber hardness suggest that the dynamic changes in pressure distribution on contact region affects material removal. Observations of the main effects plot from the depth of cut trials indicated that parameter followed the same trends as predicted

by pressure pad sensor trials.

Based on main effects plot from the depth of cut trials we can construe that material removal is directly proportional to the cutting speed (grinding rate), i.e., when the number of the interactions per unit time gets maximised. The main effect plot from the depth of cut trials also suggests that penetration depth of the grains into the work coupon surface directly depends on the force imparted for grinding. Main effect plot indicates that material removal increases with a higher dwell time of interaction suggesting that the relationship is inversely proportional to feedrate. It is also evident from the main effects plot, as the polymer loses it compliance property, the material removal depth increases significantly. As far as the grit parameters are concerned, coarser grit (grit size 60) has better material removal capabilities.

Based on the ANOVA results at a 95% confidence level from the depth of cut trials, it is apparent that grit size is the primary factor that has the highest influence on the material removal which is about five times greater than that of RPM and force imparted. Analysis of variance results at a 95% confidence level, and main effects plot from surface roughness trials suggest that it only the grit size of the belt that affects the quality of the ground surface.

The following generalised conclusions are drawn from this chapter:

- Higher stock removal commonly requires a harder polymer contact wheel, coarse abrasive grains, greater force, reduced feed, and larger cutting speed.
- Though, finishing requires a fine grade abrasive grains, roughening requires coarse grade abrasive grains embedded in the belt backing material.
- Of all the grinding parameters influencing optimum material removal and surface quality, it is essential to look in more detail of the grit size parameter. Any inconsistency to the grit size parameter may have adverse effect on the performance of grinding process with respect to material removal as well as surface quality.

Understanding the magnitude of contribution of each process variable and interaction effects on material removal and surface quality from this chapter will help in modelling of the process accurately.

Chapter 4

Material removal modelling

4.1 Abrasive belt grinding process

Abrasive belt grinding is a widely used two-body abrasive machining processes to remove undesired features such as burrs, weld seams and to achieve the required material removal and surface finish. Belt grinding is also used for polishing semi-finished components of complex shape and geometry. Similar to other abrasive machining processes, many process variables such as belt speed, belt preloaded tension, the imparted force, feed rate, workpiece geometry, polymer hardness, and belt topography features such as grit size, grain hardness etc. impact the surface quality [16]. The abrasive belt grinding is nonlinear due to the complexity of the underlying physical mechanisms, some of which remain unknown. Most industries operate belt grinding process based on empirical rules and operator experience.

The amount of material removed relies heavily on the distinct local contact conditions, which are completely influenced by the state of the grinding parameters. Although the correlation of individual parameters on material removal is understood using ANOVA and statistical techniques from Chapter 3, their combined effect on the material removal is not well established. The material removal models developed so far on contact conditions and pressure distribution are based on some assumptions. Developing analytical models for such a nonlinear process with assumptions may introduce randomness and will not be a suitable method to model the process.

A conclusive material removal model can be developed for such a dynamic process involving the actual parameters using regression techniques. A approach to

mathematically model the material removal using soft computing regression techniques is reported in this chapter. The depth of cut data from Table 3.4, which was acquired based on Taguchi's L_{27} experimental design, is used to model the material removal. Six different regression modelling methodologies, namely Multiple linear regression, Stepwise regression, Artificial Neural Networks (ANN's), Adaptive Neuro-Fuzzy Inference System (ANFIS), Support Vector Regression (SVR) and Random Forests (RF's) are applied and the results obtained by the models are compared and discussed.

4.2 Multiple linear regression

Multiple linear regression is a promising supervised learning algorithm and the most common form of linear regression analysis. As a predictive analytical tool, the multiple linear regression is used to associate one continuous dependent variable to two (or more) independent variables by finding the best fitted line [25]. The best fitted line is a line with the minimum total error to all the points. Multiple linear regression analysis helps us to comprehend the rate at which dependent variable change when changes are made in the independent variables. Regression models describe the relationship between a dependent variable, y_i or is referred to as the response variable and independent variables, X_{in}, or predictor variables, by fitting a linear equation as shown in the following equation:

$$y_i = \beta_0 + \beta_1 X_{i1} + \beta_2 X_{i2} + \beta_3 X_{i3} + ... + \beta_n X_{in} + \epsilon_i \tag{4.1}$$

where the constant β_0 represents the intercept in the model and β_n ($n \neq 0$) referred as coefficient. Since the response values for y_i vary about their means, the multiple regression model includes a residual term, ϵ_i, representing the variation. The goal of the multilinear regression is to create a linear model in hyperplane that minimises the sum of the square of the residuals concerning all predictor variables as shown in Figure 4.1. Multilinear regression identifies the hyperplane, in terms of the slope β_n and intercept β_0, through the sample data with minimum sum of the squared errors thereby predicting the regression line.

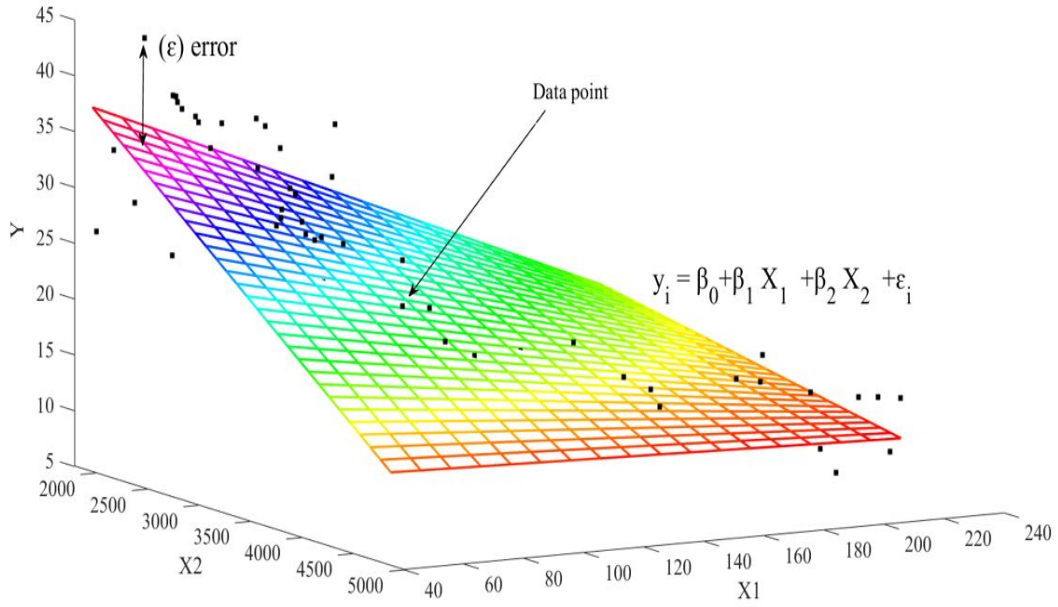

Figure 4.1: Surface that corresponds to the simplest multiple regression model.

Multilinear regression was performed to determine the relationships between the five grinding parameters, rotation per minute (RPM), force, rubber hardness, grit size, and feed rate to the depth of cut. The schematic model is illustrated in Figure 4.2.

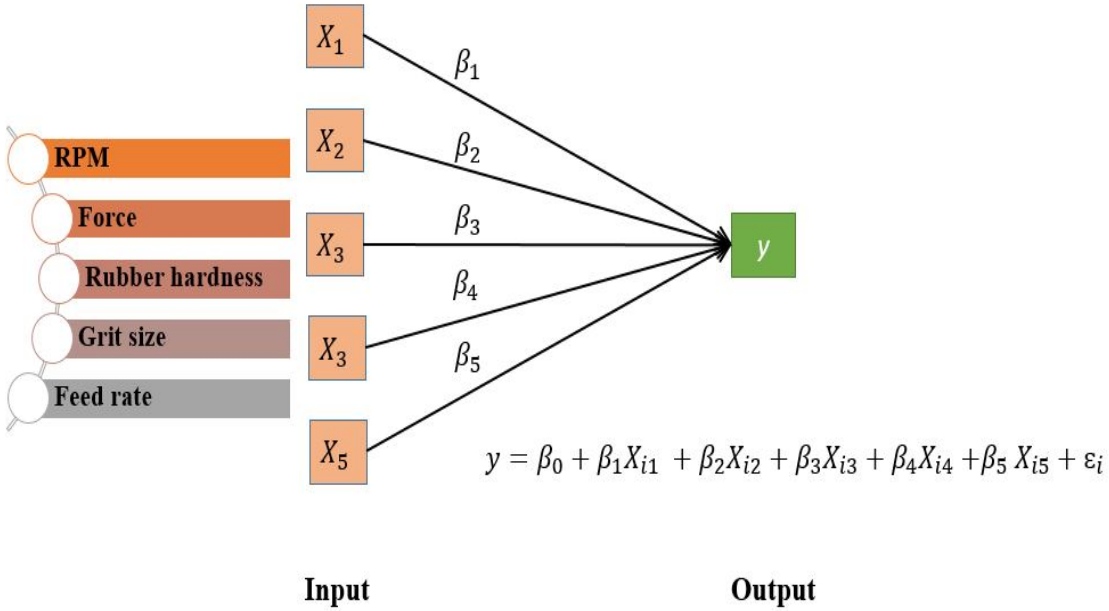

Figure 4.2: Schematic illustration of the multilinear regression model for prediction of the material removal.

The linear correlation model is developed using MATLAB. The dataset (n = 243) consisting of the five predictors and the response variable is randomly split into 70% training set and 30% testing set. The multilinear model fits the data to a hyperplane upon least square error minimisation.

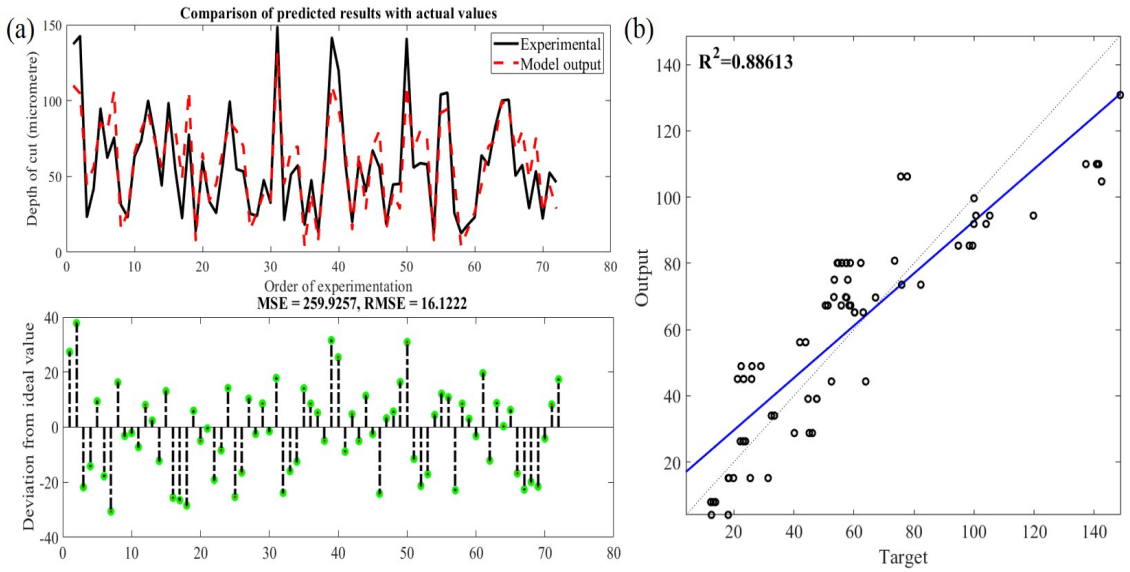

Figure 4.3: (a).Comparison of observed and predicted depth of cut using multilinear regression; (b). Statistical analysis fit of the multilinear regression model.

Figure 4.3 shows the comparison between observed and predicted material removal values on the testing dataset using the developed multilinear regression model. The figure also shows the deviation the predicted values against actual values with multilinear model highlighting a higher root mean squared error (RMSE) of 16.12 which is used as a measure to predict the performance of the model. The developed multilinear model is deficient at predicting the material removal, i.e., depth of cut. The calculated R-squared (R^2) gives a value of 0.886, which implies that the fitness of the linear model is inadequate as the targetted R^2 is a value, with a minimum deviation from 1.

4.2.1 Stepwise regression

The simple multilinear regression based on least square method from previous subsection indicates the incapability to accurately predict the depth of cut. This is attributed to the nonlinear nature of the relationship in the grinding process and the exclusion of interaction effects. Augmenting interaction effects of the predictors

on linear regression can be achieved by using the stepwise regression. Stepwise regression essentially does multiple regression a number of times, each time removing the weakest correlated variable based solely on the t-statistics of their estimated coefficients. In the end, the variables that give the best distribution will remain. A linear model containing only the linear terms is used as a starting model whereas a quadratic model containing an intercept, linear terms, interactions, and squared terms are used as a terminating model. Predictor variables are added one at a time as the regression model progresses. At each step, predictor variable or their interaction that increases R-squared (R^2) the most are considered significant whereas others are removed. The training parameters used in the stepwise regression is listed in Table 4.1.

Table 4.1: Stepwise multilinear regression training parameters.

Parameter	Value	Remarks
Training set	70%	-
Testing set	30%	-
Method	Forward stepwise regression	Predictor variable or their interaction that increases R-squared (R^2) is considered significant.
Starting model	Linear	-
Upper limit	Quadratic	Resulting model takes a quadratic form containing an intercept, linear terms, interactions, and squared terms.

The output of the developed stepwise model containing 13 terms which include 5 significant interactions and few higher order polynomials are shown in Table 4.2. Figure 4.4 shows the comparison between the observed and the predicted material removal values from the 30% testing dataset. In addition, the figure shows the deviation of the predicted values from the actual ones highlighting a reduction in RMSE of 7.77 as compared to least square based multilinear regression. The proposed model is capable, but insufficiently robust at predicting the material removal. R-squared (R^2) of value 0.975 has increased when the regression takes in a quadratic form which also takes into account the interaction effect between the belt grinding parameters. The order in which predictor variables are removed or added can provide valuable information about the quality of the predictor variables. Referring to

the t-stat value of the developed regression model, especially between the predictor interaction from Table 4.2, it is apparent that grit parameter plays a dominant role. The estimated coefficients of the regression model is significant when the interaction happens with the gritsize predictor.

Table 4.2: Estimated co-efficients from stepwise regression.

S.No	Predictors	Estimate	Std Error	t-Stat	p-Value
1	(Intercept)	86.755	7.956	10.904	5.392e-21
2	RPM	0.049856	0.0084825	5.8776	2.3937e-08
3	Feed	2.0067	0.51282	3.9131	0.00013509
4	Force	-2.7861	1.2896	-2.1605	0.032243
5	Rubber hardness	1.7358	0.18569	9.3481	8.2594e-17
6	Grit size	-1.3237	0.062244	-21.266	3.2042e-48
7	RPM: Grit size	-0.00014814	4.1438e-05	-3.575	0.00046498
8	Feed: Force	0.062239	0.011008	5.654	7.1536e-08
9	Feed: Rubber hardness	-0.069002	0.0091514	-7.5401	3.4527e-12
10	Force: Grit size	-0.0035275	0.00096854	-3.642	0.00036624
11	Rubber hardness: Grit size	-0.0010501	0.00031645	-3.3184	0.0011237
12	Force^2	0.084463	0.029849	2.8297	0.005265
13	Grit size^2	0.0039407	0.00018283	21.554	6.5639e-49

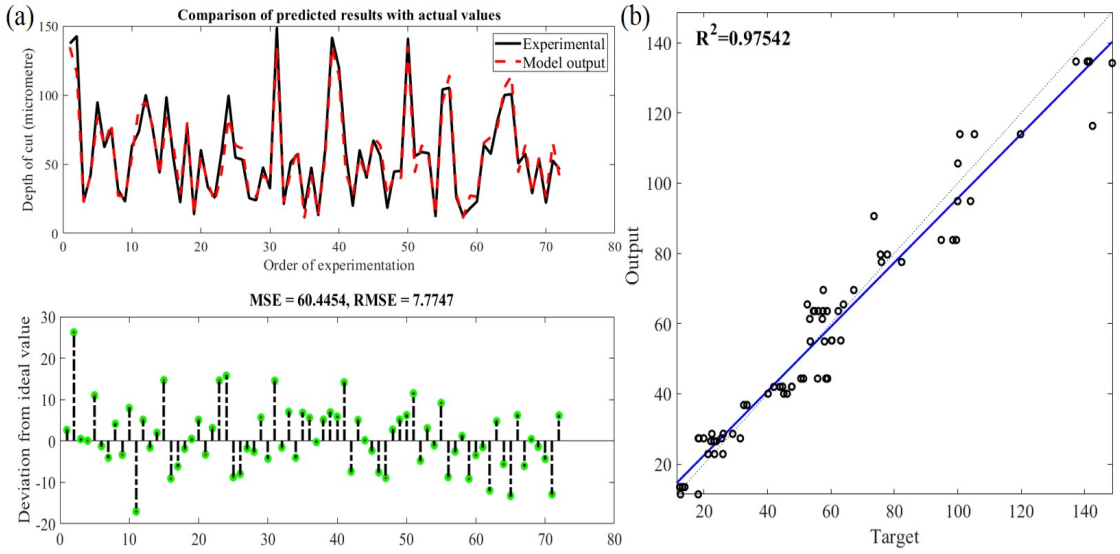

Figure 4.4: (a). Comparison of observed and predicted depth of cut using stepwise regression; (b). Statistical analysis fit of the stepwise regression model.

Figure 4.5 depicts the comparison of the residuals from the multilinear model and the stepwise multilinear model. It explicitely indicates that the latter fits the

data better. In addition, comparing the R^2 statistical metric values from both approaches, it is clear that the latter performs better than the former as it incorporates a quadratic form, which addresses the influence of the interaction between the grinding parameters and the nonlinear behaviour of the belt grinding process.

The proposed methodologies on the multilinear regression and the stepwise multilinear regression provides a useful tool to predict material removal depending on the grinding parameters. The multilinear model may not be the best choice according to the prediction accuracy and R^2, but still, we can use it to find the nature of the relationship between the two variables. Interpreting the performance of the model it is apparent that the data are intrinsically nonlinear and straight-line relationship can never be assumed in the belt grinding process. The use of a quadratic form in the stepwise regression helps to tune the model to have a better fit.

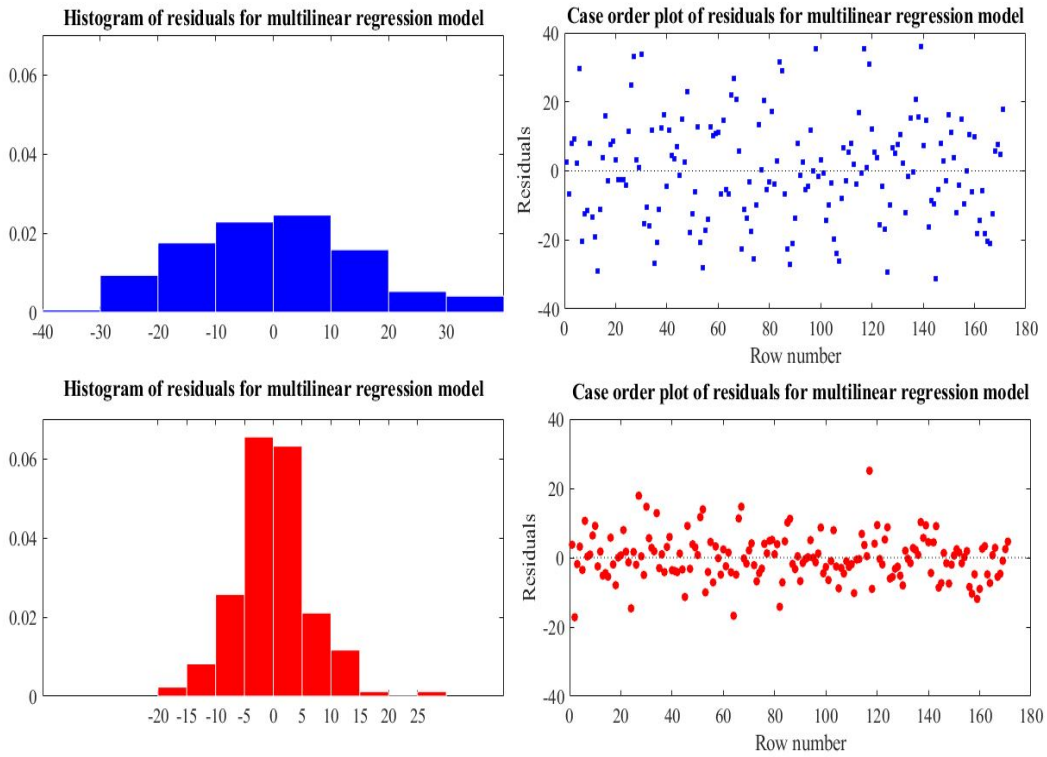

Figure 4.5: Residual plot observed between the multilinear regression model and step-wise multilinear regression model.

4.3 Artificial neural network (ANN)

Artificial Neural Networks (ANN's) are born from the approach of developing intelligent systems by simulating the biological architecture of the human brain. Estab-

lishing the connections between neurons determines the structure of the network. They typically consist of many hundred simple processing units which are wired together in a complex communication network. Neurons in ANN are arranged in a layered order. Each ANN is composed of three different layers: input, hidden and output layers. The input layer is the layer where the input values are conveyed to the network, and these neurons transmit the information to the next layer as a value. The hidden layer is the layer or layers placed between input and output layers. The experiments determine the number of layers and the number of neurons present in the hidden layers according to the problem at hand. The output layer is the layer where the output values of the network are generated. The ANN processes the information obtained from the input layer by an activation function and conveys it to the next hidden layer or directly to the output layer as shown in the Figure 4.6

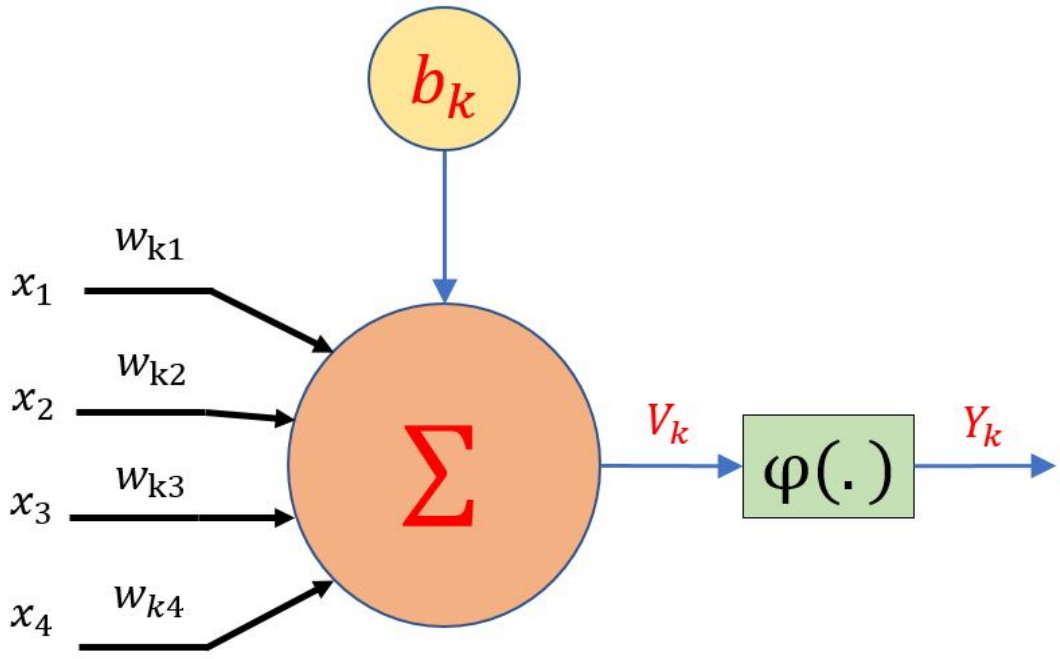

Figure 4.6: The mathematical model of a neuron.

Each connection between neurons is expressed with a weight value, and these connections are determined according to the training of the network. Expected nodes in input layer and inputs in every other node are the sum of the weighted outputs of the previous layer. Each node is brought active depending on the input, the activation function and the threshold value of the node. In mathematical terms, a neuron u_k can be described with weights w_{ji} and input x_i by

$$u_k = \sum_{j=1}^{m} w_{ji} x_i \tag{4.2}$$

and

$$v_k = u_k + b_k \tag{4.3}$$

where u_k is the linear combination output based on input signals and b_k is the bias. The output of the neuron is represented as y_k

$$y_k = \varphi(u_k + b_k) = \varphi(v_k) \tag{4.4}$$

A neuron in the network produces its output by processing its net input v_k through an activation function otherwise called a transfer function. Every neuron needs an activation function that is non-linear to bring in the much-needed non-linearity property inside the network. There are several types of activation functions used in ANN. The three forms of sigmoidal activation function as shown in equations (4.5), (4.6) and (4.7) are widely used.

$$f(x) = \frac{1}{1 + e^{-x}} range(0, 1) \tag{4.5}$$

$$f(x) = \frac{2}{1 + e^{-x}} range(-1, 1) \tag{4.6}$$

$$f(x) = \frac{e^{x} - e^{-x}}{e^{x} + e^{-x}} range(-1, 1) \tag{4.7}$$

Methodology to train connections to obtain desired results determines the learning algorithm of the network, where most common one is the back-propagation learning algorithm. Back-propagation (BP) algorithm is based on the main principle of minimisation of errors in a neural network output and modification of network values according to the minimised values. The error of network is described as the difference between the desired output D_0 and the calculated output C_0 of the network as shown in equation (4.8) and (4.9).

$$E_p = \frac{1}{2}\sum_{k=1}^{k}(D_0 - C_0)^2 \tag{4.8}$$

$$E_p = \frac{1}{2}\sum_{k=1}^{k}\sum_{p=1}^{p}(D_0 - C_0)^2 \tag{4.9}$$

where p indicates the total number of instances and K denotes the number of neurons in the output of the network. By comparing the output value of the network with the desired value, the error of network is determined which is further minimised by adjusting the weights of the networks. Back-propagation is such an algorithm that performs a gradient descent minimisation. The process of altering the weights starts at the output neuron and works backward to the hidden layer which is why it is called as back propagation. The altered weight w_{ji}^{new} is given by the η learning parameter. Once the weights of all the links of the network are decided, the decision mechanism is then developed.

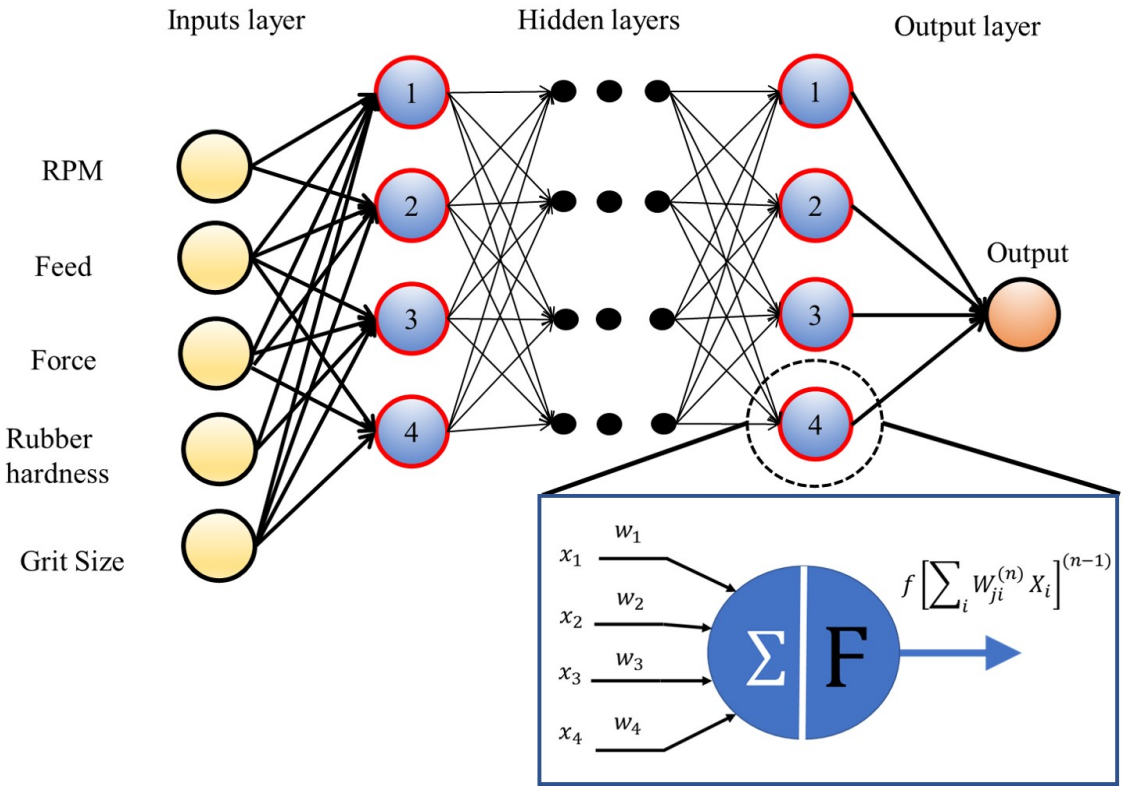

Figure 4.7: Schematic illustration of an ANN model for prediction of the material removal.

$$w_{ji}^{new} = w_{ji}^{old} \pm \triangle w_{ji} \tag{4.10}$$

$$\triangle w_{ji} = \eta \frac{\partial E_p^2}{\partial w_{ji}} \tag{4.11}$$

The architecture of the ANN that estimates the material removal in abrasive belt grinding is shown in Figure 4.7. The accuracy of an ANN model depends on its architecture and on how it is trained. The input layer of the proposed network has five neurons that represent the prediction input, while the output layer has only one neuron to predict the depth of cut. In this study, the back propagation neural network is used to construct non-linear functions between several inputs with one output. During training, the weights of the output neuron are adjusted in first place followed by adjusting the weights in the hidden layer until the expected minimum error is achieved. With hyperbolic tangent sigmoid transfer function, learning rate of 0.01 and momentum rate of 0.05, material removal is modelled using the ANN toolbox in the MATLAB software.

Table 4.3: ANN training algorithm configuration parameters.

Parameter	Value	Remarks
Maximum epochs	200	-
Performance goal	0	-
Back-propagation method	Bayesian regularisation	The function updates the weight and bias values according to Levenberg-Marquardt optimization.
Initial μ	0.005	-
Hidden layers	10, 30, 50	Number of layers between the input and output layer.
Training	70%	-
Testing	30%	-
Weight function	Dot product	-
Activation function	tansig	Hyperbolic tangent sigmoid transfer function.
Predictors	5	-
Response	1	-

The configuration parameters used to determine the best network structure of the ANN prediction model is presented in Table 4.3. The ANN algorithm uses

70% of the input data for model training with backpropagation method as Bayesian regularisation and uses the remainder for model validation. The performance of ANN depends on the number of hidden layer in the ANN network structure. It is also to be noted that the increase in the number of hidden layers has a direct impact on the cost and the modelling time. The determination of the number of layers and nodes in the hidden layers in training is based on a minimum number of iteration required to reach the required performance goal. Training stops when the error is minimised to the performance goal. Three ANNs with a different number of hidden layer configuration, i.e. 10, 20 and 30 were tested on the same training dataset. The performance of the three configurations was evaluated on minimum epochs required to achieve minimum MSE. Table 4.4 list the MSE, for the ANNs with 10, 20 and 30 hidden layers. From Table 4.4 it is clear that epochs rate decreases with the increase of hidden layers. The relationship between the number of iterations and the sum-squared error for an ANN structure with 30 hidden layers is shown in Figure 4.8.

Table 4.4: Comparison for hidden layers against epochs to reach the performance goal.

Hidder layers	Epochs
10	151
20	62
30	40

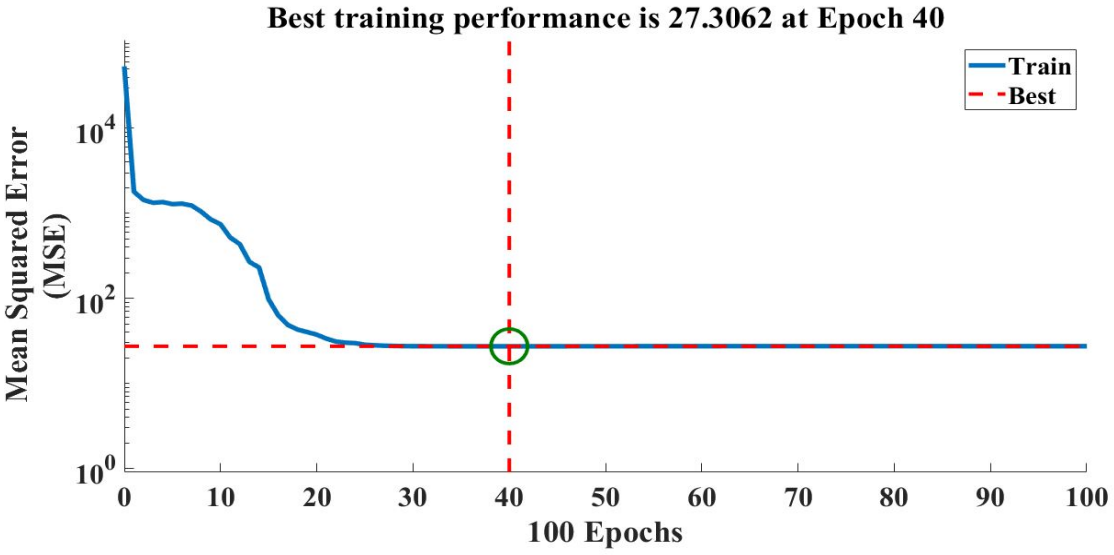

Figure 4.8: The reduction of the error with respect to the number of iterations.

It can be noted that the MSE decreases with increase of iterations. There is a sudden error reduction after 25 iterations and this reduction goes further until it saturates after 40 iterations. Though, the prediction accuracy increases as the number of hidden layers increases, the performance is not significantly improved by adding more than 30 hidden layers. Upon the completion of the training stage, the network was tested with the validation set.

Figure 4.9 shows the comparison of the actual material removal with the results of the neural network model on the validation data set (71 points). The results indicate a low deviation of the predicted values from actual values for ANN's architecture with 30 hidden layers. The trained ANN model based on backpropagation algorithm has been tested on validation data set with the RMSE of 6.64 as shown in Figure 4.9 (a). The predicted values were found to be close to the measured values. The calculated R^2 of 0.981 suggests a satisfactory fitness model. The results concludes that the proposed models can be used to predict the depth of cut in belt grinding process effectively. Though this network correlates the parameters on its own, as ANN essentially functions as a black box, it is trivial to evaluate the association between each independent variable and the dependent variable inside a neural network. Moreover, there is no specific rule for determining the structure of the ANN as the network is configured based on trial and error.

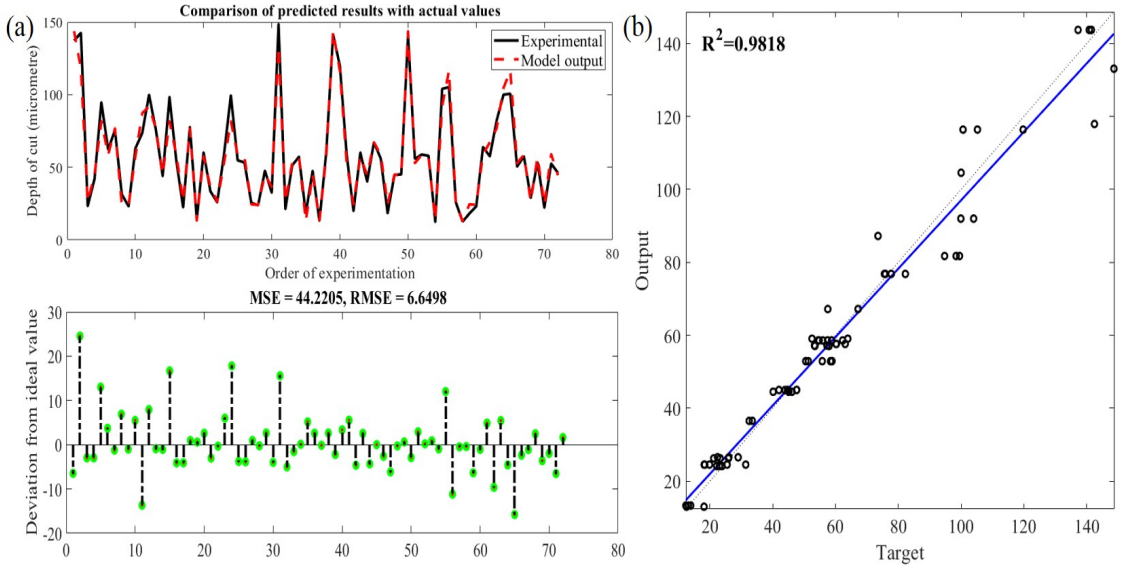

Figure 4.9: (a). Comparison of observed and predicted depth of cut using neural network regression; (b). Statistical analysis fit of the neural network regression model.

4.4 Adaptive neuro-fuzzy inference system (ANFIS)

Fuzzy inference systems have no learning capabilities regarding the input-output space and no standard tuning methods for their rule bases, which make system adaptations difficult. Adaptive neuro-fuzzy inference system (ANFIS) overcomes the fundamental problem in fuzzy if-then rules by exploiting the learning competence of ANN for automated optimisation of fuzzy if-then rules during training. This results in an automatic modification of the fuzzy system based on input-output space, which optimises the membership function for the parameters. In other wods, ANFIS architecture is a superimposition of FIS on ANN architecture, which will enable FIS to self-tune its rule base based on the output. Using an input and output space relation, ANFIS forms an FIS initially, and the membership function is altered by exploiting the back-propagation algorithm and least square method available with ANN [291].

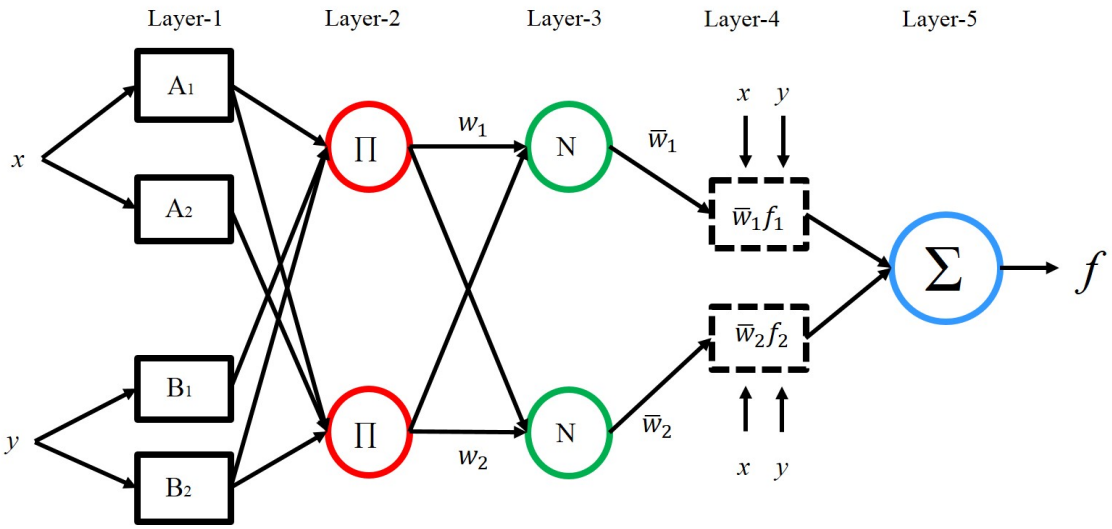

Figure 4.10: Adaptive neuro-fuzzy inference system structure.

In this section, the ANFIS architecture and its learning algorithm for the Sugeno fuzzy model will be described primarily. The ANFIS architecture is shown in Figure 4.10; ANFIS normally has five layers of neurons, of which neurons in the same layer are of the same function family. Assume that the FIS under consideration has two inputs, x and y, which form two fuzzy if–then rules based on first-order Sugeno fuzzy model [292].

Rule 1: If x is A1 and y is B1, then $f1 = p1x + q1y + r1$;

Rule 2: If x is A2 and y is B2, then $f2 = p2x + q2y + r2$;

where $p1$, $p2$, $q1$, $q2$, $r1$, and $r2$ are linear parameters and A1, A2, B1, and B2 are nonlinear parameters. The output of the i^{th} node in layer 1 is denoted as $O_{l,i}$

Layer 1: Every adaptive node i in the layer 1 has a node function.

$$O_{l,i} = \mu_{A_i}(x) \quad for \quad i = 1, 2 \quad or \quad O_{l,i} = \mu_{B_{i-2}}(y) \quad for \quad i = 3, 4 \tag{4.12}$$

where x (or y) is the input to nodes i and A_i (or B_{i-2}) generating a linguistic label coupled with the node as given by equation (4.12). The membership function for A (or B) can be any, such as a sigmoidal membership function given by equation (4.13).

$$\mu_{A_i}(x) = \frac{1}{1 + e^{-a(x-c)}} \tag{4.13}$$

where (c_i, a_i) is the parameter set. These are called premise parameters. As the values of the parameters change, the shape of the membership function varies.

Layer 2: Every node in layer 2 is a fixed node labelled $\prod$. Each node calculates the firing strength of each rule, which is the output using the simple product operator. The rule premises result is evaluated as the product of all of the incoming signals and is given by the equation (4.14)

$$O_{2,i} = w_i = \mu_{A_i}(x) \times \mu_{B_i}(y) \quad for \quad i = 1, 2 \tag{4.14}$$

Layer 3: The ratio of the i^{th} rule's firing strength to the sum of all of the rule's firing strengths is calculated by equation (4.15) in layer 3. The output of this layer is called normalised firing strengths.

$$O_{3,i} = \bar{w}_i = \frac{w_i}{\sum_i^2 w_i} = \frac{w_i}{w_1 + w_2} \quad i = 1, 2 \tag{4.15}$$

Layer 4: Every node i in layer 4 is an adaptive node with a node function. The nodes compute a parameter function on the layer output. Parameters in this layer are referred to as consequent parameters.

$$O_{4,i} = \bar{w}_i f_i = \bar{w}_i(p_i x + q_i y + r_i) \tag{4.16}$$

where w_i is a normalised firing strength from layer 3 and (pi, qi, ri) are the parameter set for the node.

Layer 5: This layer has a fixed single node labelled $\sum$, which computes the overall output as the summation of all of the incoming signals, as shown in equation (4.17). The $\sum$ gives the overall output of the constructed adaptive network, having the same functionality as the Sugeno fuzzy model.

$$O_{5,i} = \sum_i \bar{w}_i f_i = \frac{\sum_i w_i f_i}{\sum_i w_i} \tag{4.17}$$

The topology of adaptive neuro-fuzzy inference system architecture for prediction of material removal based on five belt grinding process parameters is illustrated in Figure 4.11.

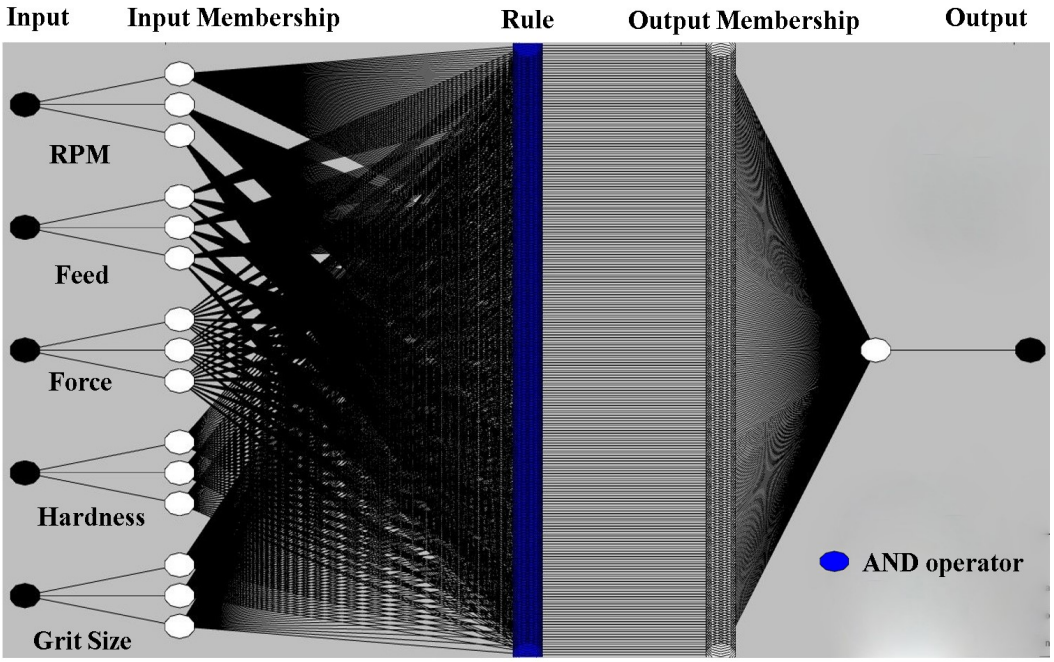

Figure 4.11: Topology of adaptive neuro-fuzzy inference system architecture.

From Figure 4.11, it can be noticed that the input membership functions of the Takagi-Sugeno model are non-linear, whereas the output membership functions are linear. The initial step of the ANFIS modelling system is to decide the input and output variables of the fuzzy logic controller.

The ANFIS model developed is a Multiple Input Single Output (MISO) system with multiple inputs and a single output. Figure 4.12 shows real inputs and real output with fuzzy rule architecture of the ANFIS. A fuzzy membership function allocates grades of membership extending from numbers between zero and one to the range of the possible values of the variable. Zero membership value specifies that it is not a member of the fuzzy-set; one signifies an extensive member.

Four types of membership functions (Sigmoidal, Gaussian bell, Gaussian, and Bell-shaped) are compared in terms of accuracy, to model and characterise the belt grinding process. The application of general sigmoidal membership functions to the neuro-fuzzy modelling process is a very attractive methodology to characterise non-linear processes [293]. The sigmoidal membership function has better approximation over other membership functions due to tapering edges. A sigmoidal membership function is created for each input variable used in belt grinding, as illustrated in Figure 4.12. The sigmoid function is differentiable for all values of the inputs to allow the use of powerful back-propagation learning algorithms [294].

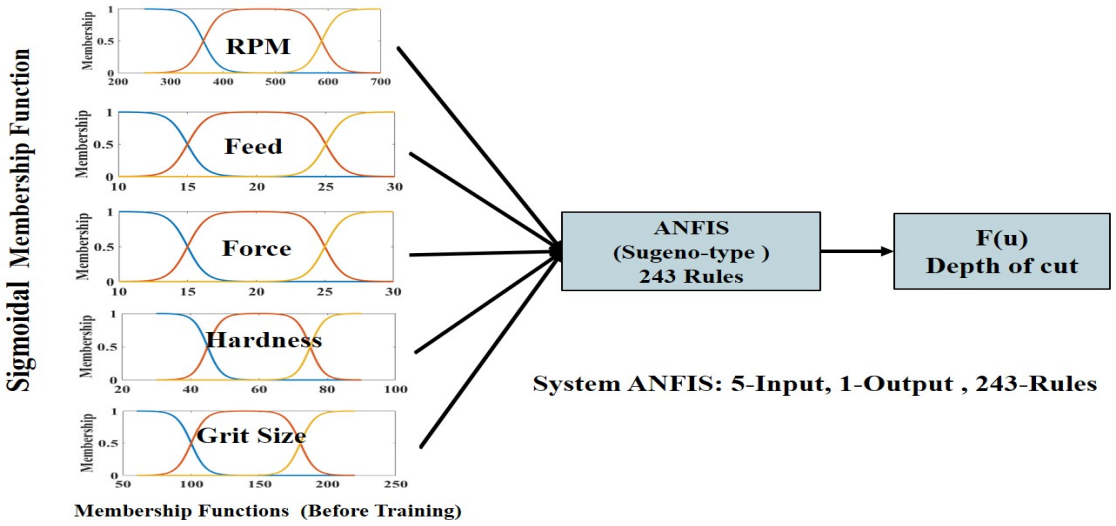

Figure 4.12: ANFIS model for belt grinding showing inputs and output.

The topology of ANFIS architecture that implements the sigmoidal membership function designed with 243 fuzzy rules for depth of cut prediction used in this research is illustrated in Figure 4.13.

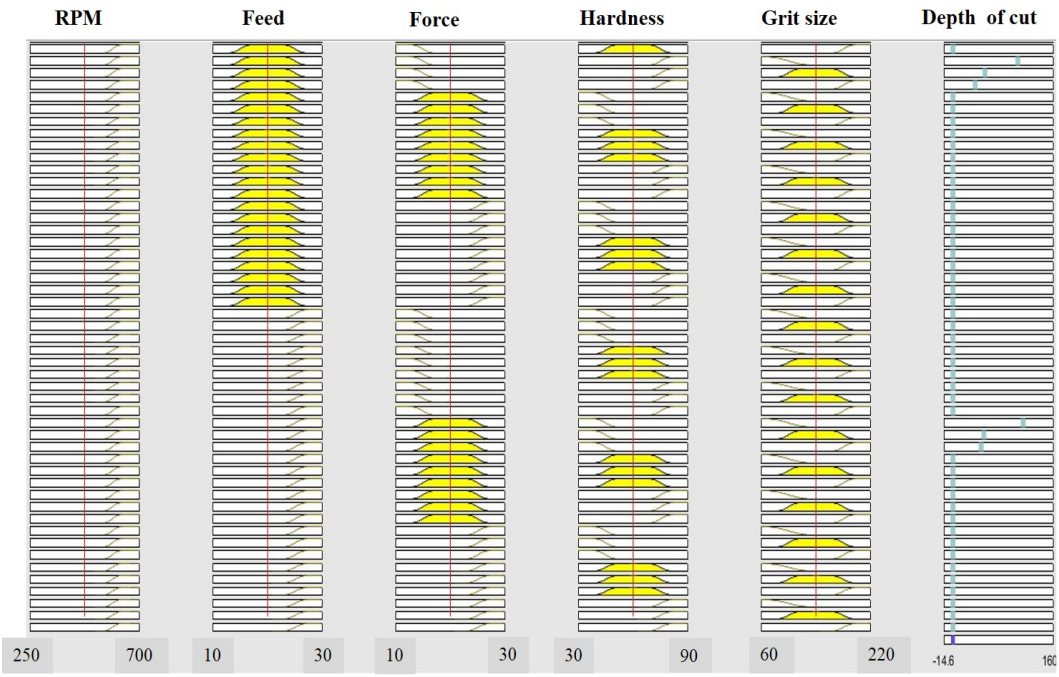

Figure 4.13: Fuzzy rules firing.

The ANFIS contains 243 rules, with sigmoidal membership functions assigned to each input variable. The total number of fitting parameters is 303, including 60 premise (nonlinear) parameters and 243 consequent (linear) parameters. The applicable control rules formulated along with the four types of membership function to model material removal were implemented in a MATLAB environment using a Sugeno-type fuzzy inference system in the fuzzy logic toolbox. Adaptive neuro-fuzzy inference system (ANFIS) learning uses back-propagation method for updating membership function parameters.

Prediction of the depth of cut of the process by ANFIS consists of two main parts i.e. training data and testing data. Hence, among data sets, 70% data is selected stochastically for the training of the ANFIS network and 30% for testing the developed model. During the training in ANFIS, 27 sets of data were used to conduct learning, and this ceased after 150 iterations, as shown in Figure 4.14. The step size for parameter adaptation had an initial value of 0.1. The proposed ANFIS training parameters are given in Table 4.5.

Figure 4.15 presents the initial and final membership functions of the five belt grinding input parameters derived by sigmoidal membership function training. It can be seen from the final membership functions of hardness and feed parameter

Table 4.5: ANFIS training parameters.

Parameter	Value	Remarks
andMethod	Prod	Product of fuzzified input values.
orMethod	Max	Maximum of fuzzified input values.
defuzzMethod	Wtaver	Weighted average of all rule outputs.
impMethod	Prod	Implication Method.
aggMethod	Max	Aggregation Method.
Membership function	Sigmoidal membership	Sigmoidal membership functions is very attractive to characterise nonlinear processes.
Learning rules	Gradient descent algorithm	Training function that updates weight and bias values according to gradient descent.

from Figure 4.15 that they are insignificant. However, on comparing the shape of initial and final membership functions of belt grinding parameters such as grit size, RPM, and force, a considerable change in the final membership function can be seen. Analysis of the sigmoidal membership function after training indicates that the factor in the belt grinding parameters that has the most impact on material removal is grit size, followed by RPM and force.

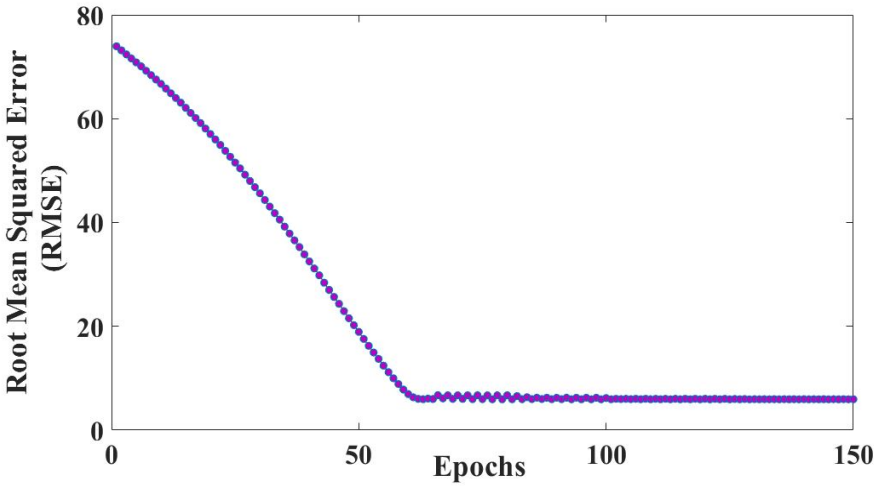

Figure 4.14: Plot of error versus epochs for modelling material removal.

ANFIS regression models were also developed for other three membership functions. Out of all the four membership functions considered sigmoidal membership had better accuracy as shown in Table 4.6. The deviation of the outputs generated by the sigmoidal fuzzy model with the experimental data is illustrated in Figure 4.16

with a RMSE of 5.64. Thus, it can be inferred that there is a co-relation between the simulated results and the experimental results obtained at the same machining conditions. The R^2 calculated based on the fitted regression line is of value 0.980 which also shows that fit of the regression model is good. The prediction results show that by employing hybrid learning algorithm such as ANFIS, the quality of generated relevant fuzzy if-then rules can be tuned to model the material removal behaviour.

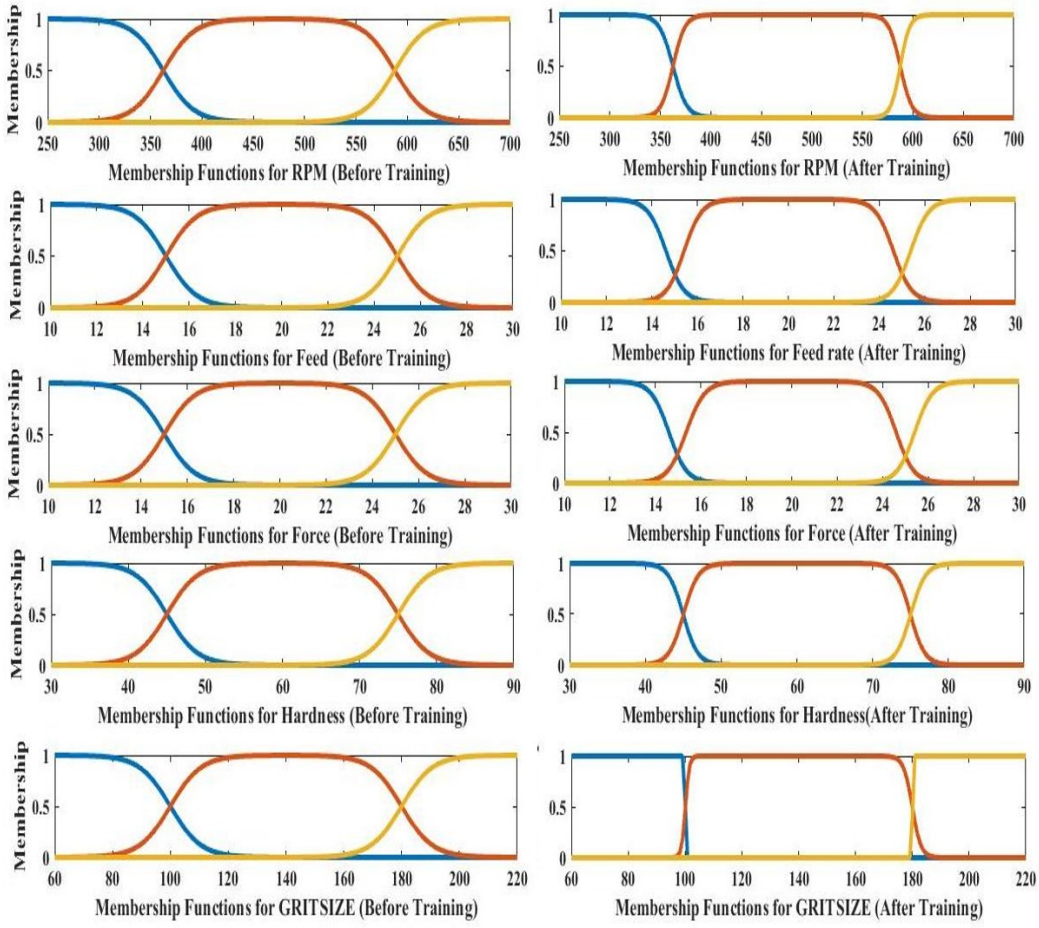

Figure 4.15: Change in shape of the sigmoidal membership function for each input before and after Training.

Table 4.6: Comparison of prediction accuracy and membership function.

Membership function	RMSE
Sigmoidal membership	5.648
Gaussian bell membership	6.7941
Gaussian membership	7.100
Bell-shaped membership	7.0341

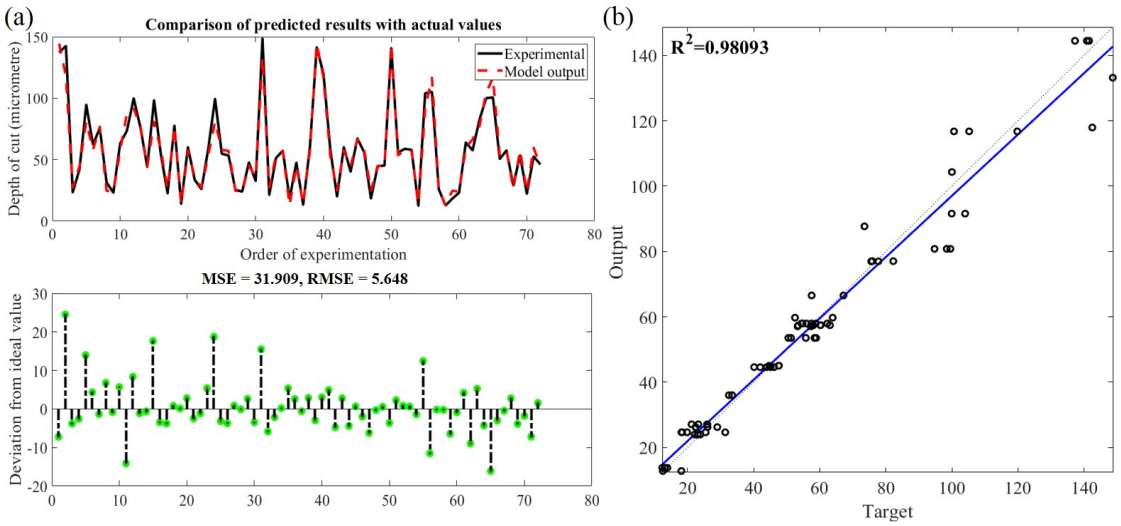

Figure 4.16: (a). Comparison of observed and predicted depth of cut using ANFIS with sigmoidal membership function; (b). Statistical analysis fit of the ANFIS model with sigmoidal membership.

Moreover, the relationship between the input parameters on material removal characteristics in belt grinding process can be interpreted which was not possible using black box models such as ANN. Understanding the input-output correlation from the proposed ANFIS architecture, it is easier to model material removal behaviour for which there is no concrete analytical description till date.

4.5 Support vector regression (SVR)

A regression version of Support Vector Machine (SVM) is referred to as support vector regression (SVR) which has emerged as an alternative and powerful technique to solve regression problems by introducing an alternative loss function. The SVR is centered on the idea of mapping the data x into a high-dimensional feature space to solve the regression problem.

Consider a data set where x_i is a D-dimensional input vector, y_i is a scalar output or target, and l is the number of points. The goal in SVR, is to find a function $f(x)$ that has at most ε deviation from the obtained targets y_i for all the training data. The nonlinear relationship between input and output is then described by a regression function $f(x)$ with weight factor $\omega = \sum_{i=1}^{n} \alpha_i x_i$ and bias b. The SVR algorithm can be extended to nonlinear cases by simply preprocessing the training patterns x_i, by a map $\phi : X \rightarrow F$, into some feature space F and then applying the

standard SV regression algorithm. In the feature space F, the regression function takes shape using a nonlinear mapping function $\phi(x)$:

$$f(x) = \omega^T \phi(x) + b = \sum_{i=1}^{n} \alpha_i \phi(x_i)^T \phi(x_j) + b \tag{4.18}$$

Nonlinear SVRs are trained by exchanging the inner products with the corresponding kernel $K(x_i, x_j) = \phi(x_i)^T \phi(x_j)$ and resultant non-linear SVR is then represented as a kernel function as shown in equation (4.19)

$$f(x) = \sum_{i=1}^{n} \alpha_i K(x_i, x_j) + b \tag{4.19}$$

For the SVR model to have good generalisation performance, ω needs to be as flat as possible. This means that the norm ($\|.\|$) of the ω vector needs to be minimised for every data $i = 1, 2, ..., l$

$$minimise \quad \frac{1}{2}\|\omega\|^2 \tag{4.20}$$

$$f(x) = \begin{cases} y_i - (\omega, x_i) - b \leq \varepsilon \\ \omega, x_i) + b - y_i \leq \varepsilon \end{cases} \tag{4.21}$$

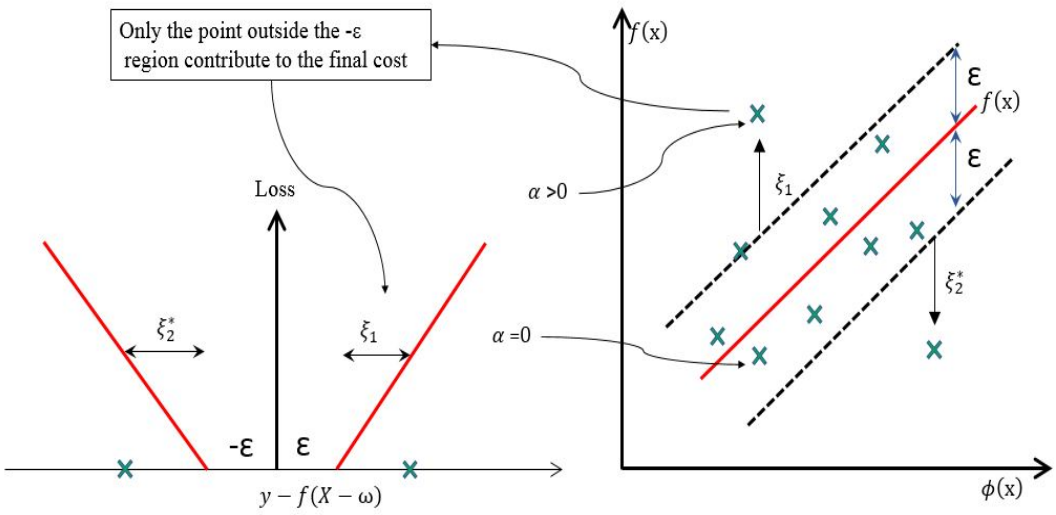

Figure 4.17: The regression line of SVR with the loss function and slack variables.

Figure 4.17 shows the regression line, the upper boundary line, lower boundary line and the radius of the $\pm\varepsilon$ insensitive loss function. The importance of the insensitive zone ($+\varepsilon \quad to - \varepsilon$) is that the points within the radius of the of insensitive loss function is deemed to be well estimated by the model, on the other hand those outside the insensitive zone contribute to the training error loss. Therefore, the radius ε of insensitive zone controls a number of support vectors. As the radius of insensitive zone increases, numbers in the support vector group reduces, and robustness of the model diminishes. A penalisation is calculated by introducing C for points outside the insensitive zone ($+\varepsilon \quad to - \varepsilon$) which decides flatness and complexity of the model. A higher value of C makes the model more complex with the chance of overfitting, and smaller value may increase training errors. An optimum choice of this two-regularisation parameter is necessary for an ideal SVR model. To obtain the optimal hyperplane, the positive slack variable ξ_i is introduced to solve the following optimisation problem as illustrated in Figure 4.17. The constraint problem can be reformulated as

$$\text{minimise} \quad \frac{1}{2}\|\omega\|^2 + C\sum_{i=1}^{l}(\xi_i + \xi_i^*) \tag{4.22}$$

$$\text{where} \quad |\xi|_\varepsilon = \begin{cases} 0, & if \quad |\xi| < \varepsilon \\ |\xi| - \varepsilon & \text{otherwise} \end{cases} \tag{4.23}$$

$$f(x) = \begin{cases} y_i - (\omega, x_i) - b \leq \xi_i + \xi_i^* \\ \omega, x_i) + b - y_i \leq \xi_i + \xi_i^* \\ (\xi_i + \xi_i^* \geq 0) \end{cases} \tag{4.24}$$

The regression function can be obtained by solving the following optimisation problem using standard dualisation principle utilising Lagrange multiplier which will give the estimates of $\omega = \sum_{i=1}^{n}(\alpha_i^* - \alpha_i)\phi(x_i)$ and b. After solving the dual form, the regression function becomes:

$$f(x) = \sum_{i=1}^{n}(\alpha_i^* - \alpha_i)K(x_i, x_j) + b \; where \; \alpha_i^*, \alpha_i = Lagrange \; multipliers \tag{4.25}$$

Gaussian radial basis function with standard deviation (γ) is commonly used, as it has the potential to handle higher dimensional input space. For accurate model fitting, three internal parameters of SVR, namely regularisation parameter (C), the radius of loss insensitive zone (ε) and standard deviation (γ) of kernel function are to be correctly set. Bayesian optimisation approach is used to identify the optimised regularisation parameter. Figure 4.18 shows the architecture of a regression machine for belt grinding process. The construction of the material removal model using support vector regression (SVR) can be summarised as follows:

1. Defining the data for learning and testing.
2. Choosing an appropriate kernel function (linear, Gaussian, radial basis function (RBF), polynomial, etc.)
3. Selecting an optimal model for training on the input data. The training is done by using a Bayesian optimisation.
4. Cross-validation on the testing data.

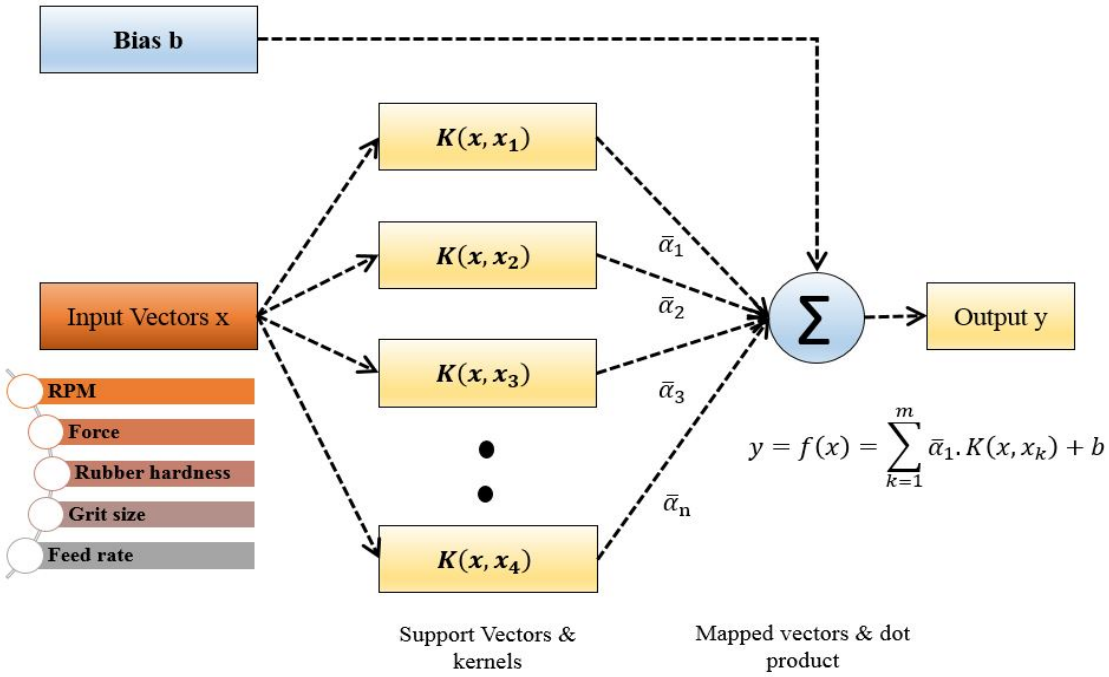

Figure 4.18: The architecture of a regression machine constructed by the SVR algorithm.

Table 4.7: Optimised SVR training parameters.

Parameter	Value	Remarks
Epsilon (ε)	0.12457	Regularisation parameter identified from Bayesian optimisation.
Box constraint (C)	989.65	Regularisation parameter identified from Bayesian optimisation.
Optimization method	Bayesian optimisation	-
Kernel	Gaussian radial basis function	Kernel to handle higher dimensional input space.
Kernel scale (γ)	0.10894	-
Training	70%	-
Testing	30%	-
Predictors	5	-
Response	1	-

Similar to the previous analyses 70% of the recorded data is selected stochastically for training and 30% for testing. The RBF is used as the kernel, where the kernel parameter γ is determined by Bayesian optimisation. The training is performed under MATLAB platform.

From our initial analysis, it was found that regularisation parameter (C= 989.65), the radius of loss insensitive zone (ε= 0.12457) and standard deviation (γ= 0.10894) give the minimal value of the MSE based on Bayesian optimisation algorithm as depicted in the Figure 4.19. There is a sudden reduction of error after five evaluations and decreases further before it saturates after 15 evaluations.

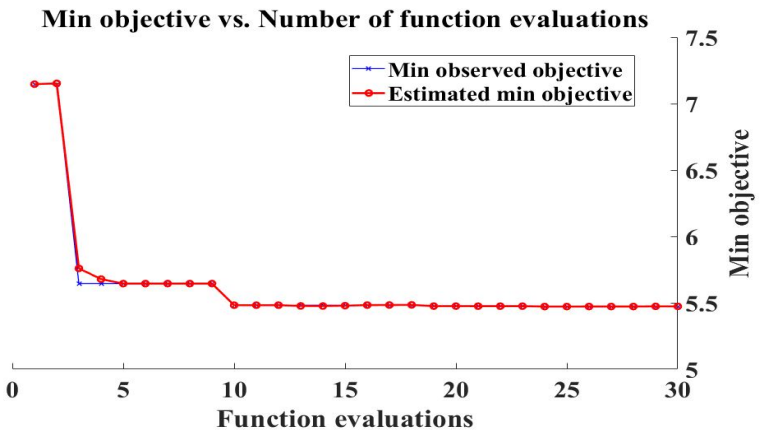

Figure 4.19: Optimisation of SVR parameters with respect to the number of iterations.

A higher value of C in the feature space signifies that the material removal model is highly complex with large random noises which also gives an indication of nonlinear behaviour of the belt grinding process. The lower values of ε for material removal indicates that the SVR model could capture the intricacy of the belt grinding process effectively. The tuned parameters used in the SVR model during learning process is listed in Table 4.7. Once the model completed the training stage, it was tested with the validation data. The effectiveness of the training can be concluded from its ability to forecast material removal from unseen data. The R^2 calculated based on the fitted regression line is 0.980 which also shows good fit of the model.

Figure 4.20 shows the deviation of the predicted values against actual values using the SVR model highlighting RMSE of 6.9989. Trained SVR model with optimum parameter settings C, ε, and γ obtained using Bayesian optimisation can efficiently predict material removal responses. Though the testing result of developed SVR algorithm favors the practical use of the model in the chosen range, the main limitation of the support vector approach is attributed to the kernel selection, which is based on trial and error.

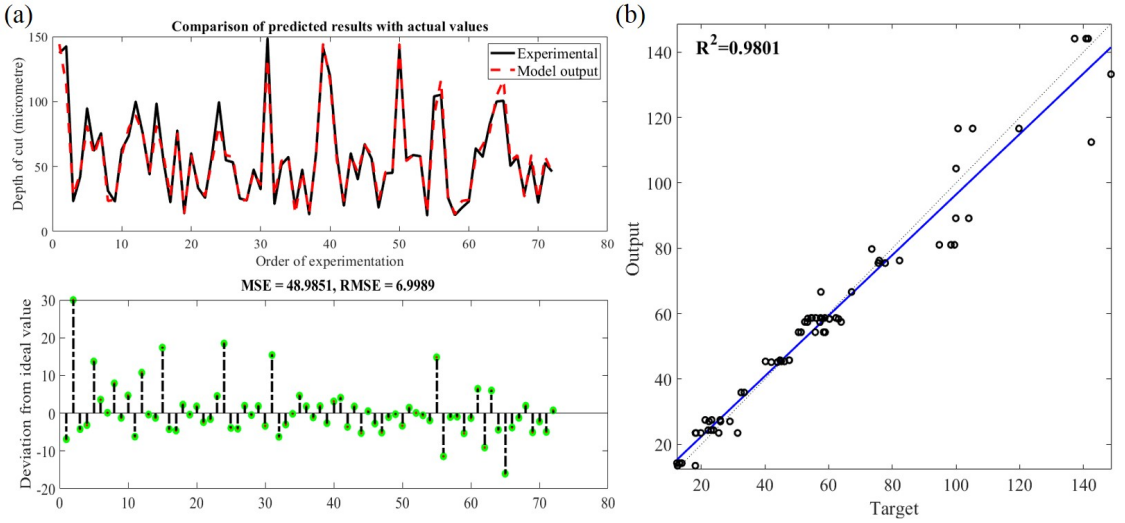

Figure 4.20: (a).Comparison of observed and predicted depth of cut using support vector regression; (b). Statistical analysis fit of the support vector regression model.

4.6 Random forest (RF)

One disadvantage of using a single decision tree (DT) is attributed to the risk of overfitting in the training data. Random forest (RF) model is a cumulative model

that makes predictions by augmenting decisions from a group of decision trees as base learners. The RF models can be written as:

$$g(x) = f0(x) + f1(x) + f2(x) + ... \tag{4.26}$$

where the final model g is the sum of simple base models f_i which is regression decision trees. Unlike linear models, random forests can capture the non-linear interaction between the features and the target. One of the biggest advantages of random forest over decision tree is that the algorithm works on boot strapping. Random forest creates a lot of individual decision trees by re-sampling the data many times with replacement and makes the final prediction at a new point by averaging the predictions from all the individual binary regression trees on this point. Averaging over all the decision trees results in a reduction of variance thereby enhancing the accuracy of the prediction. The accuracy of the random forest can be estimated from observations that are not used for individual tree otherwise called as "out of bag data" (OOB) as equation (4.27)

$$OOB \sim MSE = \frac{1}{n}\sum_{i=1}^{n}(y_i - \hat{y}_{iOOB})^2 \tag{4.27}$$

where $\hat{y}_{iOOB}$ denotes average prediction for the i^{th} observation from all trees for which this observation has been OOB. In the context of material removal prediction, each individual decision tree in a random forest is a regression tree. The dataset (n = 243) consisting of the five predictors (feed, rubber hardness, RPM, normal force, grit size) and the response variable (depth of cut) is randomly split into 70% and 30% for a training (n = 171) and validation (n = 72) respectively. The training dataset was used to optimise the random forest regression and to train the prediction model, while the validation dataset was used to test the quality and reliability of the random forest model.

The framework of predicting material removal using a RF is illustrated in Figure 4.21. The algorithm for material removal regression can be summarised as follows:

1. A bootstrap sample $(X_1, X_2, X_3, \ldots . X_n\ )$ of size N is to be drawn from the training data consisting of the five predictors and the response variable.

2. For each bootstrap sample X_i, a regression tree model is constructed by optimising the parameters, such as the number of trees t_n and leaf size based on MSE error.

3. Prediction at a new point Z is achieved by aggregating the predictions of the regression tree models.

4. The accuracy of the RF model is calculated based on the deviation of predicted value, x, from the ideal value in the validation data set.

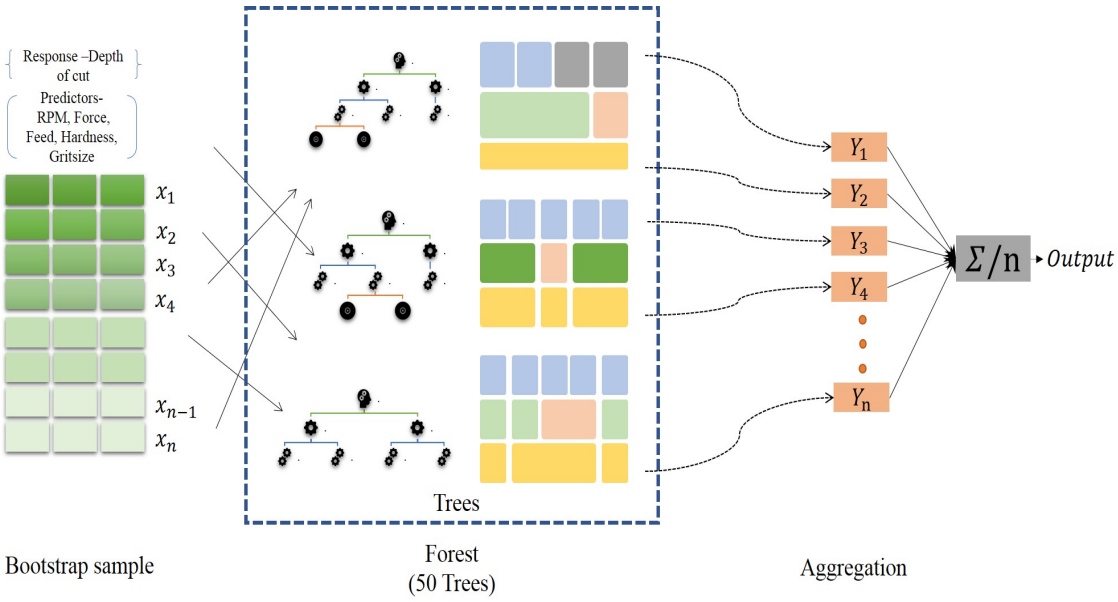

Figure 4.21: Material removal prediction using an RF.

The development of the relationship between belt grinding parameters and material removal RF model is carried out using MATLAB. Some parameters such as the minimal size of the terminal nodes of the trees, i.e., leaf size and a number of regression trees grown based on a bootstrap sample are optimised in random forest model upon the minimisation of the MSE. The number of regression trees in a random forest model defines the strength of each tree in the forest and its correlation with other trees. A number of regression trees were optimised based on the MSE by testing with five different tree values (5, 10, 20, 50 and 100) on the training dataset.

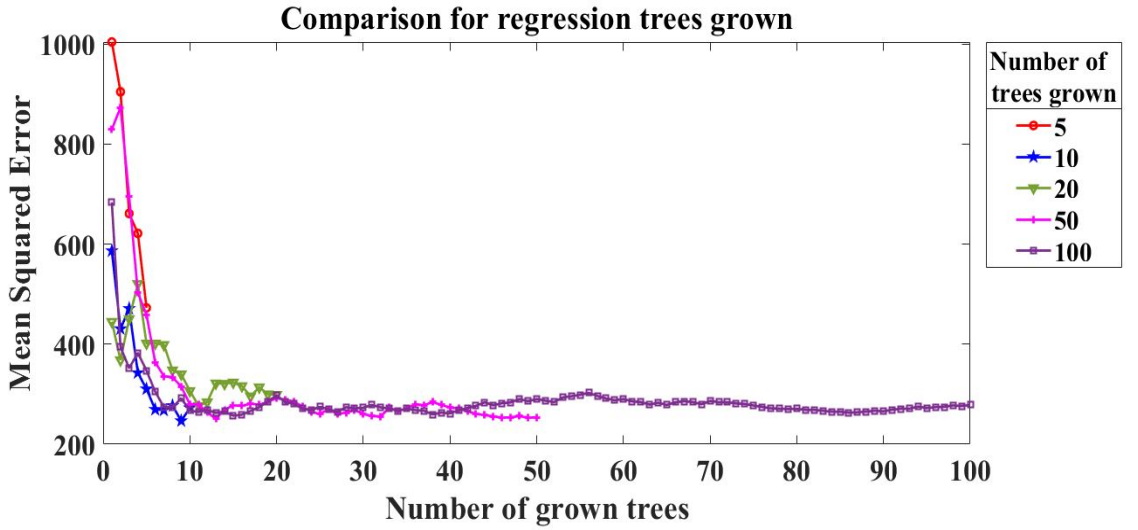

Figure 4.22: Optimisation of RF parameters (number of grown trees) using MSE.

Figure 4.22 indicates how the number of regression trees grown in RF affect the prediction error. Inferring from the figure, it is evident that the MSE saturated after 35 trees and did not improve further as the number of trees increased. The minimum leaf size parameter specifies the smallest number of observations a node can have. Letting the trees split down to leaf nodes with a minimum observation results in the most accurate random forest models. However, it is noted that smaller leaf size results in deeper trees with higher accuracy but also increases the cost of computation time and memory.

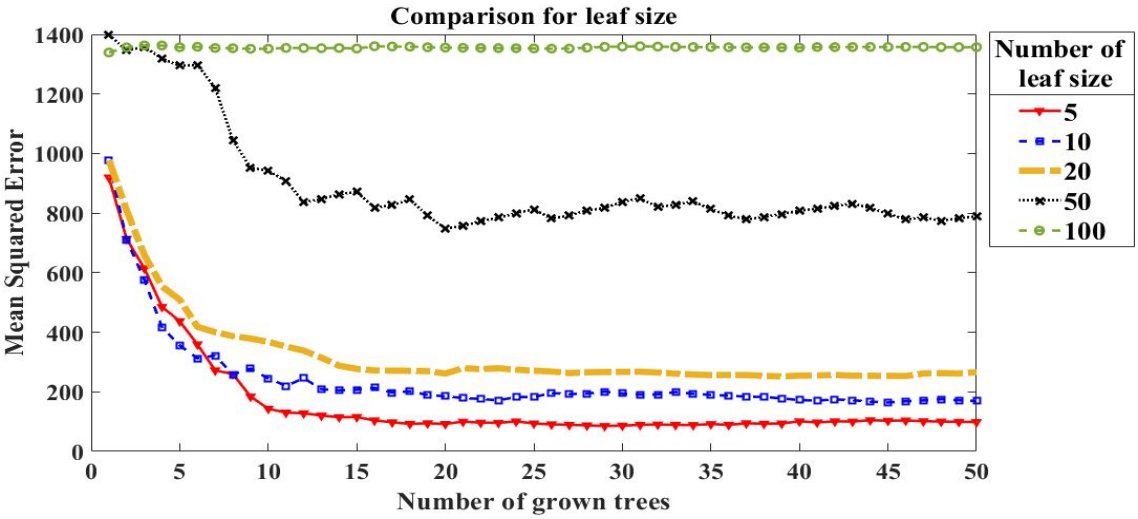

Figure 4.23: Optimisation of RF parameters (number of leaf size) using MSE.

Figure 4.23 indicates that the effect of the minimum leaf size and it is quite clear that with minimum leaf size, i.e., deeper trees the prediction ability of the model is

higher. The splitting process stops at the child node if the number of observations in a node is less than five which is used as a stopping criterion in regression model developed. Based on results from fine-tuning discussed in the section above, a random forest is constructed using 50 regression trees. A bootstrap sample of size 40 (0.25% of the training data) is drawn from the training dataset for every iteration. After 50 regression trees are constructed, a prediction at a new point can be made by aggregating the predictions from all the individual binary regression trees on this point. The tuning parameter used for developing the random forest regression model is listed in Table 4.8.

Table 4.8: Random forest training parameters.

Parameter	Value	Remarks
In bag fraction	0.25% of the training dataset	Boot strap sample size.
Method used by trees	Regression	-
Min leaf size	5	Smallest number of observations a node can have.
Number of trees	50	Number of regression trees grown.

Figure 4.24 shows an individual regression binary tree in the random forest model built based on the optimised tuning parameters listed in Table 4.8. The random forest model can rank the predictors (RPM, hardness, force, grit size and feed rate in our case) based on their importance by estimating Out-of-bag error.

The elements not included in the bootstrap sample are referred to as out-of-bag data (OOB). At each bootstrap iteration, the response value for data not included in the bootstrap sample (OOB data) is predicted and averaged over all trees t follows as shown in equation (4.28)

$$OOB \sim MSE_t = \frac{1}{n_{OOB,t}} \sum_{i=1:i\epsilon OOB_t}^{n} (y_i - \hat{y}_{i,t})^2 \tag{4.28}$$

where $\hat{y}_i,\ y_i,$ and $n_{(OOB,t)}$ denotes average prediction, observed output and the number of OOB observations in tree t. The importance of each predictor is measured by calculating the percent increase in MSE and These variable importance values are then used to rank the predictors in terms of the strength of their relationship

to the response variables. Figure 4.25 shows the predictors importance measured in terms of the increase of OOB error which states that grit size has higher correlation with material removal than others.

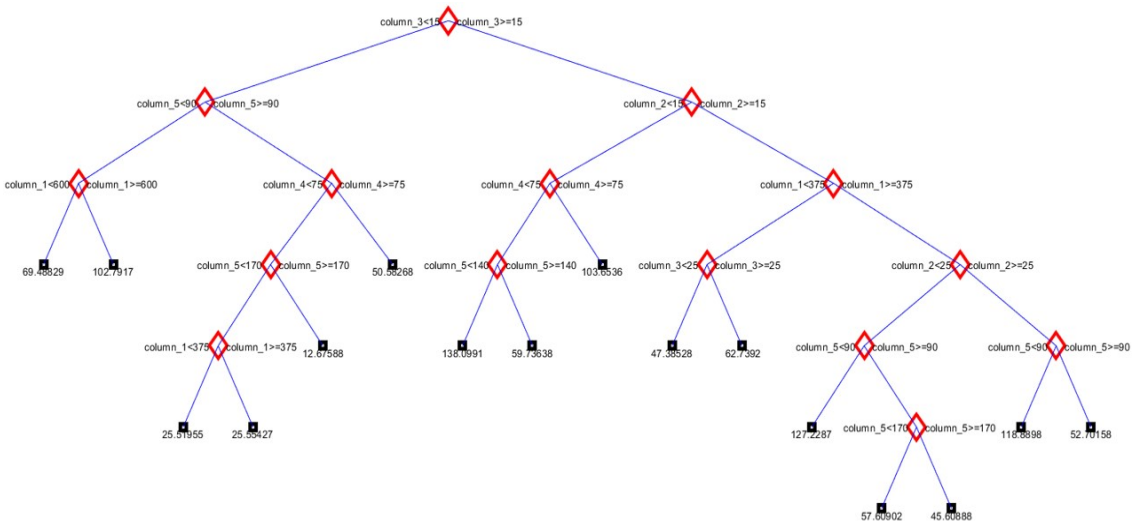

Figure 4.24: A tree used as regression function in the developed random forest model.

Figure 4.26 shows the reduction in error with number grown trees in the model developed. The developed random forest model robustness was evaluated by identifying the deviation of the observed value in the validation dataset and value predicted by the model. The random forest model predicts a new point by aggregating the predictions from all the individual 50 regression trees ensembled inside the model.

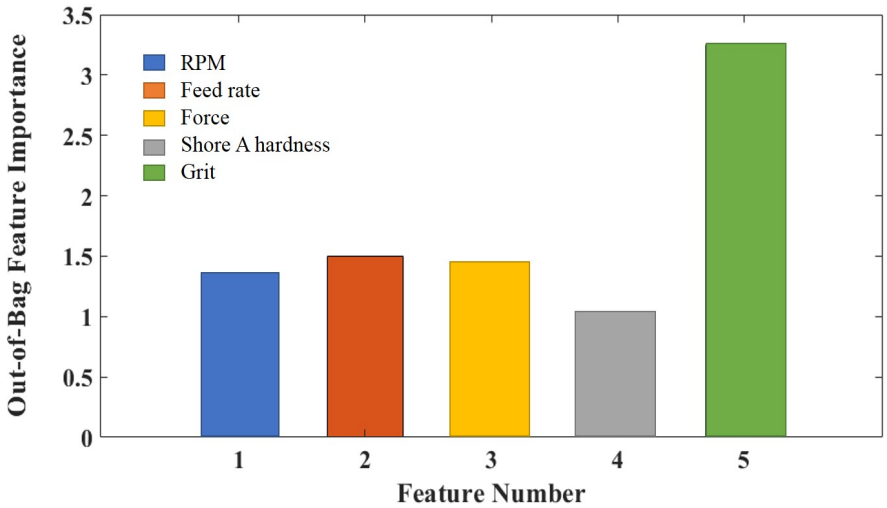

Figure 4.25: Variables importance in predicating material removal using Random forest.

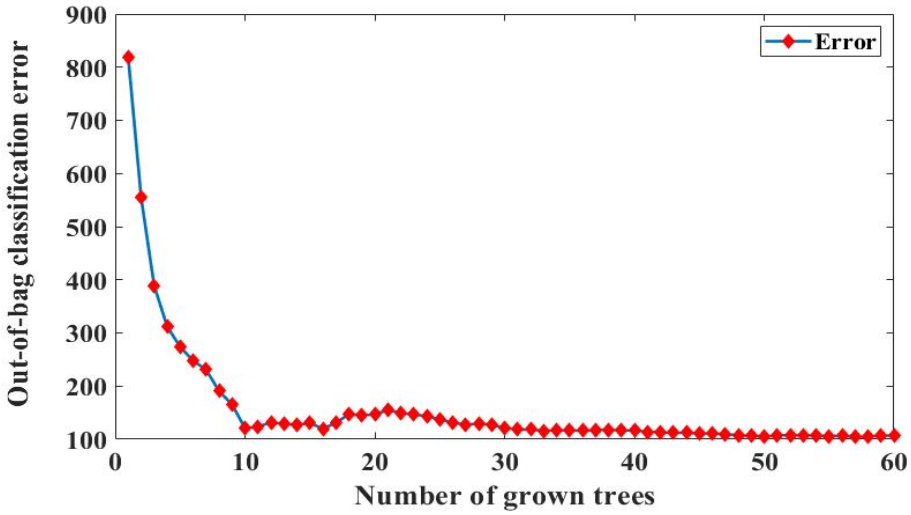

Figure 4.26: Out of bag classification error.

Figure 4.27 shows the one to one relationship between observed material removal values as predicted with the test dataset using RF regression model. It appears that the proposed model is good at predicting the material removal i.e. depth of cut. Figure 4.27 shows the deviation the predicted values against actual values with RF's highlighting the RMSE of 8.94. The R^2 calculated based on the fitted regression line is of value 0.975 which also shows that goodness of fit of the RF model is good. Although random forest seems more of a "black box" approach compared to regression trees since individual trees cannot be assessed separately, it still provides means for interpretation in giving measures of variable importance.

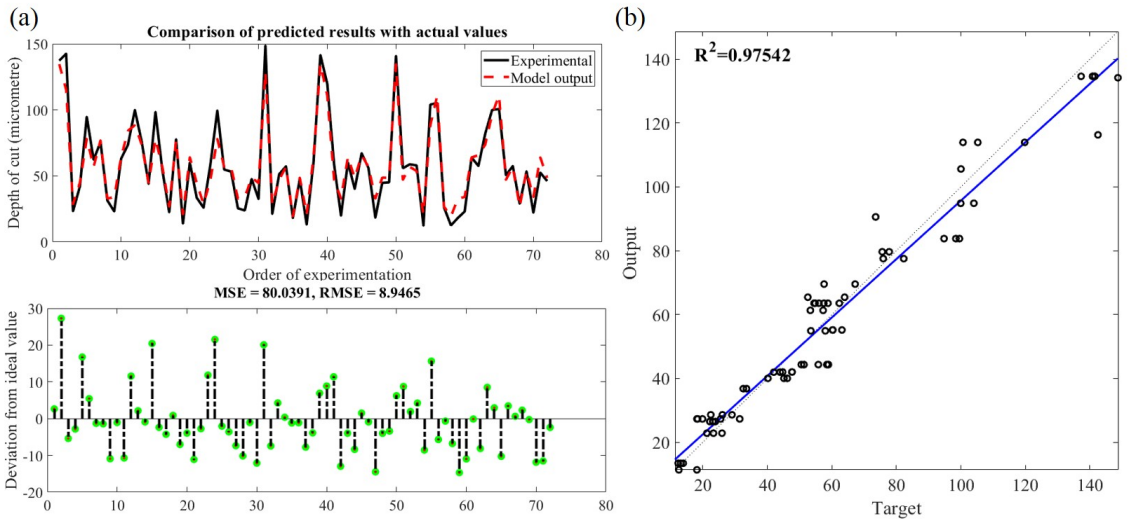

Figure 4.27: (a). Comparison of observed and predicted depth of cut using RF regression; (b). Statistical analysis fit of the RF regression model.

4.7 Conclusion

This chapter illustrates the application of different regression techniques coupled with Taguchi design of experiments. The outcome demonstrate the practicality of the techniques in developing a material removal model for abrasive belt grinding process. Based on the regression models developed the following generalised conclusions are drawn:

- Observing the performance of the multilinear and stepwise regression models it is seen that belt grinding parameters are intrinsically nonlinear and straight-line relationship assumption cannot satisfy the material removal.
- Although predicted values using ANN networks were close to the measured values, it functioned as a black box model correlating the parameters on its own, and the structure determination was based on trial and error.
- SVR modelling implemented using a Gaussian kernel function showed good accuracy on material removal. However, the drawback of the model is attributed to the selection of the kernel function that is based on trial and error.
- The ANFIS model developed in this research work has acceptable deviations between the predicted and the real results and is viable to predict the depth of cutin the abrasive belt grinding process compared to other regression techniques. The performance of the six algorithms in terms of RMSE is summarised in Figure 4.28.

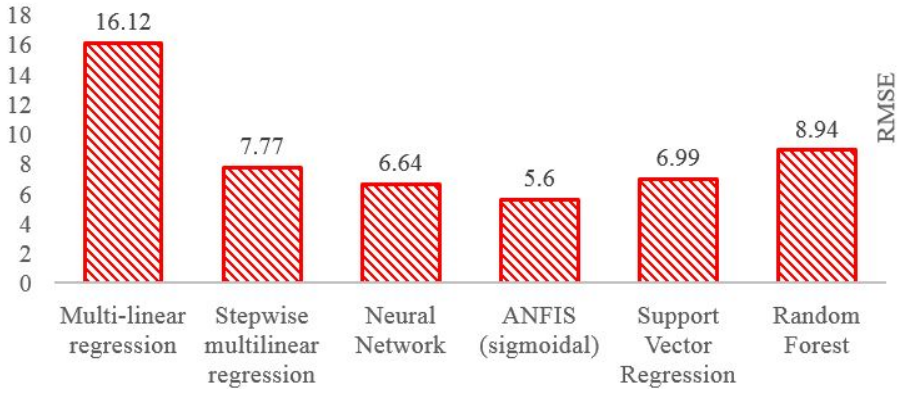

Figure 4.28: Predictive performance of the regression models.

- In addition, ANFIS could interpret the relationship between the input parameters towards the output behaviour which was not possible using other modelling techniques.
- Random forest model which is based on the frequency table was not able to predict at higher accuracy compared to other complex predictive model even though it performed better than the multilinear regression.
- Analysis of the membership functions after training in ANFIS and interpretation of variable importance measure results from RF indicates that grit size factor in belt grinding has the most impact on material removal.

Overall results from the chapter suggest that regression techniques that have the adaptability to capture nonlinear space performed well and is viable to model the material removal in abrasive belt grinding process.

Chapter 5

Material removal modes

5.1 Introduction

The changes in material removal rate and grinding force in coated abrasive belt grinding are caused principally by the formation and increase of the worn flat area on grain tips [43]. Hamann [50] had proposed a linear mathematical model which indicated that the overall material removal rate is proportional to belt wear factor. The granularity of the abrasive grain is dominant among all belt finishing parameters for material removal in belt grinding process [107,295]. Khellouki *et al.* [12] revealed the effect of abrasive grain wear on surface texture in belt finishing process and concluded that material removal rate changes based on the wear level of abrasive grains. These studies on belt grinding process emphasize on the impact of tool condition on the effectiveness of the grinding process and surface finish. Based on the authors knowledge, studies on belt grinding process have not emphasized on the influence of abrasive belt wear on the material removal mechanisms, i.e. rubbing, ploughing and cutting and this chapter tries to bridge this gap.

5.2 Material removal mechanism

The coated abrasive grinding process is characterized by the simultaneous contact of abrasive grains on the surface of the workpiece. As a result of the contact, there are many events that occur in the interaction zone as shown in the Figure 5.1. Among various events occurring in the interaction zone, only three events namely rubbing,

ploughing and cutting that are significantly responsible for the modification of the surface i.e material removal.

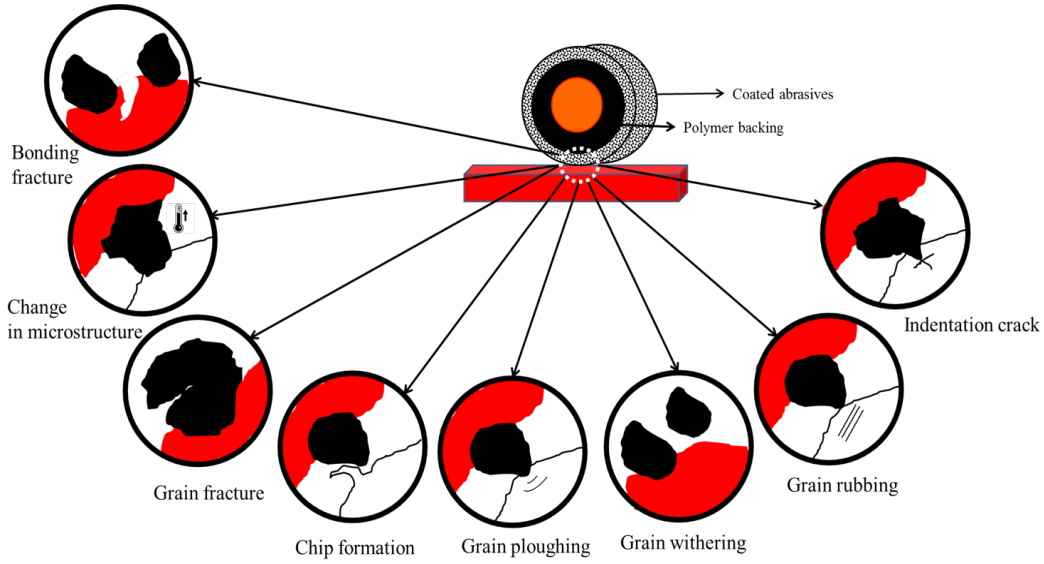

Figure 5.1: Various events occurring in the grinding zone.

In abrasive machining, material removal is caused by the interaction of the abrasive grain with the workpiece material. Abrasive grains have undefined tooltips and negative rake angle that result in high specific energy at the machining point and enable them to penetrate the workpiece upon a flat pathway. Once a sufficient force is developed, the abrasive grain tip penetrates deeply into the workpiece due to its cutting-edge geometry that causes a plastic flow of the workpiece material after it exceeds the elastic deformation. The minimum chip thickness in any abrasive machining process corresponds to the grain cutting depth on the workpiece material.

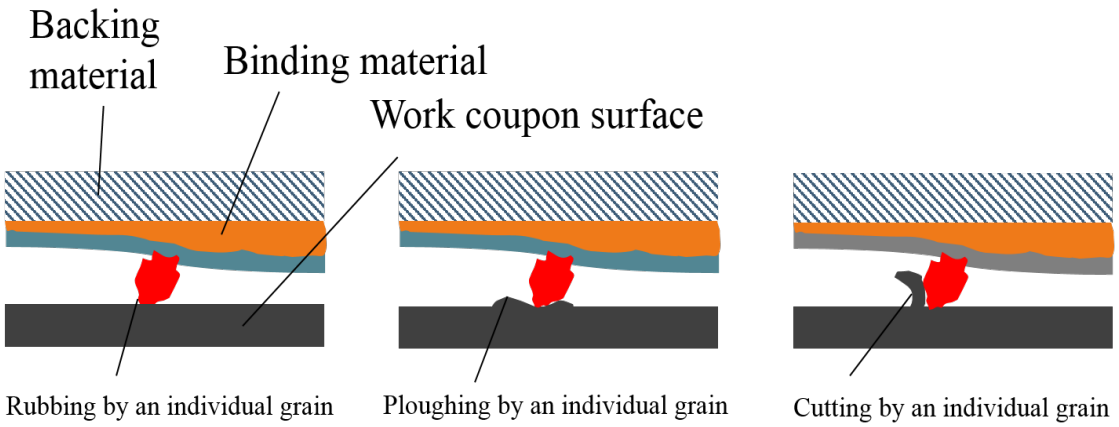

Figure 5.2: Interactions in the grinding zone as results of three material removal mechanisms.

The abrasive grains and the work material surface interact in different ways as illustrated in Figure 5.2, namely cutting (material removal), ploughing (material displacement), and rubbing (surface modification) [55–57].

Rubbing is typically characterised by elastic deformation as the grain slightly interacts with the surface without causing any plastic deformation, i.e. it does not leave any mark on the material surface. As the interaction of grain increases, it results in both elastic and plastic deformation. This is where other two phenomena, namely cutting and ploughing exist. Ploughing is a result of plastic deformation of the material as a continuous groove with ridges on both sides are formed on the surface. However no material is dislocated from the surface. When the process of grit to workpiece interaction intensifies, it results in chipping of the material from the surface, i.e. cutting. The interactions of individual grains with the workpiece cause compressive and tensile loading on the workpiece.

The direct influence of the abrasive grain wear on the material removal modes are discussed using scratch experiments in the sections below.

5.3 Single grain groove measurement analysis

Material removal mechanisms at micro scale during abrasive machining processes consists of three phases, i.e. rubbing, ploughing and cutting [296–298]. Single grain scratch tests were carried out to identify the dominant physical material removal mechanisms present during the evolution of the grain wear.

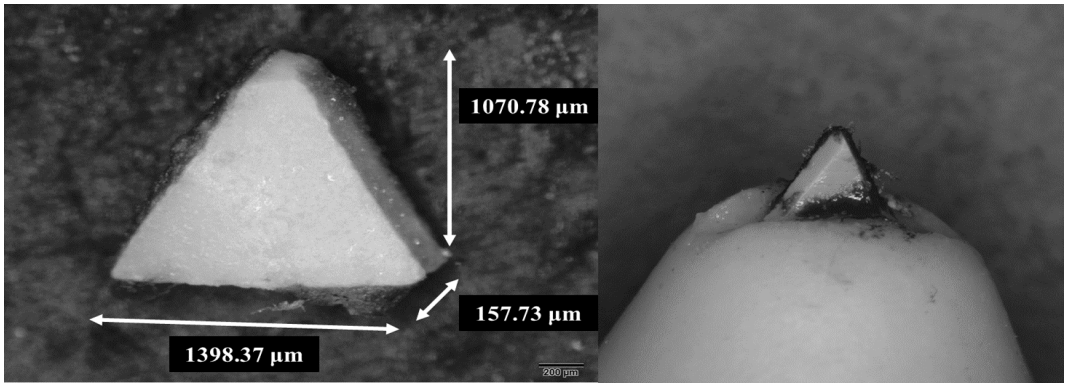

Figure 5.3: Dimension of aluminium oxide (Al_2O_3) grain considered for single grain scratch.

To perform the test, a single aluminium oxide (Al_2O_3) grain from the belt tool is

extracted. A dedicated holding fixture was designed to mount the single grain firmly in place in such a way to allow the grain to touch the workpiece during the scratch test as shown in Figure 5.3. Abrasive grain used is a prismatic triangular grain with 60 degree corner angle, with height and thickness of about 1000 μm and 150 μm as shown in Figure 5.3. The experiment was carried out within a CETR tribometer setup as shown in Figure 5.4. The experimental conditions for the single grain scratch tests are detailed in Table 5.1. The experiments were performed in such a way that triangular face of the grain faces the scratch direction. All scratch test was performed on aluminium (Al-T6061) workpieces with uniform surface conditions. Finally, the groove cut area is calculated to signify the material removal modes.

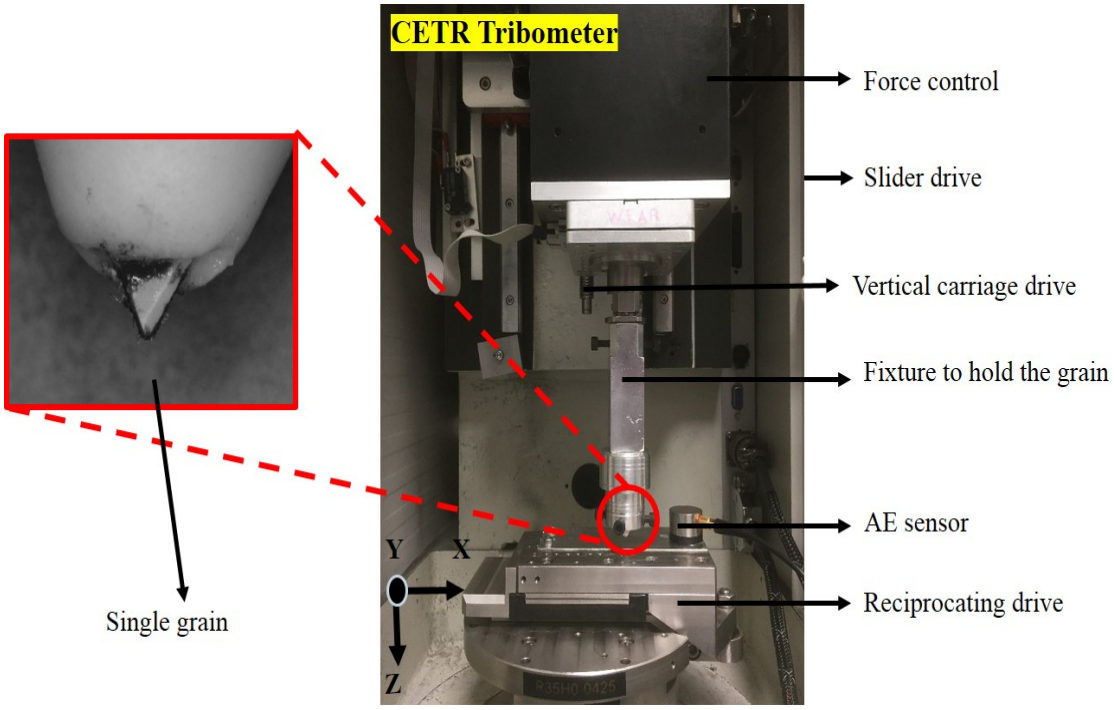

Figure 5.4: Tribometer experimental setup for single grain scratch test.

The scratch tests were carried out by feeding the aluminium oxide grain fixture by the slider drive along the X-axis towards the flat aluminium sample. A scratch groove will be formed on the surface of the flat sample with a stroke on the surface of the flat sample. Removal of material during the scratch pass depends on the cutting action of the single grain to workpiece interaction. Three states of Al_2O_3 abrasive grain as shown in Figure 5.5 were used to perform the scratch tests. Depending on the granularity of the single grain, the cutting depth varies for the abrasive grain states considered. The material removal mechanisms in a single grain scratch

experiments are quantified in terms of the material and groove geometry as shown in Figure 5.6. It is assumed that effect of events such as bond fracture and grain fracture are negligible.

Table 5.1: Experimental conditions for single grit scratch test using CETR tribometer.

Parameter	Value
Reciprocating length	4 mm
Slider speed	12.5 mm/sec
Force applied	5 N
Abrasive grain material	Aluminium oxide
Work piece material	Aluminium 6061

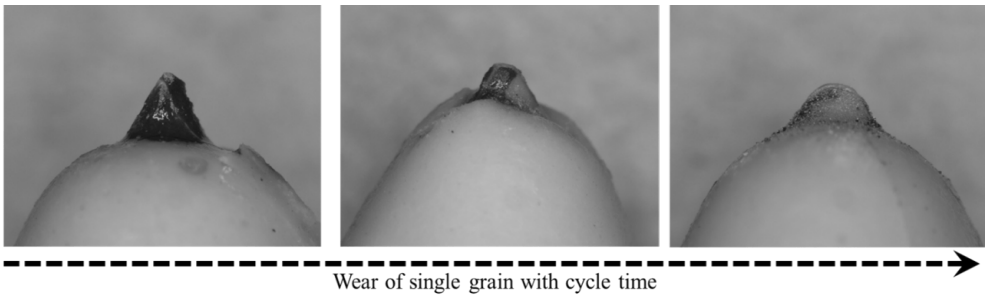

Figure 5.5: Evolution of the grain geometry after successive grinding.

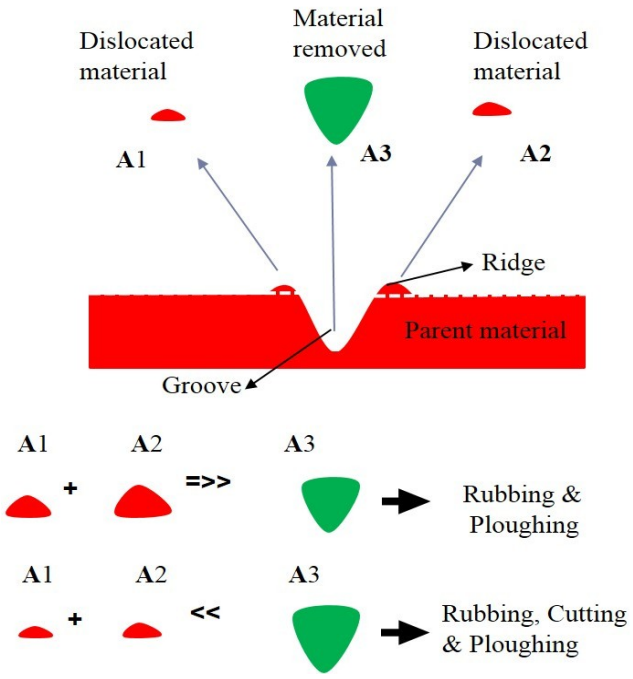

Figure 5.6: Schematics of dominant material removal mechanisms in single grain scratch experiments.

The three physical material removal modes were assessed by measuring the material profile from scratch tests. A Taly-scan profiler was used to obtain an accurate 3D measurement of the single grain scratch groove. Based on Figure 5.7, it is evident that the mechanism of material removal progresses more towards ploughing and rubbing from cutting action as the grain starts to wear down.

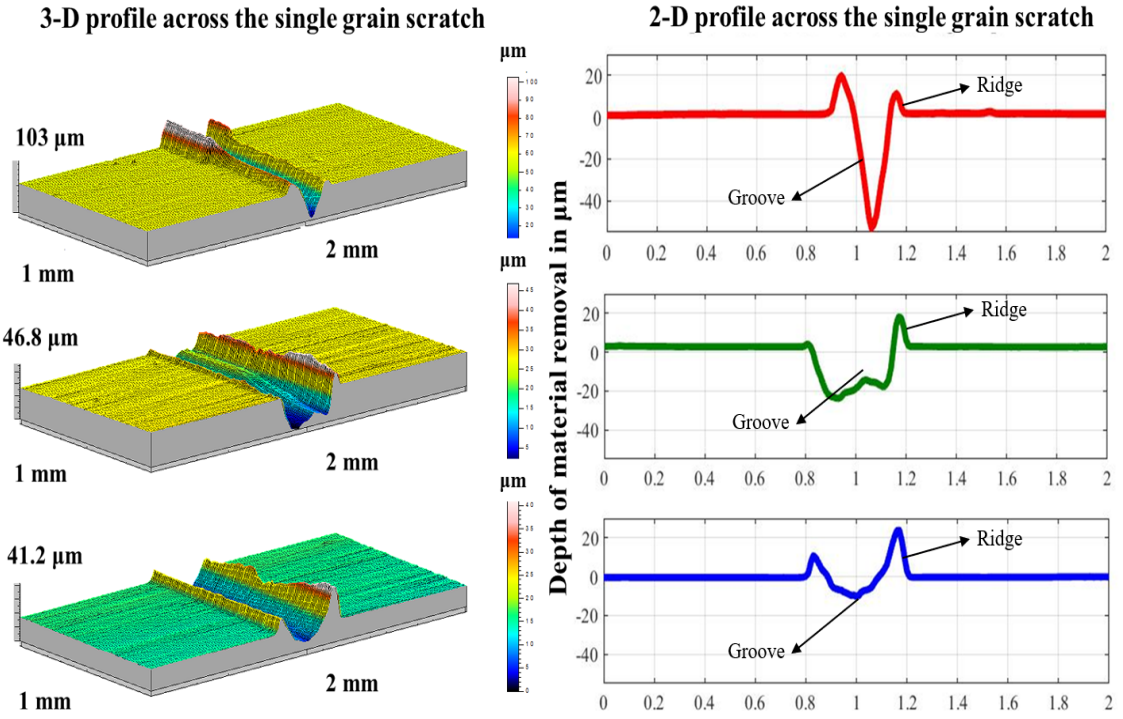

Figure 5.7: Comparison between scratch profiles acquired in 3D and 2D from three different aluminium oxide (Al_2O_3) grain states.

5.4 Dominant frequencies in different material removal modes

Transition in material removal mechanism can also be associated to the change in the geometry of the abrasive grain [57, 299]. Acoustic Emission (AE) is emitted because of material stress release process, as a result of interaction between abrasive grain and the workpiece. Spontaneously released transient elastic energy (AE) when materials undergo deformation or fracture or a combination of both can be used for investigation of grinding fundamentals [152, 153, 300]. The AE emitted during the grinding may come from elastic or plastic shear stress which can be used to

characterise the dominant material removal mechanism. Scratch test was carried out to simulate rubbing, ploughing and cutting with a new Al_2O_3 single grain using CETR tribometer setup as shown in Figure 5.4 on the scratch conditions listed in Table 5.2. It is also assumed that the grains used for all the scratch trials are of same dimension.

Table 5.2: Single grain scratch conditions to simulate three material removal modes.

Scratch parameter	Condition
Depth of cut	66 μm/sec
Slider speed	15 mm/sec
Work piece material	Aluminium 6061
Abrasive grain material	Aluminium oxide
AE sensor range	25 kHz−450 kHz (Vallen VS45-H)
Data acquisition rate	5 MHz

The scratch groove is created starting from a rubbing grain action followed by a ploughing/cutting combination, then lastly by a cutting action as illustrated in Figure 5.8.

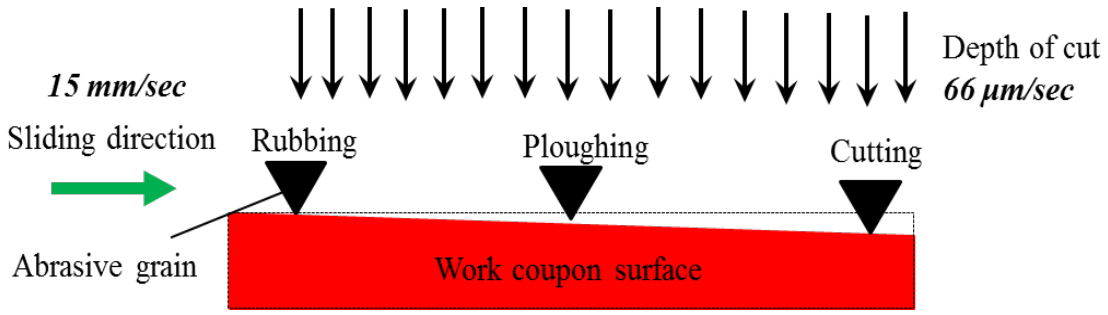

Figure 5.8: Three stages of chip generation on the surface.

Scratch groove was measured using Talysurf profilometer. From Figure 5.9, we can observe a transitional mode from ploughing to cutting. Initially, when the grain begins to interact on the workpiece surface, the normal force and elastic deformation of the workpiece is small that results in the grain sliding, which manifests itself as the rubbing phase. Subsequently, as the depth of cut increases, the vertical force becomes larger, and the grains are pressed into the workpiece surface causing material plastic deformation which results in the grain ploughing the surface. Finally, when the cutting depth of the grain into surface increases, the vertical force becomes

much larger developing higher stress creating chips from the surface resulting in the cutting stage.

The three separate grain action of rubbing, ploughing and cutting are investigated to identify the frequency signatures from the AE reading. The AE sensor is placed as close as possible to the workpiece and grain interaction zone. Figure 5.10 schematically displays how the AE system is designed from the sensor/workpiece to the computer acquisition system. The detected signals from the AE sensor were passed through pre-amplifiers with a gain of 38 dB to boost the magnitude and to eliminate the noise caused by surrounding environmental factors.

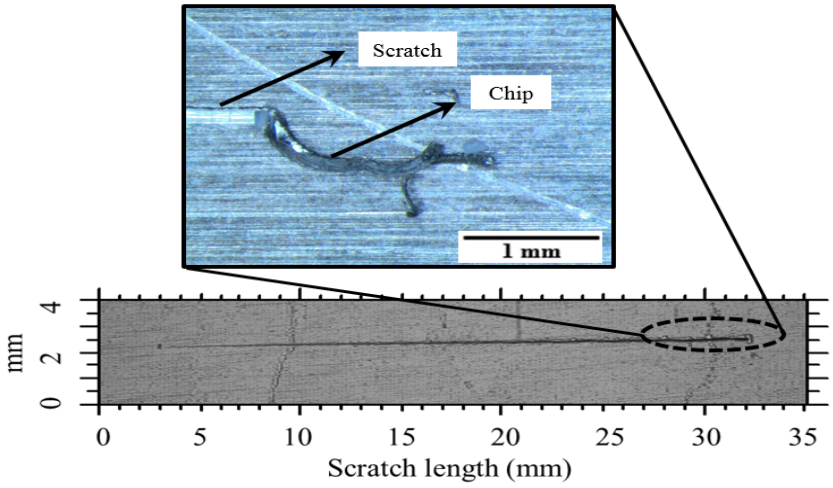

Figure 5.9: Scanned scratch groove profile using profilometer.

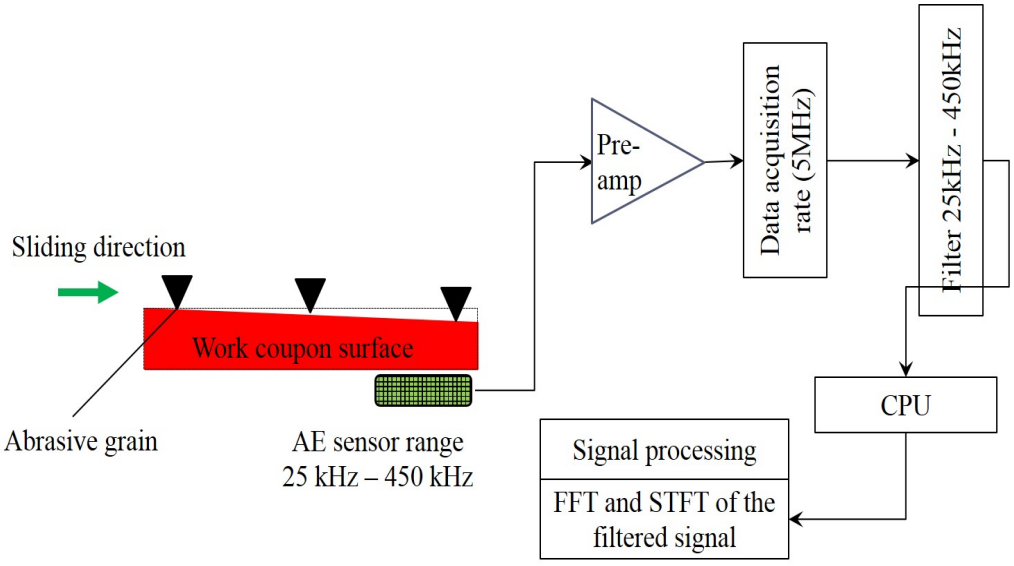

Figure 5.10: AE monitoring system for grinding process and single grain scratch tests.

The amplified AE signal is passed into bandpass filters with a cut-off frequency between 25 kHz and 450 kHz. The AE signals corresponding to these scratch slots are shown in Figure 5.11. It should also be noted that the AE intensity start to rise as the grit slightly interacts with the surface. The pre-processed time domain AE signal is transformed into the frequency domain to obtain the frequency/power spectrum of the signal. FFT calculates the frequency average over the duration of the extracted non-stationary AE signal.

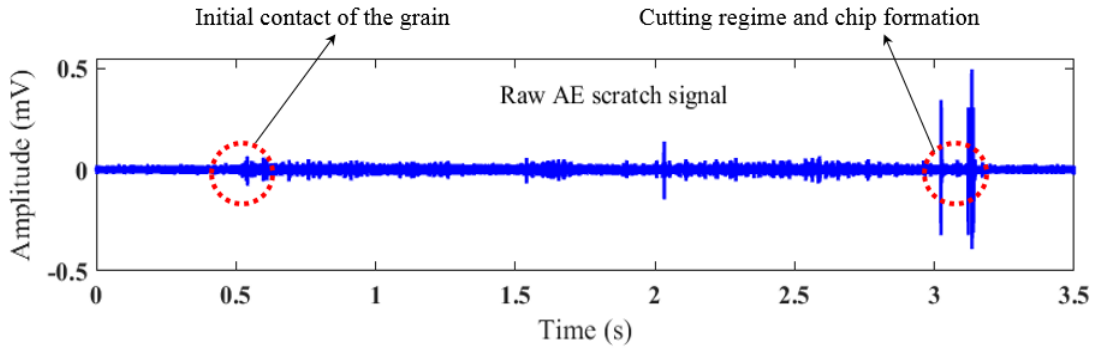

Figure 5.11: AE_{RAW} time signals extracted during single grain scratching.

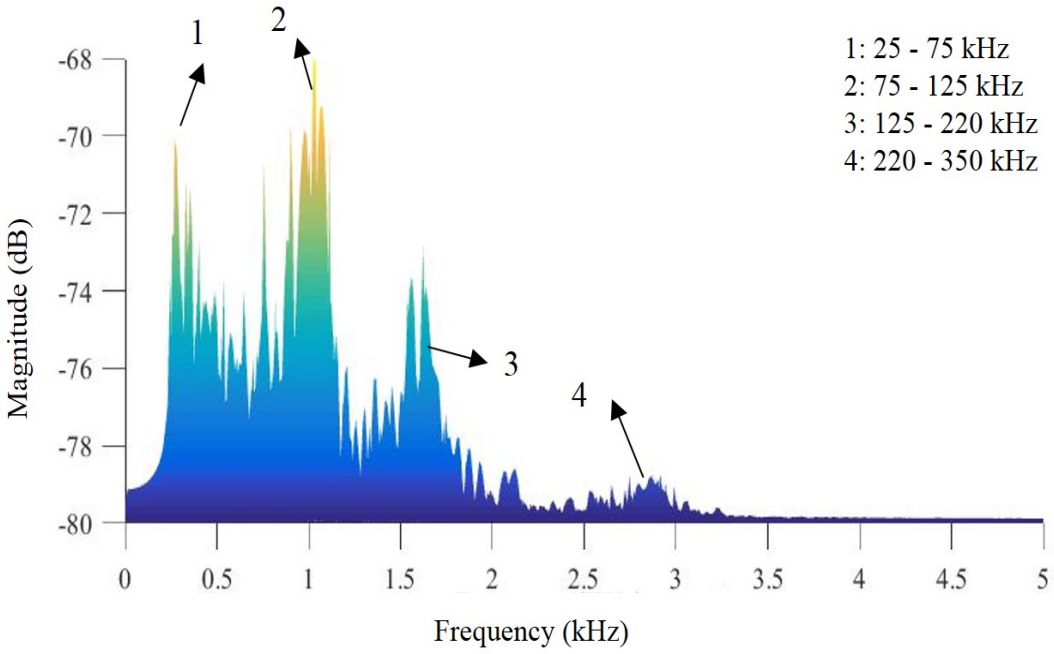

Figure 5.12: FFT analysis for extracted AE signal.

Performing a forward FFT on the AE scratch data and interpreting the results

through spectra plot, four principal peak frequency bands 1 (25−75 kHz), 2 (75−125 kHz), 3 (125−220 kHz), and 4(220−350 kHz) that could be associated with material removal modes are identified as shown in Figure 5.12. The results show that AE energy for the material removal modes is concentrated between the frequency ranges of 25−350 kHz and are typically high frequency components. However, the results from FFT do not adequately describe the transient features regarding time domain.

5.4.1 Short Time Fourier Transform (STFT)

With three different mechanisms from the single grain interaction tests, STFT was further chosen to separate the frequency signatures. STFT was applied along the length of the original time domain signal, based on parameters listed in Table 5.3. Specific to the workpiece material (Al-T6061) and grain Al_2O_3 interactions, it is found that the cutting phase dominated the frequency range within the 125-350 as shown in Figure 5.13 and Figure 5.14. The main factor to note is that ploughing and rubbing dominated in the same frequency range of 25-125 kHz and are inseparable. Analysing the STFT plot in Figure 5.13, it is evident that ploughing and rubbing occur throughout the grain interaction.

Table 5.3: Short Time Fourier Transform parameters.

Parameter	Value
Window length	65536
Hop size	16384
Number of FFT points/ window	4096
Window function	Hamming
Low-pass/ High-pass filter	25 kHz−450 kHz
Data acquisition rate	5 MHz

The four significant bands of occurrences corresponding to the material removal modes can now be classified or labelled in FFT into their respective material removal modes based on the STFT analysis as shown in Figure 5.15. Based on the STFT analysis, two classifications can be made: (1) rubbing and ploughing, and (2) cutting. Two peak frequency bands 1 (25−75 kHz) and 2 (75−125 kHz) corresponds to rubbing and ploughing modes and frequency bands 3 (125−220 kHz) and 4 (220−350 kHz) belong to cutting mode.

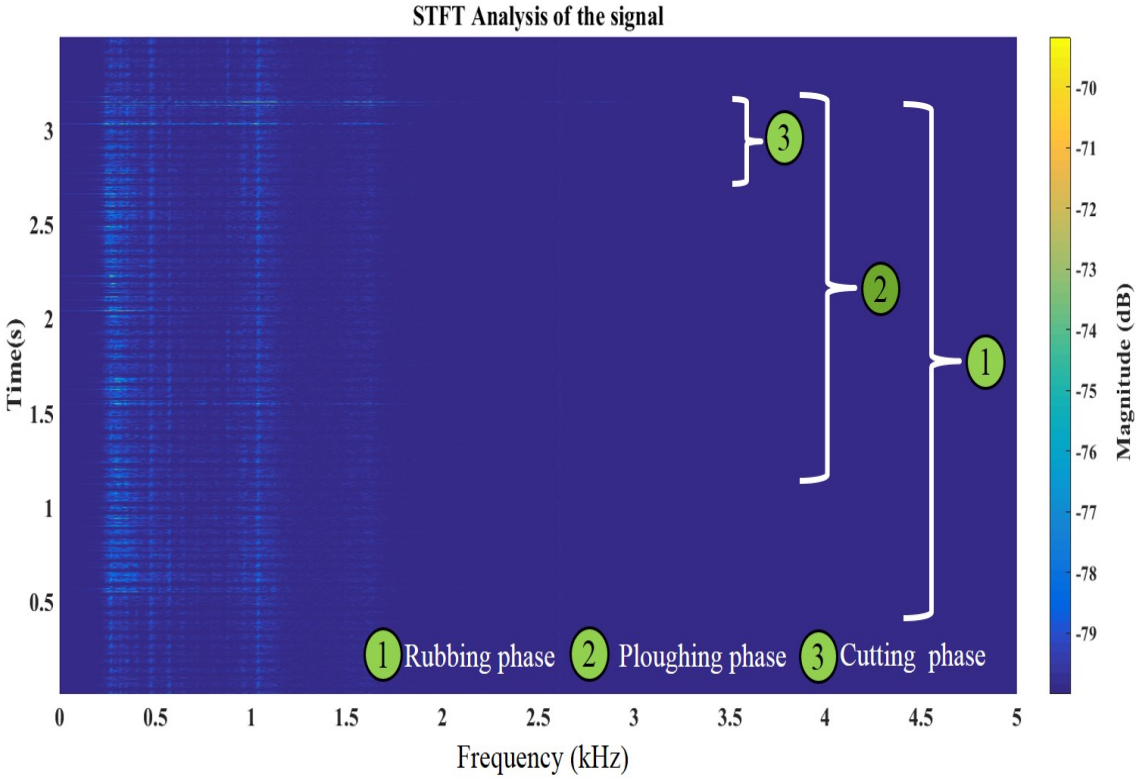

Figure 5.13: The 3D spectrogram plot of STFT analysis for extracted AE signal.

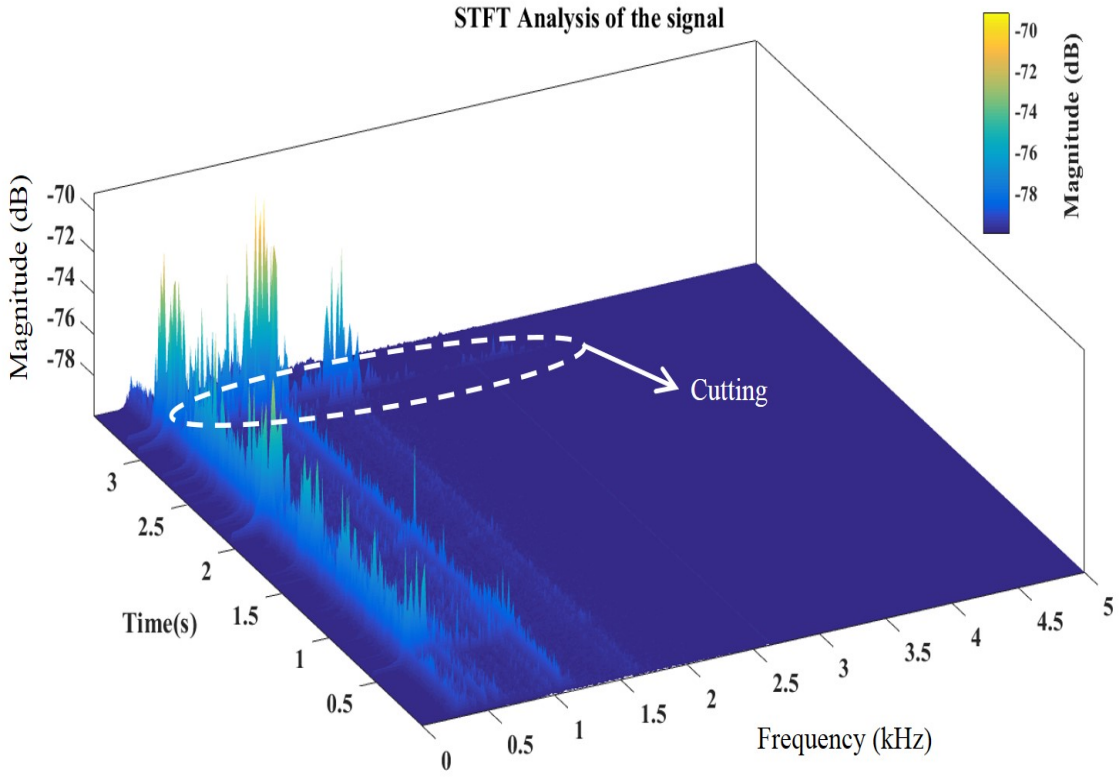

Figure 5.14: Corresponding frequency ranges for different material removal modes.

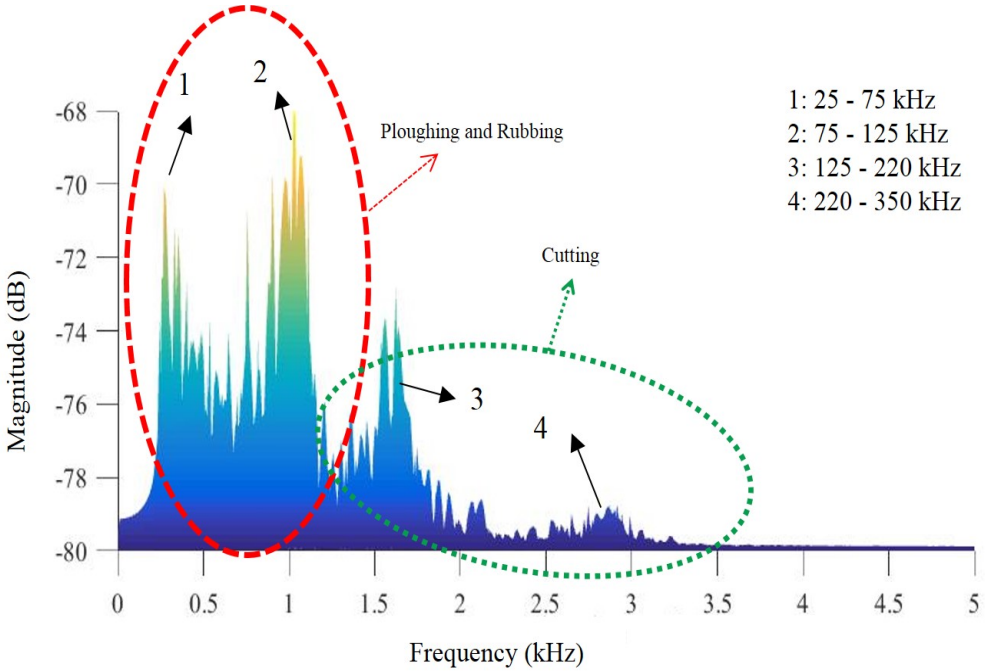

Figure 5.15: Corresponding frequency ranges for different material removal modes.

5.5 Change in material removal modes with belt wear

Moving forward, similar analysis will be carried out on abrasive belt grinding process. An electric belt grinder is customised with a fixture design to be used as a belt grinding tool as shown in Figure 5.16. The belt grinder is an electrically-powered abrasive belt tool that runs at 11,000 rpm at unloading condition and can drive belts with dimensions about 8" to 3/4" wide x 18" long. ABB 6660 robot was used to perform the experimental trials. A constant contact force of 20 N throughout the process in the normal direction (Z-axis) was imparted. Force compensation is achieved by using a force sensor (ATI force sensor) attached to the end effector of the robotic arm of ABB 6660 robot. ABB Robot Studio executes the linear tool path.

Aluminium (Al-T6061) with a planar surface of the same initial roughness is machined with the aluminium oxide (Al_2O_3) abrasive belts with three different tool wear states during experimental trials. Table 5.4 shows the experimental conditions used in the trials. Contact wheel of the belt grinder is normally kept to the surface for maintaining uniform contact condition. Experiments are carried out in dry

condition. AE Sensor is placed near to the machining zone in the workpiece with good acoustic coupling as shown in Figure 5.16.

Table 5.4: Experimental condition used during actual belt grinding.

Parameter	Values
Abrasive belt	Aluminium oxide - 40 grit size
Grinding method	Constant force of 20N using ABB robot studio
Grinding speed	11,000 RPM, 50 mm/sec
Workpiece	Aluminium (size 135 mm X 90 mm X 20 mm)
Contact wheel	Diameter:16 mm, Rubber: Hardness 80 Shore A
AE sensor range	25 kHz-450 kHz (Vallen VS45-H)
Data acquisition rate	5 MHz

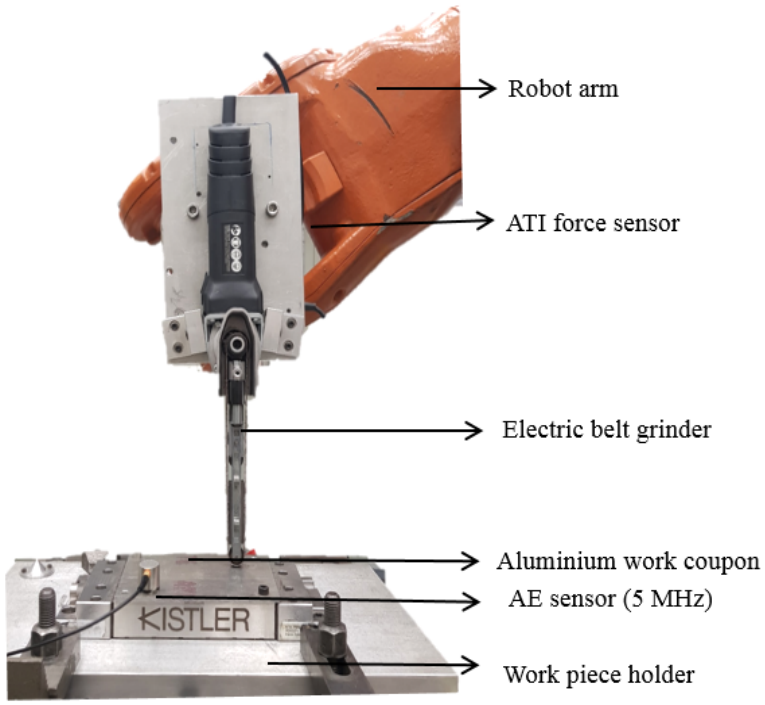

Figure 5.16: AE system for belt tool condition monitoring.

Belts with three-different state, i.e. new (fresh grains), used (partly used) and wornout (old), are used for the trials. Based on the visual comparison from 3D laser profile reading and Abbott- firestone curve for the different belt state as shown in Figure 5.17 , it is evident that the grains wither considerably from the backing material relative to the lifetime of a belt tool. It is also apparent that the grains become extinct from the backing material correspond to the cycle time of a belt tool.

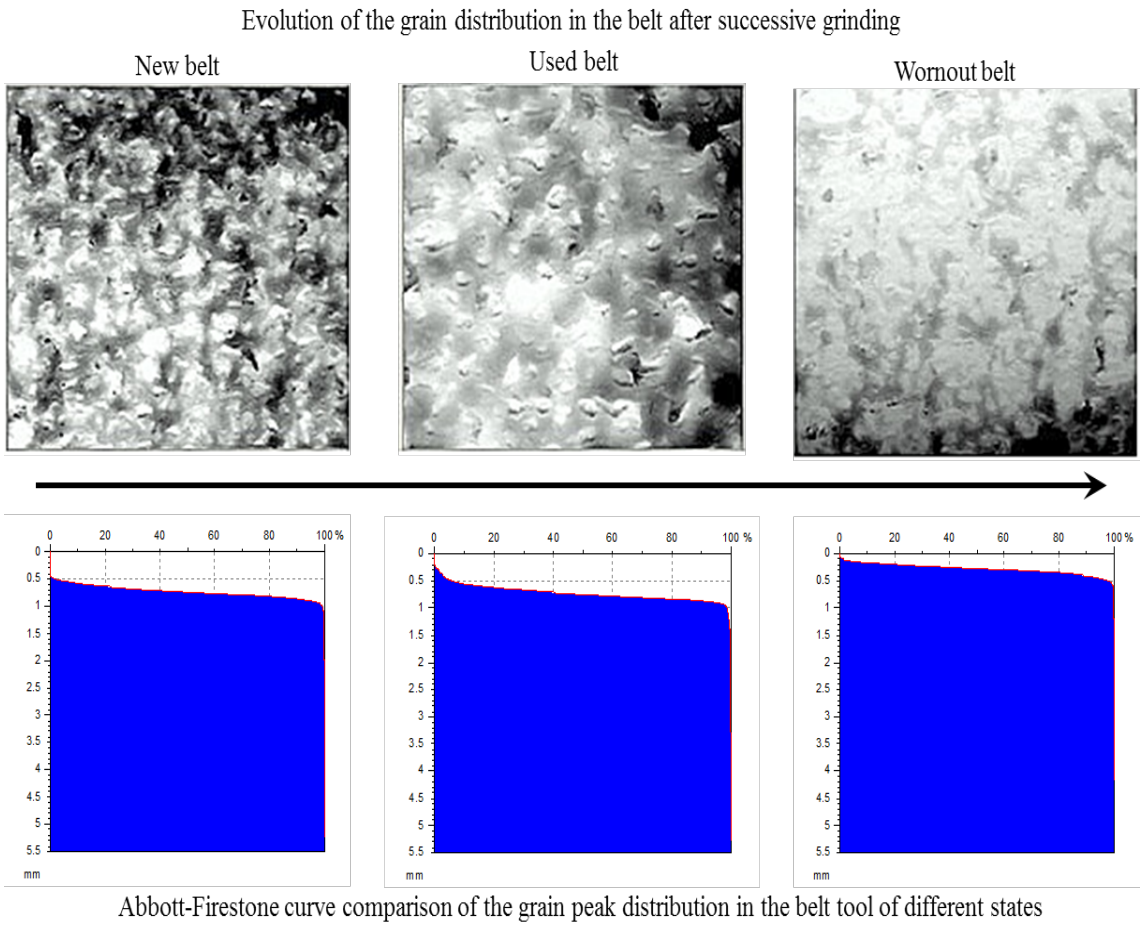

Figure 5.17: 3D laser profile scan of the grain structure evolution and Abbott-Firestone (material ratio curve) comparison of the granularity distribution in the belt tool of different states.

The AE signatures during machining with different belt states are captured at 5 MHz. The amplified AE signal is passed into bandpass filters with a cut-off frequency between 25 kHz and 450 kHz. As shown in Figure 5.18, STFT analysis for the extracted raw AE signal during the belt grinding trial shows evidence of similar frequency components to those from the single grain scratch experiments.

AE sensor signatures on contact of the belt grinder using three different belt wear states with the aluminium (Al-T6061) work coupon are shown in Figure 5.19. Evaluating the energy content of AE signal from two significant bands (25−125 kHz) and (125−350 kHz) corresponding to the material removal modes identified in Section 5.4 in experimental trials using three different tool wear states, the insight of material removal mechanism can be demonstrated.

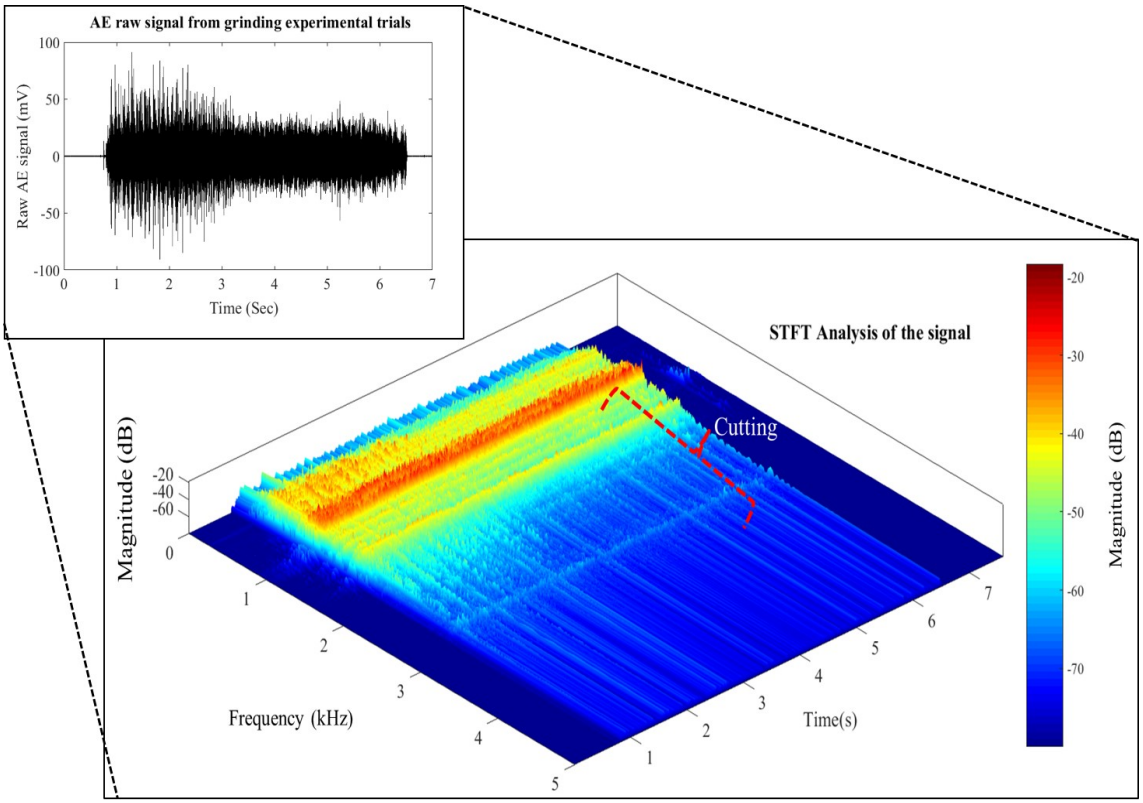

Figure 5.18: The 3D plot of STFT analysis for extracted raw AE signal during the belt grinding trial showing evidence of frequency components from single grain scratch experiments.

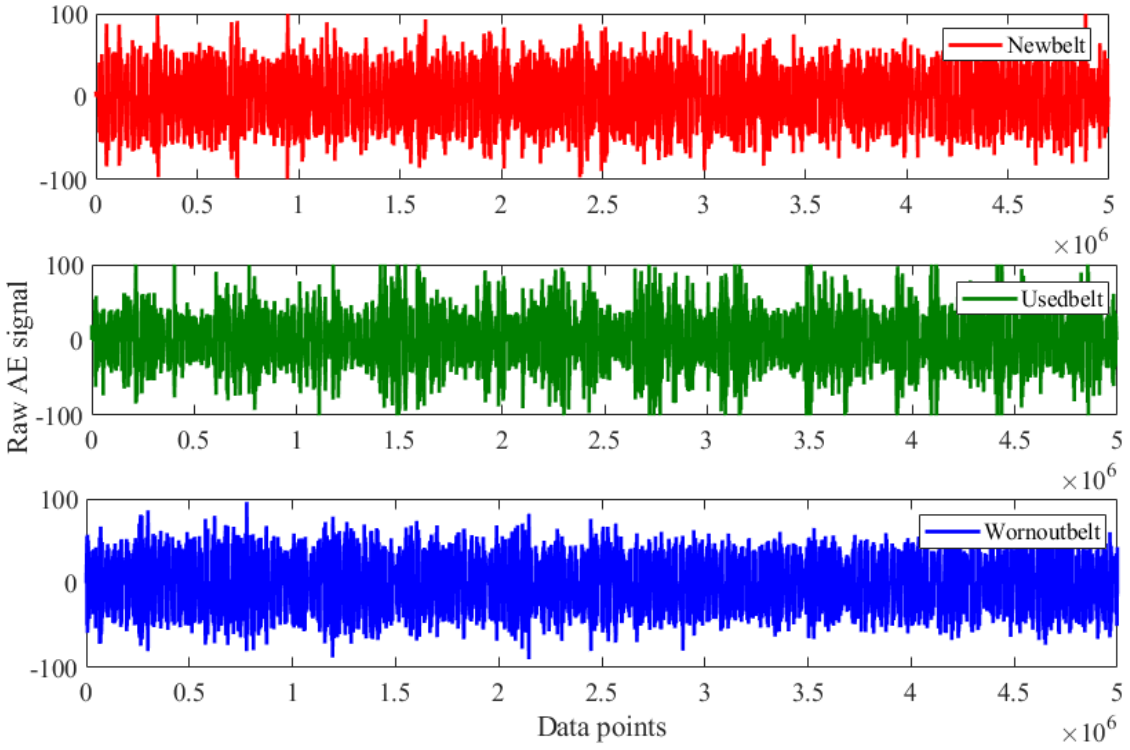

Figure 5.19: Raw extracted AE time signal during grinding trials using three different tool states.

5.5.1 Result and analysis

The following section summarizes the results of material removal mode occurrence in three different belt states during the belt grinding trials in detail. From the STFT analysis of the raw AE data in single grain scratch experiments, we can identify the dominant material removal mechanisms present based on peak frequency bands.

From STFT analysis for extracted raw AE signal during the actual belt grinding trial, it is evident that the frequency components are similar to those from the single grain scratch experiments. The energy content of the frequency ranges of two significant bands (25−125 kHz) and (125−350 kHz) from actual belt grinding trials with different tool wear states are compared to gain insight of the material removal mechanisms. Figure 5.20 shows the energy comparison in two significant frequency bands (25−125 kHz) and (125−350 kHz) corresponding to the three different belt wear states from four trials for each belt state using the experimental conditions listed in Table 5.4.

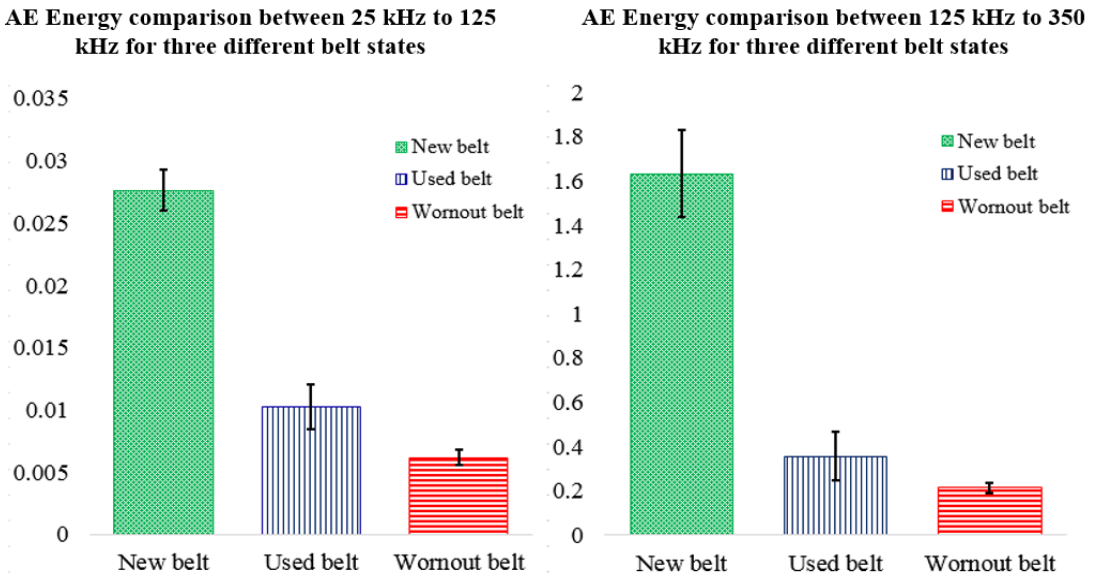

Figure 5.20: Comparison of AE energy signal for three different belt states.

Evaluating the energy signatures in the frequency band of 25−125 kHz it is apparent that rubbing and ploughing are more dominant in new belts compared with belts that have been run for considerable cycle time. There is a very obvious transition in the energy of the AE signal from high to low as the belt tool wears down which can be attributed to the granularity of the belt tool. Based on the comparison

of the energy signatures in the frequency band of 125−350 kHz it is understandable that cutting is the most prominent mode of material removal in brand new belts. It is also noticeable from Figure 5.20 that cutting gradually becomes a non-existent mode based on the energy with the cycle time of the belt tool (cutting still occurs, but it occurs significantly less). The comparison of AE energy in the two frequency bands shows that all the three material removal modes diminish as the belt tool degrades with cycle time as a result of wearing down or withering out. This study proves that the material removal modes rely heavily on the granularity of the abrasive grains and monitoring them is critical in a belt grinding process.

5.6 Conclusion

The chapter aims to quantify and characterise the frequency signatures at which material removal modes such as rubbing, ploughing and cutting occur in abrasive belt grinding process, in particular for aluminium oxide (Al_2O_3) abrasive belt on aluminium (Al-T6061) work coupon. Analysing the AE energy content of these frequencies support the fact that intensity of the material removal mechanisms changes with the granularity of the abrasive grain. With data extracted from AE sensors during scratch tests on aluminium 6061 workpieces with Al_2O_3 grain, and performing STFT analysis shows that the three material modes have their respective frequency ranges of occurrence from 25 kHz to 350 kHz. The frequency ranges that occurred at 125−350 kHz corresponds to cutting and 25−125 kHz represents ploughing and rubbing, which are inseparable.

Analysing the energy content in the three material removal modes in belt grinding trials on aluminium 6061 workpiece with three different Al_2O_3 abrasive belt states suggest that more cutting processes occur on the interaction of the material surface with new grains and gradually becomes a less-existent mode compared to with ploughing and rubbing as the grain wears gradually.

Understanding the material removal modes and the corresponding energy of frequency component help in the implementation of real-time tool wear monitoring system in abrasive belt grinding processes.

Chapter 6

Toolwear prediction

6.1 Introduction

The grinding belt is formed of coated abrasives on a backing material and fastened around at least two rotating polymer contact wheels. Figure 6.1 shows a cross-section of an abrasive belt, which includes a backing material, a base coat, and abrasive grains. Like any other abrasive machining, the grinding belt topography features grain distance, grit size, and wear rate impacting the final ground surface quality [16]. The lifecycle of a coated abrasive belt tool vitiates due to grain wear thus resulting in tool failure.

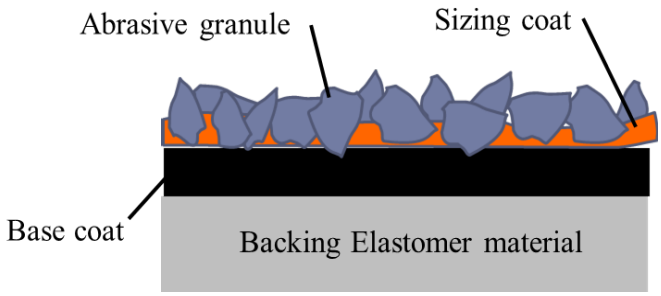

Figure 6.1: Cross section of an abrasive belt.

The pre-planned tool replacement methodologies are not suitable for belt grinding process as the machining conditions vary extensively. In most of industries, the replacement of belts in a belt grinding process is still based on operator experience. As belt wear has a direct influence on the uniformity of the material removal, real time monitoring of the tool life states helps in controlling the quality of the finished

surface. Furthermore, it will also allow for the transformation of the conventional manufacturing station to highly automated robotic manufacturing cells.

Novel logics, sensor systems, and decision-making algorithms, such as pattern recognition and statistical techniques, have been developed in the region of tool wear assessment over the years. Cutting edges are mostly unreachable during machining. Therefore, machining conditions are assessed from indirect methods based on reliable signal patterns from sensors such as temperature, vibration, cutting forces and AE. Though not much work has been explored in tool wear of coated belt abrasive tools, other works on abrasive tools have provided some insight.

This chapter presents the prediction technologies for belt condition in real time with the help of smart sensors using machine learning classifiers. Developing a predictive tool condition monitoring system for coated abrasive compliant belt machining process in real time by virtual verification adds value for the entire manufacturing process.

6.1.1 Effect of belt wear on material removal and surface quality

Abrasive belts of grit size 60 (medium coarser) made of aluminium oxide ($A1_2O_3$) grain, and canvas as the backing material of width of 10 mm is chosen for experimental trials to understand the effect of belt wear on material removal and surface quality. Four belts with different runtime are compared visually to study the evolution of grain wear on the belt surface with cycle run time.

Table 6.1: Belts conditions used for experimental trials and their respective time of usage.

Belt No	Cycle time	Usage time (minutes)
1	New belt	0
2	Belt after 5 minutes of cycle time	5
3	Belt after 15 minutes of cycle time	15
4	Worn out belt	30

Table 6.1 describes the four belts used for the experiments and their respective time of usage. A Taly-surf non-contact laser profilometer was used to profile an area

of about 5mm X 5mm. Based on the visual analysis of 3D laser profile reading as shown Figure 6.2, it is evident that the grains wear and wither considerably from the backing material relative to the lifetime of a belt tool. The degradation of the belt tool was also proportional to the cycle time.

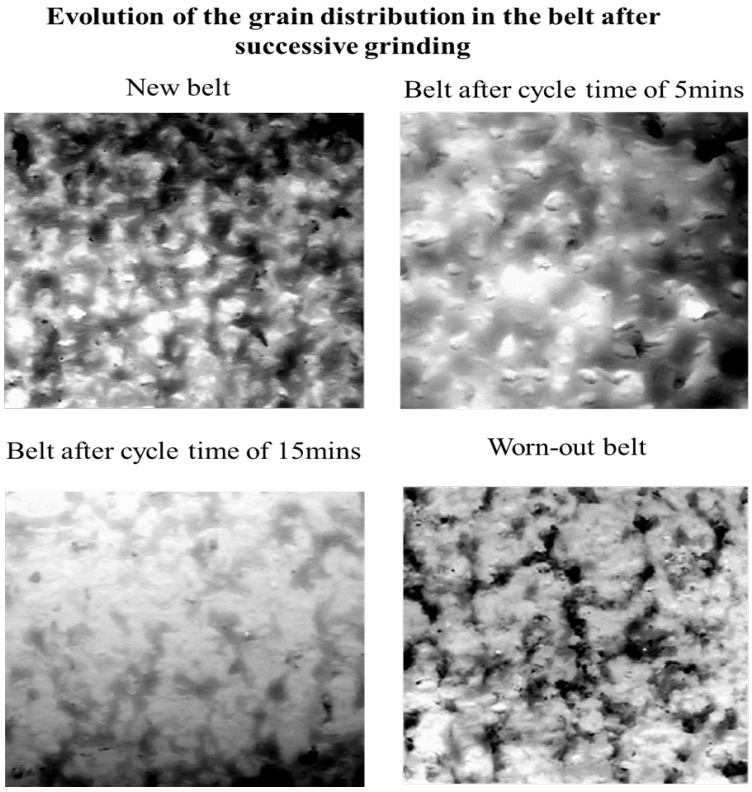

Figure 6.2: 3D laser profile scan of the grain structure evolution with belts of a different cycle time.

Analysing the surface roughness and depth of cut across the machined path in mild steel workpiece after machining with the four different tool and machining condition shown in the Table 6.2 gives information about how the surface quality and material removal varies with tool wear condition.

Table 6.2: Experimental condition used during actual belt grinding.

Parameter	Values
Abrasive belt	Aluminium oxide - 60 grit size
Grinding method	Constant force of 20 N using ABB robot studio
Grinding speed	11,000 RPM, 50 mm/sec
Workpiece	Aluminium (size 135 mm X 90 mm X 20 mm)
Contact wheel	Diameter:16 mm, Rubber: Hardness 80 Shore A

Comparison on surface roughness (R_a) generated from different belt conditions is illustrated in Figure 6.3. The figure shows that surface roughness (R_a) of workpieces varies considerably on the gradual wear of the belt. Extraction of the 2D profile from the Taly-scan profilometer across the tool path gives information on how the material removal rate varies with tool wear condition.

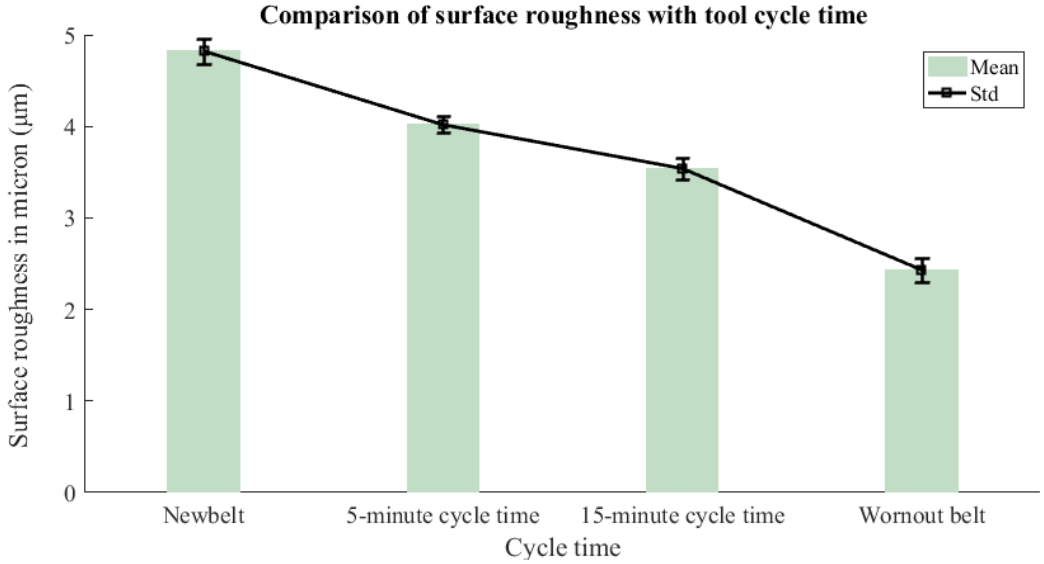

Figure 6.3: Comparison between surface roughness (R_a) generated on the mild steel coupon during machining with different belt tool states of grit size 60.

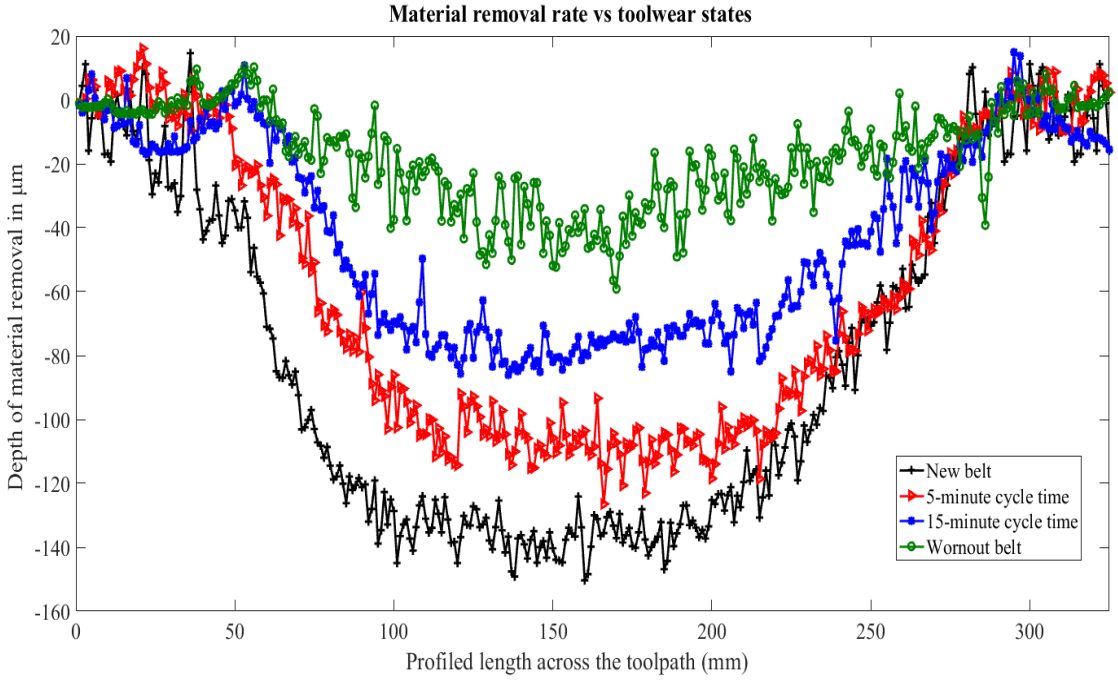

Figure 6.4: Comparison of material removal using belt grinder for different belt tool states.

Figure 6.4 indicates that a new belt has higher grain density and sharp peaks enabling higher material removal rate compared to the belts that have experienced gradual wear. This trend of material removal and surface quality emphasizes the importance of the belt tool condition monitoring.

6.2 In-process complementary based multi-sensor integration toolwear monitoring system

The use of multiple sensors is sometimes necessary for monitoring applications in a system that intermingles with and operates in a dynamic environment [154]. In-process sensors can be exercised strategically for machining process automation as they have the ability to predict the process state based on sensory feedback. Complementary multi-sensor integration system incorporating force, accelerometer and AE has been proposed as a strategy to estimate the state variables to give a complete picture of the tool condition state in an abrasive belt grinding process which is difficult to understand.

Table 6.3: Time and frequency domain features extracted from the sensor signatures for tool condition monitoring.

Feature no	Feature name
1	Mean value
2	Root Mean Square (RMS)
3-5	Autocorrelation (height of the main peak, height and position of the second peak)
6	Kurtosis
7	Skewness
8	Crest factor
9	Band-power
10	Standard deviation
11-22	Spectral peak features (height and position of first six peaks)
23-27	Spectral power (features in 5 adjacent and pre-defined frequency bands)

In this application, the signatures during machining with the different four tool wear states are captured using AE, force and accelerometer sensors placed. The raw sensor data comprises fixed-width sliding windows (10% of data acquisition rate readings/window). From each window, a vector of 27 independent features from

time domain and frequency domain are extracted at 20 kHz for the force sensor and accelerometer sensor and 1 Mhz for the acoustic sensor as shown in Table 6.3.

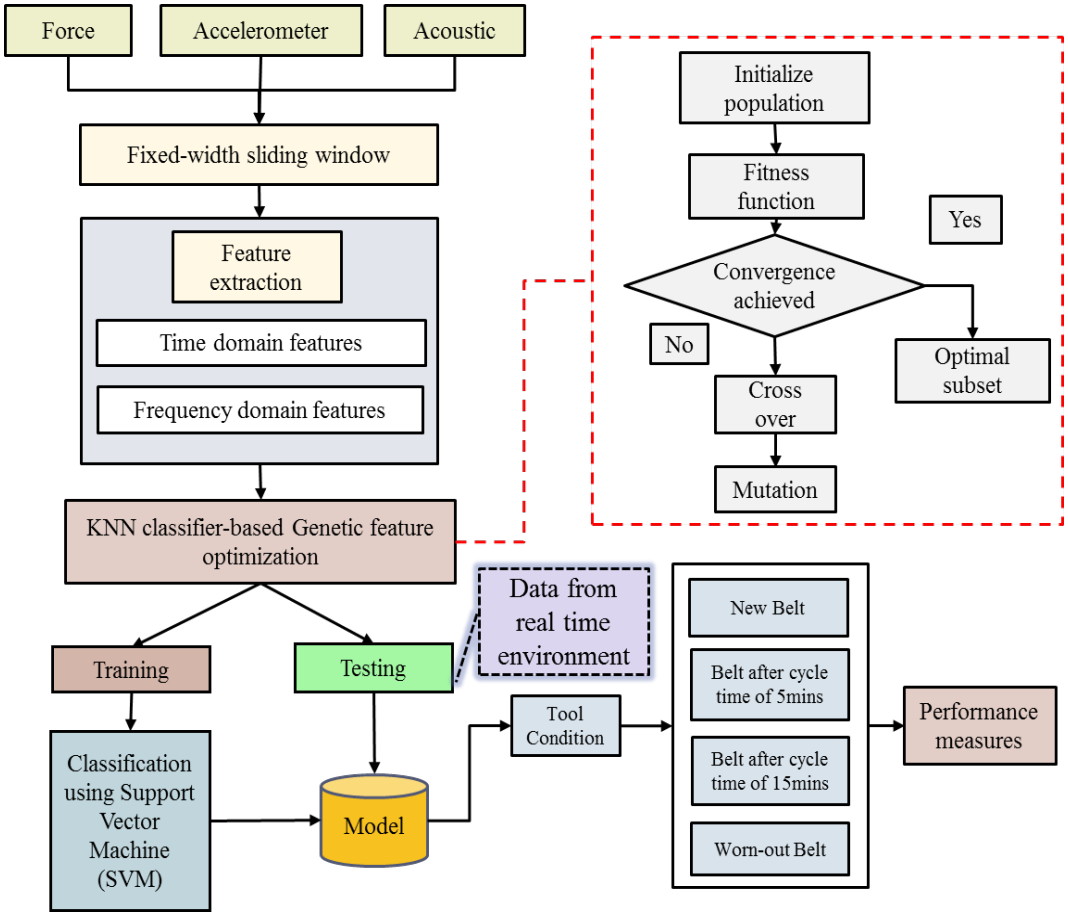

Figure 6.5: Methodology flow to predict tool wear state using SVM and GA.

Redundant data and insignificant features are eliminated by using genetic algorithm (GA) based on k-NN classifier. On optimisation, a new feature subset is introduced into supervised machine learning classification algorithm with the four different tool condition states as the classifiers in MATLAB classification learner toolbox for training. Once the model is trained with 70% of training subset data, the remaining 30% testing subset features are extracted. These subset features are passed into the developed classification models to check its robustness. Schematic flow of the methodology is described in Figure 6.5.

6.2.1 Belt grinding setup

An in-situ tool condition monitoring system based on LabVIEW platform has been developed consisting of a 3-axis Kistler 9254 dynamometer on which the mild steel

workpiece is mounted, Kistler 8763A500 triaxial accelerometer and Kistler Piezotron AE sensor. Figure 6.6 shows the overall setup and indicates the sensor placement. The triaxial accelerometer sensor is placed near the tension arm of the electric belt grinder to record the tool vibration during machining. The accelerometer has been put on the tool in such a way that it does not interrupt the belt transmission. AE sensor is located nearby to the machining zone in the mild steel workpiece with good acoustic coupling facing the machining direction.

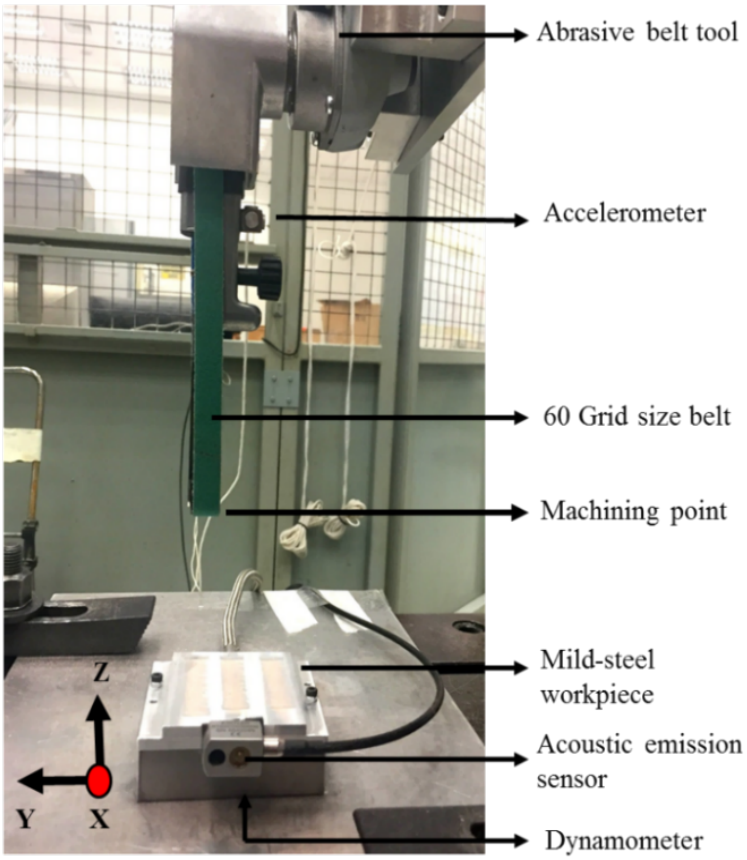

Figure 6.6: Integrated sensor system for belt tool condition monitoring.

LabVIEW environment is used to acquire the signal from AE and accelerometer whereas, in the case of the dynamometer, a data acquisition device (DAQ) supported by DEWESoft platform is used to acquire and post the process normal and tangential force signals.

The customised setup that was used for abrasive grain wear monitoring trials in Section 5.5 consisting of the ABB robot and electric belt grinder is used for experimental trials. A constant contact force of 20 N throughout the abrasive belt finishing process in the normal direction (Z-axis) was imparted. Force compensation

is achieved by using force sensor (ATI force sensor) attached to the end effector of the robotic arm of ABB 6660 robot.

Contact wheel of the belt grinder is normally kept to the surface for maintaining uniform material removal, and mild steel workpiece of same roughness is used throughout machining trials. Experiments are carried out in dry condition. Mild steel with a planar surface of the same initial roughness of 2 μm is machined with the abrasive belts with four different tool wear states as mentioned in Table 6.1 with machining condition as stated in Table 6.2.

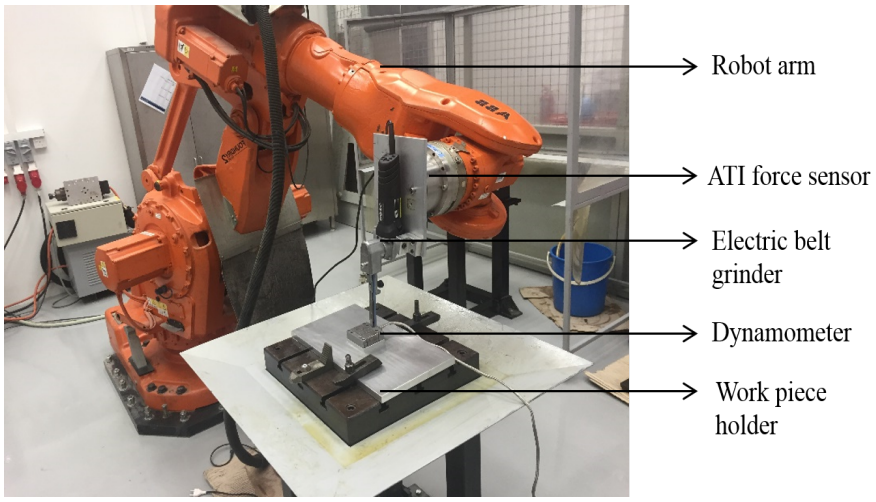

Figure 6.7: Experimental setup for belt tool condition monitoring.

6.2.2 Signal processing and feature extraction

The sensor signatures from the dynamometer suggest that forces along X-axis (the direction of the tool path) and Z-axis (normal to the workpiece) are more significant compared to the force along the Y-axis (perpendicular to the pass). In the case of the accelerometer, all the signatures from three axes gave significant readings. The accelerometer readings before the contact of abrasive tool on the workcoupon contain frequencies that might arise from the moving components namely rotating gears, spring loaded tension arm etc. as shown in Figure 6.8 (a). A Butterworth-bandstop filter is applied to screen out these frequency ranges and the design of the bandstop filter is shown in Figure 6.8 (b). Once the required signal is preprocessed, features are extracted from sensor data. From the experiments, the accelerometer, force and AE sensor reading are shown in Figure 6.9, Figure 6.10 and Figure 6.11.

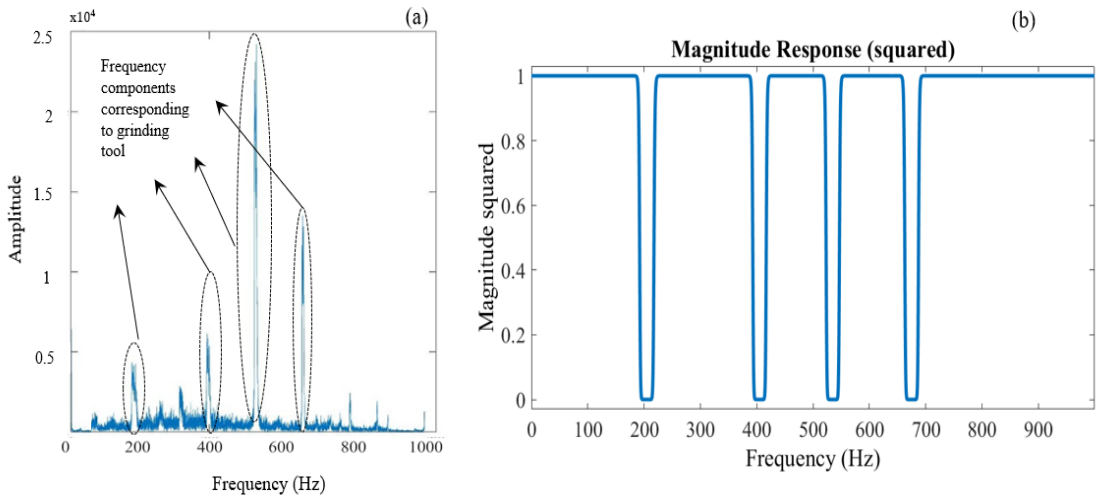

Figure 6.8: (a). Frequency of the grinding tool components from accelerometer (Z-axis) reading at non-operational state. (b). Butterworth band-stop filter design to attenuate the frequencies corresponding to the moving components of the grinding tool.

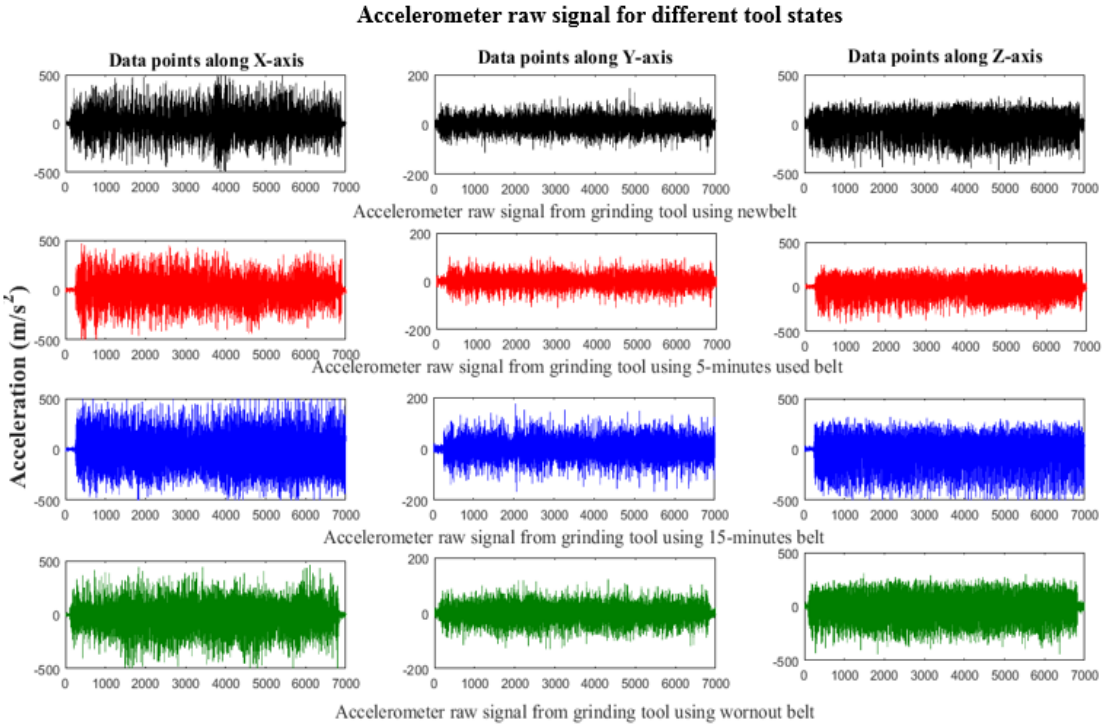

Figure 6.9: Accelerometer raw signal from grinding tool for different tool states.

The use of sensitive features is a major factor in condition monitoring and prognosis [301]. Features such as mean value, coefficient of variation and skewness of AE signals were used to classify coated tool into three categories with realistic accuracy [171]. Tax *et al.* [302] showed that time domain features such as RMS, peak

value, kurtosis, and crest factor can be used to detect damage in rolling bearings. The absolute deviation was used to measure the statistical dispersion to analyse changes in the signal during the cutting time and correlate it with the tool wear [303]. A high-frequency resonance technique was used to obtain the spectrum of the envelope signal for diagnosing bearing fault [304]. Acoustic emission based condition monitoring has some advantages over vibration-based condition monitoring and is more sensitive in tracking the progression of any defects [305].

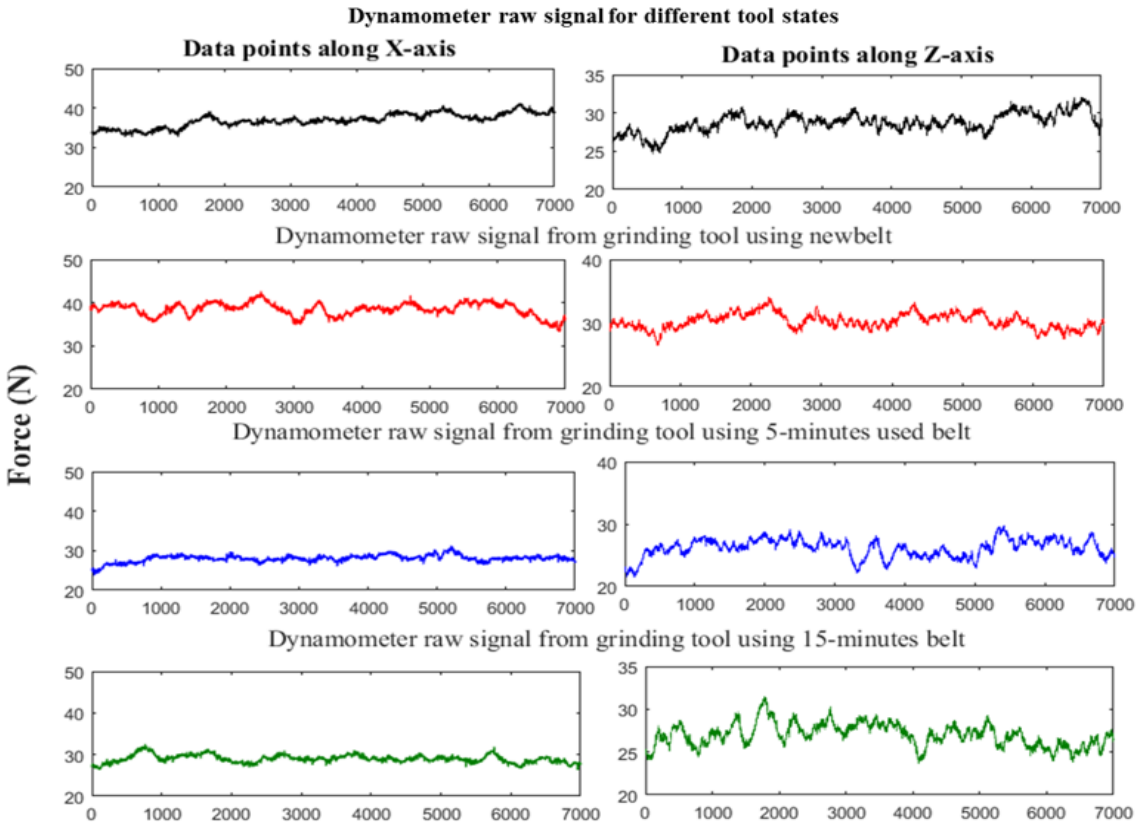

Figure 6.10: Dynamometer raw signal for different tool states during belt grinding process.

Power spectral density comparison plot of the force sensor for different belt states in Figure 6.12 demonstrates the variation in height and position of the peaks during machining with abrasive belts of different tool wear states. Auto-correlation comparison plot of accelerometer signature in Figure 6.13 shows features such as the height of main peak as well as height and position of the second peak are distinct during machining with belt tools of different usage time.

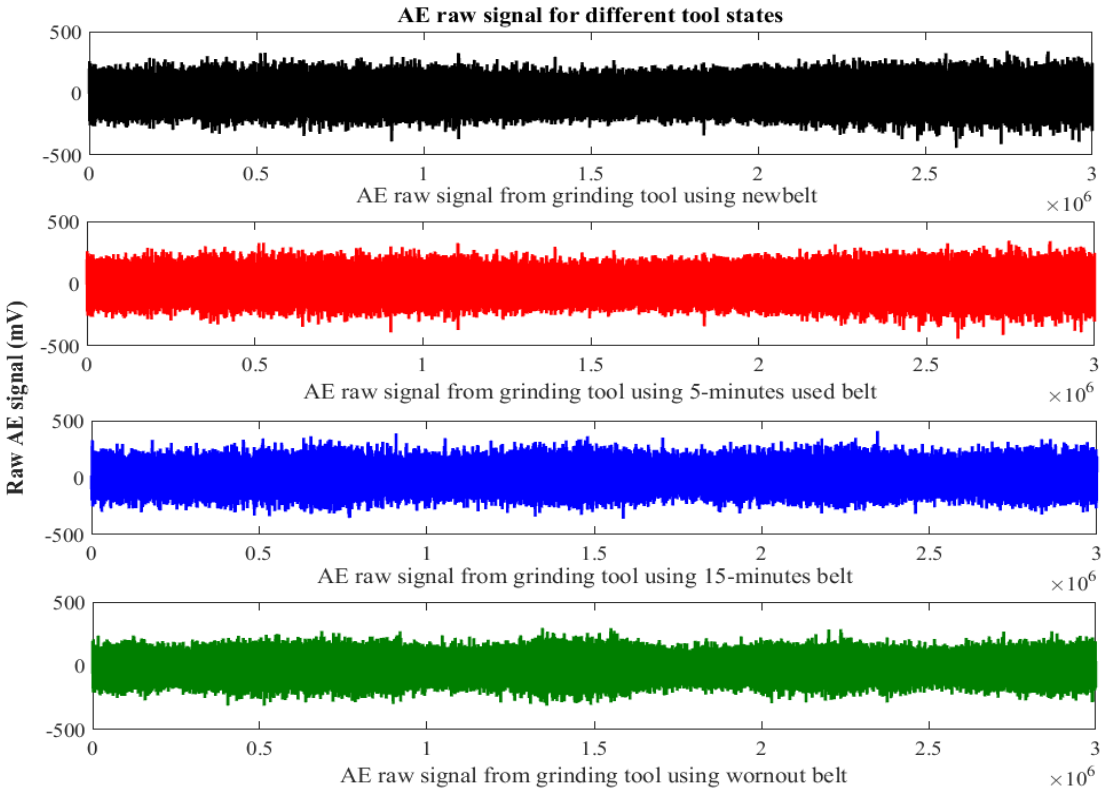

Figure 6.11: AE raw signal for different tool states during belt grinding process.

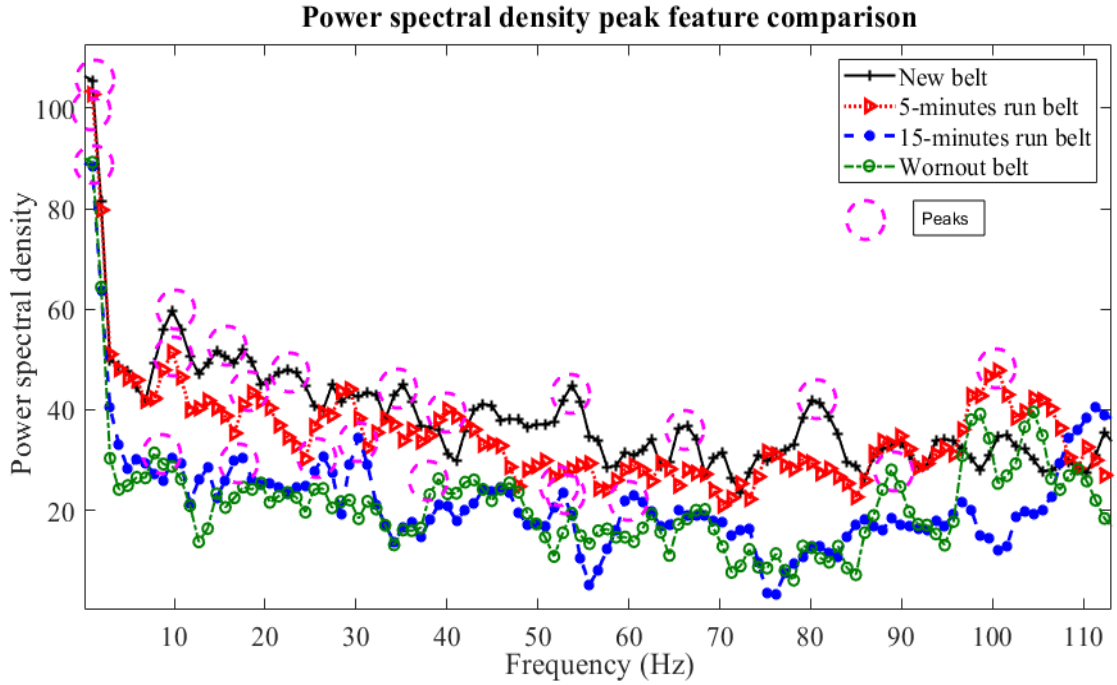

Figure 6.12: Comparison between spectral peak features for different tool states from force sensor in the x-direction.

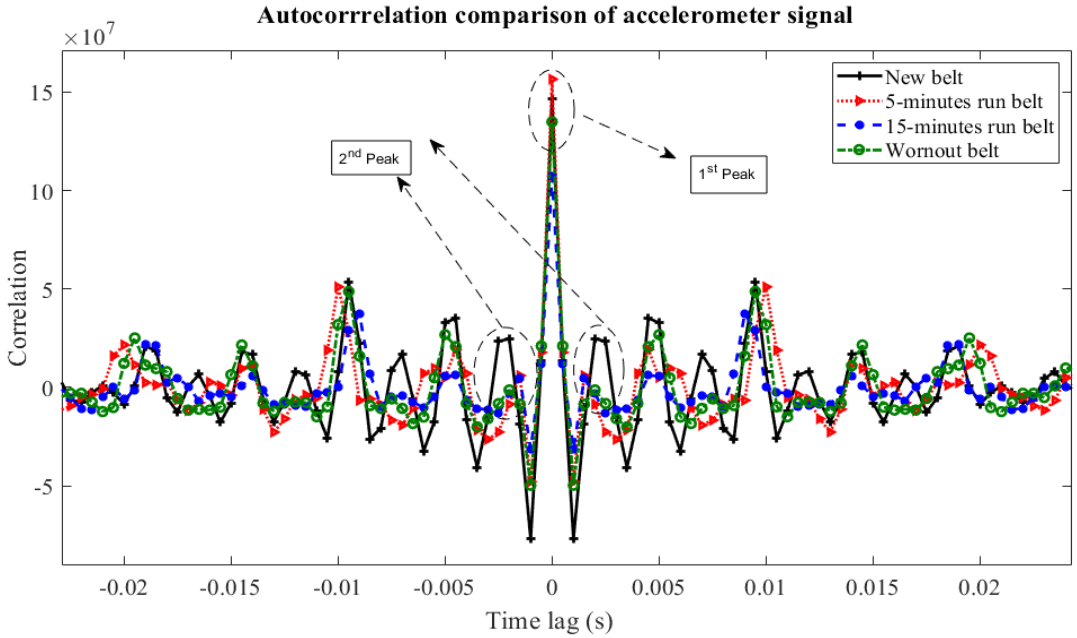

Figure 6.13: Comparison of auto-correlation features for various tool states from accelerometer sensor in the z-direction.

Figure 6.14 demonstrates the variation between power spectral features at different frequency bands for various tool wear states from AE sensor. These distinct features from sensor data are exploited to predict tool condition states in this research.

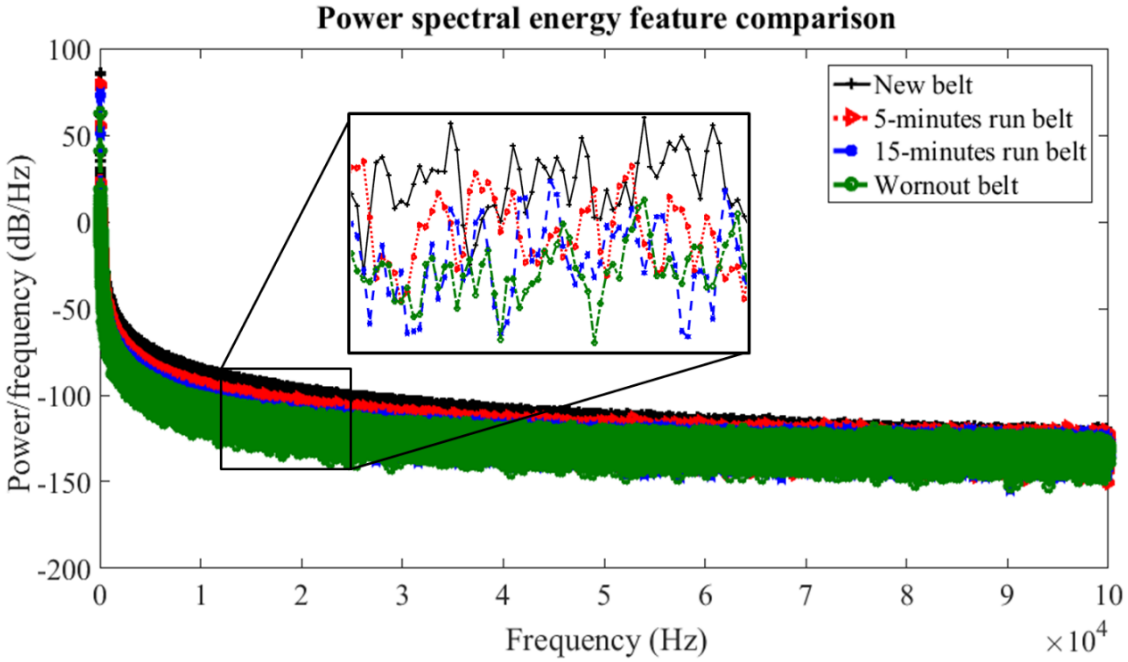

Figure 6.14: Comparison between power spectral energy features at different frequency bands for various tool wear states from AE sensor.

For the purpose of tool life cycle classification, proper features need to be identified and selected. Compared to Bartlett method, Welch method is an improved estimator of obtaining power spectral density (PSD), as overlapping and windowing reduces the spectral leakage [306]. The Welch's PSD estimate divides the time series data into overlapping segments, calculating the periodogram of each windowed segment and takes the average of the periodograms, resulting in less narrower peaks [307,308]. Hence, Welch's based spectral density extraction approach is used throughout this research work to extract location and value of peak frequencies. A Periodogram is also utilised for computing energy distribution of signals over the predefined frequency band. The choice of signal features is usually based on a priori knowledge of the nature of the signals to be classified. A total of 27 individual features from time and frequency domain as discussed in Table 6.3 from each sensor channel is used for predicting the belt tool condition. Data points are extracted from 6 channels comprising those from AE sensor, 3-axis accelerometer and 2-axis dynamometer which accounts for higher feature space of 162 features (27 features per channel).

6.2.3 Genetic Algorithm (GA) based feature selection

Classification accuracy of the recognition system reduces and time required for learning increases when the features space is redundant and non-informative [309]. The high-dimensional feature set can negatively affect classification accuracy as well as the performance during real monitoring. Feature selection is used to detect a powerful predictive subset of fields and is primarily a multi-objective problem with two main objectives of minimising classification error and the number of features. Genetic algorithm has been established to be a very adaptive and a competent means of feature selection [310].

The operations in a GA are iterative processes manipulating one population to generate a new population via genetic function such as crossover and mutation. The chromosome design, fitness function affect the feature selection using the GA. The GA generates consecutive populations of another solution that are represented by a chromosome. Fitness function evaluates the attribute of a solution in the evaluation step. The crossover and mutation functions are the main operators that randomly

impact the fitness value.

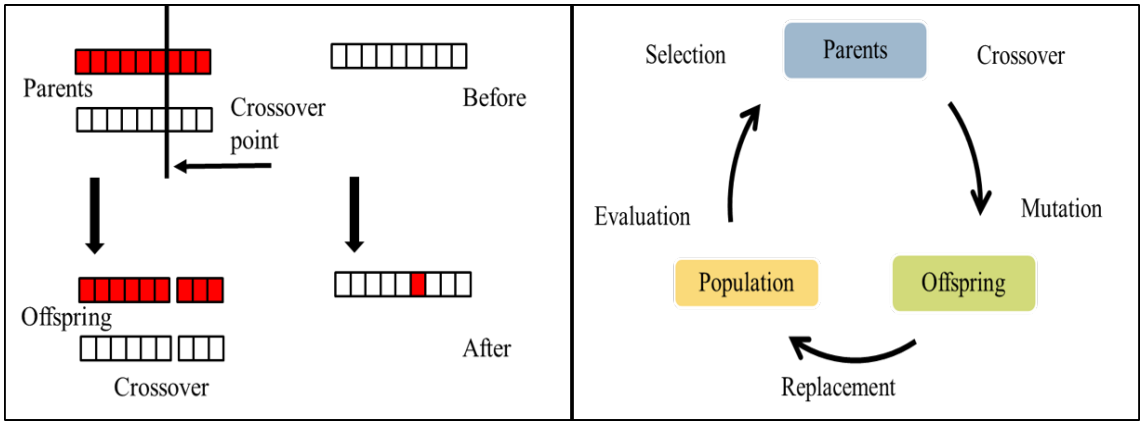

Figure 6.15: Crossover, mutation operation, and evolutionary cycle in GA.

Figure 6.15 illustrates the genetic operators of crossover and mutation and GA evolutionary process. Chromosomes are picked for reproduction by estimating the fitness value. Offspring swaps the old population using the elitism and take shape into a new population of the next generation. The better chromosomes have a higher probability to be selected into the mixing pool using the roulette wheel or the tournament selection methods. The evolutionary process operates many generations until termination condition is satisfied.

Table 6.4: Parameters used in GA simulation.

GA parameter	Values
Creation function	Creation uniform
Fitness function	k-NN based classification error
Number of generations	100
Crossover arithmetic	Arithmetic crossover
Crossover probability	0.8
Mutation probability	0.1
Elite count	15
Mutation	Mutation adapt feasible

GA finds the best possible subset of features from feature space after a series of iterative computations until acceptable results are obtained. Feature subset selection is to pick a subset of the original features to be used for the subsequent process,

thus reducing the number of features used in classification without conceding on accuracy.

Table 6.4 indicates the chromosome design, fitness function, and system architecture configuration of the GA-based feature selection implemented using the MATLAB in this research. Classification accuracy, the number of identified features, and the feature cost are the three decisive factor used to create a fitness function. The fitness function gives numerical values which are used in ranking the given chromosomes in the population. Consequently, for the chromosome with superior classification accuracy, a small number of features, and low total feature cost, fitness value will be higher.

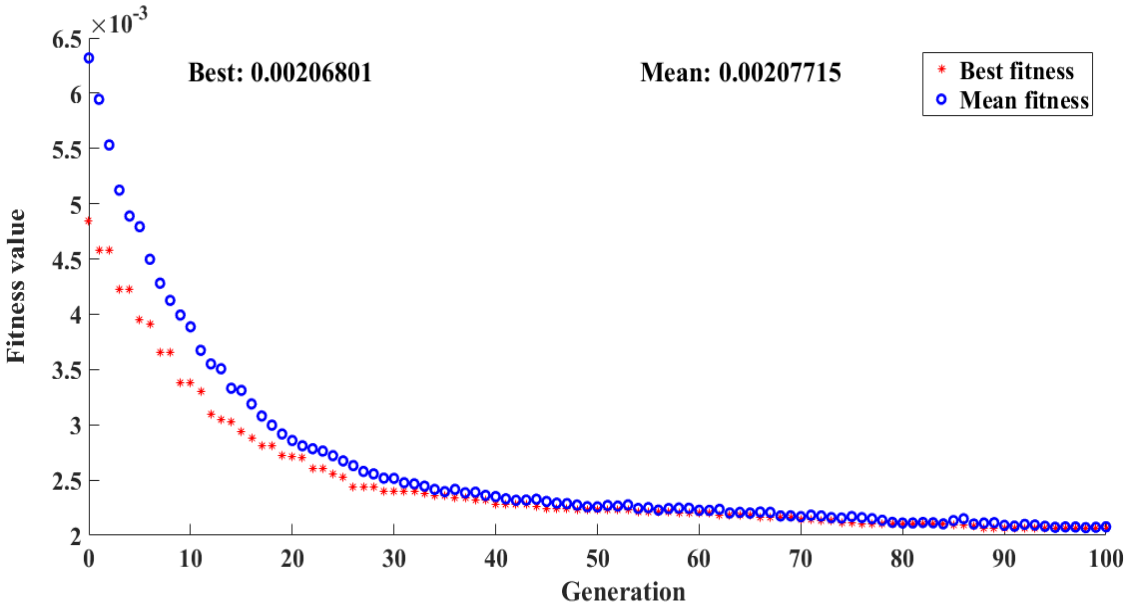

Figure 6.16: Proximity between best and mean fitness in GA simulation diagram.

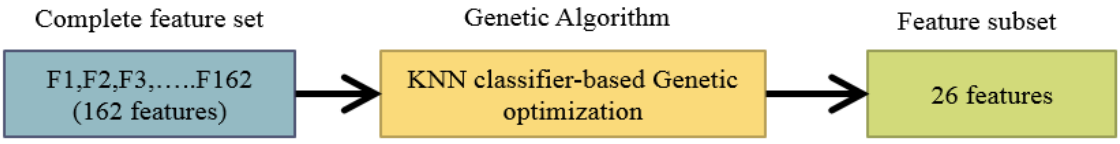

Figure 6.17: Feature subset selection.

The k-Nearest Neighbours (k-NN) based fitness function is used in GA to minimise classification error and reduce the number of features. The best fitness and mean fitness should be close in value as the GA reaches the termination condition which is also evidenced by the GA simulation diagrams as shown in Figure 6.16.

The difference between the best and mean fitness value, using the k-NN classification error for feature set were minimum. The k-NN algorithm resolves classification problem by taking into account the hamming distance in the feature space thereby lowering the features from 162 to 26 as illustrated in Figure 6.17

Figure 6.18 reveals that the correlation between band power and skewness features varies depending on the tool wear states, i.e., the topography of the abrasive belt. Such interpretation of the feature space hints us with the possibility of classifying the tool wear states and predict the condition of the belt in real-time.

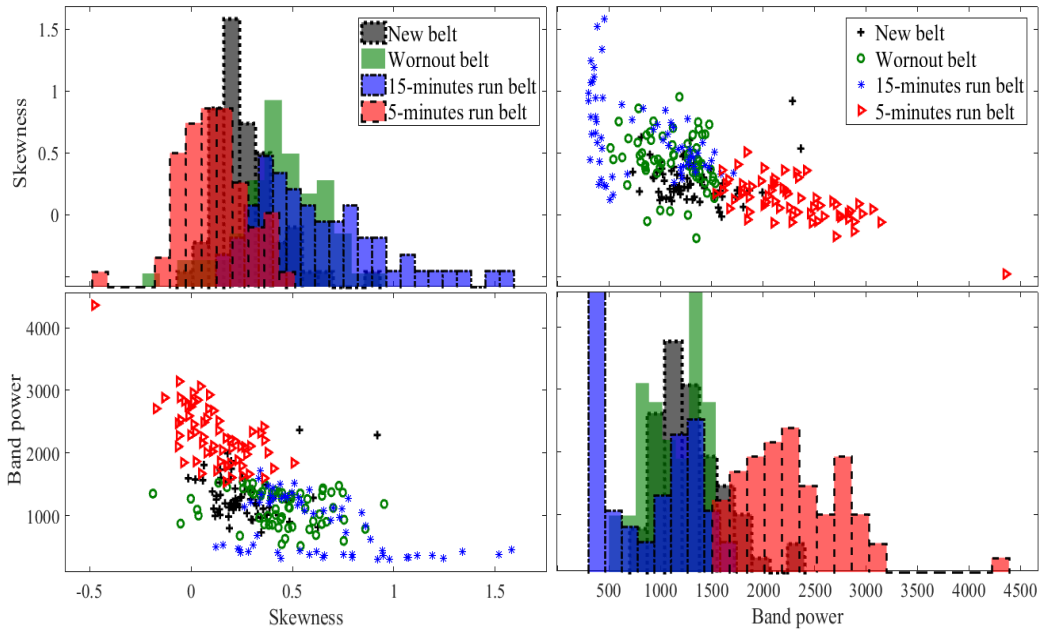

Figure 6.18: Relationship and distribution between skewness and band power feature acquired for four tool wear states.

6.2.4 Tool states classifiers

The performance-testing experiment is designed to test the predictive ability of classification models with a new subset of 26 features obtained from GA based k-NN classifier under same machining conditions. Classification of the tool wear states by the classifiers consists of two main parts, i.e training data and testing data. Hence, among data sets, 70% data is selected stochastically for the training and 30% for testing the developed models.

Five predictive models using k-NN, Naive Bayes, SVM, ANN and Bagged Trees were developed and compared. The performance of the five algorithms considered

depends primarily on their respective parameter configuration. The set of training parameters for each classifier used in this research are listed in Table 6.5. The training parameters of the chosen classifiers were based on empirical rules and their performance was evaluated based on prediction accuracy.

Table 6.5: Training parameters of the classifiers for predicting tool wear states.

GA parameter	Parameters	Values
SVM	Validation method	Hold-out validation
	SVM kernel function	Quadratic
	Kernel scale	Automatic
	Multiclass method	One-vs-One
	Standardize data	True
	Prediction speed	$\sim$ 3200 observations/sec
	Training time	0.568 secs
k-NN	Classifier	Cosine k-NN
	Number of neighbours	10
	Distance metric	Cosine
	Distance weight	Equal
	Prediction speed	$\sim$ 8200 obs/sec
	Training time	0.2232 secs
ANN	Number of neurons	30
	Output layer	4
	Training method	Back propagation
	Performance	Cross-entropy
	Epoch	25 iterations
	Training time	0.3699 secs
Naive Bayes	Distribution Names	Normal (Gaussian) distribution
	Predictors	Categorical
	Class probability	0.250
	Training time	0.4017 secs
Bagged Trees	Classifier	Complex Tree
	Maximum number of splits	100
	Split criterion	Gini's diversity
	Surrogate decision splits	Off
	Prediction speed	$\sim$ 7100 obs/sec
	Training time	0.83391 secs

It is to be noted that the training parameters of the classifiers can be further optimised based on training time and prediction accuracy. We observed quadratic kernel-based SVM having prediction accuracy higher than the other classifiers with

the set of parameters considered as shown in the Figure 6.19.

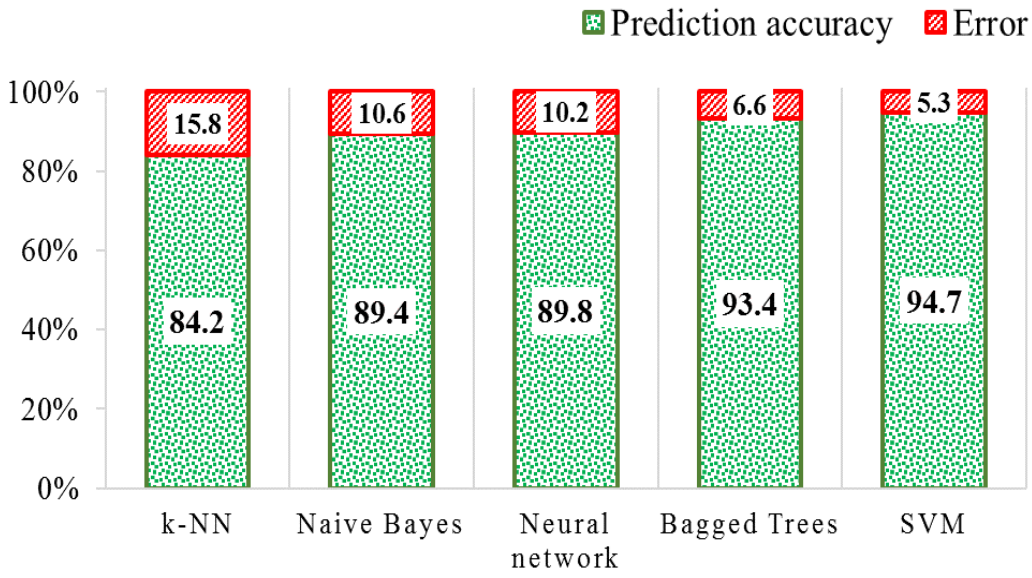

Figure 6.19: Prediction accuracy of individual classifiers.

Figure 6.20 shows 4-by-4 confusion matrices obtained with the quadratic-SVM model. The quadratic SVM kernel function maps data onto a high-dimensional feature space where the linear classification is derived from the nonlinear with different abrasive belt tool condition as classifiers. The accuracy of prediction of quadratic-SVM was 94.7% with errors occurring due to misclassification between the 15-minute used belt and wornout belt. As can be seen, there is a clear separation between different abrasive belt tool condition classifiers and the fraction of samples misclassified of the developed SVM model is minimum.

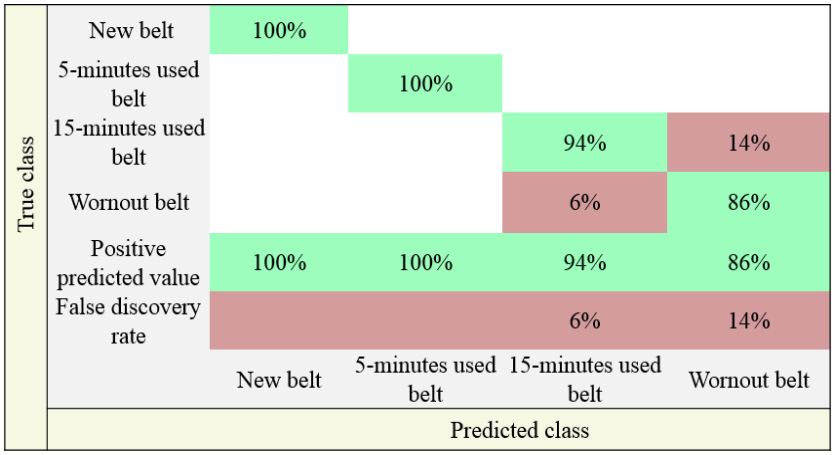

Figure 6.20: Confusion matrix of the quadratic-SVM classifier model with a prediction accuracy of 94.7%.

6.3 Conclusion

Principally, the key aim of this chapter is to determine whether a belt tool is under-utilised or overused and is due for replacement. Based on the results, the following generalised conclusions are drawn:

- A parallel multi-sensor integration system comprising of force, accelerometer and AE sensors whose signals carry the best information about the state of belt tool wear, has been developed .
- Two main kinds of waveform data analysis, i.e. time-domain and frequency domain are used to extract features that can be correlated to tool wear condition.
- Genetic Algorithm based on k-NN classifier allows for feature reduction from 162 to 26 features, thereby optimising the redundancy.
- Quadratic-SVM classifier performed better multi-classification of belt tool conditions with the prediction accuracy of 94.7% compared to other classifiers.

The current study demonstrated a methodology which could effectively monitor belt tool state and reduce the irregularities during finishing operations and has potential practical applications in industry.

Chapter 7

Weld seam removal

7.1 Introduction

Welding is an inevitable process during manufacturing, especially for aerospace industries that produces turbine blades [311,312]. Weld seam that is produced during the manufacturing cycle of these components needs to be removed as it distorts the profile precision.

Abrasive belt grinding is one of the possible ways to remove weld seams and it is also acknowledged by the workforce as a tertiary finishing process. Belt grinding does not require extra corrective work before and after [16]. Axinte *et al.* [313] reported that belt grinding process has the ability to eliminate the machining marks and to establish required surface quality.

Current industrial practice in removing weld seam involves manual grinding by the operator. The manual belt grinding process is also time consumptive as the part has to be taken from production line to the manual machining station and vice versa. There have been commercially available automated tracked weld shaving system, but the problem with such a system is the extensive time requirement for assembling and dis-assembling [314]. For ensuring a fully automated time-intensive weld seam removal work, it is necessary to build a predictive system that can monitor the weld seam removal in real time. This approach will improve the production process quality by reducing unnecessary costs and at the same time increases the level of safety.

In abrasive belt grinding process, cutting force and tool vibration signals change

when the pressure distribution of the polymer backing varies as a result of the interaction with the workpiece geometry. This variation can be suitably exploited to predict the contact conditions. To realise real time monitoring of a manufacturing process, sensors are required to serve as a feedback to the process. Vision sensor has been extensively used in sensing the initial weld point, thus providing weld seam information for assistance to the welding robot [315, 316].

The sensitivity of the measurement depends on the selection of sensors and their placement [317,318]. The sensors incorporated for monitoring the system determines the performance of the intelligent system [116, 319].

Establishment of in-process monitoring system will enable the transformation of manual manufacturing systems to unsupervised robotic machining centre's. This chapter discusses the development of a real time endpoint prediction system for weld seam removal during an abrasive belt grinding process with the help of accelerometer, force, and vision based sensor.

7.2 Real-time verification of weld seam removal using wavelet transform and classification algorithm

Schematic representation of the methodology is described in Figure 7.1. Weld seam at three different removal states is machined with the same grinding condition. The three states of weld seam are categorised by their profile geometry with new symmetrical weld seam profile labelled as Sate-1, unsymmetrical weld seam profile labelled as State-2 and the completely removed weld seam profile labelled as State-3. The signatures during grinding of three weld states are captured using force and accelerometer sensor with a sampling rate of 2 kHz. Wavelet transform is used to represent all possible types of momentary variation in vibration and force signals generated during the grinding of three weld seam states.

Daubechies-4 (Db4) wavelet function was used to extract features from vibration signal with a window size of 20 and spacing of the window of 5. The 8 level wavelet decomposition features based on Discrete Wavelet Transform (DWT) coefficients,

namely mean, variance, standard deviation, waveform length, entropy, peak2peak, Root Mean Square (RMS), Root Sum of Squares (RSSQ), band-power, kurtosis, and skewness, are extracted from the force and vibration signal. Once the features are extracted, the supervised learning technique based on classification algorithm is used to create a classification model.

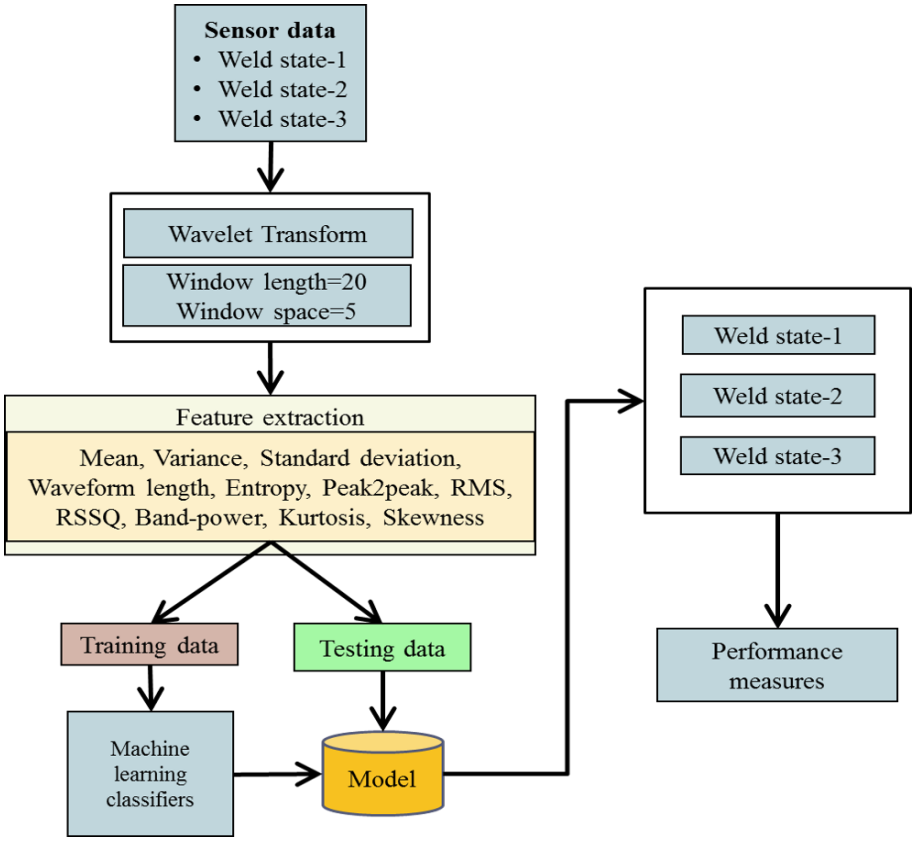

Figure 7.1: General description of the proposed methodology.

Three weld state conditions were used as the data input for classification training and testing processes. The classification was performed in MATLAB classification learner toolbox. After the model is trained, a new feature set of signatures is extracted from the weld seam states 1, 2 and 3 with the same machining condition. These wavelet decomposition features are passed into the developed classification model to check the prediction accuracy of the model.

7.2.1 Experimental setup and grinding conditions

The same setup that was used for abrasive grain wear monitoring trials in Section 5.5 consisting of the robot and belt grinder is also used in this experimental trials.

Machining was performed with abrasive belts of grit size 60 made up of silicon carbide abrasive and the contact wheel rubber backing material having a hardness of 80 Duro. It should be noted that, closed-loop control was accomplished by giving feedback to robot controller on position of the grinding point. Weld seam specimens were grinded with the process parameters as shown in Table 7.1 for all the experimental trials.

Table 7.1: Parameters used in the belt grinding experimental trials.

Parameter	Value
Belt grinding speed	18 m/s
Contact wheel diameter	16 mm
Hardness of contact wheel (polyurethane)	80 Duro
Lubrication	Dry
Feed	30 mm/s
Belt finishing duration	Variable
Operational mode	Position control

7.2.2 Weld seam removal

Weld seam are made up of stainless steel (SUS308) filler rod on mild steel work coupons using tungsten inert gas welding with argon as the inert gas. To ensure the reproducibility of the removal process weld seams of dimension 25 mm x 5 mm x 1.2 mm (LxBxH) are prepared on a flat mild steel work coupons as shown in Figure 7.2.

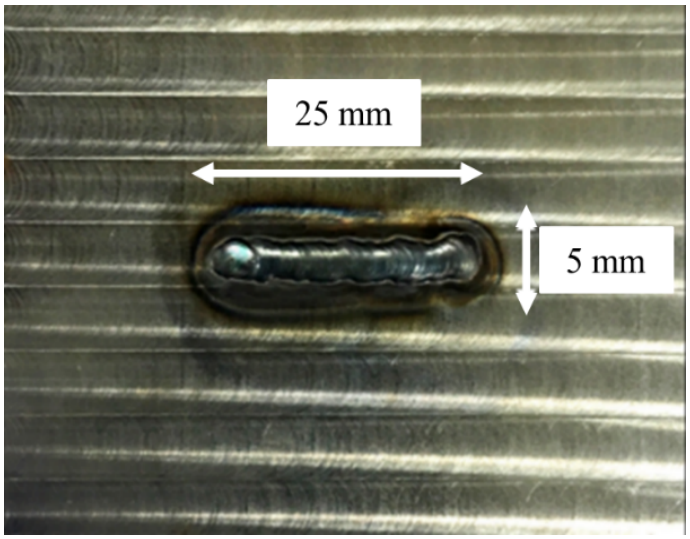

Figure 7.2: Weld seam on the mild steel coupon.

Since the weld seam is of length 25 mm and the contact width of the belt cross section is only 9 mm, tool path planning is divided into three stages for complete weld removal from the surface of the work coupon with each stage removing 1/3 of the weld seam length as shown in Figure 7.3. For each and every pass on weld seam, the weld seam profile height depletes, and the weld seam is completely removed. Tooling passes are done perpendicular to the length of the weld seam which helps to remove the weld seam as well as secure the surface integrity of the adjacent area near the weld seam as shown in Figure 7.3.

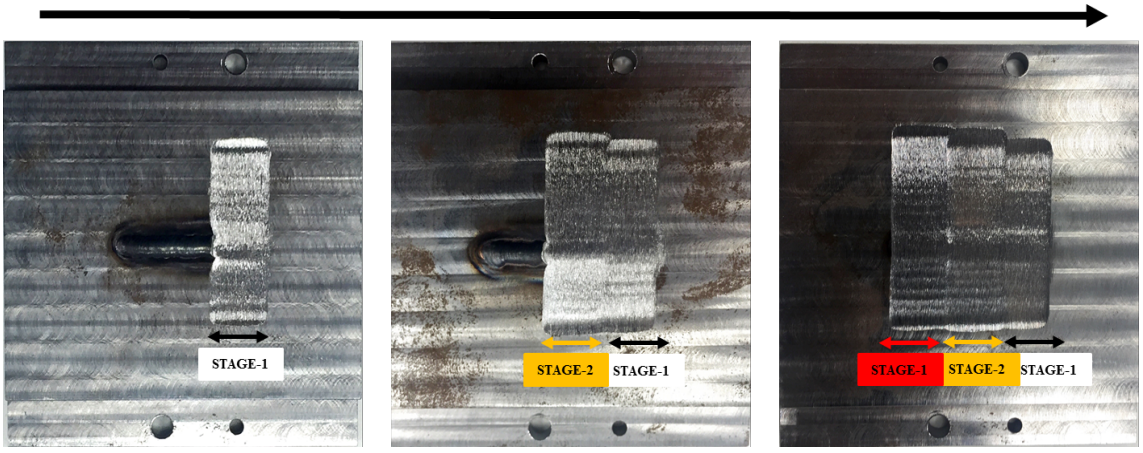

Figure 7.3: Stage-wise weld seam removal from workpiece surface in dry conditions.

7.2.3 Evolution of weld seam geometry during belt grinding

Evolution of weld seam can be categorised into three distinct states and is completely dependent on the geometry of the contact wheel of the belt grinder. The three states of weld seams are based on by their geometry of the scanned profile using Taly-scan profilometer. The shape of the weld seam profile before machining is symmetrical on both ends as shown in Figure 7.4 (a) which is labelled as State-1. The weld profile looks hemispherical with its peak at the center.

The State-2 has a weld profile evolved which is not symmetrical in shape with an apparent reduction in height compared to the weld profile obtained at initial state as shown in Figure 7.4 (b). Such a weld profile evolution can be attributed to the convolution error caused by the contact wheel diameter and inclination between the weld seam and the contact wheel of the grinder. The highest point of the profile is skewed towards the direction where the initial contact is made by the grinding

wheel on the weld seam on each and every pass.

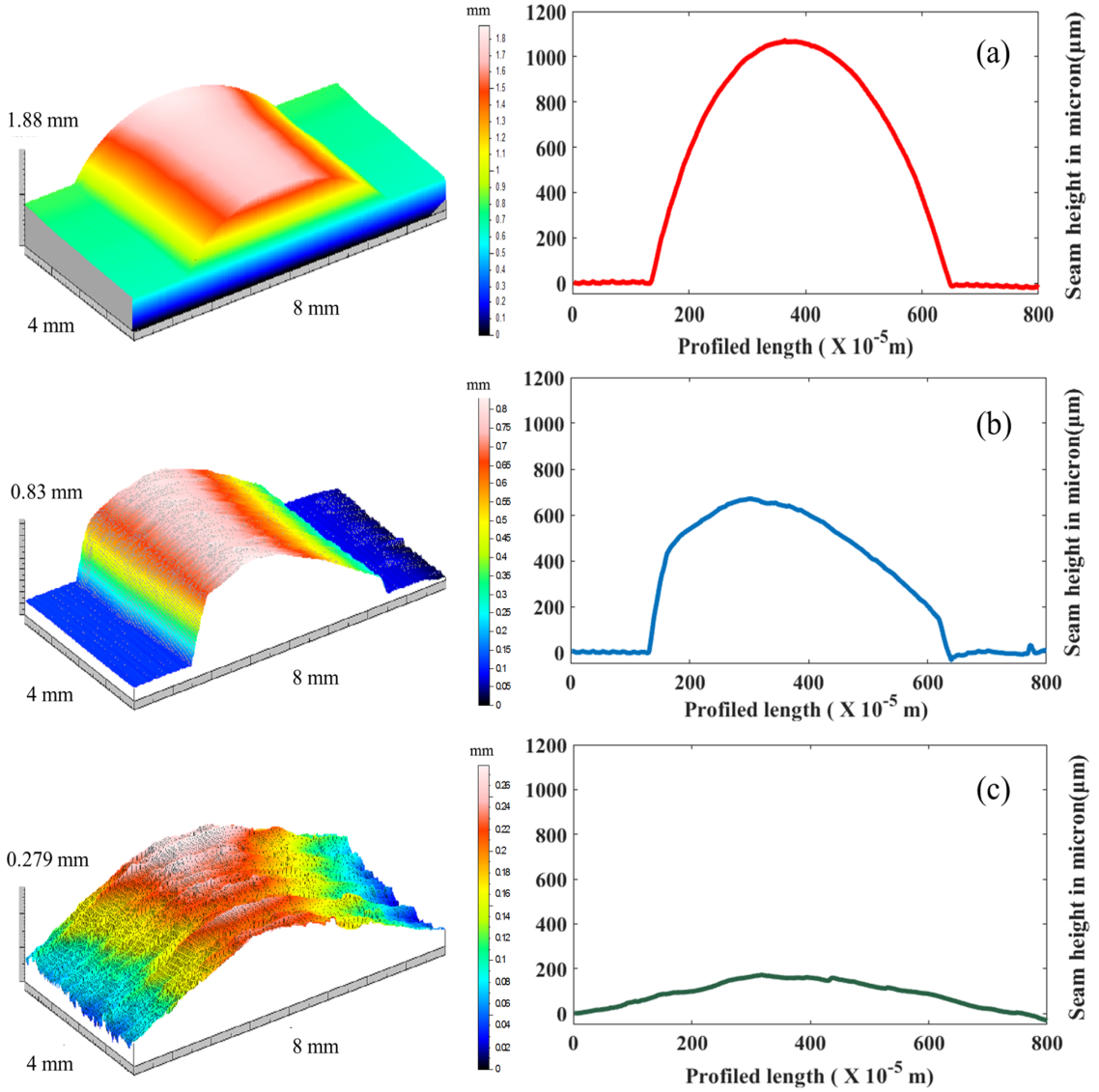

Figure 7.4: (a) 3D and 2D profile extracted from the weld seam before belt grinding process. (b) 3D and 2D non-symmetrical profile extracted from the weld seam after consecutive passes of belt grinding process (State-1). (c) 3D and 2D profile extracted when the weld seam is distinctively removed (State-2).

The State-3 is where the weld seam is distinctively removed, and there is also a reduction in the breadth of the weld seam as a result of continuous grinding as shown in Figure 7.4 (c). The contact wheel of the belt does not have convolution problem during the grinding process as it was subjected to in State-2. State-3 is the final state where the weld seam is completely removed. This research tries to predict the State-3 of weld seam virtually based on sensor signatures.

7.2.4 Complementary based multi-sensor integration system

A complementary multi-sensor integration system comprising of accelerometer and force sensor was developed and proposed as a strategy to estimate the state of the weld seam removal. Kistler 8763A500 triaxial accelerometer is placed near the tension arm of the electric belt grinder to record the tool vibration during machining. The accelerometer is placed on the tool to avoid interruption on the belt transmission. Kistler 9254, a three component dynamometer, is positioned below the work coupon to measure the forces generated during grinding.

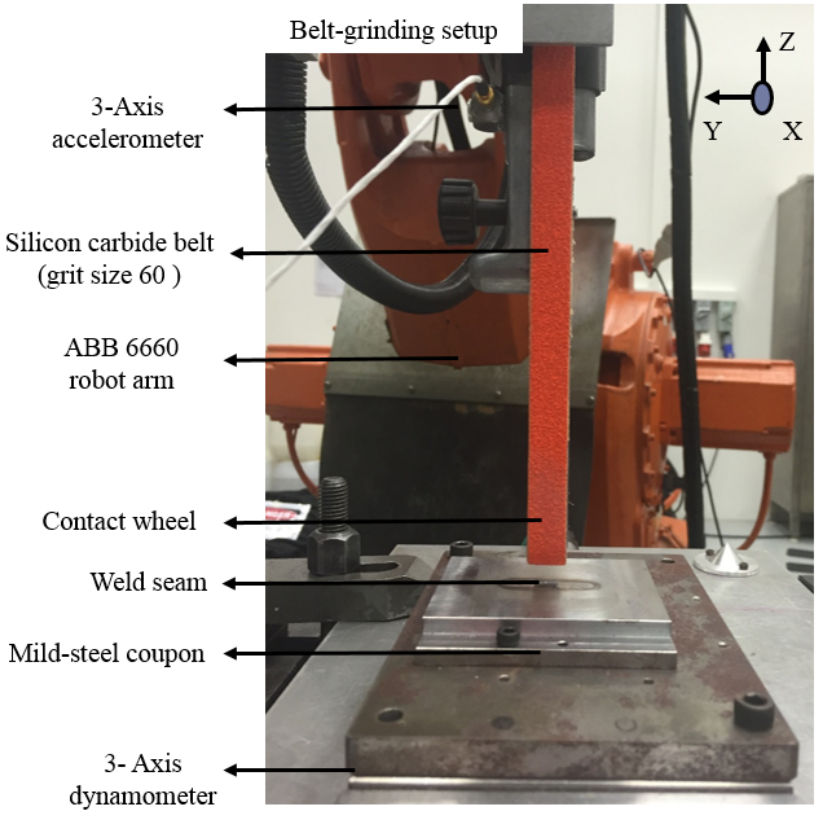

Figure 7.5: Multi-sensor belt grinding setup.

Figure 7.5 shows overall experimental setup and sensor placement. Sensor position and data sampling rate of 2 KHz set constant throughout the experiment for both accelerometer and force sensor. Data acquisition device supported by DEWE-Soft platform is used to acquire and post process the measured signal from both sensors.

7.2.5 Sensor signature analysis for different weld seam profile state

A successful weld seam end point detecting method must be responsive to the change in contact condition, i.e. change in profile geometry of the weld seam on each and every pass. Based on visual observation, the signatures from the multicomponent dynamometer on each pass suggest that forces along X (the direction of the pass), Z (normal to the work coupon surface) and Y (perpendicular to the pass) show evident significance.

The same finding is also observed from the accelerometer sensor signatures in all the three axes. Accelerometer readings are subjected to frequencies arising from moving components of the grinding tool during data acquisition as it is mounted on the grinding arm. Hence, Butterworth-bandstop filter is used to attenuate frequency ranges corresponding to the grinding tool as demonstrated in Section 6.2.2. For detecting the weld seam states efficiently in belt grinding process, monitoring signatures from the force and accelerometer signal is essential.

Analysing sensor readings during the grinding process of the weld seam at State-1, it was evident that there is a reduction in the magnitude of the signatures for both the sensor in all the axes when the grinder encounter with weld profile. Accelerometer and force sensor signatures on all three axes, when the contact wheel of the belt grinder encounters with the weld seam in State-1 are shown in Figure 7.6. and Figure 7.7.

Figure 7.8 and Figure 7.9 show the sensor signatures acquired during the grinding process of the weld seam in State-2. As the contact wheel of the belt grinder encounters the weld profiles at State-2, where the height of the seam has been reduced, there is an increase in the magnitude of the signatures. The increase in the magnitude of the signatures is attributed to the fact that the grinding contact wheel made complete contact over the weld seam and did not encounter any convolution error (see Figure 7.12. for illustration).

However, in State-3 the signatures appear to be constant throughout the belt grinding process as the weld seam is completely removed as shown in Figure 7.10 and Figure 7.11. Vibration and force sensor signals, unlike State-1 and 2, does not show any signal transitions throughout State-3.

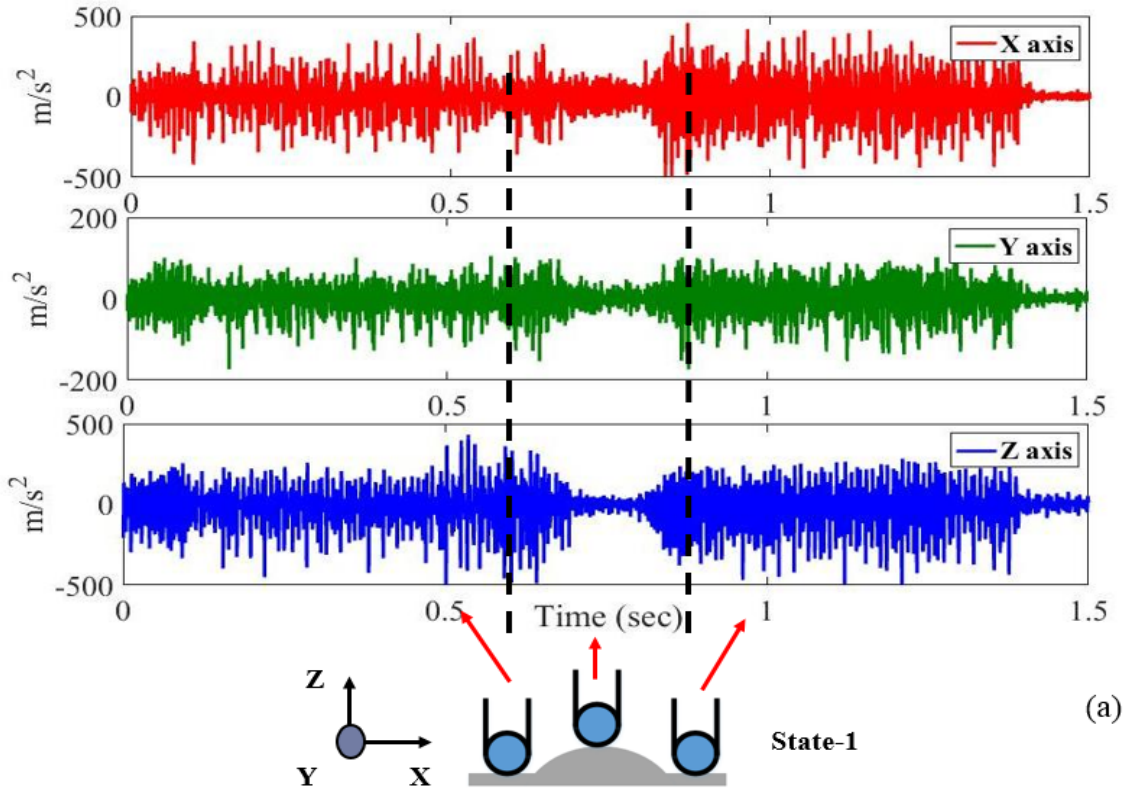

Figure 7.6: Accelerometer signatures obtained on contact of the belt grinding arm over nonsymmetrical weld seam profile State-1.

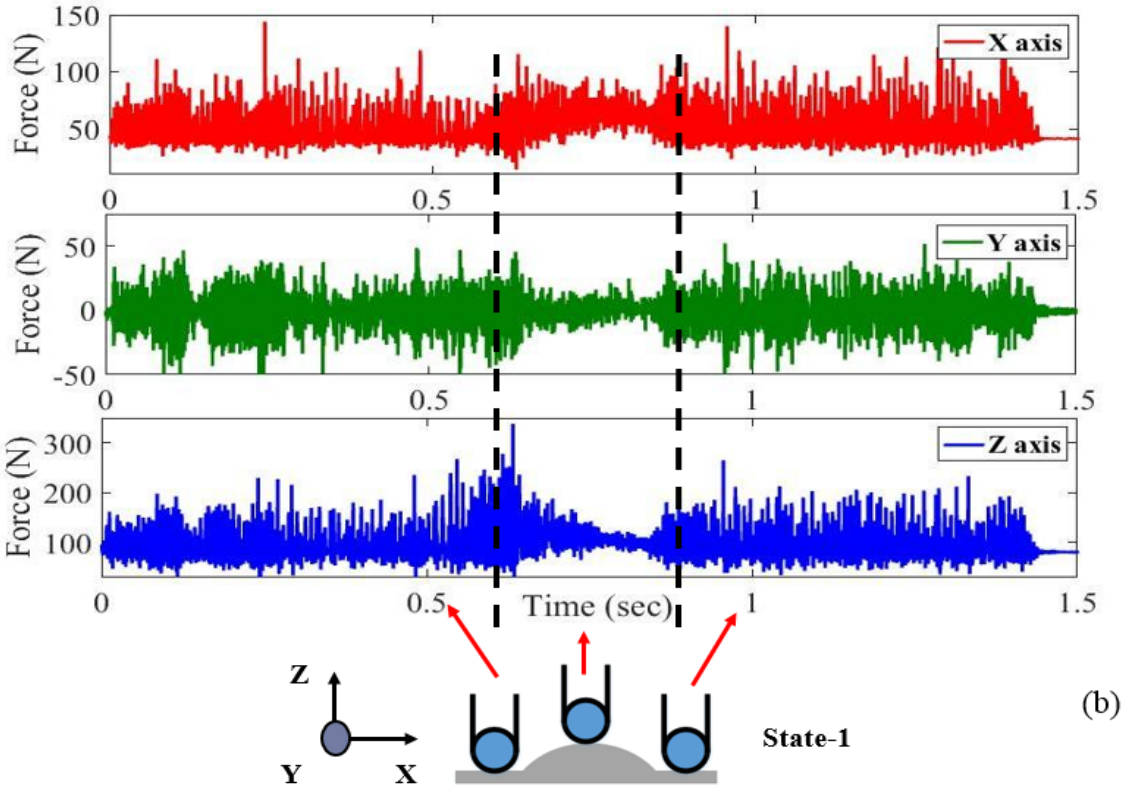

Figure 7.7: Force signatures obtained on contact of the belt grinding arm over non-symmetrical weld seam profile State-1.

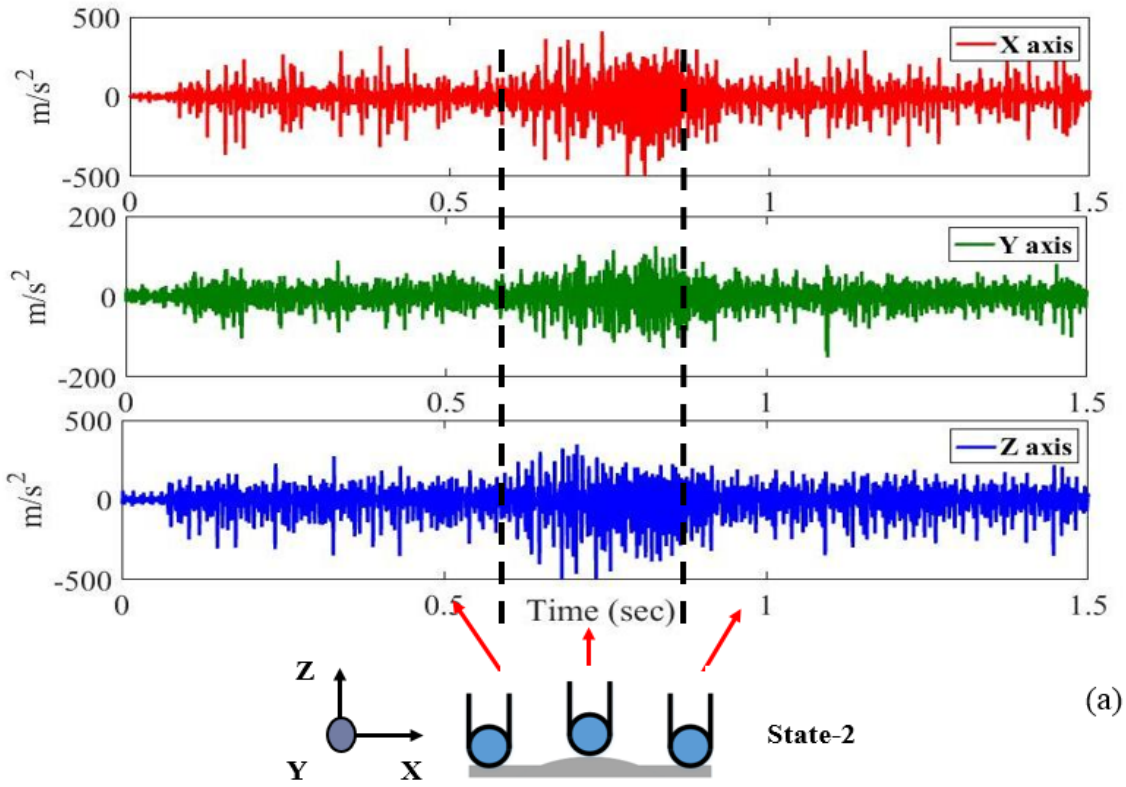

Figure 7.8: Accelerometer signatures obtained on contact of the belt grinding arm over weld seam profile State-2.

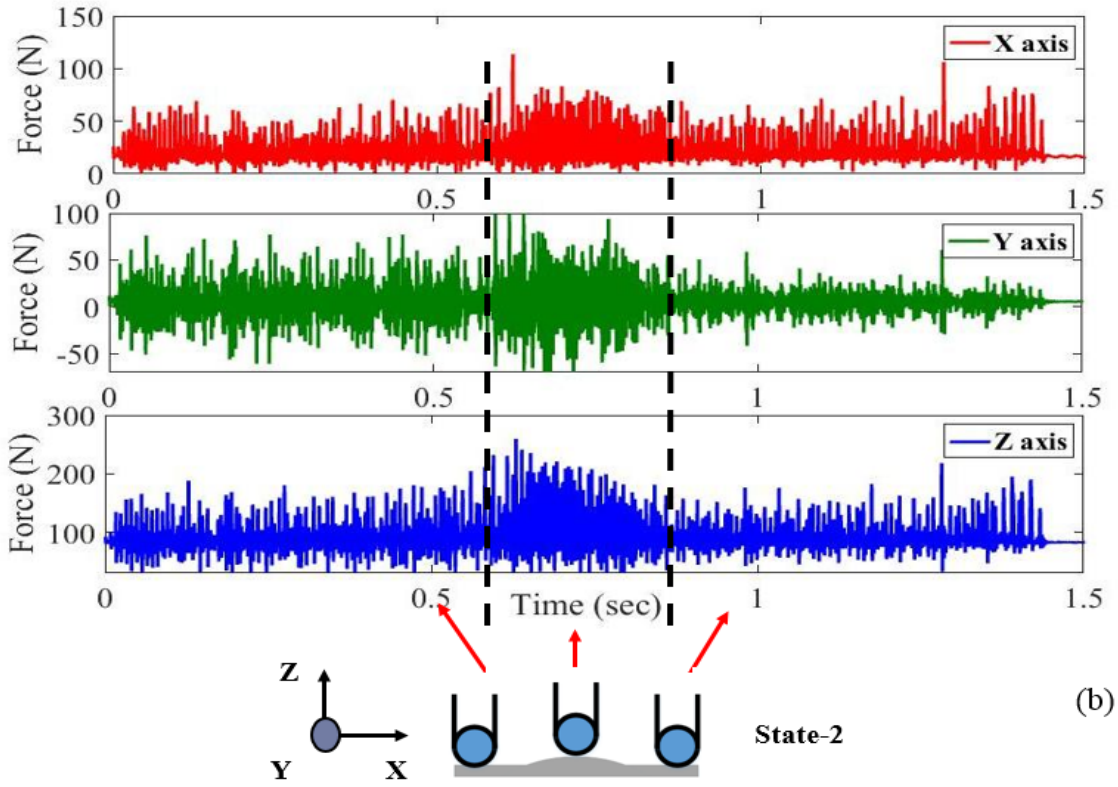

Figure 7.9: Force signatures obtained on contact of the belt grinding arm over weld seam profile State-2.

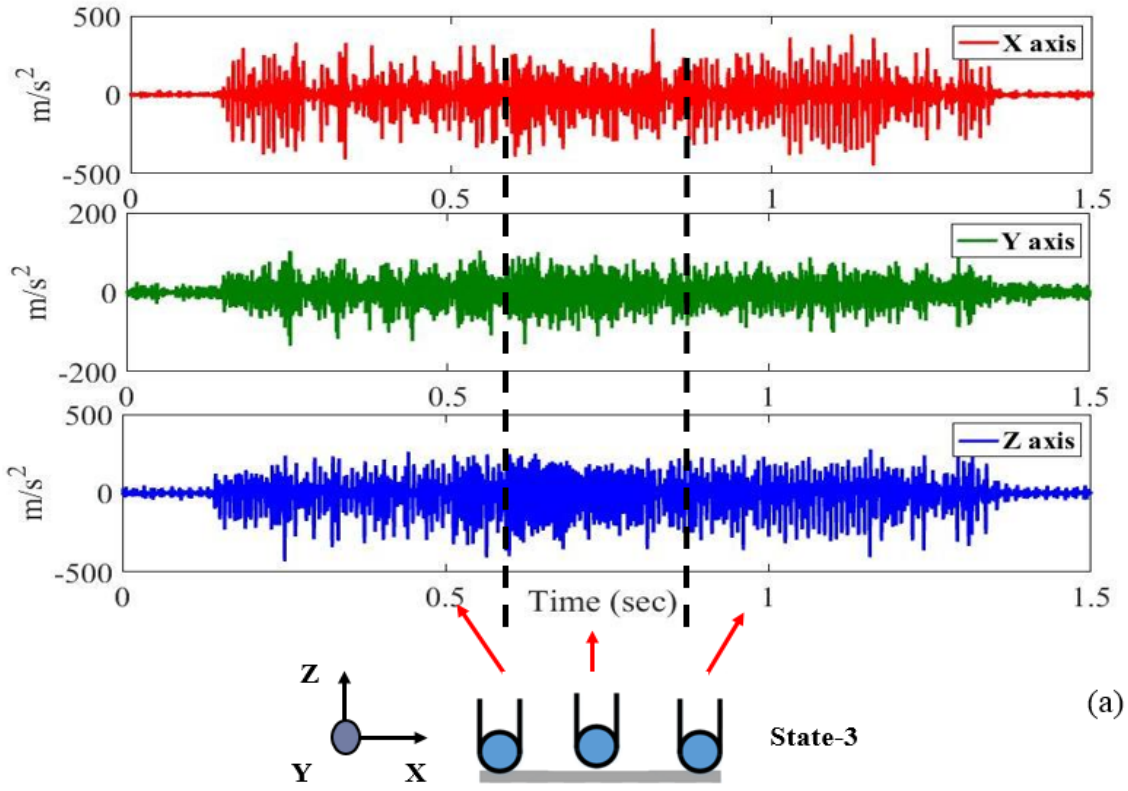

Figure 7.10: Accelerometer signatures obtained on contact of the belt grinding arm over completely removed weld State-3.

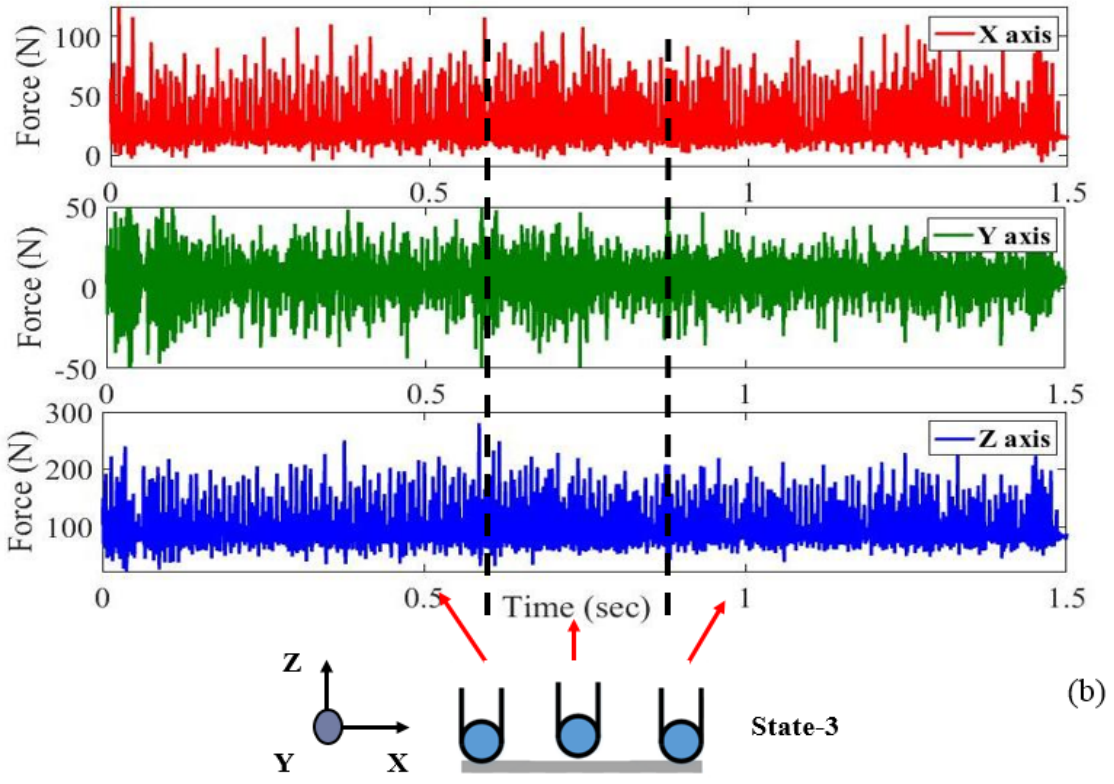

Figure 7.11: Sensor signatures obtained on contact of the belt grinding arm over completely removed weld State-3.

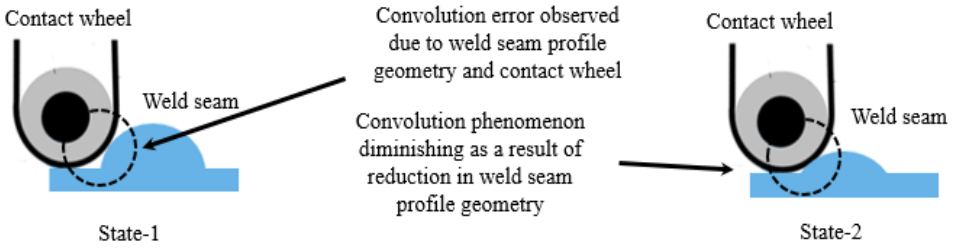

Figure 7.12: Comparison of the convolution error during machining weld seam in States-1 and 2 with the contact wheel.

7.2.6 Signal processing based on wavelet decomposition

Wavelet transform utilises an evaluating wavelet function that is localised in both frequency and time to identify transient changes in the sensor signals in time domain [320]. Wavelet transformation is an excellent tool to characterise dynamic signals as it analyses signals into different packages of energy. From classification point of view, wavelet transformation is a good contender for organising a very characteristic data set for cutting force signatures [321].

The orthogonal Daubechies filters of length 4 is applied to extract the wavelet coefficients of discrete time signals. Table 7.2 shows the frequency bands covered by the 8 decomposition levels in the performed experiments. The sensor signals from 60 experimental trials conducted using the same belt grinding condition are then decomposed up to 8 levels taking Daubechies-4 mother wavelet for extraction of features. The frequency bandwidths of approximation and detail coefficients of wavelet decompositions are shown in Figure 7.13.

Table 7.2: Wavelet-frequency bands for experimental trials.

Decomposition level	Frequency band (Hz)
Level 1	1000 - 500
Level 2	500 - 250
Level 3	250 - 125
Level 4	125 - 62.5
Level 5	62.5 - 31.25
Level 6	31.25 - 15.625
Level 7	15.625 - 7.825
Level 8	7.825 - 3.90

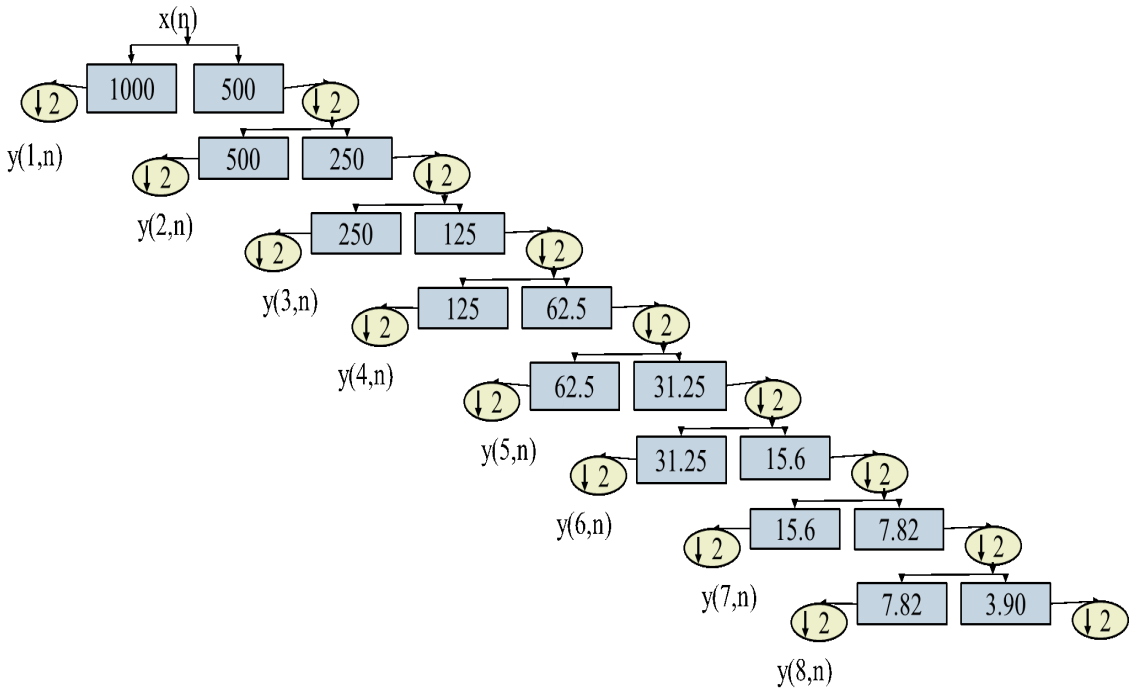

Figure 7.13: Wavelet tree decomposition with eight detail levels of time signal.

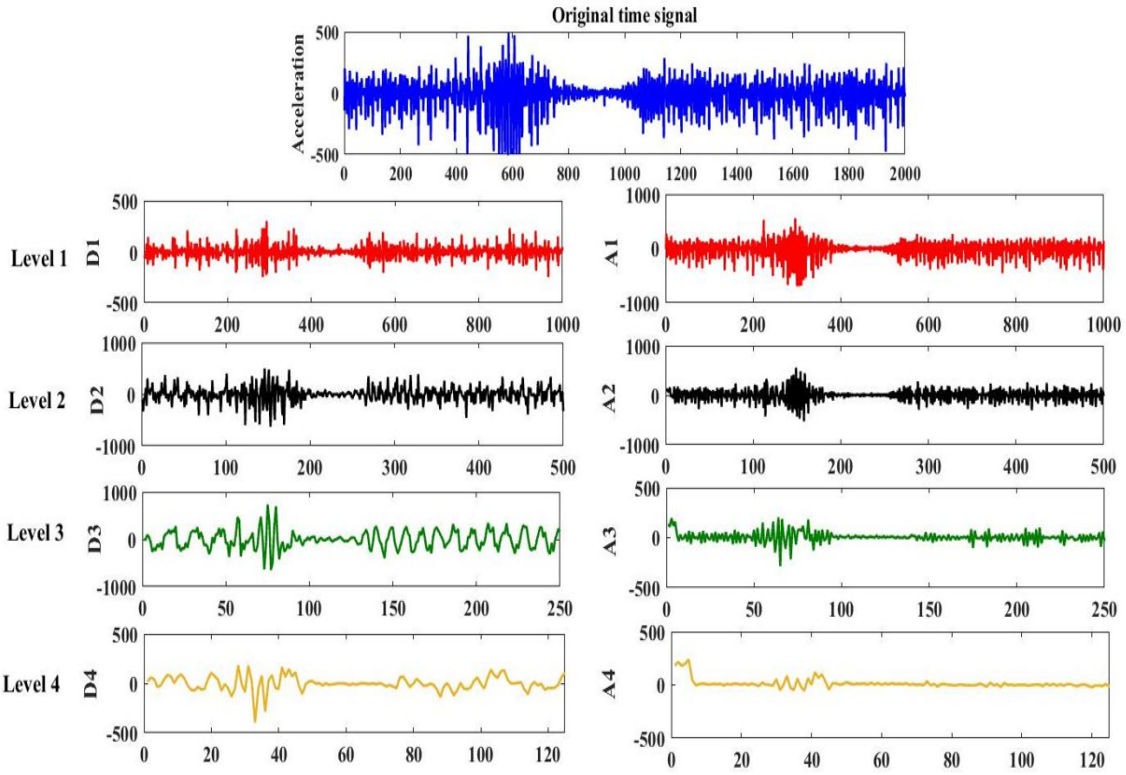

Figure 7.14: Wavelet decompositions for time signal obtained from accelerometer during grinding of weld State-1.

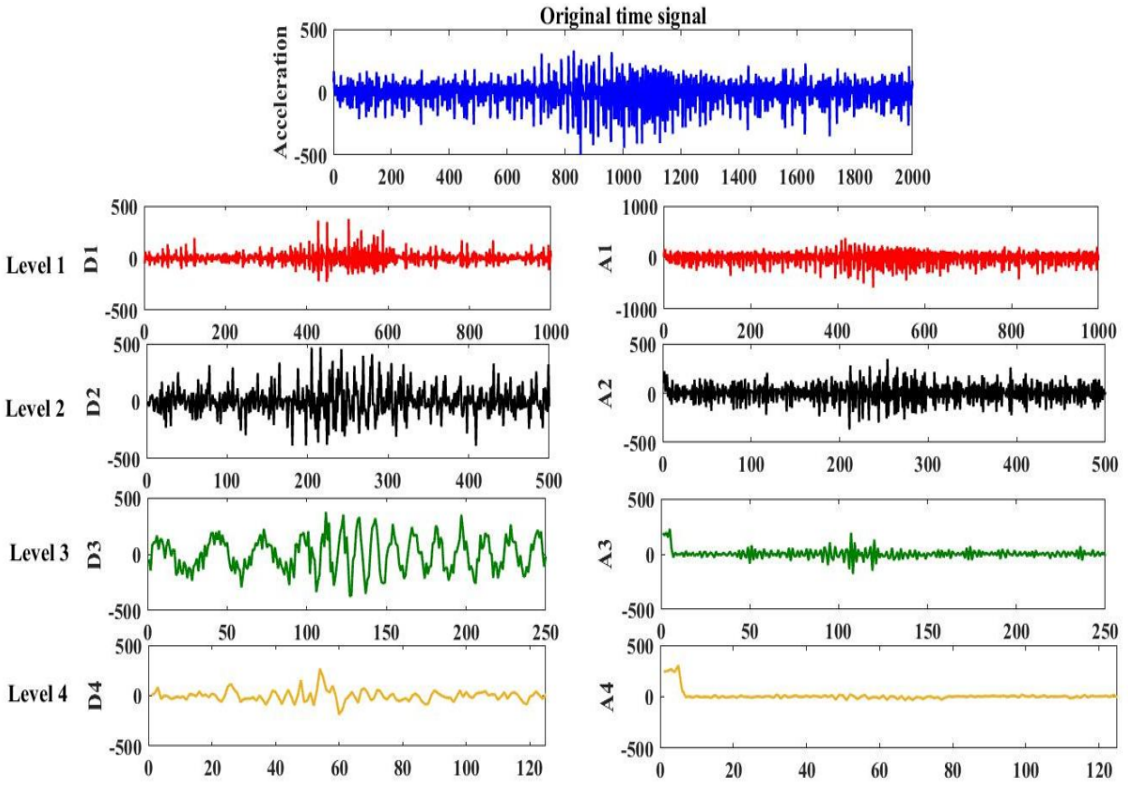

Figure 7.15: Wavelet decompositions for time signal obtained from accelerometer during grinding of weld State-2.

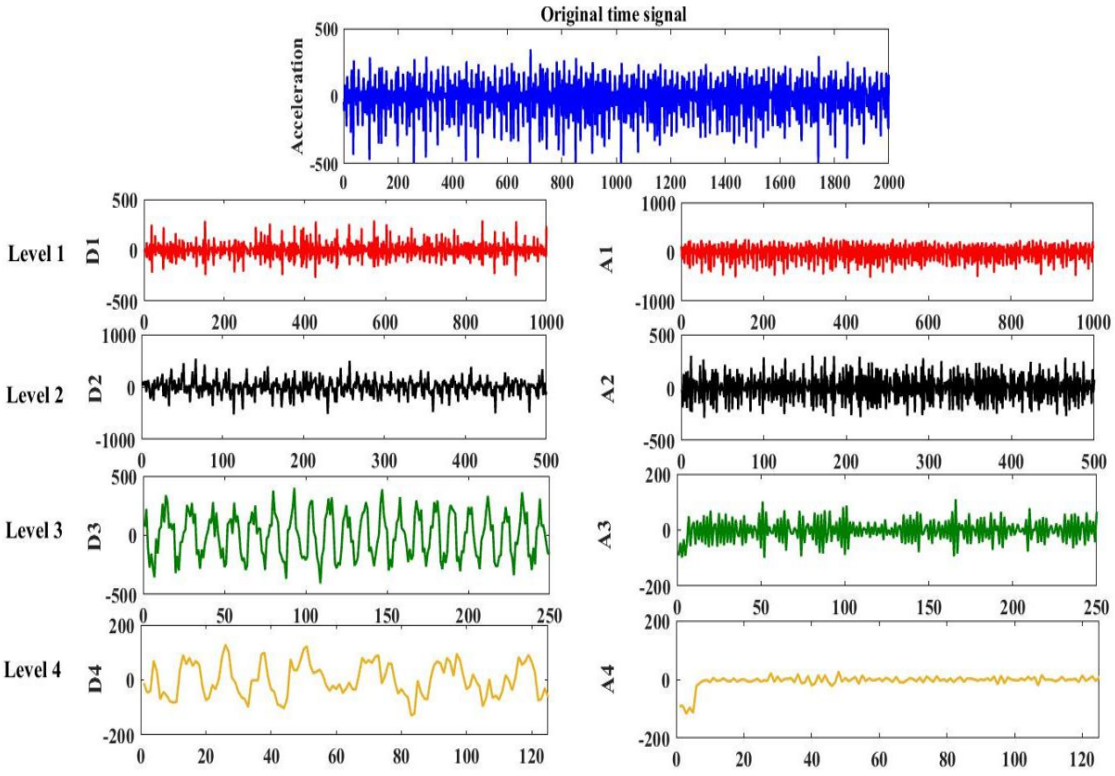

Figure 7.16: Wavelet decompositions for time signal obtained from accelerometer during grinding of weld State-3.

Figure 7.14 shows the acceleration response in State-1 when the weld seam has an symmetrical profile and the corresponding approximation and detail coefficients obtained by DWT up to four levels. The acceleration time signals of weld seam profile in State-2 and State-3 and their four-level decomposition into approximation and detail coefficients are shown in Figure 7.15 and Figure 7.16. The sensor signals obtained during grinding different states of weld seam profile geometry are distinct in wavelet decompositions when they are compared with each other. The above finding reveals DWT can be used as an effective tool for detecting weld seam removal during the compliant belt grinding process.

7.2.7 Wavelet based feature extraction

Fundamental to the success of classification and endpoint detection of the weld seam removal problem is the extraction of a set of informative features that provides the best descriptive information about the content of the input signals. Features providing more details about the signal are generated based on wavelet coefficients in the frequency sub-band when DWT is applied as discussed in the previous section 7.2.6. The features should preserve the weld seam state distinguishable as much as possible. The 11 features computed using the detail and final approximation coefficients during grinding of different weld seam profile from sensor data obtained that maximises weld state separability is listed in Table 7.3.

Table 7.3: Features extracted based on wavelet decomposition coefficients .

Feature number	Feature name
Feature 1	Mean
Feature 2	Variance
Feature 3	Standard deviation
Feature 4	Waveform length
Feature 5	Entropy
Feature 6	Peak2peak
Feature 7	Root Mean Square (RMS)
Feature 8	Root Sum of Squares (RSSQ)
Feature 9	Band power
Feature 10	Kurtosis
Feature 11	Skewness

Full tree at 8 decomposition level yields 88 features, as 11 type of feature is extracted at each level. Features extracted from force and accelerometer along three their axes channel is concatenated to form one large vector space of 528 features that will be used for endpoint prediction i.e. State-3. Figure 7.17 reveals that the correlation between energy and kurtosis features varies depending on the weld seam states, i.e. weld profile shape. Such interpretation of the feature space hints us with the possibility of classifying the weld seam states and to predict the endpoint of weld seam removal.

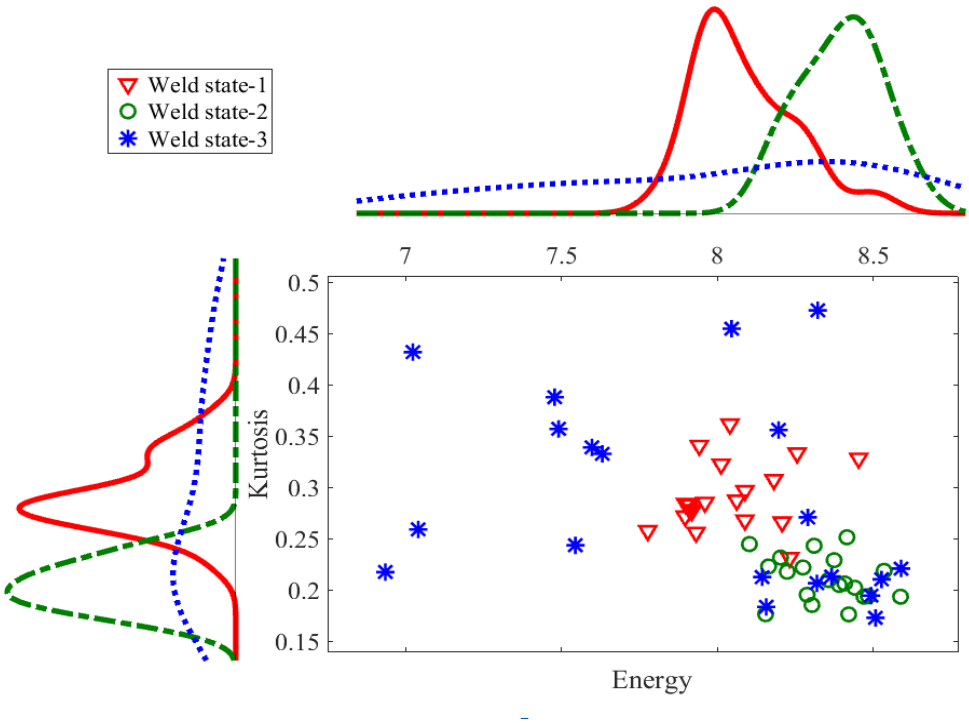

Figure 7.17: Relationship and distribution between kurtosis and energy feature acquired from accelerometer signal for level 1 decomposition for three different weld seam states.

7.2.8 Classification based endpoint detection

In this chapter, the weld seam profile geometry evolved at three different states of the belt grinding process are assigned as discrete classifiers. Classification of the weld seam states by the classifiers consists of two main parts: training data and testing data. Same like before,70% is used for training and 30% for validation. Five predictive models using k-NN, Naive Bayes, SVM, Artificial neural network and Bagged Trees were developed and compared. The performance of the five algorithms depends primarily on their respective parameter configuration. The set of training

parameters for each classifier used in this research are listed in Table 7.4.

Table 7.4: Training parameters of the classifiers for predicting weld seam states.

GA parameter	Parameters	Values
SVM	Validation method	Hold-out validation
	SVM kernel function	Quadratic
	Kernel scale	Automatic
	Multiclass method	One-vs-One
	Standardize data	True
	Prediction speed	∼120 observations/sec
	Training time	28.568 secs
kNN	Classifier	Fine KNN
	Number of neighbours	10
	Distance metric	Euclidean
	Distance weight	Equal
	Prediction speed	∼400 obs/sec
	Training time	29.94 secs
ANN	Number of neurons	10
	Output layer	3
	Training method	Backpropagation
	Performance	Cross-entropy
	Epoch	34 iterations
	Training time	1.7699 secs
Naive Bayes	Distribution Names	Normal (Gaussian) distribution
	Predictors	Categorical
	Class probability	0.33
	Training time	1.4417 secs
Bagged Trees	Classifier	Decision Tree
	Number of learners	10
	Prediction speed	∼210 obs/sec
	Training time	33.476 secs

Performance measure experiment with 30% holdout and 528-wavelet decomposition features on quadratic-SVM model had an accuracy higher than other classifiers with prediction of 95.3% as shown in Figure 7.18. Figure 7.19 exhibits that there is a clear separation drawn by the hyperplane in the feature space between different weld state using quadratic SVM classifiers. Well-chosen kernel function and finest value of parameters for the specific kernel are critical for the performance of the predictive model.

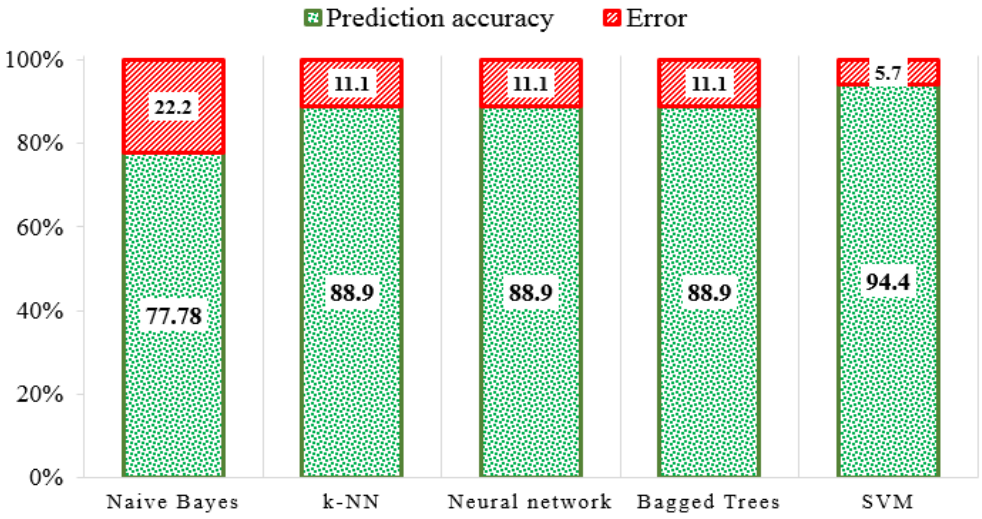

Figure 7.18: Prediction accuracy of individual classifiers.

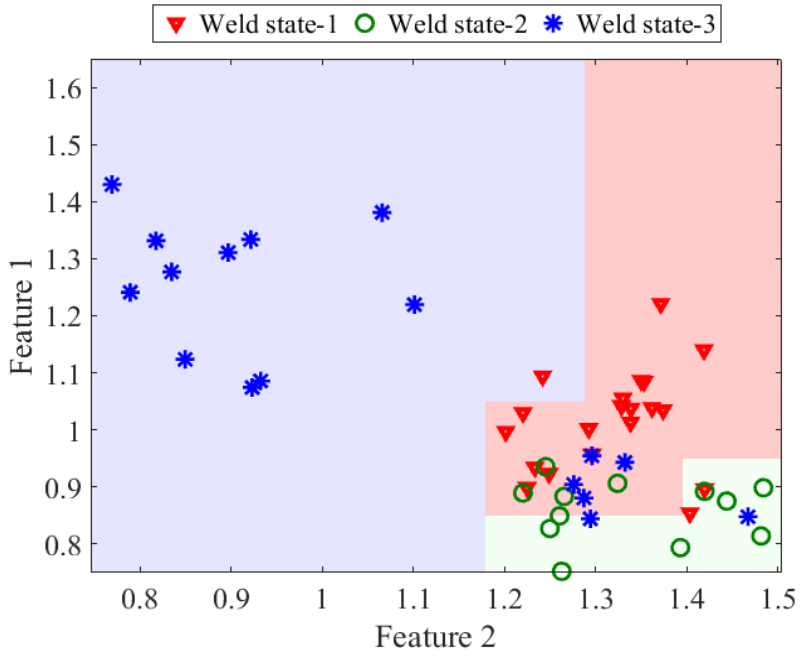

Figure 7.19: Support vector machine-based hyperplane for classification from the training set.

Figure 7.20 shows 3-by-3 confusion matrix for classification of three different weld states with 94.4% accuracy obtained using the quadratic-SVM model with a small fraction of samples misclassified. The proposed approach is composed primarily of three steps. In the first step, discrete classifiers are identified, and the corresponding sensor signatures are preprocessed. In the second step, features are extracted using wavelet decomposition based on Daubechies-4 mother wavelet discussed in

Section 7.2.6. In the final step of training and classification, exercises are performed on a machine learning based classifiers.

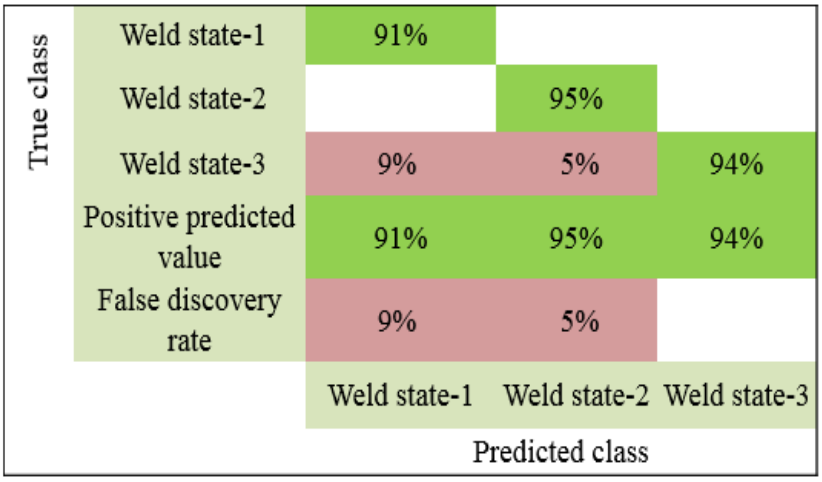

Figure 7.20: Confusion matrix depicting classifier performance in weld states 1, 2 and 3.

Though the methodology on using wavelet features can potentially correlate weld seam removal and predict removal when deployed along with the machine learning classifiers, it has the constrain of using the same model for different experimental condition. In industries, weld seam comes in complicated geometries, material and even locations that are hard to access which makes the model vulnerable as sensor signature change drastically based on machining conditions. Moreover, extra effort is required with respect to the tool path planning when weld seams of complicated shapes are to be removed. A more robust technique has to be developed to create a model which takes into account of different parameters that would suitably solve a range of problems.

7.3 Real-time verification of weld seam removal using vision sensor and deeplearning

In this section, a methodology is proposed to determine the end point of weld seam removal process such that it does not depend on the grinding parameters based on computer vision and deep learning. A novel in-process monitoring system is developed using a vision system and encoder-decoder based deep learning architecture. The section presents the results of the first investigative stage of research and

developments on semantic segmentation of weld seam removal states using encoder-decoder convolutional neural networks (EDCNN).

7.3.1 Semantic segmentation

The goal of semantic segmentation is to assign each pixel of a image to it corresponding class labels or to none of them. Semantic segmentation is expressed as a discrete labelling problem that assigns each pixel $a_i \in R^3$ an image to a label b_i from a fixed set Z. Given N observations $a = [a_1, a_2, \ldots, a_n]$ the objective is to estimate the set of labels $b = [a_1, a_2, \ldots, a_n]$ taking the values in Z^N. It can be visualised as a supervised learning problem which requires training at the pixel level. Visual scene understanding in terms of geometry, depth, perception of shape can be achieved only using semantic segmentation architecture that has an encoder network followed by a decoder network which is a natural step in the progression from coarse to fine inference.

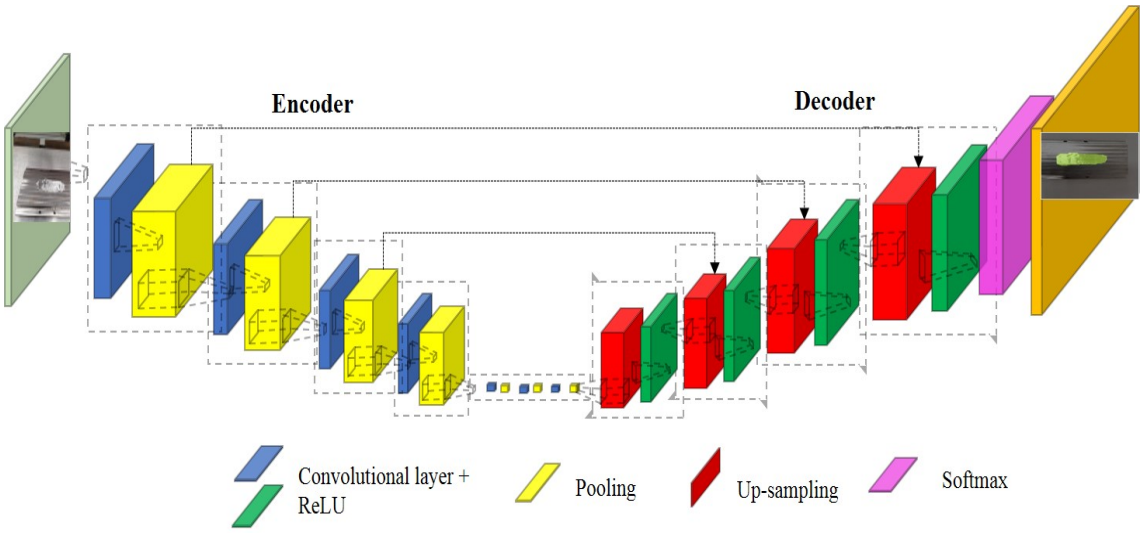

Figure 7.21: An illustration of the encoder-decoder architecture.

A typical encoder-decoder architecture is illustrated in Figure 7.21. The encoder network is used to obtain the high-level semantic feature of the images and the decoder network is applied to map the low resolution feature maps to full input resolution feature maps for pixel-wise labelling. The primary task of the decoder is to semantically project the lower resolution discriminative features acquired by the encoder onto a higher resolution pixel space to get a intense classification. There are usually shortcut connections from the encoder to the decoder to help the decoder to

recover the object details better and also to refine the upscaling process as shown in Figure 7.21. The encoder is usually a pre-trained classification network like VGG/ ResNet/ Alexnet etc.

7.3.2 Experimental setup and grinding conditions

Figure 7.22 shows the belt grinding setup used in the removing the weld seams. A vision system is introduced to capture the images of various stages of weld states which consists of a digital camera and an image processing system. The digital camera is incorporated with the help of a tripod stand adjacent to belt grinder as shown in Figure 7.22. Surface images are captured at the end of every pass of robot arm across the weld seam. The camera system is capable of capturing and storing the surface images at a resolution of 1240 x 960 pixels which are subsequently fed into a pretrained algorithm to determine the endpoint. The belt grinding parameter used during the weld seam removal are listed in Table 7.5.

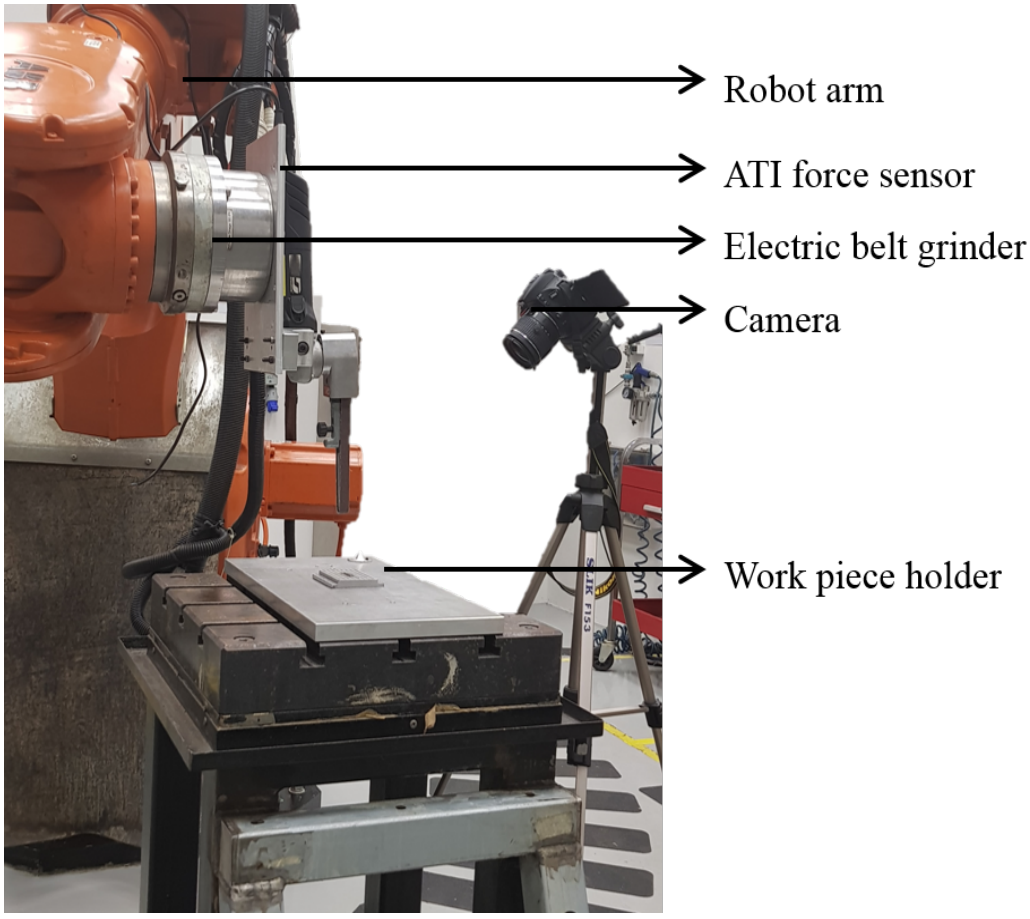

Figure 7.22: Abrasive belt grinding setup with the camera.

Table 7.5: Parameters used in the belt grinding experimental trials.

Parameter	Value
Belt grinding speed	Variable
Contact wheel diameter	Variable
Hardness of contact wheel (polyurethane)	Variable
Lubrication	Dry
Feed	Variable
Belt finishing duration	Variable
Operational mode	Position control

7.3.3 Weld seam removal

Evolution of weld seam geometry during removal process using robotised belt grinding is categorised in four distinct states based on the height of the scanned weld seam geometry that are measured using Taly-scan profilometer as shown in the form of 3-Dimensional and 2-Dimensional profiles in Figure 7.23. The shape of the weld seam profile before machining is symmetrical on both ends as shown in Figure 7.23 (a) which is labelled as State-1. The weld profile appears hemispherical and symmetrical with its peak at the center. The State-2 features an evolved weld profile as a result of grinding that is not symmetrical in shape with 30% of height removed compared to the weld profile obtained at initial state as shown in Figure 7.23 (b). The weld profile geometry of State-3 indicates the result of subsequent grinding which is not symmetrical in shape with 70% of height removed compared to the weld profile at State-1 as illustrated in Figure 7.23 (c). The State-4, the weld seam is distinctively removed as depicted in Figure 7.23 (d). This research aims to predict the State-4, i.e. the state of complete removal of weld seam from the work coupon, using vision system and deep learning.

7.3.4 Methodology

Weld seam used to produce four different removal states is machined with an abrasive belt with variable grinding conditions as listed in Table 7.5. The images at four different stages are taken in a consistent illumination, but with various angles, distances, rotation and motion blur. Each pixel of the images is labelled with its corresponding class, namely background,State-1, State-2, State-3, and State-4.

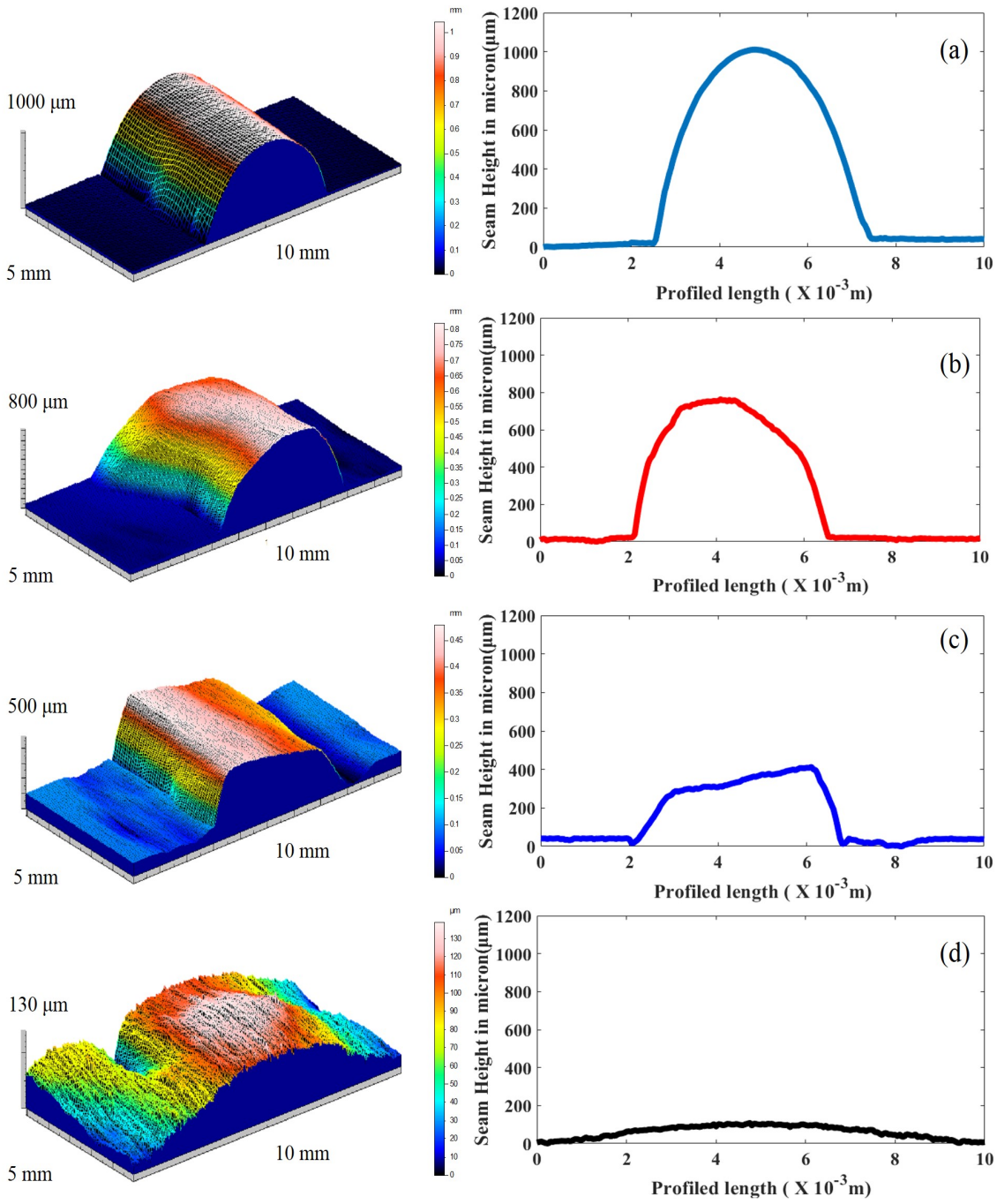

Figure 7.23: 3D and 2D profile depicting weld states during the weld seam removal using belt grinding process.

Furthermore, the augmentations such as shear, random zoom, random crops are implemented to prevent overfitting and to involve randomness on the images. The augmented final image set is further split into two with 60% of the images for training and the remaining for testing. Training and testing images are split in such a way that they represent the probability distribution of all four possible weld seam state outcomes from the weld seam grinding process.

The VGG-16 network is retrained to identify the weld seam states. VGG-16 is a convolutional neural network (CNN) architecture developed and named after the Visual Geometry Group and is also called as OxfordNet. VGG-16 has demonstrated that the depth of the network is beneficial for the classification accuracy and to give better results. The VGG neural network is a CNN for classification of 1000 real-world objects. The VGG network helps to recognize objects based on output probabilities of the different classes that an image could potentially belong. To date, it is still considered to be an excellent pretrained vision model for solving classification problem.

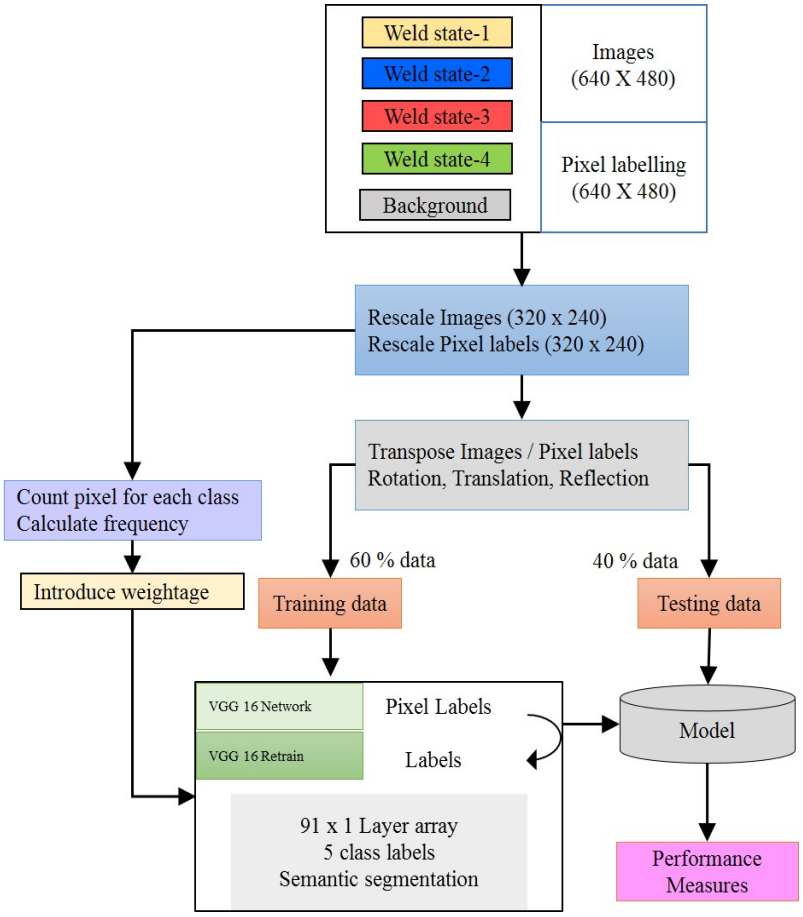

Figure 7.24: General description of the proposed methodology.

Pixel labels layer of the default VGG-16 network is replaced by the customised labels layer that would identify the weld seam state and background of an image. Distribution of pixel count for four different belt states and background is identified, and the corresponding weight is redefined on the final layer of the VGG-16 network. The weld state identification was performed in MATLAB Deep learning toolbox.

The augmented training image set is used for training, and it is ensured that the training accuracy increases and training loss decrease with iteration count. The training is terminated once the parametric conditions are met. The testing images are introduced into the retrained VGG-16 network, and the network prediction and ground truth label values of the images are equated to identify the network performance. Schematic representation of the methodology is described in Figure 7.24.

7.3.5 Image acquisition and data preparation

A vision system consisting of a Digital Single-Lens Reflex (DSLR) Nikon camera is introduced to capture the images of various states of the weld seam. The digital camera is placed adjacent to the robot arm such that its field of view is not interrupted by robots end effector and belt grinder assembly. Weld seam images at the four different states are captured at the end of every pass of belt grinder across the mild steel work coupon. The weld seam images representing four different states are taken in such a way that they contain a broad range of image distribution pattern. Please note, as indicated before, images are taken in constant illumination, but the angle, distance, rotation, and orientation are varied.

Table 7.6: Data set distribution containing weld seam states.

Class	Type	Trainingsample	Testingsample	Colourmap
Class 1	Background	1200	800	[000 000 000]
Class 2	State-1	300	200	[192 200 20]
Class 3	State-2	300	200	[000 000 192]
Class 4	State-3	300	200	[192 000 000]
Class 5	State-4	300	200	[128 192 000]

Each pixel of the images is labelled to which class they belong to. Each class is labelled using colormap as listed in Figure 7.25. Figure 7.25 illustrates the semantic pixel-wise labeling, i.e. labeling each pixel of an image for four different weld seam states with ground truth label using the colormap. The ground truth labels with the corresponding color map are implemented using the image labeler available within the Matlab framework.

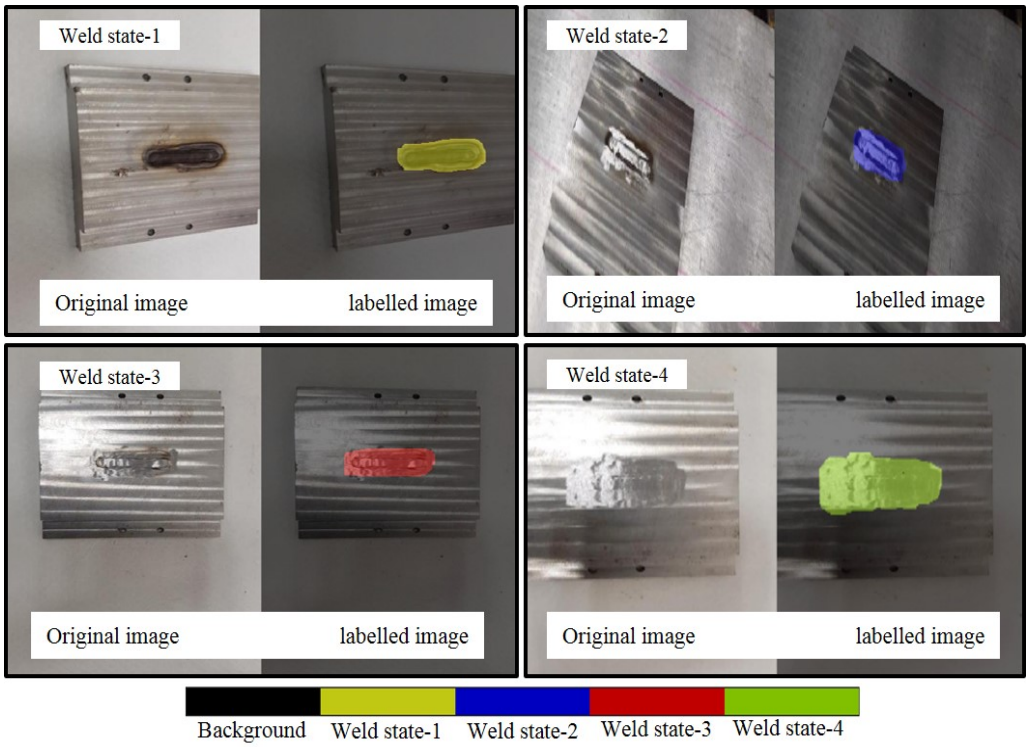

Figure 7.25: Original and pixel labelled images of four different weld seam states.

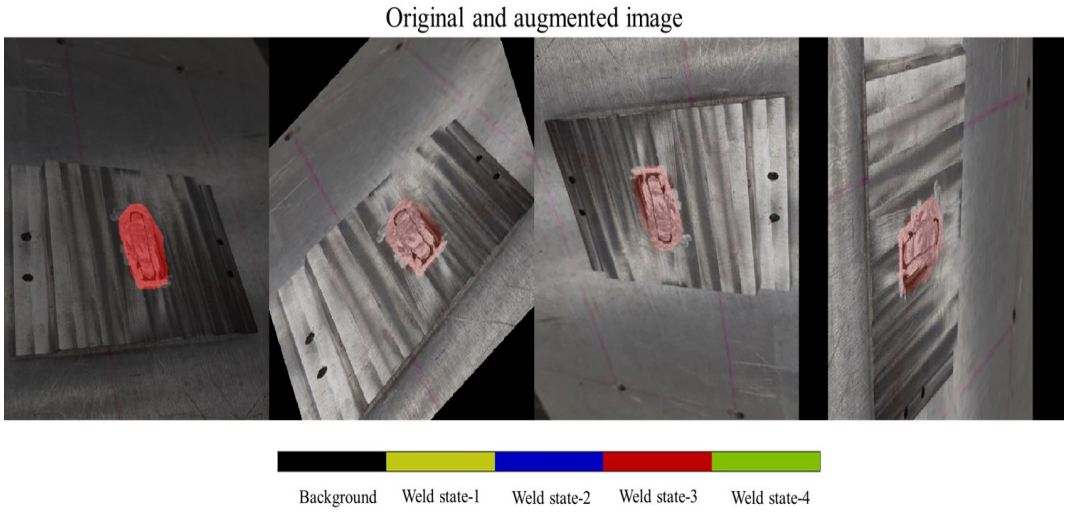

Figure 7.26: Data augmentation on the work coupon with rotation and translation.

Data augmentation provides the possibilities of increasing the input image distribution and it also helps in the generalization of the network. Data augmentation is a technique to artificially increase the training set by adding transformations or perturbations of the training data without increasing the computational cost. Figure 7.26 shows how augmentations such as rotations, horizontally or vertically flipping and random crops are implemented in the images. The augmented final

image set is further split into two with 60% of the images for training the network and the remaining for testing as listed in Table 7.6.

In total, 2000 images taken using the DSLR vision system are used for this study out of which 1200 images are used for training the network and remaining 800 images are implemented for testing purpose. These training and testing images are considered to be the representation of probability distribution of the possible four weld seam state outcomes from the grinding process. The same distribution of images is strictly considered for the training and testing of the network. The training of the network is carried out in an offline process. From the large pool of the training data, each class has 500 instances or images as listed in Table 7.6.

7.3.6 Development of the VGG-16 framework

Implementation of a sophisticated image recognition models requires tuning of millions of parameters. Building and training such model from scratch requires a lot of computing power and a lot of labelled training dataset. However, a model architecture that has already been familiar on a related task is taken and reused.

An encoder-decoder architecture is built using the pretrained VGG-16 network to perform image segmentation by assigning each pixel in an image to the corresponding class. The encoder-decoder network consists of 91 layers including convolution, batch normalization, pooling, unpooling and the pixel classification output layers, as shown in Figure 7.27. The encoder-decoder architecture has the encoder part built using VGG-16 and decoder part formed using VGG-16 network in reverse direction. The image is first down sampled by an encoder part as in a VGG-16 pretrained model, and then it is up sampled by using a decoder part that more-or-less looks like a reversed VGG-16 architecture. The encoder-decoder architecture developed using the VGG-16 network is modified by replacing a couple of layers as shown in Figure 7.26 to suit the weld state recognition problem statement.

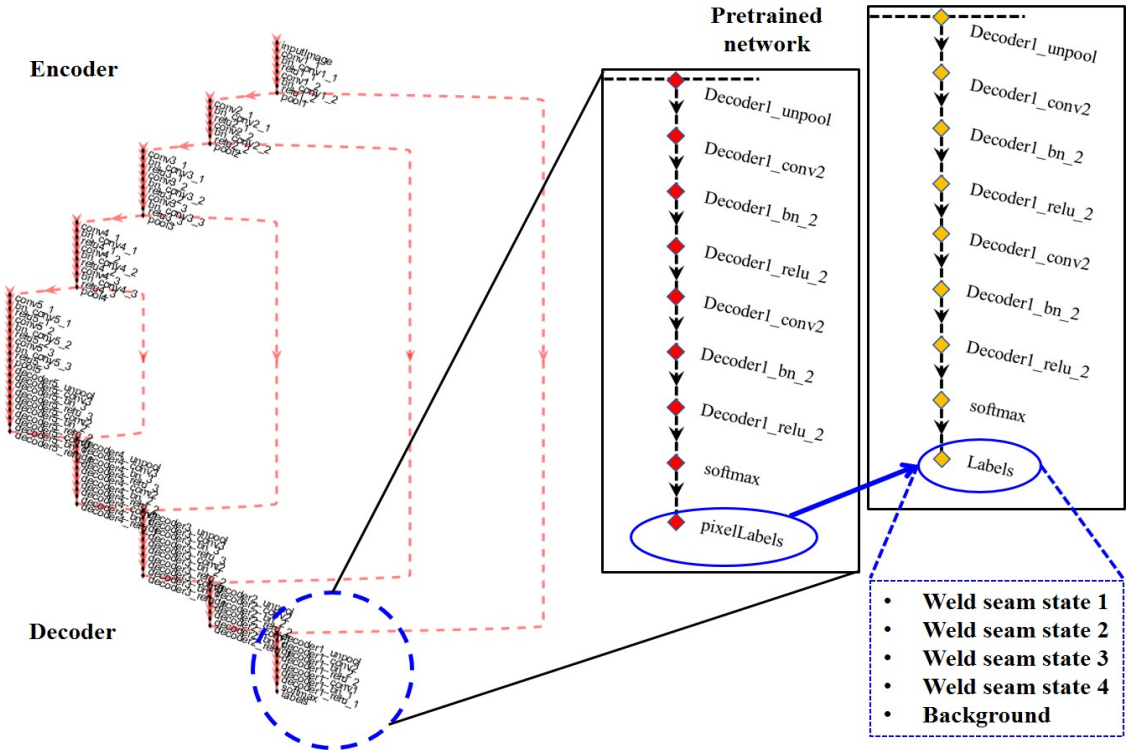

Figure 7.27: Encoder-decoder architecture developed using VGG-16 to predict the weld seam states.

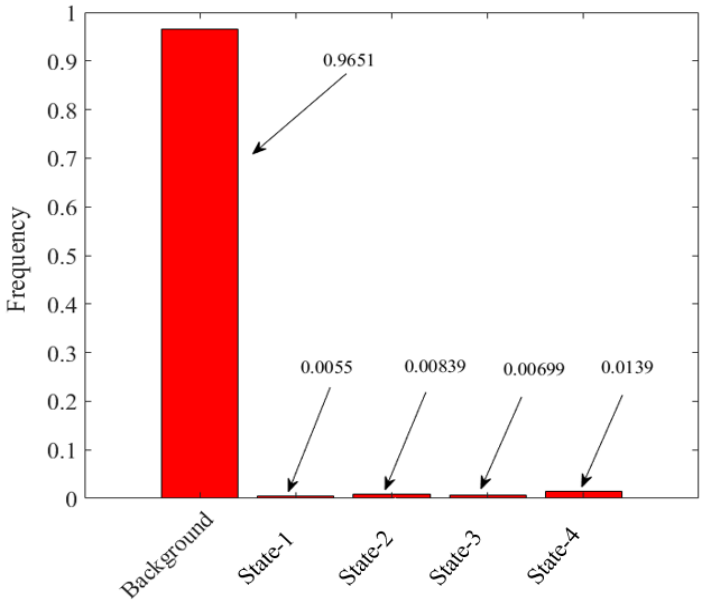

Figure 7.28: Distribution of pixels for four different belt states and background.

The classes in weld seam state data set are imbalanced as shown in Figure 7.28 as all classes did not have an equal number of pixel count. The background class covers larger area and pixel count value compared to the other weld seam state which makes the learning biased more towards the dominant background class. To

improve training effectiveness and to remove the biasing towards the dominant class the weight of the classes are balanced using median frequency. The weights of the weaker classes are given higher value and vice versa based on the median frequency score in pixelClassificationLayer.

MATLAB is used to convert the collected datasets to the SegNet data format and annotate the images. For model training, NVIDIA GeForce GTX1070 module on a desktop computer is used. The optimization algorithm used for training is stochastic gradient descent with momentum. A minibatch size of five is used to reduce memory usage while training. For model training, parameters listed in Table 7.7 are used. The average model training time in reaching a maximum number of iterations of 7200 is 8 hrs. Two different metrics such as training accuracy and training loss are used to evaluate the performance of the deep learning model during its training phase. Training loss is often used in the training process to find the best parameter values for model considered to minimize the error and training accuracy is more on the ability of the model prediction compared to the true data.

Table 7.7: SegNet training parameters.

Segementation training parameters	Values
Type of analysis	Semantic segmentation
Solver name	'sgdm'
Initial learn rate	0.001
L_2 Regularization	0.0005
Max epochs	30
Mini batch size	5
Learn rate schedule	Piecewise
Learn rate drop factor	0.2
Learn rate drop period	5
Shuffle	Every-epoch
Training set	60%
Testing set	40%

The primary objective of training a deep learning model is to reduce the loss function's value with respect to successive iteration count. Figure 7.29 shows the plot of model accuracy and Figure 7.30 shows the plot of model loss during model training. Upon visualising training accuracy and training loss plots it is evident that

there exists inverse proportionality relationship which confirms training progress is successful. From the plot of accuracy, one can see that the model has been thoroughly trained as the trend for accuracy training datasets saturates at 4,000 iterations and there is subtle performance improvement beyond this.

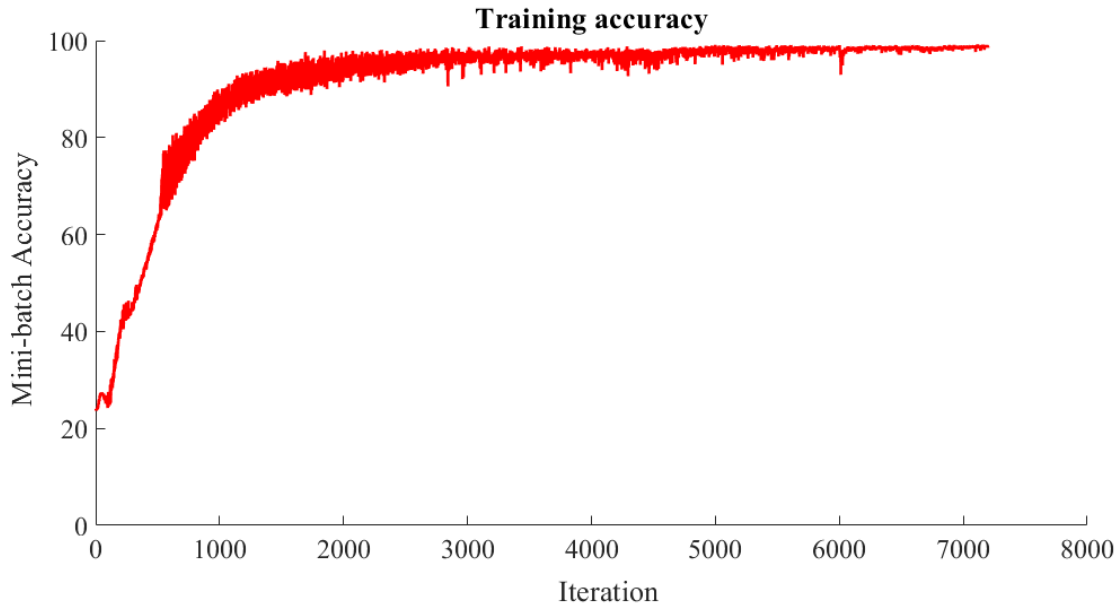

Figure 7.29: Training accuracy during retraining VGG-16 network for weld seam state prediction.

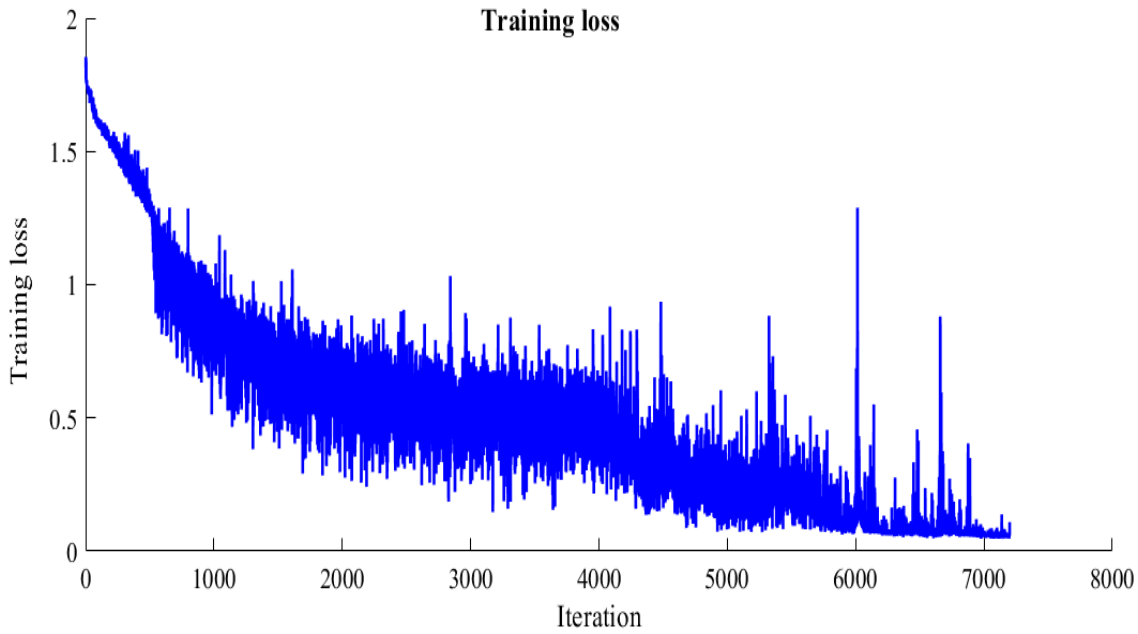

Figure 7.30: Training loss during retraining VGG-16 network for weld seam state prediction.

7.3.7 Result and discussion

The performance of the trained architecture is determined by the good prediction made over the true events. Eight hundred images are considered for testing of the trained architecture. By comparing the predictions made by the architecture over the labelled subset in testing data, the performance of the architecture can be determined as shown in Table 7.8 and Table 7.9. Intersection over Union (IoU), which is the measure of the area of overlap and area of the union, is used as an evaluation metric to measure the accuracy of the trained architecture on a testing dataset. The individual IoU of each class, mean-IoU scores and weighted-IoU scores from Table 7.8 and Table 7.9 suggest satisfactory predictions results. The absorbed true positive, true negative, false positive, false negative of the modified VGG-16 SegNet model on each pixel of the test data set are given in Figure 7.31. The figure shows that there is no misclassification among the four weld seam states.

Table 7.8: High-level overview of the network performance.

Class	Accuracy	IoU
Background	0.98838	0.98821
State-1	0.99855	0.73091
State-2	0.98398	0.75043
State-3	0.99801	0.71128
State-4	0.99858	0.78358

Table 7.9: Weld seam state detection results in using SegNet.

Parameters	Values
Mean accuracy	0.9935
Mean IoU	0.79288
Weighted IoU	0.98006
Global accuracy	0.98861

However, there is noticeable misclassification between the background class and four weld seam states. This mostly occurs when weights are not optimized in the pixel classification layer of the network. Even though we had taken into account of the bias and tendency of the network towards the dominant background using median frequency still the weight has to be further tuned to differentiate between the weld seam states and background.

	Background	State-1	State-2	State-3	State-4
Background	100%	27%	24%	29%	22%
State-1	0%	73%	0%	0%	0%
State-2	0%	0%	76%	0%	0%
State-3	0%	0%	0%	71%	0%
State-4	0%	0%	0%	0%	78%

Figure 7.31: Confusion matrix on the pixel-wise classification of weld seam state prediction.

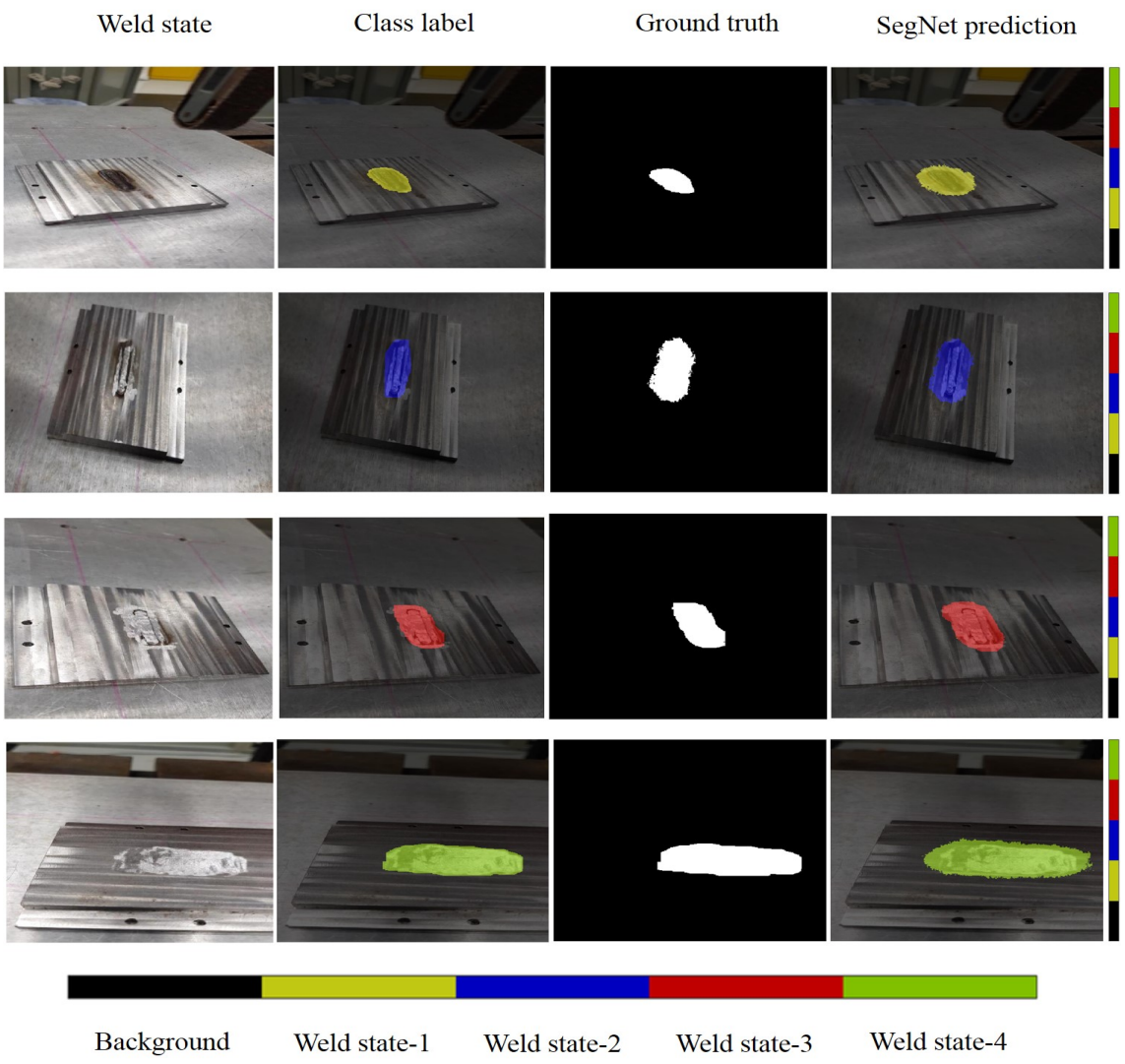

Figure 7.32: Qualitative assessment of SegNet predictions on weld seam states using modified VGG-16 architecture.

Figure 7.32 shows the qualitative evaluation of the performance of the model. Figure 7.32 presents four instances of weld state data with default color code, pixel-wise labels, ground-truth, and network prediction output for visual inspection. The first column shows the input image followed by color-coded labels and ground truth label in column two and three followed by network output in column 4 with corresponding color codes in each pixel of the image.

7.4 Conclusion

In this chapter, the evolution of weld seam geometry at different stages of removal in belt grinding process is identified and analysed. Two techniques for automatic detection of weld seam removal using vision system with the help of deep learning and physical sensors with the help of machine learning classifiers are presented.

- The chapter initially introduces a complementary based sensor integration approach to predict weld seam removal. Transitions in vibration and force signals generated during belt grinding of three different weld seam states are identified. The wavelet features that can possibly correlate weld seam removal states from sensor data is identified and deployed along with the machine learning model based on classification. The classification results demonstrate that the developed diagnostic method is a potential tool to predict removal of weld seam reliably.

- Second part of the chapter introduces a novel method for weld seam removal detection with images taken using DSLR camera and encoder-decoder based semantic segmentation. The encoder-decoder based modified VGG-16 architecture is trained on images obtained from actual belt grinding process on machining stainless steel weld seams. The trained model achieved a competitive segmentation precision on the testing dataset. This methodology based on semantic segmentation gives enough freedom for the operator in terms of tool path planning and can identify weld profile geometry irrespective of varying the grinding parameters.

Chapter 8

Conclusion and recommendations for future work

8.1 Conclusion

This thesis mainly deals with modelling and monitoring of abrasive belt grinding process in dry condition. Conclusions of the experimental observations and results in Chapters 3, 4, 5, 6, and 7 are presented and summarized in this chapter. Suggestions for further study are also discussed in this chapter.

The thesis initially explores the effect of cutting speed, force, polymer wheel hardness and feed on pressure distribution using a dynamic pressure sensor to understand material removal characteristics in Chapter 3. The observations indicate that altering any of the parameters will have a resultant shift in the magnitude of material removed.

From the experimental investigation of ANOVA results derived from Taguchi's L_{27} orthogonal array-based belt grinding trials, it was found that the dominant parameter influencing material removal is grit size parameter. Grit size effect was found to be five times greater than other influential parameters, i.e. RPM and force. ANOVA results with larger S/N suggests that 700 RPM, 10 mm/sec feed rate, 30 N force, 90 Shore A hardness and 60 grit size tend to be the optimal grinding parameters to achieve maximum depth of cut. It was also identified that pressure sensor results and main effects plot trend from ANOVA are similar.

A separate study in Chapter 3 on understanding the effect of cutting speed, force,

polymer wheel hardness, feed, and grit size on surface quality showed that grit size is the only parameter that dictates the surface roughness like any other two-body abrasive machining process.

The material removal models based on soft computing regression techniques were developed in Chapter 4. Six different modelling methodologies, namely multiple linear regression, stepwise regression, ANN, ANFIS, SVR and RF have been applied to data determined using the Taguchi design of experiments. All five models, except for multiple linear regression, demonstrated a relatively low prediction error. It is likely that the proposed regression models can be applied for defining parameter levels for achieving desired material removal without the need to conduct physical belt grinding experiments. Interpreting the results of ANFIS and RF models, it was also found that grit parameter plays a dominant role in the modelling of the belt grinding process.

The significance of abrasive grain wear was studied in Chapter 5 by correlating material removal modes and wear state of the grains. The different material removal modes (cutting, ploughing and rubbing) and their respective occurrence frequency on aluminium 6061 workpiece were identified with single grit scratch experiments using tribometer and Al_2O_3 grains. STFT analysis of AE sensor data extracted while performing scratch tests on aluminium 6061 proved that the frequency ranges occurring at 125-350 kHz corresponds to cutting and 25-125 kHz corresponds to ploughing and rubbing.

Evaluating the energy content of the dominant frequencies in the actual belt grinding process using AE data showed that cutting occurs dominantly on the interaction of the material surface with new grains and gradually becomes a non-existent mode as the grain wears. It also suggested that the material removal modes are correlated to abrasive grain wear.

Having understood the evolution of the abrasive grain degradation in the belt tool with process time from Chapter 5, an in-process abrasive belt wear monitoring system based on classification were developed and discussed in Chapter 6. Predicting tool life in real time for coated abrasives not only helps to optimise the utilisation of the tool's life cycle, but also secures the surface quality of finished components.

A complementary based sensor integration approach was successfully developed

using accelerometer, AE, and force sensor to predict tool wear for belt tool. Required pre-processing and signal processing was established for getting time and frequency domain features by appropriate use of hardware, off-line filtering techniques etc. The subset feature that can correlate to tool wear was identified using GA. The k-Nearest Neighbour (k-NN), was used as the fitness function for the GA. The subset features extracted were used to train five different classification algorithms in MATLAB. Performance testing results showed that SVM based in-process tool condition monitoring model has high accuracy rate for predicting the belt states.

Finally, Chapter 7 proposes two novel approaches for in-process endpoint detection of weld seam removal during robotic abrasive belt grinding process using physical and vision-based sensors. The first approach involves developing a virtual inspecting system using force sensor, accelerometer sensor, and machine learning algorithm. The wavelet decomposition coefficient was used to represent all possible types of transients in vibration and force signals generated during grinding over the weld seam. The "Daubechies-4" wavelet function was used to extract features from the sensor data that represented different weld states. The SVM based classifier predicted the weld state more accurately compared to other classifiers considered.

The second approach demonstrates a technique for automatic endpoint detection of weld seam removal with the help of deep learning and vision system. An experimental investigation using images from four different weld seam states were trained using VGG-16 network based on encoder-decoder architecture. The results demonstrate that the second approach can be considered as a promising tool for predicting weld seam removal in real time compared to the first approach as it does not have tool path and grinding condition constraints.

8.2 Future work

Based on this study, the author suggests following further research topics for benefiting industrial needs.

1. This study was attempted to establish a relationship between five input parameters in abrasive belt grinding on material removal. The understanding can be further improved by associating more parameters that were not con-

sidered in the study. Some of them could be grit composition, serration in rubber, workpiece material hardness, geometry of the wheel, number of passes etc. The study was conducted for aluminium, while the magnitude in the influence of process variables may vary for other materials. A comparative study of the various material such as titanium, steel alloys and most importantly composites which are widely used in industries is required, to define the abrasive belt grinding process completely.

2. Most of the experiments performed for parameter analysis were done in flat workpiece. It is vital to understand the effect of parameters/ variables during grinding intricate shapes.

3. ANOVA results show that grit parameter significantly affects the depth of cut. A study on achieving grinding performance compensation in case of grain degradation using other parameter has to be conducted.

4. Successful implementation of regression models for material removal requires the contact between work coupon and grinding wheel to be normal. As a result, it is also important to establish a tool path planning model especially for the components with intricate shapes.

5. Understanding the cutting, ploughing and rubbing phenomenon along with corresponding frequency components in harder materials, such as titanium, mild steel etc., using single grit scratch experiments is also essential.

6. Although a real time belt wear monitoring system has been established, it is important to note that there are areas such as feature selection, model parameter selection and sensor location, which require further optimisation to realise conclusive belt wear monitoring system.

7. Tool wear and material removal modelling had been explored using conventional machine learning algorithms in this thesis. Alternatively, deep learning algorithms could also be explored to model and monitor the process.

8. The performance of proposed SegNet network in inspecting weld seam removal can be further improved by localising the work coupon from the background

and feeding the region of interest into the encoder-decoder network to narrow down the search region. It will be a much faster and efficient architecture to facilitate a real-time predicting of weld seam removal.

9. The whole work performed in this thesis on modelling and monitoring of the belt grinding process was in dry condition, i.e. without lubrication, and it is essential to note the performance of belt grinding parameters and sensor signals in wet conditions.

References

[1] T. Kubela, A. Pochyly, and V. Singule, "Assessment of industrial robots accuracy in relation to accuracy improvement in machining processes," 2016.

[2] S. Ferrada Ibacache and H. Omeragic, "Optimizing a production line of packaging material by the use of discrete-event simulation," 2010.

[3] S. Kalpakjian, S. R. Schmid, and K. V. Sekar, *Manufacturing, Engineering and Technology*. Pearson, 2014.

[4] E. P. DeGarmo, J. T. Black, R. A. Kohser, and B. E. Klamecki, *Materials and process in manufacturing*. Prentice Hall Upper Saddle River, 1997.

[5] P. Seyfried, H. Kunzmann, P. McKeown, and M. Weck, *Progress in Precision Engineering. [electronic resource] : Proceedings of the 6th International Precision Engineering Seminar (IPES 6)/2nd International Conference on Ultraprecision in Manufacturing Engineering (UME 2), May, 1991 Braunschweig, Germany*. Berlin, Heidelberg : Springer Berlin Heidelberg, 1991., 1991.

[6] J. F. G. Oliveira, E. J. Silva, C. Guo, and F. Hashimoto, "Industrial challenges in grinding," *CIRP Annals - Manufacturing Technology*, vol. 58, no. 2, pp. 663–680, 2009.

[7] M. J. Jackson and J. P. Davim, *Machining with abrasives*. Springer, 2011.

[8] M. Moore, "A review of two-body abrasive wear," *Wear*, vol. 27, no. 1, pp. 1–17, 1974.

[9] S. Kalpakjian and S. Schmid, *Manufacturing Processes for Engineering Materials*. Prentice Hall, 2003.

[10] A. P. S. Arunachalam, S. Idapalapati, and S. Subbiah, "Multi-criteria decision making techniques for compliant polishing tool selection," *The International Journal of Advanced Manufacturing Technology*, vol. 79, no. 1-4, pp. 519–530, 2015.

[11] X. Zhang, B. Kuhlenkötter, and K. Kneupner, "An efficient method for solving the signorini problem in the simulation of free-form surfaces produced by belt grinding," *International Journal of Machine Tools and Manufacture*, vol. 45, no. 6, pp. 641–648, 2005.

[12] A. Khellouki, J. Rech, and H. Zahouani, "The effect of abrasive grain's wear and contact conditions on surface texture in belt finishing," *Wear*, vol. 263, no. 1, pp. 81–87, 2007.

[13] A. Khellouki, J. Rech, and H. Zahouani, "The effect of abrasive grain's wear and contact conditions on surface texture in belt finishing," *Wear*, vol. 263, no. 1-6, pp. 81–87, 2007.

[14] I. D. Marinescu, W. B. Rowe, B. Dimitrov, and I. Inaski, *Tribology of abrasive machining processes*. Elsevier, 2004.

[15] S. Wang and C. Li, "Application and development of high-efficiency abrasive process," *International Journal of Advanced Science and Technology*, vol. 47, no. 10, pp. 51–64, 2012.

[16] X. Ren, M. Cabaravdic, X. Zhang, and B. Kuhlenkötter, "A local process model for simulation of robotic belt grinding," *International Journal of Machine Tools and Manufacture*, vol. 47, no. 6, pp. 962–970, 2007.

[17] ticienne.com, 'Polishing of Turbine Blades', 1999. [Online]. Available: http://www.ticienne.com/EN/lucidatura.html. [Accessed: 09-July-2018].

[18] M. Awhale, N. Chinchkar, V. Gunjawate, N. Phule, and Amrute, "Surface belt grinder for keys-a review," *International Journal of Recent Research in Civil and Mechanical Engineering (IJRRCME)*, vol. Vol. 2,, no. Issue 2,, pp. pp: (56–59), October 2015.

[19] S. Mezghani, M. El Mansori, and H. Zahouani, "New criterion of grain size choice for optimal surface texture and tolerance in belt finishing production," *Wear*, vol. 266, no. 5, pp. 578–580, 2009.

[20] K. Rajurkar, J. Kozak, and A. Chatterjee, *Civil Engineering Handbook - Corrosion Resistance*. 2016.

[21] H. Tschatsch, *Applied Machining Technology*. Berlin, Heidelberg : Springer-Verlag Berlin Heidelberg., 2009.

[22] J. Griffin, "Pattern recognition of micro and macro grinding phenomenon with a generic strategy to machine process monitoring," 2008.

[23] X. Ren and B. Kuhlenkötter, "Real-time simulation and visualization of robotic belt grinding processes," *The International Journal of Advanced Manufacturing Technology*, vol. 35, no. 11-12, pp. 1090–1099, 2006.

[24] 3M. '3M Abrasive Belts for Metalworking.' 2019. [Online]. Available: www.3m.com/3M/en-US/metalworking-us/featured-products/cubitronII. [Accessed: 08-January-2019].

[25] Robowork. 'ACF-Active Contact Flange.' 2019. [Online]. Available: www.robowork.pt/en/products-accessories/ferrobotics-/acf-active-contact-flange. [Accessed: 08-January-2019].

[26] C. H. Li, Z. Fang, and H. Y. Zhao, "Investigation of high-efficiency abrasive finishing," in *2010 International Conference on E-Business and E-Government*, pp. 2716–2719.

[27] X. Zhang, M. Cabaravdic, K. Kneupner, and B. Kuhlenkötter, *Real-Time Simulation of Robot Controlled Belt Grinding Processes of Sculptured Surfaces*, vol. 1. 2004.

[28] W. Konig, H. K. Tonshoff, J. Fromlowitz, and P. Dennis, "Belt grinding," *CIRP Annals*, vol. 35, no. 2, pp. 487–494, 1986.

[29] V. Pandiyan, W. Caesarendra, T. Tjahjowidodo, and H. H. Tan, "In-process tool condition monitoring in compliant abrasive belt grinding process using

support vector machine and genetic algorithm," *Journal of Manufacturing Processes*, vol. 31, pp. 199–213, 2018.

[30] J. Bak, "High speed abrasive belt grinding," report, DTIC Document, 1989.

[31] S. Malkin and C. Guo, *Grinding technology : theory and applications of machining with abrasives*. New York : Industrial Press, 2008., 2nd ed. ed., 2008.

[32] H. Huang, Z. Gong, X. Chen, and L. Zhou, "Robotic grinding and polishing for turbine-vane overhaul," *Journal of materials processing technology*, vol. 127, no. 2, pp. 140–145, 2002.

[33] M. Jackson and J. Davim, *Machining with Abrasives*. Springer US, 2010.

[34] F. M. F. d. A. Varasquim, M. C. d. S. Alves, M. T. T. Gonçalves, L. F. F. Santiago, and A. J. D. d. Souza, "Influence of belt speed, grit sizes and pressure on the sanding of eucalyptus grandis wood," *Cerne*, vol. 18, no. 2, pp. 231–237, 2012.

[35] Y. Sun, T. T. Vu, Z. Halil, and S. H. Yeo, "Pressure distribution of serrated contact wheels—experimental and numerical analysis," *The International Journal of Advanced Manufacturing Technology*, vol. 90, no. 9, pp. 3407–3419, 2017.

[36] Y. Wang, B. Hou, F. Wang, and Z. Ji, "A controllable material removal strategy considering force-geometry model of belt grinding processes," *The International Journal of Advanced Manufacturing Technology*, vol. 93, no. 1, pp. 241–251, 2017.

[37] X. Zhang, K. Kneupner, and B. Kuhlenkötter, "A new force distribution calculation model for high-quality production processes," *The International Journal of Advanced Manufacturing Technology*, vol. 27, no. 7-8, pp. 726–732, 2006.

[38] X. Ren, B. Kuhlenkötter, and H. Müller, "Simulation and verification of belt grinding with industrial robots," *International Journal of Machine Tools and Manufacture*, vol. 46, no. 7, pp. 708–716, 2006.

[39] X. Ren and B. Kuhlenkötter, "Real-time simulation and visualization of robotic belt grinding processes," *The International Journal of Advanced Manufacturing Technology*, vol. 35, no. 11, pp. 1090–1099, 2008.

[40] S. Wu, K. Kazerounian, Z. Gan, and Y. Sun, "A simulation platform for optimal selection of robotic belt grinding system parameters," *The International Journal of Advanced Manufacturing Technology*, vol. 64, no. 1, pp. 447–458, 2013.

[41] A. Jourani, M. Dursapt, H. Hamdi, J. Rech, and H. Zahouani, "Effect of the belt grinding on the surface texture: modeling of the contact and abrasive wear," *Wear*, vol. 259, no. 7, pp. 1137–1143, 2005.

[42] S. Mezghani, M. E. Mansori, and H. Zahouani, "New criterion of grain size choice for optimal surface texture and tolerance in belt finishing production," *Wear*, vol. 266, no. 5–6, pp. 578–580, 2009.

[43] J. Shibata, I. Inasaki, and S. Yonetsu, "The relation between the wear of grain cutting edges and their metal removal ability in coated abrasive belt grinding," *Wear*, vol. 55, no. 2, pp. 331–344, 1979.

[44] V. T. Thien, Z. B. A. Halil, S. Yajuan, Y. S. Hock, and A. Wee, "Surface finishing: Experimental study of pressure distribution by compliant contact wheels," in *Proceedings of the 3rd International Conference on Mechatronics and Robotics Engineering*, pp. 88–94, ACM, 2017.

[45] Y. Sun, T. Vu, and S. Yeo, "Study of pressure distribution in compliant contact wheels for robotic surface finishing," *MATEC Web of Conferences*, vol. 42, p. 03007, 2016.

[46] H. Lv, Y. Song, P. Jia, Z. Gan, and L. Qi, "An adaptive modeling approach based on esn for robotic belt grinding," in *The 2010 IEEE International Conference on Information and Automation*, pp. 787–792.

[47] W. Wang, F. Liu, Z. Liu, and C. Yun, "Prediction of depth of cut for robotic belt grinding," *The International Journal of Advanced Manufacturing Technology*, vol. 91, no. 1, pp. 699–708, 2017.

[48] Y. Sun, T. T. Vu, Z. Halil, S. H. Yeo, and A. Wee, "Material removal prediction for contact wheels based on a dynamic pressure sensor," *The International Journal of Advanced Manufacturing Technology*, vol. 93, no. 1, pp. 945–951, 2017.

[49] Y. J. Wang, Y. Huang, Y. X. Chen, and Z. S. Yang, "Model of an abrasive belt grinding surface removal contour and its application," *The International Journal of Advanced Manufacturing Technology*, vol. 82, no. 9, pp. 2113–2122, 2016.

[50] G. Hamann, *Modellierung des abtragsverhaltens elastischer robotergefuehrter schleifwerkzeuge*. Thesis, 1998.

[51] Y. Q. Wang, B. Hou, H. B. Liu, and F. B. Wang, "Propeller material belt grinding parameters optimisation using taguchi technique," *International Journal of Industrial and Systems Engineering*, vol. 25, no. 1, pp. 1–13, 2017.

[52] M. Schinhaerl, G. Smith, R. Stamp, R. Rascher, L. Smith, E. Pitschke, P. Sperber, and A. Geiss, "Mathematical modelling of influence functions in computer-controlled polishing: Part ii," *Applied Mathematical Modelling*, vol. 32, no. 12, pp. 2907–2924, 2008.

[53] K. H. Z. Gahr, "Formation of wear debris by the abrasion of ductile metals," *Wear*, vol. 74, no. 2, pp. 353–373, 1981.

[54] K. H. Z. Gahr, "Modelling of two-body abrasive wear," *Wear*, vol. 124, no. 1, pp. 87–103, 1988.

[55] Z. B. Hou and R. Komanduri, "On the mechanics of the grinding process – part i. stochastic nature of the grinding process," *International Journal of Machine Tools and Manufacture*, vol. 43, no. 15, pp. 1579–1593, 2003.

[56] J. Griffin, *Pattern recognition of micro and macro grinding phenomenon with a generic strategy to machine process monitoring*. Thesis, 2008.

[57] S. Mezghani, M. El Mansori, and E. Sura, "Wear mechanism maps for the belt finishing of steel and cast iron," *Wear*, vol. 267, no. 1–4, pp. 86–91, 2009.

[58] K. H. T. Kayaba and K. Kato, "Analysis of the abrasive wear mechanism by successive observations of wear processes in a scanning electron microscope," vol. 110, pp. 419–430, 1986.

[59] D. E. Dimla, "Sensor signals for tool-wear monitoring in metal cutting operations—a review of methods," *International Journal of Machine Tools and Manufacture*, vol. 40, no. 8, pp. 1073–1098, 2000.

[60] L. P. Heck, "Signal processing research in automatic tool wear monitoring," in *1993 IEEE International Conference on Acoustics, Speech, and Signal Processing*, vol. 1, pp. 55–58 vol.1.

[61] F. Girardin, D. Rémond, and J.-F. Rigal, "A new method for detecting tool wear and breakage in milling," *International Journal of Material Forming*, vol. 3, no. 1, pp. 463–466, 2010.

[62] S. Kurada and C. Bradley, "A review of machine vision sensors for tool condition monitoring," *Computers in Industry*, vol. 34, no. 1, pp. 55–72, 1997.

[63] J. G. Chow and P. K. Wright, "On-line estimation of tool/chip interface temperatures for a turning operation," *Journal of Engineering for Industry*, vol. 110, no. 1, pp. 56–64, 1988.

[64] S. Lin and C. Ting, "Tool wear monitoring in drilling using force signals," *Wear*, vol. 180, no. 1, pp. 53–60, 1995.

[65] S. Choudhury and S. Rath, "In-process tool wear estimation in milling using cutting force model," *Journal of Materials Processing Technology*, vol. 99, no. 1, pp. 113–119, 2000.

[66] H. Ravindra, Y. Srinivasa, and R. Krishnamurthy, "Acoustic emission for tool condition monitoring in metal cutting," *Wear*, vol. 212, no. 1, pp. 78–84, 1997.

[67] N. Ghosh, Y. Ravi, A. Patra, S. Mukhopadhyay, S. Paul, A. Mohanty, and A. Chattopadhyay, "Estimation of tool wear during cnc milling using neural network-based sensor fusion," *Mechanical Systems and Signal Processing*, vol. 21, no. 1, pp. 466–479, 2007.

[68] S. Kakade, L. Vijayaraghavan, and R. Krishnamurthy, "In-process tool wear and chip-form monitoring in face milling operation using acoustic emission," *Journal of Materials Processing Technology*, vol. 44, no. 3, pp. 207–214, 1994.

[69] S. C. Lin and R. J. Yang, "Force-based model for tool wear monitoring in face milling," *International Journal of Machine Tools and Manufacture*, vol. 35, no. 9, pp. 1201–1211, 1995.

[70] S.-L. Chen and Y. W. Jen, "Data fusion neural network for tool condition monitoring in cnc milling machining," *International Journal of Machine Tools and Manufacture*, vol. 40, no. 3, pp. 381–400, 2000.

[71] N. Ghosh, Y. B. Ravi, A. Patra, S. Mukhopadhyay, S. Paul, A. R. Mohanty, and A. B. Chattopadhyay, "Estimation of tool wear during cnc milling using neural network-based sensor fusion," *Mechanical Systems and Signal Processing*, vol. 21, no. 1, pp. 466–479, 2007.

[72] M. Malekian, S. S. Park, and M. B. G. Jun, "Tool wear monitoring of micro-milling operations," *Journal of Materials Processing Technology*, vol. 209, no. 10, pp. 4903–4914, 2009.

[73] J. H. Zhou, C. K. Pang, Z. W. Zhong, and F. L. Lewis, "Tool wear monitoring using acoustic emissions by dominant-feature identification," *IEEE Transactions on Instrumentation and Measurement*, vol. 60, no. 2, pp. 547–559, 2011.

[74] B. Cuka and D.-W. Kim, "Fuzzy logic based tool condition monitoring for end-milling," *Robotics and Computer-Integrated Manufacturing*, vol. 47, pp. 22–36, 2017.

[75] D. Wu, C. Jennings, J. Terpenny, R. X. Gao, and S. Kumara, "A comparative study on machine learning algorithms for smart manufacturing: Tool wear prediction using random forests," *Journal of Manufacturing Science and Engineering*, vol. 139, no. 7, pp. 071018–071018–9, 2017.

[76] D. E. Dimla and P. M. Lister, "On-line metal cutting tool condition monitoring," *International Journal of Machine Tools and Manufacture*, vol. 40, no. 5, pp. 739–768, 2000.

[77] F. J. Alonso and D. R. Salgado, "Analysis of the structure of vibration signals for tool wear detection," *Mechanical Systems and Signal Processing*, vol. 22, no. 3, pp. 735–748, 2008.

[78] A. Ghasempoor, J. Jeswiet, and T. N. Moore, "Real time implementation of on-line tool condition monitoring in turning," *International Journal of Machine Tools and Manufacture*, vol. 39, no. 12, pp. 1883–1902, 1999.

[79] L. Wang, M. G. Mehrabi, and J. E. Kannatey-Asibu, "Hidden markov model-based tool wear monitoring in turning," *Journal of Manufacturing Science and Engineering*, vol. 124, no. 3, pp. 651–658, 2002.

[80] A. Gajate, R. Haber, R. del Toro, P. Vega, and A. Bustillo, "Tool wear monitoring using neuro-fuzzy techniques: a comparative study in a turning process," *Journal of Intelligent Manufacturing*, vol. 23, no. 3, pp. 869–882, 2012.

[81] S. C. Lin and C. J. Ting, "Tool wear monitoring in drilling using force signals," *Wear*, vol. 180, no. 1, pp. 53–60, 1995.

[82] X. Li, S. Dong, and P. K. Venuvinod, "Hybrid learning for tool wear monitoring," *The International Journal of Advanced Manufacturing Technology*, vol. 16, no. 5, pp. 303–307, 2000.

[83] H. M. Ertunc, K. A. Loparo, and H. Ocak, "Tool wear condition monitoring in drilling operations using hidden markov models (hmms)," *International Journal of Machine Tools and Manufacture*, vol. 41, no. 9, pp. 1363–1384, 2001.

[84] C. Sanjay, M. L. Neema, and C. W. Chin, "Modeling of tool wear in drilling by statistical analysis and artificial neural network," *Journal of Materials Processing Technology*, vol. 170, no. 3, pp. 494–500, 2005.

[85] D. Shi and N. N. Gindy, "Tool wear predictive model based on least squares support vector machines," *Mechanical Systems and Signal Processing*, vol. 21, no. 4, pp. 1799–1814, 2007.

[86] E. Brinksmeier and F. Werner, "Monitoring of grinding wheel wear," *CIRP Annals - Manufacturing Technology*, vol. 41, no. 1, pp. 373–376, 1992.

[87] P. Lezanski, "An intelligent system for grinding wheel condition monitoring," *Journal of Materials Processing Technology*, vol. 109, no. 3, pp. 258–263, 2001.

[88] T. Warren Liao, C.-F. Ting, J. Qu, and P. J. Blau, "A wavelet-based methodology for grinding wheel condition monitoring," *International Journal of Machine Tools and Manufacture*, vol. 47, no. 3, pp. 580–592, 2007.

[89] L. Wang, M. G. Mehrabi, and E. Kannatey-Asibu, "Hidden markov model-based tool wear monitoring in turning," *Journal of Manufacturing Science and Engineering*, vol. 124, no. 3, pp. 651–658, 2002.

[90] L. Dan and J. Mathew, "Tool wear and failure monitoring techniques for turning—a review," *International Journal of Machine Tools and Manufacture*, vol. 30, no. 4, pp. 579–598, 1990.

[91] X. Li, "A brief review: acoustic emission method for tool wear monitoring during turning," *International Journal of Machine Tools and Manufacture*, vol. 42, no. 2, pp. 157–165, 2002.

[92] D. E. Dimla and P. M. Lister, "On-line metal cutting tool condition monitoring.: I: force and vibration analyses," *International Journal of Machine Tools and Manufacture*, vol. 40, no. 5, pp. 739–768, 2000.

[93] N. H. Cook, "Tool wear sensors," *Wear*, vol. 62, no. 1, pp. 49–57, 1980.

[94] A. Villa, G. Quaglia, R. Chiara, G. Rutelli, and R. Levi, "An expert control system for tool life management in flexible manufacturing cells," *CIRP Annals*, vol. 34, no. 1, pp. 87–90, 1985.

[95] J. V. Abellan-Nebot and F. Romero Subirón, "A review of machining monitoring systems based on artificial intelligence process models," *The International Journal of Advanced Manufacturing Technology*, vol. 47, no. 1, pp. 237–257, 2010.

[96] K. Wegener, H. W. Hoffmeister, B. Karpuschewski, F. Kuster, W. C. Hahmann, and M. Rabiey, "Conditioning and monitoring of grinding wheels," *CIRP Annals*, vol. 60, no. 2, pp. 757–777, 2011.

[97] B. Varghese, S. Pathare, R. Gao, C. Guo, and S. Malkin, "Development of a sensor-integrated "intelligent" grinding wheel for in-process monitoring," *CIRP Annals*, vol. 49, no. 1, pp. 231–234, 2000.

[98] Z. Yang and Z. Yu, "Grinding wheel wear monitoring based on wavelet analysis and support vector machine," *The International Journal of Advanced Manufacturing Technology*, vol. 62, no. 1, pp. 107–121, 2012.

[99] B. Karpuschewski, M. Wehmeier, and I. Inasaki, "Grinding monitoring system based on power and acoustic emission sensors," *CIRP Annals*, vol. 49, no. 1, pp. 235–240, 2000.

[100] A. Hassui, A. E. Diniz, J. F. G. Oliveira, J. Felipe, and J. J. F. Gomes, "Experimental evaluation on grinding wheel wear through vibration and acoustic emission," *Wear*, vol. 217, no. 1, pp. 7–14, 1998.

[101] M. J. Jackson and M. P. Hitchiner, *Abrasive Tools and Bonding Systems*, pp. 1–77. Boston, MA: Springer US, 2011.

[102] P. Balakrishnan, H. Trabelsy, E. Kannatey-Asibu, and E. Emel, "A sensor fusion approach to cutting tool monitoring," in *Proc. 15th NSF Conf. on Production Research and Technology, SME, University of California, Berkeley*, p. 101.

[103] J.-S. Kwak and M.-K. Ha, "Detection of dressing time using the grinding force signal based on the discrete wavelet decomposition," *The International Journal of Advanced Manufacturing Technology*, vol. 23, no. 1, pp. 87–92, 2004.

[104] A. Hosokawa, K. Mashimo, K. Yamada, and T. Ueda, "Evaluation of grinding wheel surface by means of grinding sound discrimination," *JSME International Journal Series C Mechanical Systems, Machine Elements and Manufacturing*, vol. 47, no. 1, pp. 52–58, 2004.

[105] D. Lipinski, W. Kacalak, and R. Tomkowski, "Methodology of evaluation of abrasive tool wear with the use of laser scanning microscopy," *Scanning*, vol. 36, no. 1, pp. 53–63, 2013.

[106] W. Wang, F. Salvatore, J. Rech, and J. Li, "Investigating effects of adhesion wear on cutting efficiency and energy cost in dry belt finishing," *The International Journal of Advanced Manufacturing Technology*, 2017.

[107] A. Khellouki, H. Maiz, J. Rech, and H. Zahouani, "Application de la méthode des plans d'expériences à la caractérisation du procédé de toilage de superfinition," in *Integrated Desing and Production, 4th International Conference, Casablanca, Maroc.*

[108] S. K. V. Pramod Kumar N, Avinash N V and U. K. S, "Thermal and tool wear studies on mild steel turning," vol. 1, no. 5, pp. 477–486, 2014.

[109] T. Vorburger, N. Orji, L. Sung, and T. Rodriguez, "Surface finish and subsurface metrology," in *V-SEMETRA-Fifth Aerospace Metrology Seminar, São Jose dos Campos, Brazil, July*, pp. 21–24.

[110] M. Conroy and J. Armstrong, "A comparison of surface metrology techniques," in *Journal of Physics: Conference Series*, vol. 13, p. 458, IOP Publishing.

[111] B. Bhushan, *Modern Tribology Handbook, Two Volume Set.* Crc Press, 2000.

[112] J. M. Bennett, M. M. Tehrani, J. Jahanmir, J. C. Podlesny, and T. L. Balter, "Topographic measurements of supersmooth dielectric films made with a mechanical profiler and a scanning force microscope," *Applied optics*, vol. 34, no. 1, pp. 209–212, 1995.

[113] T. V. Vorburger, H.-G. Rhee, T. B. Renegar, J.-F. Song, and A. Zheng, "Comparison of optical and stylus methods for measurement of surface texture," *The International Journal of Advanced Manufacturing Technology*, vol. 33, no. 1-2, pp. 110–118, 2007.

[114] H. Shinno, H. Hashizume, and H. Sato, "In-process monitoring method for machining environment based on simultaneous multiphenomena sensing," *CIRP Annals - Manufacturing Technology*, vol. 46, no. 1, pp. 53–56, 1997.

[115] D. Dornfeld A, "In process recognition of cutting states," *JSME international journal. Ser. C, Dynamics, control, robotics, design and manufacturing*, vol. 37, no. 4, pp. 638–650, 1994.

[116] R. C. Luo and M. G. Kay, "A tutorial on multisensor integration and fusion," in *Industrial Electronics Society, 1990. IECON'90., 16th Annual Conference of IEEE*, pp. 707–722, IEEE.

[117] R. Teti and S. R. T. Kumara, "Intelligent computing methods for manufacturing systems," *CIRP Annals*, vol. 46, no. 2, pp. 629–652, 1997.

[118] A. Thangaraj and P. K. Wright, "Drill wear sensing and failure prediction for untended machining," *Robotics and Computer-Integrated Manufacturing*, vol. 4, no. 3–4, pp. 429–435, 1988.

[119] D.-W. Cho, S. J. Lee, and C. N. Chu, "The state of machining process monitoring research in korea," *International Journal of Machine Tools and Manufacture*, vol. 39, no. 11, pp. 1697–1715, 1999.

[120] J. Tlusty and G. Andrews, "A critical review of sensors for unmanned machining," *CIRP Annals-Manufacturing Technology*, vol. 32, no. 2, pp. 563–572, 1983.

[121] P. Bhattacharyya, D. Sengupta, and S. Mukhopadhyay, "Cutting force-based real-time estimation of tool wear in face milling using a combination of signal processing techniques," *Mechanical Systems and Signal Processing*, vol. 21, no. 6, pp. 2665–2683, 2007.

[122] D. K. Baek, T. J. Ko, and H. S. Kim, "Real time monitoring of tool breakage in a milling operation using a digital signal processor," *Journal of Materials Processing Technology*, vol. 100, no. 1, pp. 266–272, 2000.

[123] J. Dong, K. V. R. Subrahmanyam, Y. S. Wong, G. S. Hong, and A. R. Mohanty, "Bayesian-inference-based neural networks for tool wear estimation," *The International Journal of Advanced Manufacturing Technology*, vol. 30, no. 9, pp. 797–807, 2006.

[124] Y. M. Ertekin, Y. Kwon, and T.-L. Tseng, "Identification of common sensory features for the control of cnc milling operations under varying cutting conditions," *International Journal of Machine Tools and Manufacture*, vol. 43, no. 9, pp. 897–904, 2003.

[125] D. Y. Jang, Y.-G. Choi, H.-G. Kim, and A. Hsiao, "Study of the correlation between surface roughness and cutting vibrations to develop an on-line roughness measuring technique in hard turning," *International Journal of Machine Tools and Manufacture*, vol. 36, no. 4, pp. 453–464, 1996.

[126] P. Eisele and R. Griffin, "Some vibration effects on surfaces produced by turret lathes," ASME.

[127] S. Lin and M. Chang, "A study on the effects of vibrations on the surface finish using a surface topography simulation model for turning," *International Journal of Machine Tools and Manufacture*, vol. 38, no. 7, pp. 763–782, 1998.

[128] D. A. Dornfeld, Y. Lee, and A. Chang, "Monitoring of ultraprecision machining processes," *The International Journal of Advanced Manufacturing Technology*, vol. 21, no. 8, pp. 571–578, 2003.

[129] D. A. Dornfeld, *Acoustic Emission Monitoring and Analysis in Manufacturing: Presented at the Winter Annual Meeting of the American Society of Mechanical Engineers, New Orleans, Louisiana, December 9-14, 1984*, vol. 14. The Society, 1984.

[130] Z. Yuchen, P. Orban, and S. Nikumb, "Sensors for intelligent machining-a research and application survey," in *1995 IEEE International Conference on Systems, Man and Cybernetics. Intelligent Systems for the 21st Century*, vol. 2, pp. 1005–1010 vol.2.

[131] W. L. Weingaertner and A. Boaron, "Contact recognition between grinding wheel and workpiece," in *20 th International Congress of Mechanical Engineering, Gramado-RS, Brazil*.

[132] T. Hwang, E. P. Whitenton, N. N. Hsu, G. V. Blessing, and C. Evans, "Acoustic emission monitoring of high speed grinding of silicon nitride," *Ultrasonics*, vol. 38, no. 1, pp. 614–619, 2000.

[133] R. C. Asher, *Ultrasonic Sensors for chemical and process plant*. Taylor & Francis, 1997.

[134] D. Dornfeld and J. B. Liu, "Abrasive texturing and burnishing process monitoring using acoustic emission," *CIRP Annals-Manufacturing Technology*, vol. 42, no. 1, pp. 397–400, 1993.

[135] D. Dornfeld, "Application of acoustic emission techniques in manufacturing," *NDT & E International*, vol. 25, no. 6, pp. 259–269, 1992.

[136] A. Diniz, J. Liu, and D. Dornfeld, "Correlating tool life, tool wear and surface roughness by monitoring acoustic emission in finish turning," *Wear*, vol. 152, no. 2, pp. 395–407, 1992.

[137] B. Karpuschewski, *Sensoren zur Prozessüberwachung beim Spanen.* VDI-Verlag, 2001.

[138] P. Benardos and G.-C. Vosniakos, "Predicting surface roughness in machining: a review," *International journal of machine tools and manufacture*, vol. 43, no. 8, pp. 833–844, 2003.

[139] J. Chen and B. Huang, "An in-process neural network-based surface roughness prediction (inn-srp) system using a dynamometer in end milling operations," *The International journal of Advanced Manufacturing Technology*, vol. 21, no. 5, pp. 339–347, 2003.

[140] K. Risbood, U. Dixit, and A. Sahasrabudhe, "Prediction of surface roughness and dimensional deviation by measuring cutting forces and vibrations in turning process," *Journal of Materials Processing Technology*, vol. 132, no. 1, pp. 203–214, 2003.

[141] M. Selvam, "Tool vibration and its influence on surface roughness in turning," *Wear*, vol. 35, no. 1, pp. 149–157, 1975.

[142] Y.-H. Tsai, J. C. Chen, and S.-J. Lou, "An in-process surface recognition system based on neural networks in end milling cutting operations," *International Journal of Machine Tools and Manufacture*, vol. 39, no. 4, pp. 583–605, 1999.

[143] O. Abouelatta and J. Madl, "Surface roughness prediction based on cutting parameters and tool vibrations in turning operations," *Journal of materials processing technology*, vol. 118, no. 1, pp. 269–277, 2001.

[144] N. R. Abburi and U. S. Dixit, "A knowledge-based system for the prediction of surface roughness in turning process," *Robotics and Computer-Integrated Manufacturing*, vol. 22, no. 4, pp. 363–372, 2006.

[145] A. Hassui and A. E. Diniz, "Correlating surface roughness and vibration on plunge cylindrical grinding of steel," *International Journal of Machine Tools and Manufacture*, vol. 43, no. 8, pp. 855–862, 2003.

[146] E. N. Diei and D. A. Dornfeld, "Acoustic emission sensing of tool wear in face milling," *Journal of Engineering for Industry*, vol. 109, no. 3, pp. 234–240, 1987.

[147] I. Marinescu and D. A. Axinte, "A critical analysis of effectiveness of acoustic emission signals to detect tool and workpiece malfunctions in milling operations," *International Journal of Machine Tools and Manufacture*, vol. 48, no. 10, pp. 1148–1160, 2008.

[148] I. Marinescu and D. Axinte, "A time–frequency acoustic emission-based monitoring technique to identify workpiece surface malfunctions in milling with multiple teeth cutting simultaneously," *International Journal of Machine Tools and Manufacture*, vol. 49, no. 1, pp. 53–65, 2009.

[149] A. E. Diniz, J. J. Liu, and D. A. Dornfeld, "Correlating tool life, tool wear and surface roughness by monitoring acoustic emission in finish turning," *Wear*, vol. 152, no. 2, pp. 395–407, 1992.

[150] H. K. Tonshoff, M. Jung, S. Männel, and W. Rietz, "Using acoustic emission signals for monitoring of production processes," *Ultrasonics*, vol. 37, no. 10, pp. 681–686, 2000.

[151] C. Beggan, M. Woulfe, P. Young, and G. Byrne, "Using acoustic emission to predict surface quality," *The International Journal of Advanced Manufacturing Technology*, vol. 15, no. 10, pp. 737–742, 1999.

[152] W. Hundt, D. Leuenberger, F. Rehsteiner, and P. Gygax, "An approach to monitoring of the grinding process using acoustic emission (ae) technique," *CIRP Annals*, vol. 43, no. 1, pp. 295–298, 1994.

[153] J. Webster, I. Marinescu, R. Bennett, and R. Lindsay, "Acoustic emission for process control and monitoring of surface integrity during grinding," *CIRP Annals*, vol. 43, no. 1, pp. 299–304, 1994.

[154] G. Mauris, E. Benoit, and L. Foulloy, *Fuzzy linguistic methods for the aggregation of complementary sensor information*, pp. 214–230. Springer, 1998.

[155] D. Dornfeld, Y. Lee, and A. Chang, "Monitoring of ultraprecision machining processes," *The International Journal of Advanced Manufacturing Technology*, vol. 21, no. 8, pp. 571–578, 2003.

[156] A. J. Jerri, "The shannon sampling theorem; its various extensions and applications: A tutorial review," *Proceedings of the IEEE*, vol. 65, no. 11, pp. 1565–1596, 1977.

[157] N. Tandon and A. Choudhury, "A review of vibration and acoustic measurement methods for the detection of defects in rolling element bearings," *Tribology International*, vol. 32, no. 8, pp. 469–480, 1999.

[158] J. Z. Zhang and J. C. Chen, "The development of an in-process surface roughness adaptive control system in end milling operations," *The International Journal of Advanced Manufacturing Technology*, vol. 31, no. 9, pp. 877–887, 2007.

[159] A. Al-Habaibeh and N. Gindy, "A new approach for systematic design of condition monitoring systems for milling processes," *Journal of Materials Processing Technology*, vol. 107, no. 1, pp. 243–251, 2000.

[160] P. G. Benardos and G. C. Vosniakos, "Prediction of surface roughness in cnc face milling using neural networks and taguchi's design of experiments," *Robotics and Computer-Integrated Manufacturing*, vol. 18, no. 5, pp. 343–354, 2002.

[161] Z. Wang, P. Willett, P. R. DeAguiar, and J. Webster, "Neural network detection of grinding burn from acoustic emission," *International Journal of Machine Tools and Manufacture*, vol. 41, no. 2, pp. 283–309, 2001.

[162] J. H. Tarn and M. Tomizuka, "On-line monitoring of tool and cutting conditions in milling," *Journal of Engineering for Industry*, vol. 111, no. 3, pp. 206–212, 1989.

[163] Z. Deyuan, H. Yuntai, and C. Dingchang, "On-line detection of tool breakages using telemetering of cutting forces in milling," *International Journal of Machine Tools and Manufacture*, vol. 35, no. 1, pp. 19–27, 1995.

[164] B. Bahr, S. Motavalli, and T. Arfi, "Sensor fusion for monitoring machine tool conditions," *International Journal of Computer Integrated Manufacturing*, vol. 10, no. 5, pp. 314–323, 1997.

[165] K. Jemielniak, "Some aspects of ae application in tool condition monitoring," *Ultrasonics*, vol. 38, no. 1, pp. 604–608, 2000.

[166] J. Webster, W. P. Dong, and R. Lindsay, "Raw acoustic emission signal analysis of grinding process," *CIRP Annals*, vol. 45, no. 1, pp. 335–340, 1996.

[167] J.-S. Kwak and M.-K. Ha, "Neural network approach for diagnosis of grinding operation by acoustic emission and power signals," *Journal of Materials Processing Technology*, vol. 147, no. 1, pp. 65–71, 2004.

[168] R. E. Haber, J. E. Jiménez, C. R. Peres, and J. R. Alique, "An investigation of tool-wear monitoring in a high-speed machining process," *Sensors and Actuators A: Physical*, vol. 116, no. 3, pp. 539–545, 2004.

[169] R. J. Kuo and P. H. Cohen, "Multi-sensor integration for on-line tool wear estimation through radial basis function networks and fuzzy neural network," *Neural Networks*, vol. 12, no. 2, pp. 355–370, 1999.

[170] S. D. E. Dimla, "The correlation of vibration signal features to cutting tool wear in a metal turning operation," *The International Journal of Advanced Manufacturing Technology*, vol. 19, no. 10, pp. 705–713, 2002.

[171] T. Moriwaki and M. Tobito, "A new approach to automatic detection of life of coated tool based on acoustic emission measurement," *Journal of Engineering for Industry*, vol. 112, no. 3, pp. 212–218, 1990.

[172] Y. M. Niu, Y. S. Wong, and G. S. Hong, "An intelligent sensor system approach for reliable tool flank wear recognition," *The International Journal of Advanced Manufacturing Technology*, vol. 14, no. 2, pp. 77–84, 1998.

[173] J. C. Chen and W.-L. Chen, "A tool breakage detection system using an accelerometer sensor," *Journal of Intelligent Manufacturing*, vol. 10, no. 2, pp. 187–197, 1999.

[174] O. B. Abouelatta and J. Mádl, "Surface roughness prediction based on cutting parameters and tool vibrations in turning operations," *Journal of Materials Processing Technology*, vol. 118, no. 1, pp. 269–277, 2001.

[175] I. Inasaki and K. Okamura, "Monitoring of dressing and grinding processes with acoustic emission signals," *CIRP Annals*, vol. 34, no. 1, pp. 277–280, 1985.

[176] G. C. Smith and S. S. Lee, "A method for detecting tool wear on a cnc lathe using a doppler radar detector," *The International Journal of Advanced Manufacturing Technology*, vol. 25, no. 3, pp. 270–280, 2005.

[177] S. Y. Liang, R. L. Hecker, and R. G. Landers, "Machining process monitoring and control: The state–of–the–art," no. 3641X, pp. 599–610, 2002.

[178] J. CusidOCusido, L. Romeral, J. A. Ortega, J. A. Rosero, and A. G. Espinosa, "Fault detection in induction machines using power spectral density in wavelet decomposition," *IEEE Transactions on Industrial Electronics*, vol. 55, no. 2, pp. 633–643, 2008.

[179] L. Cohen, *Time-frequency analysis*, vol. 778. Prentice Hall PTR Englewood Cliffs, NJ:, 1995.

[180] W. Caesarendra and T. Tjahjowidodo, "A review of feature extraction methods in vibration-based condition monitoring and its application for degradation trend estimation of low-speed slew bearing," *Machines*, vol. 5, no. 4, p. 21, 2017.

[181] X. Chen and T. Limchimchol, "Monitoring grinding wheel redress-life using support vector machines," *International Journal of Automation and Computing*, vol. 3, no. 1, pp. 56–62, 2006.

[182] F. Torres and J. Griffin, "Control with micro precision in abrasive machining through the use of acoustic emission signals," *International Journal of Precision Engineering and Manufacturing*, vol. 16, no. 3, pp. 441–449, 2015.

[183] Z. Zhu, R. Yan, L. Luo, Z. Feng, and F. Kong, "Detection of signal transients based on wavelet and statistics for machine fault diagnosis," *Mechanical Systems and Signal Processing*, vol. 23, no. 4, pp. 1076–1097, 2009.

[184] K. Shukla and A. K. Tiwari, *Filter Banks and DWT*, pp. 21–36. Springer, 2013.

[185] L. Xiaoli, T. Shiu Kit, and W. Jun, "Real-time tool condition monitoring using wavelet transforms and fuzzy techniques," *IEEE Transactions on Systems, Man, and Cybernetics, Part C (Applications and Reviews)*, vol. 30, no. 3, pp. 352–357, 2000.

[186] K. Zhu, Y. S. Wong, and G. S. Hong, "Wavelet analysis of sensor signals for tool condition monitoring: A review and some new results," *International Journal of Machine Tools and Manufacture*, vol. 49, no. 7, pp. 537–553, 2009.

[187] R. Azouzi and M. Guillot, "On-line prediction of surface finish and dimensional deviation in turning using neural network based sensor fusion," *International Journal of Machine Tools and Manufacture*, vol. 37, no. 9, pp. 1201–1217, 1997.

[188] M. Chandrasekaran, M. Muralidhar, C. M. Krishna, and U. S. Dixit, "Application of soft computing techniques in machining performance prediction and optimization: a literature review," *The International Journal of Advanced Manufacturing Technology*, vol. 46, no. 5, pp. 445–464, 2010.

[189] D. Axinte and N. Gindy, "Assessment of the effectiveness of a spindle power signal for tool condition monitoring in machining processes," *International Journal of Production Research*, vol. 42, no. 13, pp. 2679–2691, 2004.

[190] C. XiaoQi, Z. Hao, and D. Wildermuth, "In-process tool monitoring through acoustic emission sensing," *Automated Material Processing Group, Automation Technology Division*, vol. 1, 2001.

[191] K.-M. Tsai and P.-J. Wang, "Predictions on surface finish in electrical discharge machining based upon neural network models," *International Journal of Machine Tools and Manufacture*, vol. 41, no. 10, pp. 1385–1403, 2001.

[192] T. Ozel and Y. Karpat, "Prediction of surface roughness and tool wear in finish dry hard turning using back propagation neural networks," in *CD-Proceedings of 17th International Conference on Production Research*.

[193] C.-X. Feng and X.-F. Wang, "Surface roughness predictive modeling: neural networks versus regression," *IIE Transactions*, vol. 35, no. 1, pp. 11–27, 2003.

[194] S. S. Lee and J. C. Chen, "On-line surface roughness recognition system using artificial neural networks system in turning operations," *The International Journal of Advanced Manufacturing Technology*, vol. 22, no. 7-8, pp. 498–509, 2003.

[195] S. V. Kamarthi, S. R. T. Kumara, and P. H. Cohen, "Flank wear estimation in turning through wavelet representation of acoustic emission signals," *Journal of Manufacturing Science and Engineering*, vol. 122, no. 1, pp. 12–19, 1997.

[196] T. Ozel and Y. Karpat, "Predictive modeling of surface roughness and tool wear in hard turning using regression and neural networks," *International Journal of Machine Tools and Manufacture*, vol. 45, no. 4, pp. 467–479, 2005.

[197] D. E. Dimla, P. M. Lister, and N. J. Leighton, "Neural network solutions to the tool condition monitoring problem in metal cutting—a critical review of methods," *International Journal of Machine Tools and Manufacture*, vol. 37, no. 9, pp. 1219–1241, 1997.

[198] S. Das, P. P. Bandyopadhyay, and A. B. Chattopadhyay, "Neural-networks-based tool wear monitoring in turning medium carbon steel using a coated carbide tool," *Journal of Materials Processing Technology*, vol. 63, no. 1, pp. 187–192, 1997.

[199] S. Das, R. Roy, and A. B. Chattopadhyay, "Evaluation of wear of turning carbide inserts using neural networks," *International Journal of Machine Tools and Manufacture*, vol. 36, no. 7, pp. 789–797, 1996.

[200] S. D. E. Dimla, "Application of perceptron neural networks to tool-state classification in a metal-turning operation," *Engineering Applications of Artificial Intelligence*, vol. 12, no. 4, pp. 471–477, 1999.

[201] V. S. Sharma, S. Dhiman, R. Sehgal, and S. K. Sharma, "Estimation of cutting forces and surface roughness for hard turning using neural networks," *Journal of Intelligent Manufacturing*, vol. 19, no. 4, pp. 473–483, 2008.

[202] I. Asilturk and M. CUnkas, "Modeling and prediction of surface roughness in turning operations using artificial neural network and multiple regression method," *Expert Systems with Applications*, vol. 38, no. 5, pp. 5826–5832, 2011.

[203] Z. W. Zhong, L. P. Khoo, and S. T. Han, "Prediction of surface roughness of turned surfaces using neural networks," *The International Journal of Advanced Manufacturing Technology*, vol. 28, no. 7, pp. 688–693, 2006.

[204] K. A. Risbood, U. S. Dixit, and A. D. Sahasrabudhe, "Prediction of surface roughness and dimensional deviation by measuring cutting forces and vibrations in turning process," *Journal of Materials Processing Technology*, vol. 132, no. 1, pp. 203–214, 2003.

[205] D. A. Axinte, "Approach into the use of probabilistic neural networks for automated classification of tool malfunctions in broaching," *International Journal of Machine Tools and Manufacture*, vol. 46, no. 12, pp. 1445–1448, 2006.

[206] H. Oktem, T. Erzurumlu, and F. Erzincanli, "Prediction of minimum surface roughness in end milling mold parts using neural network and genetic algorithm," *Materials & Design*, vol. 27, no. 9, pp. 735–744, 2006.

[207] A. M. Zain, H. Haron, and S. Sharif, "Prediction of surface roughness in the end milling machining using artificial neural network," *Expert Systems with Applications*, vol. 37, no. 2, pp. 1755–1768, 2010.

[208] G. Quintana, M. L. Garcia-Romeu, and J. Ciurana, "Surface roughness monitoring application based on artificial neural networks for ball-end milling operations," *Journal of Intelligent Manufacturing*, vol. 22, no. 4, pp. 607–617, 2011.

[209] S. Karabulut, "Optimization of surface roughness and cutting force during aa7039/al2o3 metal matrix composites milling using neural networks and taguchi method," *Measurement*, vol. 66, pp. 139–149, 2015.

[210] S. K. Choudhury and G. Bartarya, "Role of temperature and surface finish in predicting tool wear using neural network and design of experiments," *International Journal of Machine Tools and Manufacture*, vol. 43, no. 7, pp. 747–753, 2003.

[211] B. Kaya, C. Oysu, and H. M. Ertunc, "Force-torque based on-line tool wear estimation system for cnc milling of inconel 718 using neural networks," *Advances in Engineering Software*, vol. 42, no. 3, pp. 76–84, 2011.

[212] H. Saglam and A. Unuvar, "Tool condition monitoring in milling based on cutting forces by a neural network," *International Journal of Production Research*, vol. 41, no. 7, pp. 1519–1532, 2003.

[213] U. Caydas and A. Hascalik, "A study on surface roughness in abrasive waterjet machining process using artificial neural networks and regression analysis method," *Journal of Materials Processing Technology*, vol. 202, no. 1, pp. 574–582, 2008.

[214] C. Tsao and H. Hocheng, "Evaluation of thrust force and surface roughness in drilling composite material using taguchi analysis and neural network," *Journal of materials processing technology*, vol. 203, no. 1-3, pp. 342–348, 2008.

[215] C. Sanjay and C. Jyothi, "A study of surface roughness in drilling using mathematical analysis and neural networks," *The International Journal of Advanced Manufacturing Technology*, vol. 29, no. 9, pp. 846–852, 2006.

[216] I. Abu-Mahfouz, "Drilling wear detection and classification using vibration signals and artificial neural network," *International Journal of Machine Tools and Manufacture*, vol. 43, no. 7, pp. 707–720, 2003.

[217] E. Govekar and I. Grabec, "Self-organizing neural network application to drill wear classification," *Journal of Engineering for Industry*, vol. 116, no. 2, pp. 233–238, 1994.

[218] S. C. Lin and C. J. Ting, "Drill wear monitoring using neural networks," *International Journal of Machine Tools and Manufacture*, vol. 36, no. 4, pp. 465–475, 1996.

[219] M. E. Nakai, P. R. Aguiar, H. Guillardi, E. C. Bianchi, D. H. Spatti, and D. M. D'Addona, "Evaluation of neural models applied to the estimation of tool wear in the grinding of advanced ceramics," *Expert Systems with Applications*, vol. 42, no. 20, pp. 7026–7035, 2015.

[220] D. F. G. Moia, I. H. Thomazella, P. R. Aguiar, E. C. Bianchi, C. H. R. Martins, and M. Marchi, "Tool condition monitoring of aluminum oxide grinding wheel in dressing operation using acoustic emission and neural networks," *Journal of the Brazilian Society of Mechanical Sciences and Engineering*, vol. 37, no. 2, pp. 627–640, 2015.

[221] F. Cus and U. Zuperl, "Real-time cutting tool condition monitoring in milling," *Strojniški vestnik-Journal of Mechanical Engineering*, vol. 57, no. 2, pp. 142–150, 2011.

[222] C. Chungchoo and D. Saini, "On-line tool wear estimation in cnc turning operations using fuzzy neural network model," *International Journal of Machine Tools and Manufacture*, vol. 42, no. 1, pp. 29–40, 2002.

[223] T. J. Ko, D. W. Cho, and J. M. Lee, "Fuzzy pattern recognition for tool wear monitoring in diamond turning," *CIRP Annals*, vol. 41, no. 1, pp. 125–128, 1992.

[224] S.-Y. Ho, K.-C. Lee, S.-S. Chen, and S.-J. Ho, "Accurate modeling and prediction of surface roughness by computer vision in turning operations using

an adaptive neuro-fuzzy inference system," *International Journal of Machine Tools and Manufacture*, vol. 42, no. 13, pp. 1441–1446, 2002.

[225] Y. Jiao, S. Lei, Z. J. Pei, and E. S. Lee, "Fuzzy adaptive networks in machining process modeling: surface roughness prediction for turning operations," *International Journal of Machine Tools and Manufacture*, vol. 44, no. 15, pp. 1643–1651, 2004.

[226] X. D. Fang and I. S. Jawahir, "Predicting total machining performance in finish turning using integrated fuzzy-set models of the machinability parameters," *International Journal of Production Research*, vol. 32, no. 4, pp. 833–849, 1994.

[227] J. C. Chen and V. Susanto, "Fuzzy logic based in-process tool-wear monitoring system in face milling operations," *The International Journal of Advanced Manufacturing Technology*, vol. 21, no. 3, pp. 186–192, 2003.

[228] A. Iqbal, N. He, N. U. Dar, and L. Li, "Comparison of fuzzy expert system based strategies of offline and online estimation of flank wear in hard milling process," *Expert Systems with Applications*, vol. 33, no. 1, pp. 61–66, 2007.

[229] Z. Uros, C. Franc, and K. Edi, "Adaptive network based inference system for estimation of flank wear in end-milling," *Journal of Materials Processing Technology*, vol. 209, no. 3, pp. 1504–1511, 2009.

[230] S.-P. Lo, "An adaptive-network based fuzzy inference system for prediction of workpiece surface roughness in end milling," *Journal of Materials Processing Technology*, vol. 142, no. 3, pp. 665–675, 2003.

[231] W.-H. Ho, J.-T. Tsai, B.-T. Lin, and J.-H. Chou, "Adaptive network-based fuzzy inference system for prediction of surface roughness in end milling process using hybrid taguchi-genetic learning algorithm," *Expert Systems with Applications*, vol. 36, no. 2, pp. 3216–3222, 2009.

[232] J. C. Chen and M. Savage, "A fuzzy-net-based multilevel in-process surface roughness recognition system in milling operations," *The International Journal of Advanced Manufacturing Technology*, vol. 17, no. 9, pp. 670–676, 2001.

[233] F. Dweiri, M. Al-Jarrah, and H. Al-Wedyan, "Fuzzy surface roughness modeling of cnc down milling of alumic-79," *Journal of Materials Processing Technology*, vol. 133, no. 3, pp. 266–275, 2003.

[234] S. J. Lou and J. C. Chen, "In-process surface recognition of a cnc milling machine using the fuzzy nets method," *Computers & Industrial Engineering*, vol. 33, no. 1, pp. 401–404, 1997.

[235] J. C. Chen and M. S. Lou, "Fuzzy-nets based approach to using an accelerometer for an in-process surface roughness prediction system in milling operations," *International Journal of Computer Integrated Manufacturing*, vol. 13, no. 4, pp. 358–368, 2000.

[236] Q. Liu, X. Chen, and N. Gindy, "Fuzzy pattern recognition of ae signals for grinding burn," *International Journal of Machine Tools and Manufacture*, vol. 45, no. 7, pp. 811–818, 2005.

[237] Y. M. Ali and L. C. Zhang, "A fuzzy model for predicting burns in surface grinding of steel," *International Journal of Machine Tools and Manufacture*, vol. 44, no. 5, pp. 563–571, 2004.

[238] A. K. Nandi and D. K. Pratihar, "Design of a genetic-fuzzy system to predict surface finish and power requirement in grinding," *Fuzzy Sets and Systems*, vol. 148, no. 3, pp. 487–504, 2004.

[239] P. G. Li and S. M. Wu, "Monitoring drilling wear states by a fuzzy pattern recognition technique," *Journal of Engineering for Industry*, vol. 110, no. 3, pp. 297–300, 1988.

[240] O. S. Mesina and R. Langari, "A neuro-fuzzy system for tool condition monitoring in metal cutting," *Journal of Manufacturing Science and Engineering*, vol. 123, no. 2, pp. 312–318, 2000.

[241] L. Monostori and C. S. Egresits, "Modelling and monitoring of milling through neuro-fuzzy techniques," *IFAC Proceedings Volumes*, vol. 27, no. 4, pp. 463–468, 1994.

[242] A. I. Azmi, "Monitoring of tool wear using measured machining forces and neuro-fuzzy modelling approaches during machining of gfrp composites," *Advances in Engineering Software*, vol. 82, pp. 53–64, 2015.

[243] S. Kumanan, C. P. Jesuthanam, and R. Ashok Kumar, "Application of multiple regression and adaptive neuro fuzzy inference system for the prediction of surface roughness," *The International Journal of Advanced Manufacturing Technology*, vol. 35, no. 7, pp. 778–788, 2008.

[244] I. Maher, M. E. H. Eltaib, A. A. D. Sarhan, and R. M. El-Zahry, "Cutting force-based adaptive neuro-fuzzy approach for accurate surface roughness prediction in end milling operation for intelligent machining," *The International Journal of Advanced Manufacturing Technology*, vol. 76, no. 5, pp. 1459–1467, 2015.

[245] K.-C. Lee, S.-J. Ho, and S.-Y. Ho, "Accurate estimation of surface roughness from texture features of the surface image using an adaptive neuro-fuzzy inference system," *Precision Engineering*, vol. 29, no. 1, pp. 95–100, 2005.

[246] M. Rizal, J. A. Ghani, M. Z. Nuawi, and C. H. C. Haron, "Online tool wear prediction system in the turning process using an adaptive neuro-fuzzy inference system," *Applied Soft Computing*, vol. 13, no. 4, pp. 1960–1968, 2013.

[247] R. Tetl and D. D'Addona, "Grinding wheel management through neuro-fuzzy forecasting of dressing cycle time," *CIRP Annals*, vol. 52, no. 1, pp. 407–410, 2003.

[248] W. Caesarendra, T. Wijaya, T. Tjahjowidodo, B. K. Pappachan, A. Wee, and M. I. Roslan, "Adaptive neuro-fuzzy inference system for deburring stage classification and prediction for indirect quality monitoring," *Applied Soft Computing*, 2018.

[249] S. T. Kumaran, T. J. Ko, R. Kurniawan, C. Li, and M. Uthayakumar, "Anfis modeling of surface roughness in abrasive waterjet machining of carbon fiber reinforced plastics," *Journal of Mechanical Science and Technology*, vol. 31, no. 8, pp. 3949–3954, 2017.

[250] L. Owsley, L. E. Atlas, and G. D. Bernard, "Self-organizing feature maps and hidden markov models for machine-tool monitoring," *Signal Processing, IEEE Transactions on*, vol. 45, no. 11, pp. 2787–2798, 1997.

[251] L. Heck and J. McClellan, "Mechanical system monitoring using hidden markov models," in *Acoustics, Speech, and Signal Processing, 1991. ICASSP-91., 1991 International Conference on*, pp. 1697–1700, IEEE.

[252] V. Vapnik, *The nature of statistical learning theory*. Springer Science & Business Media, 2013.

[253] C. Campbell, "Kernel methods: a survey of current techniques," *Neurocomputing*, vol. 48, no. 1, pp. 63–84, 2002.

[254] S. Cho, S. Asfour, A. Onar, and N. Kaundinya, "Tool breakage detection using support vector machine learning in a milling process," *International Journal of Machine Tools and Manufacture*, vol. 45, no. 3, pp. 241–249, 2005.

[255] B. Kaya, C. Oysu, H. M. Ertunc, and H. Ocak, "A support vector machine-based online tool condition monitoring for milling using sensor fusion and a genetic algorithm," *Proceedings of the Institution of Mechanical Engineers, Part B: Journal of Engineering Manufacture*, vol. 226, no. 11, pp. 1808–1818, 2012.

[256] T. Benkedjouh, K. Medjaher, N. Zerhouni, and S. Rechak, "Health assessment and life prediction of cutting tools based on support vector regression," *Journal of Intelligent Manufacturing*, vol. 26, no. 2, pp. 213–223, 2015.

[257] B. Lela, D. Bajić, and S. Jozić, "Regression analysis, support vector machines, and bayesian neural network approaches to modeling surface roughness in face milling," *The International Journal of Advanced Manufacturing Technology*, vol. 42, no. 11, pp. 1082–1088, 2009.

[258] K. Kadirgama, M. M. Noor, and M. M. Rahman, "Optimization of surface roughness in end milling using potential support vector machine," *Arabian Journal for Science and Engineering*, vol. 37, no. 8, pp. 2269–2275, 2012.

[259] R. Ramesh, K. S. Ravi Kumar, and G. Anil, "Automated intelligent manufacturing system for surface finish control in cnc milling using support vector machines," *The International Journal of Advanced Manufacturing Technology*, vol. 42, no. 11, pp. 1103–1117, 2009.

[260] D. R. Salgado and F. J. Alonso, "An approach based on current and sound signals for in-process tool wear monitoring," *International Journal of Machine Tools and Manufacture*, vol. 47, no. 14, pp. 2140–2152, 2007.

[261] U. Caydas and S. Ekici, "Support vector machines models for surface roughness prediction in cnc turning of aisi 304 austenitic stainless steel," *Journal of Intelligent Manufacturing*, vol. 23, no. 3, pp. 639–650, 2012.

[262] L. Atlas, M. Ostendorf, and G. D. Bernard, "Hidden markov models for monitoring machining tool-wear," in *2000 IEEE International Conference on Acoustics, Speech, and Signal Processing. Proceedings (Cat. No.00CH37100)*, vol. 6, pp. 3887–3890 vol.6.

[263] K. Zhu, Y. S. Wong, and G. S. Hong, "Multi-category micro-milling tool wear monitoring with continuous hidden markov models," *Mechanical Systems and Signal Processing*, vol. 23, no. 2, pp. 547–560, 2009.

[264] T. W. Liao, G. Hua, J. Qu, and P. J. Blau, "Grinding wheel condition monitoring with hidden markov model-based clustering methods," *Machining Science and Technology*, vol. 10, no. 4, pp. 511–538, 2006.

[265] M. Elangovan, S. B. Devasenapati, N. R. Sakthivel, and K. I. Ramachandran, "Evaluation of expert system for condition monitoring of a single point cutting tool using principle component analysis and decision tree algorithm," *Expert Systems with Applications*, vol. 38, no. 4, pp. 4450–4459, 2011.

[266] C. L. Jiaa and D. A. Dornfeld, "A self-organizing approach to the prediction and detection of tool wear," *ISA Transactions*, vol. 37, no. 4, pp. 239–255, 1998.

[267] L. Breiman, "Random forests," *Machine Learning*, vol. 45, no. 1, pp. 5–32, 2001.

[268] R. Shanmugamani, M. Sadique, and B. Ramamoorthy, "Detection and classification of surface defects of gun barrels using computer vision and machine learning," *Measurement*, vol. 60, pp. 222–230, 2015.

[269] X. Zhang, C. Krewet, and B. Kuhlenkötter, "Automatic classification of defects on the product surface in grinding and polishing," *International Journal of Machine Tools and Manufacture*, vol. 46, no. 1, pp. 59–69, 2006.

[270] G. Senthil Kumar, U. Natarajan, and S. S. Ananthan, "Vision inspection system for the identification and classification of defects in mig welding joints," *The International Journal of Advanced Manufacturing Technology*, vol. 61, no. 9, pp. 923–933, 2012.

[271] V. Lashkia, "Defect detection in x-ray images using fuzzy reasoning," *Image and Vision Computing*, vol. 19, no. 5, pp. 261–269, 2001.

[272] C. Fan, F. Lv, and S. Chen, "Visual sensing and penetration control in aluminum alloy pulsed gta welding," *The International Journal of Advanced Manufacturing Technology*, vol. 42, no. 1, pp. 126–137, 2009.

[273] S. Ravikumar, K. I. Ramachandran, and V. Sugumaran, "Machine learning approach for automated visual inspection of machine components," *Expert Systems with Applications*, vol. 38, no. 4, pp. 3260–3266, 2011.

[274] J. Hongbin, Y. L. Murphey, S. Jinajun, and C. Tzyy-Shuh, "An intelligent real-time vision system for surface defect detection," in *Proceedings of the 17th International Conference on Pattern Recognition, 2004. ICPR 2004.*, vol. 3, pp. 239–242 Vol.3.

[275] H. Zheng, L. X. Kong, and S. Nahavandi, "Automatic inspection of metallic surface defects using genetic algorithms," *Journal of Materials Processing Technology*, vol. 125-126, pp. 427–433, 2002.

[276] Y. LeCun and Y. Bengio, "Convolutional networks for images, speech, and time series," *The handbook of brain theory and neural networks*, vol. 3361, no. 10, p. 1995, 1995.

[277] Y. LeCun, "Generalization and network design strategies," *Connectionism in perspective*, pp. 143–155, 1989.

[278] Y. LeCun, P. Haffner, L. Bottou, and Y. Bengio, *Object recognition with gradient-based learning*, pp. 319–345. Springer, 1999.

[279] Y. LeCun, Y. Bengio, and G. Hinton, "Deep learning," *nature*, vol. 521, no. 7553, p. 436, 2015.

[280] C. Thornton, F. Hutter, H. H. Hoos, and K. Leyton-Brown, "Auto-weka: Combined selection and hyperparameter optimization of classification algorithms," in *Proceedings of the 19th ACM SIGKDD international conference on Knowledge discovery and data mining*, pp. 847–855, ACM.

[281] J. Petrak, "Fast subsampling performance estimates for classification algorithm selection," in *Proceedings of the ECML-00 Workshop on Meta-Learning: Building Automatic Advice Strategies for Model Selection and Method Combination*, pp. 3–14, Citeseer.

[282] E. Chong, C. Han, and F. C. Park, "Deep learning networks for stock market analysis and prediction: Methodology, data representations, and case studies," *Expert Systems with Applications*, vol. 83, pp. 187–205, 2017.

[283] M. Sheinfeld, S. Levinson, and I. Orion, "Highly accurate prediction of specific activity using deep learning," *Applied Radiation and Isotopes*, vol. 130, pp. 115–120, 2017.

[284] I. Sa, Z. Chen, M. Popović, R. Khanna, F. Liebisch, J. Nieto, and R. Siegwart, "weednet: Dense semantic weed classification using multispectral images and mav for smart farming," *IEEE Robotics and Automation Letters*, vol. 3, no. 1, pp. 588–595, 2018.

[285] N. Audebert, B. Le Saux, and S. Lefèvre, "Segment-before-detect: Vehicle detection and classification through semantic segmentation of aerial images," *Remote Sensing*, vol. 9, no. 4, 2017.

[286] R. Yasrab, N. Gu, and X. Zhang, "An encoder-decoder based convolution neural network (cnn) for future advanced driver assistance system (adas)," *Applied Sciences*, vol. 7, no. 4, 2017.

[287] G. Taguchi, *Introduction to quality engineering: designing quality into products and processes*. 1986.

[288] H. R. Lindman, *Analysis of variance in experimental design*. Springer Science & Business Media, 2012.

[289] 'Xsensor Technology Corporation', 2018. [Online]. Available: www.xsensor.com/products/high-pressure-sensors. [Accessed: 09-July-2018].

[290] 'Capacitive Tactile Sensing', 2018. [Online]. Available: http://www.pressureprofile.com/capacitive-sensors. [Accessed: 09-July-2018].

[291] L.-C. Ying and M.-C. Pan, "Using adaptive network based fuzzy inference system to forecast regional electricity loads," *Energy Conversion and Management*, vol. 49, no. 2, pp. 205–211, 2008.

[292] L. A. Zadeh, "Fuzzy sets," *Information and control*, vol. 8, no. 3, pp. 338–353, 1965.

[293] O. Yilmaz, A. T. Bozdana, and M. A. Okka, "An intelligent and automated system for electrical discharge drilling of aerospace alloys: Inconel 718 and ti-6al-4v," *The International Journal of Advanced Manufacturing Technology*, vol. 74, no. 9-12, pp. 1323–1336, 2014.

[294] P. J. Werbos, "Backpropagation through time: what it does and how to do it," *Proceedings of the IEEE*, vol. 78, no. 10, pp. 1550–1560, 1990.

[295] V. Pandiyan, W. Caesarendra, T. Tjahjowidodo, and G. Praveen, "Predictive modelling and analysis of process parameters on material removal characteristics in abrasive belt grinding process," *Applied Sciences*, vol. 7, no. 4, p. 363, 2017.

[296] X. Chen and W. Brian Rowe, "Analysis and simulation of the grinding process. part ii: Mechanics of grinding," *International Journal of Machine Tools and Manufacture*, vol. 36, no. 8, pp. 883–896, 1996.

[297] E. Atzeni and L. Iuliano, "Experimental study on grinding of a sintered friction material," *Journal of Materials Processing Technology*, vol. 196, no. 1, pp. 184–189, 2008.

[298] L. Zhang, *Numerical Analysis and Experimental Investigation of Energy Partition and Heat Transfer in Grinding*, p. Ch. 04. Rijeka: InTech, 2012.

[299] H. Sin, N. Saka, and N. P. Suh, "Abrasive wear mechanisms and the grit size effect," *Wear*, vol. 55, no. 1, pp. 163–190, 1979.

[300] D. Dornfeld and H. G. Cai, "An investigation of grinding and wheel loading using acoustic emission," *Journal of Engineering for Industry*, vol. 106, no. 1, pp. 28–33, 1984.

[301] W. Caesarendra, B. Kosasih, K. Tieu, and C. A. Moodie, "An application of nonlinear feature extraction-a case study for low speed slewing bearing condition monitoring and prognosis," in *Advanced Intelligent Mechatronics (AIM), 2013 IEEE/ASME International Conference on*, pp. 1713–1718, IEEE.

[302] D. M. Tax, A. Ypma, and R. P. Duin, *Pump failure detection using support vector data descriptions*, pp. 415–425. Springer, 1999.

[303] Y. Tarng, Y. Hseih, and S. Hwang, "Sensing tool breakage in face milling with a neural network," *International Journal of Machine Tools and Manufacture*, vol. 34, no. 3, pp. 341–350, 1994.

[304] P. McFadden and J. Smith, "Vibration monitoring of rolling element bearings by the high-frequency resonance technique—a review," *Tribology international*, vol. 17, no. 1, pp. 3–10, 1984.

[305] W. Caesarendra, B. Kosasih, A. K. Tieu, H. Zhu, C. A. S. Moodie, and Q. Zhu, "Acoustic emission-based condition monitoring methods: Review and application for low speed slew bearing," *Mechanical Systems and Signal Processing*, vol. 72–73, pp. 134–159, 2016.

[306] F. J. Harris, "On the use of windows for harmonic analysis with the discrete fourier transform," *Proceedings of the IEEE*, vol. 66, no. 1, pp. 51–83, 1978.

[307] P. K. Rahi and R. Mehra, "Analysis of power spectrum estimation using welch method for various window techniques," *International Journal of Emerging Technologies and Engineering*, vol. 2, no. 6, pp. 106–109, 2014.

[308] S. L. Marple and S. L. Marple, *Digital spectral analysis: with applications*, vol. 5. Prentice-Hall Englewood Cliffs, NJ, 1987.

[309] M. Dash and H. Liu, "Consistency-based search in feature selection," *Artificial intelligence*, vol. 151, no. 1, pp. 155–176, 2003.

[310] R. Akbari and K. Ziarati, "A multilevel evolutionary algorithm for optimizing numerical functions," *International Journal of Industrial Engineering Computations*, vol. 2, no. 2, pp. 419–430, 2011.

[311] M. U. Islam, L. Xue, and G. McGregor, "Process for manufacturing or repairing turbine engine or compressor components," Aug. 7 2001. US Patent 6,269,540.

[312] P. W. Heitman, S. N. Hammond, and L. E. Brown, "Method for joining single crystal turbine blade halves," Dec. 10 1991. US Patent 5,071,059.

[313] D. Axinte, M. Kritmanorot, M. Axinte, and N. Gindy, "Investigations on belt polishing of heat-resistant titanium alloys," *Journal of Materials Processing Technology*, vol. 166, no. 3, pp. 398–404, 2005.

[314] "Automated weld seam removal system promises removal rates over 20 times faster than manual grinding," *Industrial Robot: An International Journal*, vol. 38, no. 4, 2011.

[315] X. Chen, S. Chen, T. Lin, and Y. Lei, "Practical method to locate the initial weld position using visual technology," *The International Journal of Advanced Manufacturing Technology*, vol. 30, no. 7, pp. 663–668, 2006.

[316] H. Luo and X. Chen, "Laser visual sensing for seam tracking in robotic arc welding of titanium alloys," *The International Journal of Advanced Manufacturing Technology*, vol. 26, no. 9, pp. 1012–1017, 2005.

[317] Y. Ito, *In-Process Measurement for Machining States: Sensing Technology in Noisy Space*, pp. 17–40. Cham: Springer International Publishing, 2014.

[318] J. C. Chen, L. Huang, A. Lan, and S. Lee, "Analysis of an effective sensing location for an in-process surface recognition system in turning operations," *Journal of Industrial Technology*, vol. 15, no. 3, pp. 1–6, 1999.

[319] D. Dornfeld, "Acoustic emission process monitoring for untended manufacturing," in *Proc. Japan-USA Symposium on Flexible Automation*, pp. 831–836.

[320] R. E. Learned and A. S. Willsky, "A wavelet packet approach to transient signal classification," *Applied and Computational Harmonic Analysis*, vol. 2, no. 3, pp. 265–278, 1995.

[321] I. N. Tansel, C. Mekdeci, and C. Mclaughlin, "Detection of tool failure in end milling with wavelet transformations and neural networks (wt-nn)," *International Journal of Machine Tools and Manufacture*, vol. 35, no. 8, pp. 1137–1147, 1995.